

Chapter 9

Antarctic environmental change and ice sheet evolution through the Miocene to Pliocene – a perspective from the Ross Sea and George V to Wilkes Land Coasts

Richard H. Levy^{1,2}, Aisling M. Dolan³, Carlota Escutia⁴,
Edward G.W. Gasson⁵, Robert M. McKay², Tim Naish¹,
Molly O. Patterson⁶, Lara F. Pérez⁷, Amelia E. Shevenell⁸,
Tina van de Flierdt⁹, Warren Dickinson², Douglas E. Kowalewski¹⁰,
Stephen R. Meyers¹¹, Christian Ohneiser¹², Francesca Sangiorgi¹³,
Trevor Williams¹⁴, Hannah K. Chorley², Laura De Santis¹⁵,
Fabio Florindo¹⁶, Nicholas R. Golledge², Georgia R. Grant¹,
Anna Ruth W. Halberstadt¹⁷, David M. Harwood¹⁸, Adam R. Lewis¹⁹,
Ross Powell²⁰ and Marjolaine Verret²

¹GNS Science, Lower Hutt, New Zealand, ²Antarctic Research Centre, Victoria University of Wellington, Wellington, New Zealand, ³School of Earth and Environment, University of Leeds, Leeds, United Kingdom, ⁴Andalusian Institute of Earth Sciences, CSIC and Universidad de Granada, Armilla, Spain, ⁵Centre for Geography and Environmental Science, University of Exeter, Cornwall Campus, Penryn, United Kingdom, ⁶Department of Geological Sciences and Environmental Studies, Binghamton University, Binghamton, NY, United States, ⁷British Antarctic Survey, Cambridge, United Kingdom, ⁸College of Marine Science, University of South Florida, St. Petersburg, FL, United States, ⁹Department of Earth Science and Engineering, Imperial College London, London, United Kingdom, ¹⁰Department of Earth, Environment, and Physics, Worcester State University, Worcester, MA, United States, ¹¹Department of Geoscience, University of Wisconsin-Madison, Madison, WI, United States, ¹²Department of Geology, University of Otago, Dunedin, New Zealand, ¹³Laboratory of Palaeobotany and Palynology, Department of Earth Sciences, Marine Palynology and Paleoceanography, Utrecht University, Utrecht, The Netherlands, ¹⁴International Ocean Discovery Program, Texas A&M University, College Station, TX, United States, ¹⁵National Institute of Oceanography and Applied Geophysics – OGS, Sgonico, Italy, ¹⁶National Institute of Geophysics and Volcanology, Rome, Italy, ¹⁷Climate System Research Center, University of Massachusetts, Amherst, MA, United States,

¹⁸*Department of Earth and Atmospheric Sciences, University of Nebraska, Lincoln, NE, United States,*¹⁹*Department of Geosciences, North Dakota State University, Fargo, ND, United States,*²⁰*Department of Geology and Environmental Geosciences, Northern Illinois University, DeKalb, IL, United States*

9.1 Introduction

9.1.1 Overview and relevance

The Miocene to Pliocene interval of Earth's history occurred between 23.04 and 2.58 million years ago (Ma) (Gradstein and Ogg, 2020; Raffi et al., 2020). During this time, Earth's climate transitioned from relatively warm conditions in the Oligocene, where ice sheets in Antarctica were largely land-based, to the onset of bi-polar glaciation. The long-term cooling trend was punctuated by several, global-scale climatic events and transitions (De Vleeschouwer et al., 2017; Westerhold et al., 2020; Zachos et al., 2001a) including the Miocene Climatic Optimum (MCO) (Flower, 1999; Flower and Kennett, 1994; Steinthorsdottir et al., 2021), Middle Miocene Climate Transition (MMCT) (Flower and Kennett, 1994; Shevenell et al., 2004; Tian et al., 2013), Tortonian Thermal Maximum (Holbourn et al., 2013; Westerhold et al., 2020), Late Miocene Cooling (Herbert et al., 2016; Holbourn et al., 2018; Loutit and Kennett, 1979), and the Pliocene Warm Period (Beu, 1974; Dowsett et al., 1996; Haywood et al., 2016; Poore and Sloan, 1996). These events are captured in regional paleoenvironmental proxy records and their global nature is reflected in the deep-sea benthic foraminifer oxygen and carbon isotope records (Fig. 9.1). Importantly, variations in the oxygen isotopic composition of sea water recorded in the tests of benthic foraminifers reflect changes in bottom water temperature and ice volume, which are used to infer the evolution of high latitude climate and ice sheets (De Vleeschouwer et al., 2017; Kennett, 1977; Miller et al., 1991a; Westerhold et al., 2020; Zachos et al., 2001a, 2008). Sea level reconstructions from geological archives (Carlson et al., 2019; Grant et al., 2019; John et al., 2011; Kominz et al., 2008, 2016; Miller et al., 2005; Miller et al., 2005, 2012, 2020) provide independent records of ice volume variability but can be contradictory due to uncertainty in age control and non-climatic processes (e.g., glacial isostatic adjustment, dynamic topography and tectonics) that affect local sea level. In this chapter, we set the global climate scene and then focus on Antarctica's climate and ice sheet evolution through the Miocene and Pliocene. We review and summarise paleoclimate observations from Antarctica during these global climatic episodes and discuss modelling studies. We take a regional approach and focus our discussion towards geological data from the Ross Sea, George V Coast and Wilkes Land (Fig. 9.2). However, we acknowledge that data and insights into Miocene and Pliocene

climate change and ice dynamics are available from other regions around Antarctica (Haywood et al., 2008; McKay et al., 2021).

By the end of this century, atmospheric carbon dioxide (CO_2) is projected to reach concentrations between 430 and 1000 parts per million in volume (ppmv), depending upon future emission scenarios (IPCC, 2013; Meinshausen et al., 2011) (Fig. 9.1). Proxy-based atmospheric CO_2 reconstructions suggest that the Pliocene was the last time when atmospheric CO_2 levels exceeded 400 ppm (Badger et al., 2013a; Bartoli et al., 2011; Martinez-Botí et al., 2015; Pagani et al., 2010; Seki et al., 2010) and global mean temperatures were 2°C – 3°C warmer than pre-industrial, making this time period an important target for understanding environmental conditions in light of ongoing climate change (Burke et al., 2018; Dolan et al., 2012; Dowsett et al., 2012; Haywood et al., 2013, 2016; Lawrence et al., 2009; Lunt et al., 2012; Masson-Delmotte et al., 2013; Raymo, 1994). The long-term trend of the global benthic marine oxygen isotope stack implies that during the early to mid Pliocene global ice volume was reduced, compared to today (Lisiecki and Raymo, 2005; Miller et al., 2012), with estimates of global mean sea level (GMSL) ranging between 6 and 25 metres higher than present (Dumitru et al., 2019; Dutton et al., 2015; Grant et al., 2019; Miller et al., 2012; Raymo et al., 2011; Rovere et al., 2020). Proxy-based reconstructions suggest CO_2 concentrations were even higher during the MCO, at times exceeding 600 ppm, although the range of concentration estimates is high (Greenop et al., 2014; Sosdian et al., 2018; Steinthorsdottir et al., 2021). Global mean surface temperatures during this interval were between 3°C and 8°C warmer than today (Shevenell et al., 2004; Steinthorsdottir et al., 2021; You, 2010; You et al., 2009) and sea level records suggest Antarctica's ice sheets were at times much smaller than now (John et al., 2011; Kominz et al., 2008, 2016; Miller et al., 2005, 2020). Significant research effort is focused on the Miocene as it is recognised as an important target for evaluating the Earth system response to future warming (Steinthorsdottir et al., 2020), particularly if efforts to mitigate greenhouse emissions fall short.

Warm climate intervals from the Miocene and Pliocene help us understand the sensitivity of Antarctica's ice sheets and the high southern latitudes to climate change; information that can inform our planet's possible future. Presently, a disconnect exists between paleoceanographic interpretations of ice volume change derived from the deep-sea records and ice-proximal records of environmental variability and ice sheet dynamics from the margins of Antarctica. An example is the long-lasting debate over Antarctic ice sheet stability (Clapperton and Sugden, 1990; Sugden et al., 1993) vs dynamism (Webb and Harwood, 1991; Wilson, 1995) since the middle Miocene. The stability hypothesis is based, in part, on the deep-sea oxygen-isotope record, which shows a stepwise and sustained increase in $\delta^{18}\text{O}$ values beginning at ~ 14 Ma ago (Flower and Kennett, 1993a; Kennett et al., 1975) and

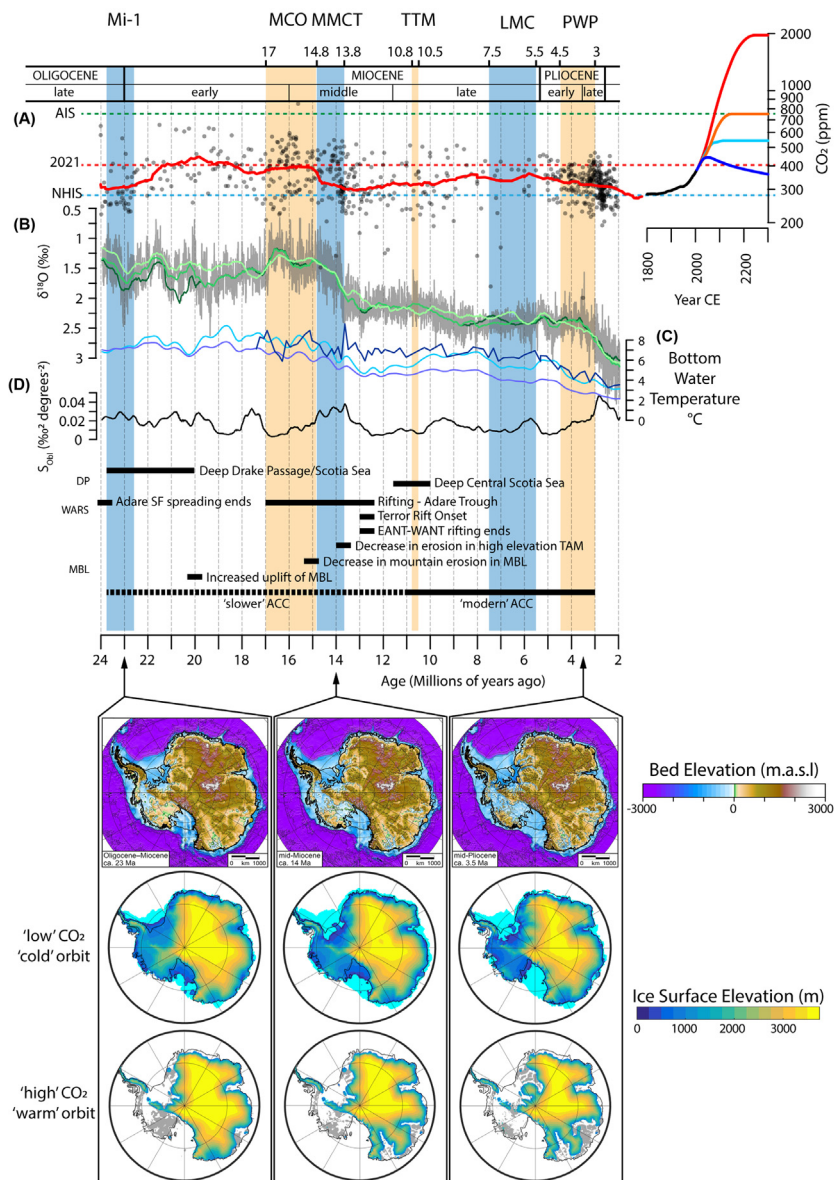


FIGURE 9.1 Summary of key environmental records and tectonic events that have influenced Antarctic climate and ice sheet evolution through the Miocene to Pliocene. Major climatic transitions include the Oligocene/Miocene Boundary (Mi-1) event, the Miocene Climatic Optimum (MCO), Middle Miocene Climate Transition (MMCT), Tortonian Thermal Maximum (TTM), Late Miocene Cooling (LMC), and Pliocene Warm Period (PWP). (A) Atmospheric CO₂ compilation comprises data from a range of proxies including boron isotopes (Bartoli et al., 2011; (Continued)

has been interpreted to represent ice build-up and stabilisation of the East Antarctic Ice Sheet (EAIS). However, as: (1) the geographic distribution of geological studies around the Antarctic margin has increased and the fidelity of the records has improved (Bertram et al., 2018; Cook et al., 2013, 2017; Escutia et al., 2019; Gulick et al., 2017; Levy et al., 2019; McKay et al., 2012; Patterson et al., 2014; Sangiorgi et al., 2018; Wilson et al., 2018), (2) new sea level reconstructions have been produced (Dumitru et al., 2019; Grant et al., 2019; Miller et al., 2012; Rovere et al., 2020), and (3) modelling approaches have improved (Berends et al., 2019; de Boer et al., 2014; DeConto and Pollard, 2016; DeConto et al., 2012; Dolan et al., 2012; Gasson et al., 2016b; Haywood et al., 2016; Pollard and DeConto, 2009; Pollard et al., 2015), it is now clear that Antarctica's ice sheets behaved dynamically throughout the Neogene and into the Quaternary.

Here we outline recent advances in knowledge of Antarctic Ice Sheet (AIS) behaviour and climate evolution through the Neogene. We focus our review on ice proximal geological records from the Ross Sea and offshore George V Land and Wilkes Land (Fig. 9.2); three regions where important data sets have become available over the past 15 years. We also present

-
- ◀ Foster et al., 2012; Greenop et al., 2014, 2019; Martinez-Botí et al., 2015; Raitzsch et al., 2021; Seki et al., 2010; Sosdian et al., 2018), B/Ca (Badger et al., 2013b), phytoplankton/alkenones (Badger et al., 2013b, 2019; Bolton et al., 2016; Pagani et al., 2011; Seki et al., 2010; Super et al., 2018; Zhang et al., 2013), leaf stomata (Beerling et al., 2009; Kürschner et al., 1996, 2008; Retallack, 2009a; Van der Burgh et al., 1993), paleosols (Cerling, 1992; Ekart et al., 1999; Ji et al., 2018; Retallack, 2009b), phytanes (Witkowski et al., 2018) and diatoms (Mejía et al., 2017). Solid red line displays a two million year moving average. CO₂ concentrations from 1765 to 2300 are shown for representative concentration pathways (RCPs) 2.6 (dark blue), 4.5 (light blue), 6 (orange) and 8.5 (red) (Meinshausen et al., 2011). Atmospheric CO₂ concentration thresholds for Antarctic ice sheet formation (green dashed line) and Northern Hemisphere (bi-polar) glaciation (blue dashed line) are based on modelling results (DeConto and Pollard, 2003; DeConto et al., 2008). Present day average atmospheric CO₂ concentration shown by the red dashed line and is like those that characterised much of the early to middle Miocene. (B) Splice of deep sea benthic foraminifera δ¹⁸O data (light grey) reflect changes in ice volume and deep/bottom water temperature (De Vleeschouwer et al., 2017). A comparison between three different records/splices is shown by the three green lines that display a 500 kyr moving average through the splice of Miller et al. (2020) (dark green), De Vleeschouwer et al. (2017) (medium green), and Cramer et al. (2009) (light green). (C) Bottom water temperature (BWT) records are derived from Ocean Drilling Program (ODP) Site 806 (dark blue) (Lear et al., 2015) Equation 7a (light blue) and 7b (purple) from the compilation of Cramer et al. (2011). (D) Obliquity sensitivity (S_{obl}) offers a proxy for ice sheet extent where higher values reflect times during which ice sheets expanded across Antarctica's continental shelves (Levy et al., 2019). Timing and duration of significant tectonic and oceanic events in the region around the Drake Passage (DP), West Antarctic Rift System (WARS), and Marie Byrd Land (MBL) are indicated by black horizontal bars (see text for details). Reconstructed topography for Antarctica is shown for three key time slices (23, 14, and 3.5 Ma) with associated ice sheet model simulations under low (280 ppm) CO₂ forcing and cold astronomical configuration and high (840 ppm) CO₂ forcing and warm astronomical configuration (Paxman et al., 2020).

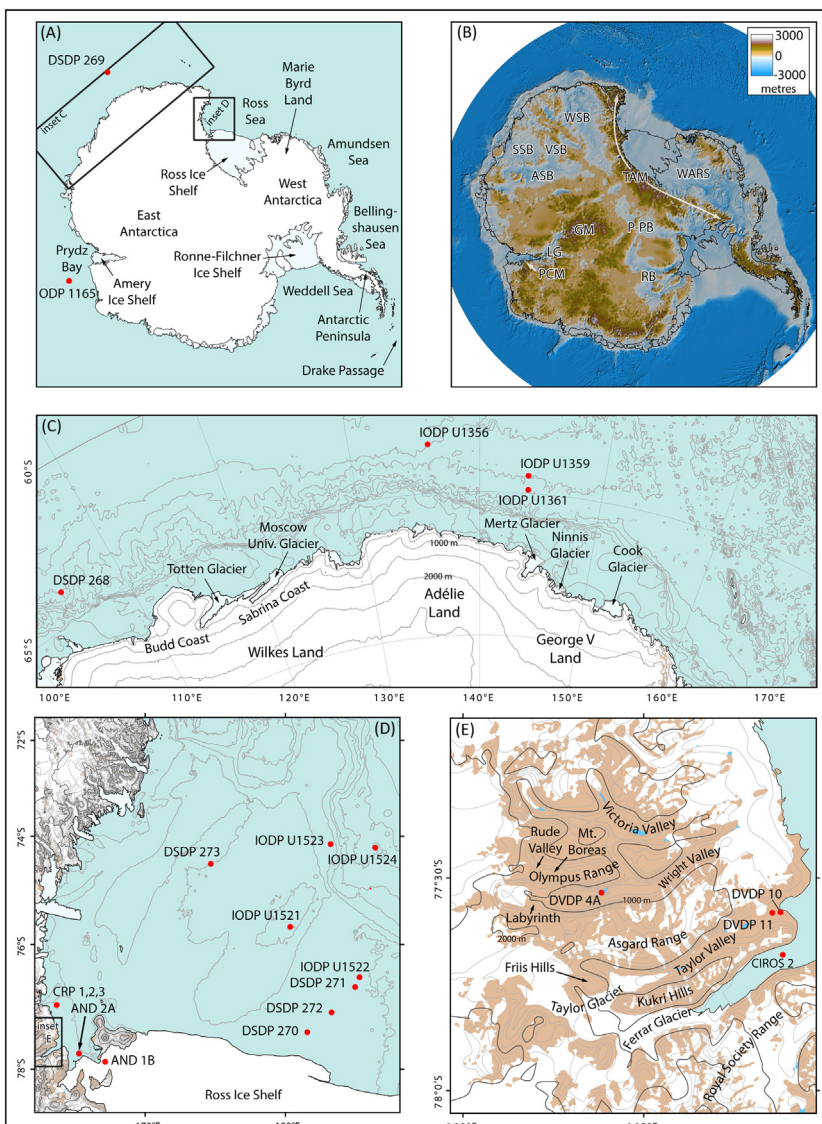


FIGURE 9.2 Location of key terrestrial and marine geological records discussed in the text. Deep Sea Drilling Project (DSDP), Ocean Drilling Program (ODP), Integrated Ocean Discovery Program (IODP), Dry Valleys Drilling Project (DVDP), Cenozoic Investigation of the Ross Sea Core (CIROS-1), Cape Roberts Project (CRP), and ANDRILL (AND) drill sites are indicated by red dots. Blue regions = ocean, white = ice, brown = exposed rock and sediment. Ice sheet elevation and ocean bathymetric contours are every 500 m. (A) Antarctica. (B) Subglacial geography of Antarctica derived from Bedmap2 (Fretwell et al., 2013) with major subglacial basins: WSB, Wilkes Subglacial Basin; ASB, Aurora Subglacial Bain; SSB, Sabrina Subglacial Basin; VSB, (Continued)

and discuss recent modelling studies that investigate climate–ice sheet interactions in the Miocene and Pliocene. For a broader review of other data sets from around the Antarctic, particularly offshore Prydz Bay and the Antarctic Peninsula, we refer the reader to the previous version of this chapter (Haywood et al., 2008) and other review papers and documents (Barrett, 2013; Bart and De Santis, 2012; Escutia et al., 2019; McKay et al., 2021).

9.1.2 Far-field records of climate and ice sheet variability

9.1.2.1 The Early Miocene

The onset of the Miocene is marked by a major transition in global climate from relative warmth of the late Oligocene to the generally cooler climates that persisted through much of the Neogene (Naish et al., 2021). Atmospheric CO₂ declined in the latest Oligocene (Zhang et al., 2013) reaching concentrations below 400 ppm across the Oligocene-Miocene Transition (OMT) (Fig. 9.1) (Greenop et al., 2019; Super et al., 2018). A large (~1‰) transient positive oxygen isotope excursion, broadly known as the Mi-1 event (Miller et al., 1991a; Zachos et al., 2001a; Zachos et al., 2001c) coincides with globally-distributed evidence for sea level lowstands of 20 to 40 m (Miller et al., 2020; Miller et al., 2005; Śliwińska et al., 2014; Zelilidis et al., 2002). Early Miocene cooling coincides with the onset of modern monsoon-like climate and widespread loess deposition in northern China (Guo et al., 2008; Zhang et al., 2018), ~2°C cooling in NW Europe (Śliwińska et al., 2014), and cooler sea surface temperature (SST) in the north Atlantic Ocean (Egger et al., 2018; Super et al., 2020; Super et al., 2018). High resolution ice-distal benthic foraminifer stable isotope records suggest that the AIS expanded across the OMT and reached a volume comparable to present (Liebrand et al., 2017; Liebrand et al., 2011). Ice volume was potentially up to 25% larger than today if assumptions are made about the stability of the δ¹⁸O composition of Antarctica's ice sheets (Pekar et al., 2006). Far field records suggest that the AIS decreased in size over the one million years after the OMT, in response to climatic warming and a hypothesised subsidence-induced reduction in terrestrial Antarctic land mass (Liebrand et al., 2017). Earliest Miocene proxy CO₂ concentrations are variable, with post-OMT estimates as high as 1000 ppm (Reichgelt et al.,

◀ Vincennes Subglacial Basin; *P-PB*, Pensacola-Pole Basin; *RB*, Recovery Basin; *WARS*, West Antarctic Rift System; *LG*, Lambert Graben; *TAM*, Transantarctic Mountains, *GM*, Gamburtsev Mountains; *PCM*, Prince Charles Mountains. (C) George V Land, Adélie Land, and Wilkes Land region of East Antarctica. (D) Ross Sea Region, in the panel D a square indicating the location of panel E. (E) McMurdo Dry Valleys. Land contours in (D) and (E) are every 200 m.

2016). However, a majority of the proxy data indicate values between 350 and 450 ppm from 23 to 19.5 Ma (Greenop et al., 2019; Londoño et al., 2018; Reichgelt et al., 2020; Super et al., 2018; Zhang et al., 2013). Glacial-interglacial variability through much of the early Miocene was paced by variations in short and long-period eccentricity (Holbourn et al., 2005; Liebrand et al., 2017) and likely saw fluctuations between 50% and 125% of the modern EAIS (Pekar and DeConto, 2006). Bottom water temperatures (BWT) likely varied up to 3°C on million year time scales (Cramer et al., 2011).

9.1.2.2 *The mid-Miocene*

Following the relatively cool climate of the earliest Miocene, environmental proxies indicate that the Planet entered an interval of relative warmth. The Miocene Climatic Optimum (MCO; ~17 to ~14.8 Ma) is characterised by low average deep sea benthic foraminifera $\delta^{18}\text{O}$ values (De Vleeschouwer et al., 2017; Flower and Kennett, 1993a; Holbourn et al., 2015; Westerhold et al., 2020; Woodruff and Savin, 1991) (Figs 9.1 and 9.3). Fossil floral and faunal evidence indicate that this was the warmest interval of the past 35 million years (Böhme, 2003; Hornbrook, 1992; Mosbrugger et al., 2005; Prebble et al., 2017; Utescher et al., 2011). Average global surface temperatures were likely 3°C to 4°C warmer than present (You, 2010), with intervals of peak warmth during which average surface temperatures were ~7°C to 8°C warmer than today (Goldner et al., 2014; Steinthorsdottir et al., 2020, 2021). Near surface and surface water temperature (upper 200 m) in the Southern Ocean were at times between 7°C and ~16°C warmer than present (Sangiorgi et al., 2018; Shevenell et al., 2004) and global deep sea water temperatures were between 5°C and 9°C warmer than today (Billups and Schrag, 2003; Lear et al., 2010, 2015; Modestou et al., 2020; Shevenell et al., 2008). Causes of warming and cooling through the MCO have largely been attributed to changes in carbon cycling (e.g., greenhouse gas concentrations) (Foster and Rohling, 2013; Foster et al., 2012; Vincent and Berger, 1985; Woodruff and Savin, 1989). There is a wide range of estimates of atmospheric CO₂ concentrations during the MCO of between <400 and >1000 ppm (Cui et al., 2020; Greenop et al., 2014; Ji et al., 2018; Sosdian et al., 2018; Steinthorsdottir et al., 2021). The inferred increase in CO₂ has been linked to rapid eruption of the Columbia River Flood basalts between 16.7 and 15.9 Ma (Foster et al., 2012; Kasbohm and Schoene, 2018). Statistical analysis of available proxy data suggests that average values through the MCO were ~400 ppm (Figs 9.1 and 9.3) but estimates based on boron proxy data from Ocean Drilling Program (ODP) Site 761 off NW Australia suggest eccentricity-paced (100 kyr) variations between 200 and 600 ppm occurred (Greenop et al., 2014). Mechanisms and processes driving these relatively large high

frequency changes in the carbon cycle require further exploration. However, there is little doubt they support other climate proxies that indicate a dynamic astronomically-paced climate during the MCO (Holbourn et al., 2015) (Fig. 9.3) and that climate sensitivity may have been higher than present.

A more detailed examination of benthic foraminifera $\delta^{18}\text{O}$ data suggests that, like most intervals in Earth's history, the MCO cannot be characterised by a single 'time slice' reconstruction. The onset of the MCO is marked by a large ($\sim 1\%$), relatively rapid shift in mean $\delta^{18}\text{O}$ values (Fig. 9.1) and is followed by low to moderate variability on eccentricity-paced time scales (Holbourn et al., 2015) (Figs 9.1 and 9.3). These data suggest subdued environmental variability during the early MCO (~ 17 to 16 Ma) and reflect warmer ocean bottom waters and/or reduced ice volume relative to the early Miocene (Figs 9.1 and 9.3). This period of relative warmth and stability was followed by an interval from 16 to 15 Ma characterised by high amplitude $\delta^{18}\text{O}$ variability (Flower and Kennett, 1994) with shifts up to 1.5% on eccentricity-paced glacial/interglacial timescales (Holbourn et al., 2015) (Fig. 9.3B). MCO bottom water temperatures (BWT) fluctuated by as much as 3°C in the Southern Ocean on hundred thousand year timescales (Shevenell et al., 2008) and up to 6°C at lower latitude sites across million year periods (Lear et al., 2015) (Fig. 9.3F). These relatively large BWT changes may explain a significant portion of the $\delta^{18}\text{O}$ variability between 16 and 15 Ma, although global sea level reconstructions suggest that large ice volume variations during this time cannot be ruled out (Miller et al., 2020). These large $\delta^{18}\text{O}$ variations also coincide with eccentricity-paced (~ 400 kyr) changes in benthic foraminifera $\delta^{13}\text{C}$ data. The astronomically-paced excursions are superimposed on the ~ 2 million year-long global $\sim 1\%$ increase in $\delta^{13}\text{C}$ referred to as the Monterey Carbon Isotopic Excursion (Vincent and Berger, 1985) (Fig. 9.3D). The Monterey Excursion has nine 400 kyr-paced $\delta^{13}\text{C}$ maxima (Holbourn et al., 2007; Pagani et al., 1999a; Woodruff and Savin, 1989) that reflect changes in global carbon cycling, an interpretation further supported by observations of global Carbonate Compensation Depth variability (Holbourn et al., 2015) and intervals of enhanced organic carbon deposition and preservation on the circum-Pacific continental shelves (Sosdian et al., 2020; Vincent and Berger, 1985).

Sedimentary records from the New Jersey margin (Kominz et al., 2008, 2016; Miller et al., 2005) and the Marion Plateau, south of Australia (John et al., 2011), indicate sea level rose and fell up to ~ 35 m during the MCO (Fig. 9.3), requiring fluctuations of up to 60% of the present AIS. SSTs in high northern latitudes were up to 15°C warmer than present during the MCO but were not significantly higher than the early Miocene (Super et al., 2018) and there is little evidence for ice-rafting in the Arctic from 17.5 to 16 Ma (St. John, 2008). These data suggest that the fluctuating

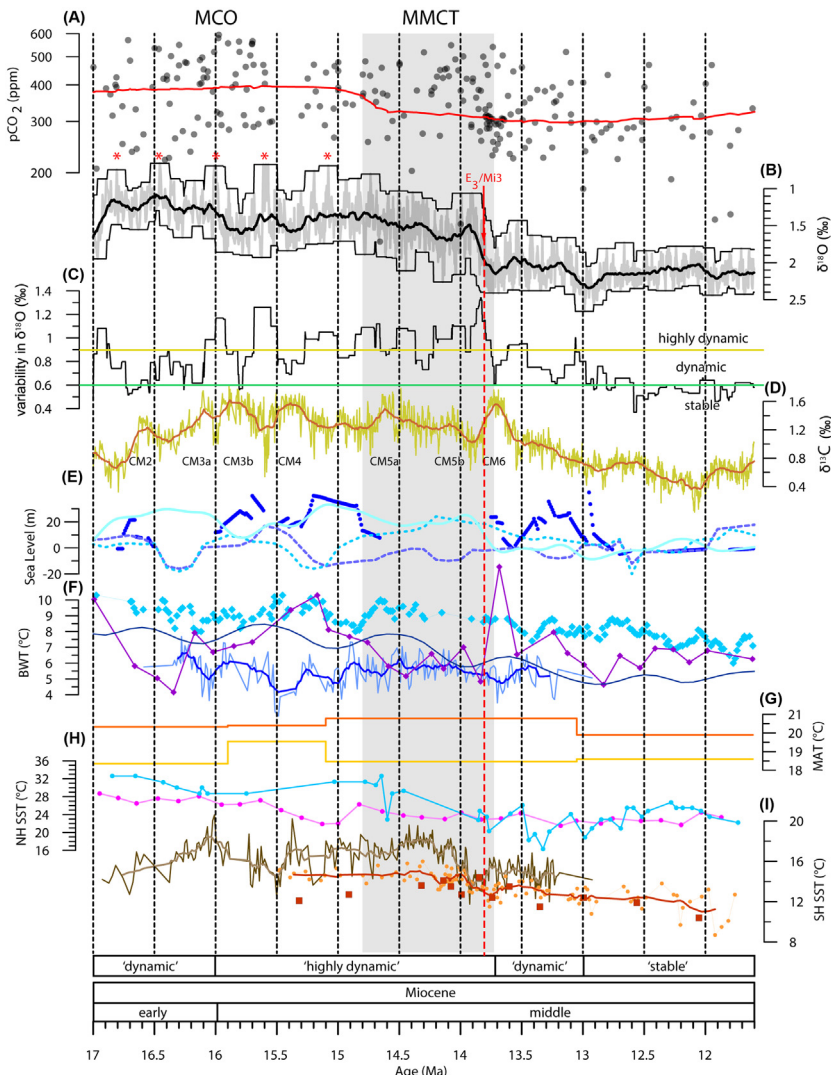


FIGURE 9.3 Environmental data from the late early Miocene through middle Miocene (17 to 11.6 Ma). (A) Atmospheric CO_2 compilation comprises data from a range of proxies outlined in Fig. 9.1. Solid red line displays a two million year moving average. (B) Splice of deep sea benthic foraminifera $\delta^{18}\text{O}$ data (light grey) reflect changes in ice volume and deep/bottom water temperature (De Vleeschouwer et al., 2017). Solid black line displays a 150 kyr moving average. Maximum and minimum values are determined within each 150 kyr window and create the envelope (black lines) that bound the $\delta^{18}\text{O}$ data. Red asterisks indicate intervals of peak warmth and maximum carbonate dissolution in the eastern equatorial Pacific (Holbourn et al., 2015). $E_3/\text{Mi-3}$ is the large stepwise $\delta^{18}\text{O}$ increase (Flower and Kennett, 1993a; Miller et al., 1991b; Woodruff and Savin, 1991) that marks the end of the MMCT. (C) A $\delta^{18}\text{O}$ variability ‘index’, (Continued)

glaciers and ice sheets that drove changes in sea level during the MCO were in Antarctica. However, questions remain regarding the minimum extent of Antarctic ice during this time. Did the AIS completely melt during the MCO or did high elevation and inland areas remain ice covered during the warmest interglacials? Recent studies using far-field records suggest that ice completely disappeared from Antarctica during intervals of peak warmth in the MCO (Miller et al., 2020). However, equilibrium ice sheet simulations (Gasson et al., 2016b; Halberstadt et al., 2021; Paxman et al., 2020) and proxy data (Levy et al., 2016; Shevenell et al., 2008) suggest these ‘total deglaciation’ events were rare or did not occur. Whereas data presented throughout this review shed some light regarding AIS behaviour in the MCO, new ice-proximal sedimentary records are required to determine the sensitivity of the AIS to middle Miocene warmth (McKay et al., 2021).

Termination of the MCO and the onset of cooling and glacial expansion through the Middle Miocene Climate Transition (MMCT) is indicated by an increase in $\delta^{18}\text{O}$ maxima starting at ~ 14.8 Ma, which was followed by a gradual increase of $\sim 0.3\text{\textperthousand}$ in average $\delta^{18}\text{O}$ values during the subsequent

-
- interpreted as a measure of glacial/interglacial variability, is determined by subtracting the maximum values in (B) from the minimum value, for each 150 kyr window. We indicate arbitrary ‘thresholds’ in these data (green and yellow solid lines) and suggest that values below 0.6‰ reflect a relatively ‘stable’ high latitude environment and values that exceed 0.9‰ indicate a highly dynamic environment with large changes in BWT and/or ice volume over glacial–interglacial time scales. (D) Yellow line shows high resolution deep sea benthic foraminifera $\delta^{13}\text{C}$ splice (Westerhold et al., 2020). Solid deep orange line displays a 150 kyr moving average and carbon maxima events (Vincent and Berger, 1985; Woodruff and Savin, 1991) are labelled (CM2–6). (E) Sea level curves are from Kominz et al. (2016) (blue dots), Kominz et al. (2008) (pale blue dashed line), Miller et al. (2005) (blue dashed line), and Miller et al. (2020) (pale blue line). (F) BWT data from ODP Site 761 (east Indian Ocean: 16.738°S, 115.535°E) (Lear et al., 2010) (light blue), ODP Site 806 (western equatorial Pacific Ocean: 0.319°N, 159.361°E) (Lear et al., 2015) (purple), ODP Site 1171 (southwest Tasman Sea: 48.4999°S, 146.1115°E) (Shevenell et al., 2008) (blue), and derived from the compilation of Cramer et al. (2011) using Equation 7a (dark blue). Solid line through data from ODP Site 1171 displays a 9-pt running average. (G) Pollen-based Mean Annual Temperature estimates for New Zealand display ‘envelope’ where upper bound (dark orange) = mean of warmest 20% of samples and lower bound (light orange) = mean of coldest 20% of samples (Prebble et al., 2017). (H) SST data for the Northern Hemisphere from DSDP Site 608 (northwest Atlantic Ocean: 42.8367°N, 23.0875°W) (Super et al., 2018) (light blue) and ODP Site 982 (northwest Atlantic Ocean: 57.516°N, 15.866°W) (Super et al., 2020) (pink). (I) SST data for the Southern Hemisphere from ODP Site 1171 using the Mg/Ca proxy (Shevenell et al., 2004) (dark brown) and the TEX₈₆ proxy (orange) (Leutert et al., 2020) using the calibration of Ho and Laepple (2016). Solid lines through the Mg/Ca and TEX₈₆ data display a 9-pt running average. Red squares display temperature estimates derived from clumped isotopes (Δ_{47}) (Leutert et al., 2020). Grey vertical band highlights the Middle Miocene Climate Transition and vertical red dashed line indicates likely threshold in the climate system, across which high latitudes cooled and sea ice and Antarctic marine-based ice sheets became a more frequent and persistent feature.

~800 kyr (Holbourn et al., 2014) (Fig. 9.3B). By the end of the MMCT (at ~13.8 Ma), global $\delta^{18}\text{O}$ had increased by 1‰ to 1.5‰ (Holbourn et al., 2005, 2014; Kennett, 1977; Shackleton and Kennett, 1975a). A ~100 ppm decrease (400 to 300 ppm) in average CO₂ concentrations occurred at the onset of the MMCT (Fig. 9.3A), although proxy data indicate a high degree of variability continued following the initial drop, with values exceeding 500 ppm at times and dropping below 200 ppm at others (Fig. 9.3A). In contrast to the MCO, BWT variability during the MMCT was low, generally fluctuating by ~1°C on 100 and 400 kyr time scales in the Southern Ocean (Shevenell et al., 2008). BWT generally decreased during the MMCT by ~2°C (Cramer et al., 2011; Modestou et al., 2020; Shevenell et al., 2008). SSTs records suggest mid southern latitudes cooled by 3°C to 4°C between 14.1 and 13.8 Ma (Leutert et al., 2020; Shevenell et al., 2004, 2008).

Sea level records through much of the MMCT are somewhat ambiguous (Fig. 9.3E). Records from the New Jersey margin indicate sea level amplitudes varied by at least 10 m (Kominz et al., 2016), but different data sets produce significantly different maximum and minimum magnitudes (Fig. 9.3E). Furthermore, data from the Marion Plateau indicate sea level rose and fell by ~35 m between 14.7 and 14 Ma (John et al., 2011). Large amplitude (1‰) high frequency variations in the $\delta^{18}\text{O}$ record occur through the interval (Holbourn et al., 2014; Shevenell et al., 2008). Given that BWTs remained relatively stable, these large excursions suggest glacial–interglacial changes in ice volume were significant. A gradual increase in ice-raftered debris (IRD) from 15.6 to 14 Ma in the North Atlantic suggests sea ice presence and/or ice growth and glacial advance to coastlines around the margins of the Greenland Sea (St. John, 2008). While a modelling study suggests northern hemisphere ice sheets may have grown when CO₂ dropped below 280 ppm (DeConto et al., 2008), it is still unclear if significant growth of ice occurred in the northern hemisphere at this time. This implies that the AIS was highly dynamic and advanced and retreated throughout the MMCT. However, an overall shift to more positive $\delta^{18}\text{O}$ values from the MCO to MMCT suggests the AIS grew larger during glacials and retreated less during interglacials between 14.8 and 13.9 Ma (Holbourn et al., 2014; Shevenell et al., 2008).

The gradual increase in average $\delta^{18}\text{O}$ values across the MMCT culminated between 13.9 and 13.8 Ma with a global ~1.2‰ increase, the most striking feature in Neogene oxygen isotope records (Figs 9.1 and 9.3). Prior to 13.8 Ma, $\delta^{18}\text{O}$ values generally fluctuated by 1‰ on glacial–interglacial timescales. However, at ~13.8 Ma it appears that an environmental tipping point was reached (Kennett, 1977). Rather than ‘rebounding’ to prior interglacial values, an additional rapid increase in $\delta^{18}\text{O}$ occurred, driving a ~0.6‰ stepwise increase in average deep sea $\delta^{18}\text{O}$ values. This pronounced increase was first recorded in low resolution records from Deep Sea Drilling Project (DSDP) Sites 289 (0.4987°S, 158.5115°E) and 291 (12.8072°N,

127.8308°E) in the western Pacific Ocean (Shackleton and Kennett, 1975b). Moderate resolution benthic and planktic foraminifera isotopic data from DSDP Site 590 (31.167°S, 163.3585°E) first showed a two-step increase occurred during this interval (Kennett et al., 1986). As the resolution of the deep sea benthic isotope records improved, this interval of maximum $\delta^{18}\text{O}$ values was formally identified as oxygen isotope zone Mi3 (Miller et al., 1991a) and $\delta^{18}\text{O}$ maximum E₃ (Woodruff and Savin, 1991). High-resolution data from DSDP Site 588 (26.1117°S, 161.2267°E) in the north Tasman Sea resolved three distinct increases through Mi3/event E, that were identified as E₁, E₂, and E₃ (Flower and Kennett, 1993a). Most recently, well-dated high-resolution records from the mid to low latitudes (Holbourn et al., 2007, 2014) and astronomically-tuned $\delta^{18}\text{O}$ splices (De Vleeschouwer et al., 2017; Miller et al., 2020; Westerhold et al., 2020) place the final step of the MMCT (Mi3/E₃) between 13.9 and 13.8 Ma.

Approximately 70% of the observed $\sim 1.2\%$ shift between 13.9 and 13.8 Ma is attributed to AIS growth (Shevenell et al., 2004; Wright et al., 1992), which implies ~ 76 to 100 m of sea level fall if the Pleistocene calibration of 0.08%–0.11% per 10 metres of sea level is applied (Adkins et al., 2002; Fairbanks and Matthews, 1978). However, sea level records through this final MMCT step are ambiguous and somewhat contradictory. A major sequence boundary characterises the entire MMCT at the shallow continental shelf sites offshore New Jersey (Kominz et al., 2016). However, it is impossible to identify whether a series of sea level rise and fall events occurred across the MMCT or that a single sea level fall at ~ 13.8 Ma eroded older sediments. A sea level fall of ~ 30 m between 13.9 and 13.7 Ma is inferred from sea level calibrations applied to $\delta^{18}\text{O}$ records (Miller et al., 2020) and a sea level fall of 59 ± 6 m at 13.8 Ma is inferred from stratigraphic sequences on the Marion Plateau (John et al., 2011). The Marion Plateau data suggest global ice volume grew by ~ 26 m sea level equivalent (s.l.e.) more at ~ 13.8 Ma than during previous glacial maxima within the MMCT (e.g., at 14.7 Ma). This ‘additional’ ice likely filled Antarctica’s marine basins and expanded to the edge of Antarctica’s prograding and advancing continental shelves (Colleoni et al., 2018; De Santis et al., 1995, 1999; Levy et al., 2016, 2019; McKay et al., 2019; Pérez et al., 2021a) but may have also formed in the northern hemisphere (DeConto et al., 2008). Whereas there is no definitive evidence for ice sheet growth in the northern hemisphere during the MMCT, a pronounced cooling of 6°C in the north Atlantic Ocean occurred between 14.5 Ma and 13.8 Ma (Super et al., 2018). Furthermore, a major change in foraminifera assemblage (Kender and Kaminski, 2013) suggests that perennial sea ice persisted in the Arctic Ocean since 14 Ma. Clearly, the Earth’s high latitudes cooled at this time.

Understanding the drivers of environmental change recorded by increasing $\delta^{18}\text{O}$ across the MMCT, and the large rapid stepwise increase at its end has been a focus of many studies (Flower and Kennett, 1993a, 1994; Kennett,

1977; Shevenell et al., 2004). Changes in ocean circulation (Shevenell et al., 2004) and the draw down in atmospheric CO₂ concentration (Holbourn et al., 2005, 2013) are often cited as likely catalysts of the MMCT. Warm surface ocean temperatures at ODP Site 1171 (48.4999°S 149.1115°E) suggest that changes in the hydrological cycle and an increase in precipitation over Antarctica beginning at ~15.4 Ma may have contributed to initial ice sheet expansion (Shevenell et al., 2004). Constriction of the Tethys seaway (Hamon et al., 2013; Hsü and Bernoulli, 1978; Woodruff and Savin, 1989), ongoing deepening of the Drake Passage, and enhanced circulation of the Antarctic Circumpolar Current (Dalziel et al., 2013) may have slowly reduced meridional heat and vapour transport to Antarctica (Lewis et al., 2006; Shevenell et al., 2004, 2008). Subsequent Southern Ocean surface cooling and intensified climatic response to changes in Earth's orbital eccentricity increased thermal isolation of Antarctica and drove maximum ice sheet expansion recorded by the E₃ δ¹⁸O isotope event (Holbourn et al., 2005; Shevenell et al., 2004) (Fig. 9.3E). SSTs at high northern latitudes also cooled between 2°C and 6°C (Super et al., 2020). Terrestrial records in central Europe also indicate a ~17°C decline in soil temperature occurred over ~350 kyrs between 14.5 and 14 Ma (Methner et al., 2020).

Astronomical variations in insolation likely also played a role in driving high latitude cooling and ice growth at this time. Records from ODP Site 1171 in the Southern Ocean suggest that climate was paced by long-period eccentricity variations (~400 kyr) between 15.4 and 13.5 Ma (Shevenell et al., 2004). Higher resolution records from IODP Site U1338 (2.5078°N 117.9693°W) in the eastern Pacific indicate that while prominent 400 and 100 kyr eccentricity cycles dominated the warm MCO, a switch to obliquity-paced climate variability occurred at 14.7 Ma, with an increase in response to eccentricity (100 kyr) forcing occurring after 14.1 Ma (Holbourn et al., 2014). The major shift in δ¹⁸O and inferred advance of the AIS coincides with an obliquity node between 14.2 and 13.8 Ma (Holbourn et al., 2005).

The role of carbon cycling across the MMCT remains unclear (Shevenell et al., 2008), in part due to the range of atmospheric CO₂ estimates from the proxy data and the cessation of the Monterey δ¹³C Excursion (Fig. 9.3D). Whereas average CO₂ values remained relatively constant across the E₃ event (Fig. 9.3), high resolution data from the Ras il-Pellegrin section in Malta suggest atmospheric CO₂ concentration dropped and remained below 300 ppm for at least 200 kyrs following the event (Badger et al., 2013b). This drop in atmospheric CO₂ occurred as δ¹³C values increased during the last major excursion of the Monterrey event (CM6) (Woodruff and Savin, 1991) (Fig. 9.3E). Large increases in opal accumulation in the eastern equatorial Pacific at 14 and 13.8 Ma and uplifted marginal marine sedimentary sequences around the Pacific Rim suggest high silica-based productivity contributed to atmospheric CO₂ drawdown (Flower and Kennett, 1993a, 1993b;

Holbourn et al., 2014; Vincent and Berger, 1985). These observations are consistent with hypotheses that an increase in organic carbon burial drove a decrease in atmospheric CO₂ and contributed to global cooling (Vincent and Berger, 1985).

The interval of climatic cooling and ice expansion reflected by the Mi3/E₃ isotope shift was a transient event. Sea surface and bottom water temperatures warmed by 2°C to 3°C between 13.7 and 13.5 Ma (Lear et al., 2010; Modestou et al., 2020; Shevenell et al., 2004, 2008). Notably, the large variations in δ¹³C that characterised the MCO and MMCT ceased by ~13.5 Ma and began a gradual decline of ~0.5‰ in average values through to the end of the middle Miocene (Fig. 9.3E) (Vincent and Berger, 1985). This drop in carbon isotope values and coincident warming suggests that feedbacks associated with ice expansion may have influenced global carbon cycling (Shevenell et al., 2004, 2008) and is supported by modelling experiments (Knorr and Lohmann, 2014). Deep sea δ¹⁸O records indicate the AIS remained variable at this time and δ¹⁸O minima of <1.5‰ (Fig. 9.3B) suggest the AIS retreated to, and possibly inland of, the terrestrial continental margin during interglacial intervals.

Surface temperatures at mid latitudes in the Southern Ocean began to cool again at ~13.5 Ma and gradually declined by 2°C to 3°C through the late middle Miocene (Leutert et al., 2020; Shevenell et al., 2004). Mean annual terrestrial temperatures in New Zealand also cooled by ~1°C (Prebble et al., 2017). However, cooling was not ubiquitous, as indicated by data from the North Atlantic, which show SSTs warmed by approximately 5°C (Super et al., 2018, 2020). An interval during which average deep sea δ¹⁸O values remained relatively low and glacial–interglacial amplitude variability was relatively small (<0.6‰), occurred between 13.5 and 13 Ma. Relatively large ice sheets may have persisted during this interval. However, variability in BWT was also muted (~1°C) during this interval (Cramer et al., 2011) and may account for ~0.22‰ of the 0.6‰ δ¹⁸O shift. It follows that the remaining ~0.38‰ of δ¹⁸O not accounted for by temperature may reflect ice volume changes equivalent to between 47 and 35 metres sea level equivalent if the Pleistocene calibration of 0.08–0.11‰ per 10 metres of sea level is applied (Adkins et al., 2002; Fairbanks and Matthews, 1978). This magnitude of sea level change requires relatively large-scale growth and retreat of ice on Antarctica. However, if ice sheets occupied the northern hemisphere, then these bi-polar ice masses could have each varied by smaller amounts. Data from northern hemisphere IODP Site 302 (87.8666°N, 136.1774°E) hints that glacier ice may have reached the coast around the Arctic at this time (St. John, 2008). Proxy data indicate atmospheric CO₂ concentration dropped below 300 ppm (Badger et al., 2013b) (Fig. 9.3A) and an idealised modelling study suggests ice may have grown in the northern hemisphere under these climatic conditions (DeConto et al., 2008). New

geological data are required to confirm or refute whether significant volumes of ice grew in high northern latitudes following the MMCT.

9.1.2.3 The Late Miocene

The late Miocene was recently dubbed the ‘cool house’ because it comprises the bridge from the middle Miocene ‘warm house’ to the modern ‘icehouse’ (Westerhold et al., 2020). However, global SST reconstructions indicate ocean surface temperatures remained significantly warmer than present even after the final ‘cooling step’ in $\delta^{18}\text{O}$ records at the end of the MMCT (Herbert et al., 2016). Furthermore, whereas bottom water temperatures cooled across the MMCT (Cramer et al., 2011; Lear et al., 2015; Modestou et al., 2020; Shevenell et al., 2008), they were still 6°C to 9°C warmer than present in the Indian Ocean in the late Miocene (Modestou et al., 2020). SSTs at high northern latitudes were also significantly warmer (up to 17°C) relative to modern conditions in the late Miocene and latitudinal temperature gradients remained low (Super et al., 2020).

Sea level reconstructions from the New Jersey margin record an episode of major sea level fall between ~11 and 10.5 Ma (Kominz et al., 2008; Miller et al., 2005) (Fig. 9.4E). This drop is one of the largest Cenozoic low-stand events recorded in classic sequence stratigraphic studies (Haq et al., 1987) but is less obvious in recent reconstructions based on analysis of the $\delta^{18}\text{O}$ record (Miller et al., 2020, 2005). A dramatic shoaling of the carbon compensation depth at ~10.5 Ma marks the start of the late Miocene ‘carbonate crash’ (Diester-Haass et al., 2004; Lyle et al., 1995; Pälike et al., 2012; Peterson et al., 1992; Preiss-Daimler et al., 2021), which has been attributed to changes in the intensity of chemical weathering and riverine input of calcium and carbonate ions to the ocean (Lübbbers et al., 2019) and/or changes in ocean circulation related to the restriction of the central American seaway (Newkirk and Martin, 2009). The Benguela upwelling system off southern Africa is thought to have initiated at ~10 Ma (Diester-Haass et al., 2004; Rommerskirchen et al., 2011; Siesser, 1980). Today this major upwelling system delivers cold and nutrient-rich Antarctic sourced waters to support vast populations of phytoplankton and its inception may reflect change at high southern latitudes in the late Miocene. Pollen records from New Zealand indicate a shift to cooler and wetter climate in the mid southern latitudes occurred at this time (Prebble et al., 2017). An increase in the altitude of the Tibetan Plateau is thought to have occurred between 10 and 8 Ma and may have caused enhanced aridity in the Asian interior and contributed to the onset of the Indian and east Asian monsoons (Raymo and Ruddiman, 1992; Zhisheng et al., 2001). However, questions remain around the timing of uplift in the Neogene, the orographic influence on regional

climate dynamics, and the synchronicity of paleoclimatic indicators in the region (Molnar et al., 2010).

Whereas textural analysis of sand grains from ODP Site 918 (63.0928°N 38.6389°W) suggests glaciers were present on Greenland ~ 11 Ma (Helland and Holmes, 1997), drop stones in glacial marine records from the same site suggest glaciers first reached the coastline of Greenland approximately 7 Ma (Larsen et al., 1994; St John and Krissek, 2002). In addition, analysis of beryllium and aluminium isotopes in sand grains from marine sediments show that the East Greenland Ice Sheet existed over the past 7.5 million years (Bierman et al., 2016). These data and analysis of regional seismic data around the Greenland margin (Pérez et al., 2018) offer compelling evidence for continental-scale ice sheets in both polar regions by the late Miocene. A major shift in marine $\delta^{13}\text{C}$ occurs between 8 and 7 Ma (Diester-Haass et al., 2002; Farrell et al., 1995; Holbourn et al., 2018; Loutit and Kennett, 1979) (Fig. 9.4D) and is coincident with the onset of global cooling and inferred bi-polar glaciation. This shift has been attributed to changes in the Southern Hemisphere due to either reduced ventilation of Southern Component Water (SCW) following expansion of the West Antarctic Ice Sheet (WAIS) (Kennett and Barker, 1990), or decreased input of Northern Component Water (NCW) to the Southern Ocean and/or decreased exchange of CO_2 between the atmosphere and surface water in Antarctic source areas (Hodell and Venz-Curtis, 2006). Expansion of C_4 grasslands at the expense of C_3 vegetation occurred at this time (Osborne and Beerling, 2006; Pagani et al., 1999b; Tipple and Pagani, 2007) and coincides with major changes in large terrestrial fauna to a dominance by browsers (Badgley et al., 2008). Rare but important specimens assigned to *Sahelanthropus tchadensis* suggest the hominin lineage first appeared at 7 Ma (Brunet, 2010; Brunet et al., 2002; Vignaud et al., 2002), although the taxonomy of these fossil taxa is still developing (Haile-Selassie et al., 2004) and their linkages to modern humans are debated (Wood and Harrison, 2011).

Modest cooling of global SSTs that characterised the early-late Miocene accelerated in the Messinian (Herbert et al., 2016). SSTs decreased by 2°C to 3°C in the Southern Ocean and by up to 5°C at high northern latitudes (Herbert et al., 2016) (Fig. 9.4H). This Late Miocene Cooling (LMC) episode coincides with an increase in zonal and meridional temperature gradients in the Pacific at ~ 7 Ma (Zhang et al., 2014), aridification in the subtropical regions (e.g., south-central Andes) (Amidon et al., 2017), and establishment of the Sahara Desert (Schuster et al., 2006). Mid-latitude SSTs reached near modern values at ~ 6 Ma (Fig. 9.4H) (Herbert et al., 2016), coincident with pronounced cooling and an increase in precipitation in New Zealand (Prebble et al., 2017). The Messinian Salinity Crisis (MSC) (6.2 to 5.5 Ma) was perhaps the most dramatic oceanographic event in the latest Miocene (Hsü et al., 1973). Sea level fall and subsequent desiccation of the Mediterranean is recorded by >1000 m of evaporite deposits in the Mediterranean Basin

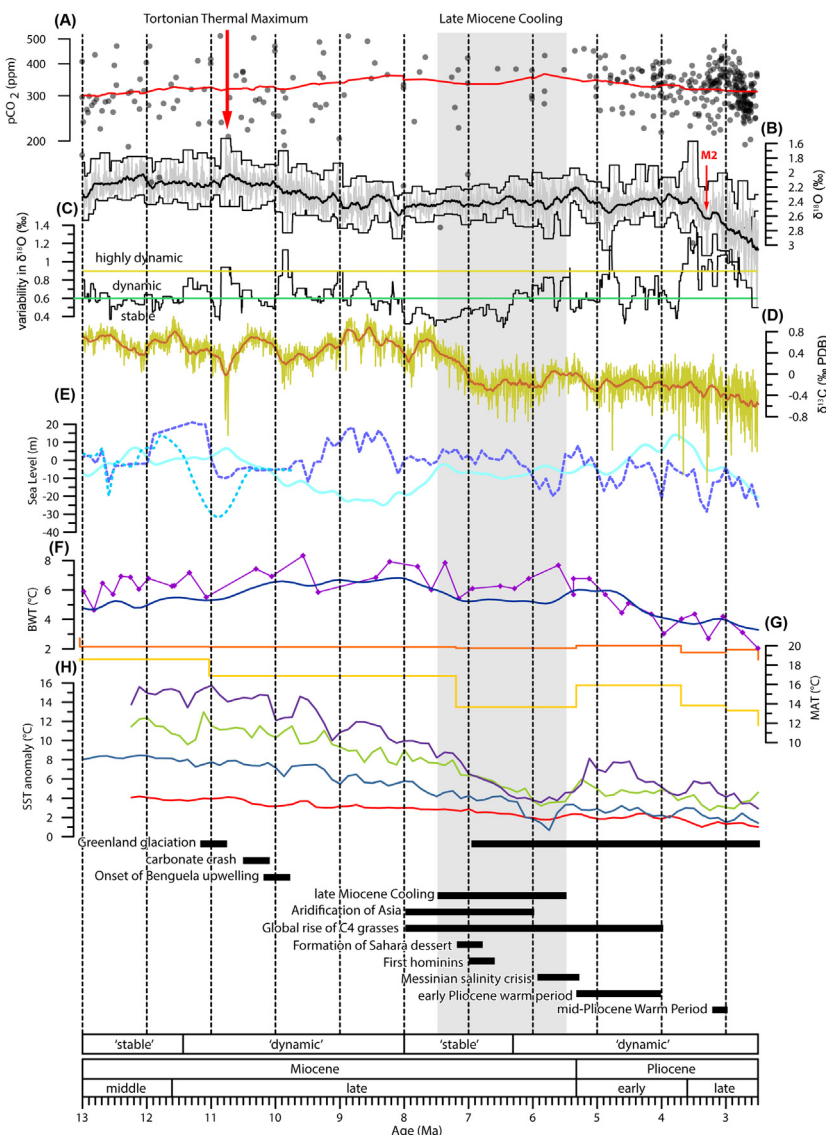


FIGURE 9.4 Environmental data from the late middle Miocene through Pliocene (13 to 2.58 Ma). (A) Atmospheric CO_2 compilation comprises data from a range of proxies outlined in Fig. 9.1. Solid red line displays a two million year moving average. (B) Splice of deep sea benthic foraminifera $\delta^{18}\text{O}$ data (light grey) reflect changes in ice volume and deep/bottom water temperature (De Vleeschouwer et al., 2017). Solid black line displays a 150 kyr moving average. Maximum and minimum values are determined within each 150 kyr window and create the envelope (black lines) that bound the $\delta^{18}\text{O}$ data. (C) A $\delta^{18}\text{O}$ variability ‘index’, interpreted as a measure of glacial/interglacial variability, is determined by subtracting the maximum values in

(Continued)

(Barber, 1981; Hodell et al., 1986). Debate on the causes of the MSC persists, with tectonic restriction between the Mediterranean Sea and the Atlantic Ocean (Garcia-Castellanos and Villaseñor, 2011), and glacial eustatic controls (Zhang and Scott, 1996) or an interplay between the two being the most likely scenario (Ohneiser et al., 2015).

The episode of Late Miocene Cooling culminated in the MSC and terminated with relatively rapid warming of $\sim 3^{\circ}\text{C}$ to 4°C in the mid-latitudes into the early Pliocene (Herbert et al., 2016). This climatic ‘rebound’ at the end of the Miocene is also reflected in Southern Hemisphere mid-latitude records of terrestrial palynomorphs (Prebble et al., 2017), marine molluscs (Beu, 1990) and shallow water foraminifera (Hornbrook, 1992) from New Zealand.

9.1.2.4 The Pliocene

Geological proxies indicate that the warm Early to mid-Pliocene (5.3 to 3.0 Ma) interval is the last time in Earth’s history that atmospheric CO₂ concentrations (ca. 400 ppm) were similar to present day and global mean surface temperatures were 2°C – 3°C warmer than modern (Martinez-Botí et al., 2015; Masson-Delmotte et al., 2013). Other prominent features during this warm interval include a perennially ice-free Arctic Ocean (Ballantyne et al., 2010, 2013; Dowsett et al., 2012), Arctic summer temperatures approximately 8°C – 19°C warmer than modern (Brigham-Grette et al., 2013; Salzmann et al., 2011), reduced meridional and zonal SST gradients (Brierley et al., 2015; Fedorov et al., 2013; Tierney et al., 2019), and enhanced production and export of Northern Component Water (NCW) – the ancient correlative to North Atlantic Deep Water (NADW) (Billups et al., 1997; Frank et al., 2002; Kwiek and Ravelo, 1999; Ravelo and Andreasen, 2000). Vegetation

-
- ◀ (B) from the minimum value, for each 150 kyr window. We indicate arbitrary ‘thresholds’ in these data (green and yellow solid lines) and suggest that values below 0.6‰ reflect a relatively ‘stable’ high latitude environment and values that exceed 0.9‰ indicate a highly dynamic environment with large changes in BWT and/or ice volume over glacial–interglacial time scales. (D) Yellow line shows high resolution deep sea benthic foraminifera $\delta^{13}\text{C}$ splice (Westerhold et al., 2020). Solid deep orange line displays a 150 kyr moving average and carbon maxima events (Vincent and Berger, 1985; Woodruff and Savin, 1991) are labelled (CM2–6). (E) Sea level curves are from Kominz et al. (2008) (pale blue dashed line), Miller et al. (2005) (blue dashed line), and Miller et al. (2020) (pale blue line). (F) BWT data from ODP Site 926 (western Atlantic Ocean: 3.7191°N , 42.9081°W) (Lear et al., 2003, 2020) and derived from the compilation of Cramer et al. (2011) using Equation 7a (dark blue). (G) Pollen-based Mean Annual Temperature estimates for New Zealand display ‘envelope’ where upper bound (dark orange) = mean of warmest 20% of samples and lower bound (light orange) = mean of coldest 20% of samples (Prebble et al., 2017). (H) Stacked SST curves from alkenone based reconstructions for the SST anomalies for the Northern Hemisphere $>50^{\circ}\text{N}$ (purple line) and 30 to 50°N (green line), Tropics (red line), and Southern Hemisphere 30 to 50°S (blue line) (Herbert et al., 2016). Grey vertical band highlights Late Miocene Cooling. Timing and duration of key global events through indicated by horizontal black bars (see text for details).

reconstructions (Salzmann et al., 2008) imply that the global extent of arid deserts decreased and boreal forests replaced tundra. Atmosphere-Ocean Global Circulation Models (AOGCMs) predict an enhanced hydrological cycle, but with large inter-model spread (Haywood et al., 2013, 2020). The East Asian Summer Monsoon, as well as other monsoon systems, may have been enhanced at this time (Wan et al., 2010). Furthermore, high southern latitudes were characterised by episodic retreat and collapse of the marine-based WAIS (Naish et al., 2009; Pollard and DeConto, 2009) and the marine margins of the EAIS (Bertram et al., 2018; Cook et al., 2013; Patterson et al., 2014; Reinardy et al., 2015), with reduced coastal sea ice (relative to modern) in the Ross Sea, Prydz Bay and Antarctic Peninsula regions (Escutia et al., 2009; McKay et al., 2012; Scherer et al., 2016; Whitehead and Bohaty, 2003; Whitehead et al., 2005; Winter et al., 2010a).

SSTs reconstructions and diatom assemblage data from the Ross Sea, imply contraction or breakdown of the Antarctic Polar Front allowed sub-Antarctic diatom flora to migrate across the Antarctic continental shelf (McKay et al., 2012). Mean annual near surface temperatures in the Ross Sea were up to 6°C and inhibited growth of sea ice (McKay et al., 2012). Reduced sea ice extent in the Southern Ocean between ~3.6 to 2.75 Ma has been associated with enhanced air-sea gas exchange with the deep ocean resulting from increased ventilation of water masses in the South Atlantic sector of the Southern Ocean (Hodell and Venz-Curtis, 2006; Waddell et al., 2009; Woodard et al., 2014). In terms of areal extent, the majority of marine-based ice sheet loss would have occurred in the Pacific sectors of the WAIS and EAIS (e.g., Ross Sea and Wilkes Land), with implications for the overturning ocean circulation and marine biogeochemistry (Bertram et al., 2018; Cook et al., 2013; DeConto and Pollard, 2016; McKay et al., 2012; Naish et al., 2009; Pollard et al., 2015; Taylor-Silva and Riesselman, 2018). Pan-Antarctic ice sheet simulations for the warm early to mid-Pliocene yield ice volume loss equivalent to between 8.5 and 16 m of sea-level from these marine-based sectors (de Boer et al., 2015; DeConto and Pollard, 2016; Golledge et al., 2017b; Pollard and DeConto, 2009). The climatic implications of the increase in oceanic area as water occupied regions previously occupied by ice is currently underrepresented in climate and ice sheet modelling studies (Woodard et al., 2014). However, one recent study suggests that changes in ice sheet extent may have affected the rate of the Pacific overturning circulation (Hill et al., 2017).

Pliocene sea-level changes have been reconstructed using a variety of geological techniques including: (1) marine benthic oxygen-isotope ($\delta^{18}\text{O}$) records paired with Mg/Ca paleothermometry (Miller et al., 2012), (2) an algorithm incorporating sill-depth, salinity and the $\delta^{18}\text{O}$ record from the Mediterranean and Red Seas (Rohling et al., 2014), (3) uplifted paleo-shorelines (Miller et al., 2012; Rovere et al., 2014), (4) submerged

speleothems (Dumitru et al., 2019), and (5) backstripped continental margins (Grant et al., 2019; Miller et al., 2012; Naish and Wilson, 2009). An assessment of the suite of far-field estimates (Dutton et al., 2015) suggests a range for highest GMSL during the Pliocene of between 5–40 m above present. PlioSeaNZ (Grant et al., 2019) is a continuous floating sea-level record for the Mid-Pliocene Warm Period (3.3–3 Ma) derived from Whanganui, New Zealand and is independent of the global benthic $\delta^{18}\text{O}$ record. Sea level estimates are based on a theoretical relationship between sediment transport by waves and water depth that is applied to a grain size record from a well-dated, continuous, shallow marine sequence. If all the glacial–inter-glacial variability in the PlioSeaNZ record was above present-day sea level, then GMSL during the warmest mid-Pliocene interglacial was at least +4.1 m and no more than +20.7 m, with a median of +10.7 m and likely (66%) range between 6.2 m (16th percentile) and 16.7 m (84th percentile) (Grant and Naish, 2021).

9.1.3 Southern Ocean Paleogeography and Paleoceanography

The dominant oceanographic feature of the Southern Ocean circulation is the Antarctic Circumpolar Current (ACC) (Carter et al., 2021). The ACC is the largest global ocean current. It flows clockwise around Antarctica with an average transport volume of \sim 130–160 Sv and is strongly constrained by seafloor topography (Barker and Thomas, 2004; Olbers et al., 2004; Orsi et al., 1995; Rintoul, 1991; Rintoul et al., 2001). Most of the circumpolar flow takes place along the Polar Front (PF) and Subantarctic Front (SAF), which extend from the surface to the seafloor (Sokolov and Rintoul, 2007). The deep layers of the ACC comprise relatively warm Circumpolar Deep Water (CDW), which reaches the surface along steeply rising isopycnal (line of equal density) surfaces to the south of the PF. Northward advection of nutrient-rich upwelled waters feed subduction of Antarctic Intermediate Water, and southward advection feeds the subduction of Antarctic Bottom Waters. Due to the absence of land barriers, the Southern Ocean circulation connects the three main ocean basins, making it a critical feature of the modern global overturning circulation, which distributes heat, carbon, and nutrients around the globe, compensating the sinking of deep waters in the North Atlantic Ocean (Marshall and Speer, 2012; Rintoul, 2018). Today, incursions of warm CDW onto the Antarctic continental shelves have been shown to cause melting and thinning of Antarctic ice shelves through basal melting (Paolo et al., 2015; Pritchard et al., 2012; Rintoul et al., 2016; Thoma et al., 2008).

The transport and storage of heat, carbon dioxide, and fresh water, by the ACC have a significant influence on global and regional climate (Rintoul and da Silva, 2019). Opening of a path for flow between Australia and Antarctica and South America and Antarctica was required to allow

circum-Antarctic flow of the ACC. Initial formation and subsequent variability in the strength of the ACC may have played a key role in modulating climate at high southern latitudes, with implications for ice sheet dynamics (Kennett, 1977; Lyle et al., 2007; Sijp and England, 2004). However, development of the ACC may have played a secondary role to changes in greenhouse gas concentrations in driving initial growth of the AIS (DeConto and Pollard, 2003; Huber and Nof, 2006).

The time of opening and deepening of the Tasman Strait to deep water flow is widely accepted at ~ 37 Ma (Exon et al., 2001, 2004; Lawver and Gahagan, 2003; Stickley et al., 2004). In addition, neodymium isotopes from records on opposite sides of Tasmania suggest that an eastward flowing deep-water current has been present since 30 Ma (Scher et al., 2015). Analysis of grain size at ODP and DSDP sites across the Tasmanian Gateway, as well as hiatuses, indicate water current speed increased and water masses became more homogeneous at 23.95 Ma and suggest the ACC was well established at this time (Barron and Keller, 1982; Pfuhl and McCave, 2005). Furthermore, a late Oligocene-early Miocene (~ 25 – 23 Ma) onset of the ACC is also inferred from evidence for current activity in the South Pacific along the path of the ACC (Lyle et al., 2007). Numerical modelling studies also show that, while an open circum-Antarctic gateway existed since the late Eocene, throughflow of the ACC was still limited during the Oligocene (Hill et al., 2013) because Australia and South America were substantially closer to Antarctica than today (Markwick, 2007). Recent analysis of sediment cores from conjugate margins of the modern Southern Ocean between Australia and Antarctica (Bijl et al., 2018b; Evangelinos et al., 2020; Hartman et al., 2018; Salabarnada et al., 2018; Sangiorgi et al., 2018) suggest a strong, ‘near-modern’ ACC did not form until the late Miocene (~ 11 Ma).

Onset of a ‘modern and strong’ ACC is likely linked to the establishment of deep-water circulation through the Drake Passage and Scotia Sea. However, the timing of opening, widening, and deepening of this key ocean gateway is still widely debated (Barker et al., 2007; Eagles and Jokat, 2014; Hodel et al., 2021; Maldonado et al., 2014; van de Lagemaat et al., 2021). Tectonic reconstructions based on age constraints from oceanic spreading magnetic anomalies and heat flow suggest continental blocks began to separate in the middle Eocene ~ 45 to 41 Ma (Eagles and Jokat, 2014; Livermore et al., 2007). Paleoceanographic reconstructions, based on neodymium isotopic ratios, propose shallow flows across the Drake Passage started in the late Eocene (Scher and Martin, 2006). However, stronger through flow of a proto-ACC may not have been possible until the late Oligocene to early Miocene (Hill et al., 2013; Hodel et al., 2021; Martos et al., 2013). Tectonic studies suggest that broad (100–300 km wide) and deep (>2.5 km) to intermediate depth (2.5 to 1 km) oceanic pathways were well developed in the Scotia Sea by 20 Ma (Barker et al.,

2007; Eagles and Jokat, 2014) allowing circulation of deep water that may have enhanced formation of year-round sea-ice and increased cooling of surface air temperature (Sijp and England, 2004). Sparse contourite deposits in the Scotia Sea suggest through flow of the CDW began in the early/middle Miocene (Maldonado et al., 2003; Pérez et al., 2019) but strong and widespread deep water currents associated with Southern Component Water production first occurred in the region during the middle to late Miocene (13.8 to 8.4 Ma) (Maldonado et al., 2003; Pérez et al., 2021b). Unobstructed deep through flow of the ACC that characterises the region today may not have occurred until the late middle to late Miocene (Carter et al., 2014; Dalziel et al., 2013; Pérez et al., 2019, 2021b). Clearly more information is required to improve our knowledge regarding the evolution of Southern Ocean circulation and dynamics and its influence on climate and the cryosphere.

9.1.4 Land elevation change and influences on Antarctic Ice Sheet evolution

Tectonic changes have played a significant role in the evolution of water mass circulation in the Southern Ocean and around the Antarctic margin (Carter et al., 2021). But tectonic uplift and subsidence across the Antarctic continental shelves and interior regions has also influenced the growth and extent of the AIS through the Cenozoic (Halberstadt et al., 2021; Hochmuth et al., 2020; Kerr et al., 1999, 2000; Paxman et al., 2020; Sorlien et al., 2012; Wilson et al., 2009, 2012a, 2013). Furthermore, physical processes, including erosion, transport, and deposition of sediment, modify the landscape and can form over deepened basins that inhibit ice sheet growth or create sedimentary platforms across which ice can expand (Pollard and DeConto, 2007, 2020). The interaction between climate, tectonics, ice sheets, and sedimentary processes has been a focus of the Scientific Committee on Antarctic Research (SCAR) ANTscape (Barrett et al., 2009) coordinated initiative within the ACE program, that developed in the Circum-Antarctic Stratigraphy and Paleobathymetry subcommittee activity within the PAIS program for the past two decades. Key results from these efforts include time slice reconstructions for the Eocene-Oligocene (~34 Ma), Oligocene-Miocene (~23 Ma), Middle Miocene (~14 Ma), and Pliocene (~3.5 Ma) (Hochmuth et al., 2020; Paxman et al., 2019b) (Fig. 9.1).

These reconstructions highlight the significant topographic changes that occurred across West Antarctica as it evolved from a subaerial landmass in the late Eocene (Wilson et al., 2009) to a region characterised by deep subglacial basins today (Drewry and Jordan, 1983; Fretwell et al., 2013; Morlighem et al., 2020). Formation of this submarine topography occurred throughout the Miocene and Pliocene as rifting and thermal subsidence caused the region to deepen (Fielding et al., 2005, 2007; Henrys et al., 2007; Kulhanek et al.,

2019; McKay et al., 2021; Sorlien et al., 2012) and glacial erosion scoured deep basins across the continental shelves (Bart and De Santis, 2012; Bart and Owolana, 2012; Levy et al., 2019; McKay et al., 2019). Similar processes likely deepened interior basins in East Antarctica including the Wilkes, Aurora, Pensacola-Pole and Recovery subglacial basins, which occupy large regions of the continental interior (Drewry and Jordan, 1983; Fretwell et al., 2013; Morlighem et al., 2020; Paxman et al., 2019a, 2019b). Today, these areas contain ice that is grounded well below sea level and is vulnerable to warming ocean temperatures with the potential to raise sea level by ~19 m if it were to melt (Fretwell et al., 2013).

9.2 Records of Miocene to Pliocene climate and ice sheet variability from the Antarctic margin

9.2.1 Introduction to stratigraphic records

Because deep-sea $\delta^{18}\text{O}$ records provide insight into both bottom water temperature and ice volume change (Emiliani, 1955, 1966; Shackleton, 1967; Shackleton and Kennett, 1975b), ice-proximal records of climate change and ice volume fluctuations from Antarctica's continental margins are required to augment the continuous but distal data from the deep sea. Geological records of past environmental change from the Antarctic continental margin are relatively rare, as much of the sedimentary stratigraphic archive is covered by ocean and ice (Escutia et al., 2019). However, geophysical surveys and geological mapping in Antarctica have uncovered stratigraphic sequences preserved on, and along the margins of, Antarctica's continental shelves and at the mouths of outlet glaciers around the continent (McKay et al., 2021). Over the past 50 years, the Deep Sea Drilling Project (DSDP), Ocean Drilling Program (ODP), and Integrated Ocean Drilling Program (IODP) and International Ocean Discovery Program (IODP) have undertaken seventeen legs and expeditions in sub-Antarctic and Antarctic waters to recover rock and sediment cores from the ocean basins and continental shelves around the continent (Escutia et al., 2019; Gohl et al., 2019; Lamy et al., 2019; McKay et al., 2019; Weber et al., 2019). In addition to drilling in the deep ocean basins and on the outer continental shelf, records from locations proximal to the modern Antarctic coast in the Ross Sea have also been recovered by international drilling efforts including the Dry Valley Drilling Project (DVDP) (McGinnis, 1981), Cenozoic Investigations in the Western Ross Sea (CIROS) Project (Barrett, 1989), Cape Roberts Project (CRP) (Barrett, 2007, 2009), and Antarctic Drilling (ANDRILL) Program (Harwood et al., 2008, 2009; Naish et al., 2007). Here we take a regional approach and summarise the available geological data from Neogene outcrop and drill cores from the Ross Sea region and offshore George V Land (Wilkes subglacial

basin) (Fig. 9.5). We acknowledge that significant information from the Neogene is also available from onshore and offshore Prydz Bay (Barron et al., 1991; Cooper et al., 2004) and the Antarctic Peninsula (Barker et al., 2002) and that the majority of new information from recent drilling expeditions is forthcoming (Gohl et al., 2019; Lamy et al., 2019; McKay et al., 2019; Weber et al., 2019).

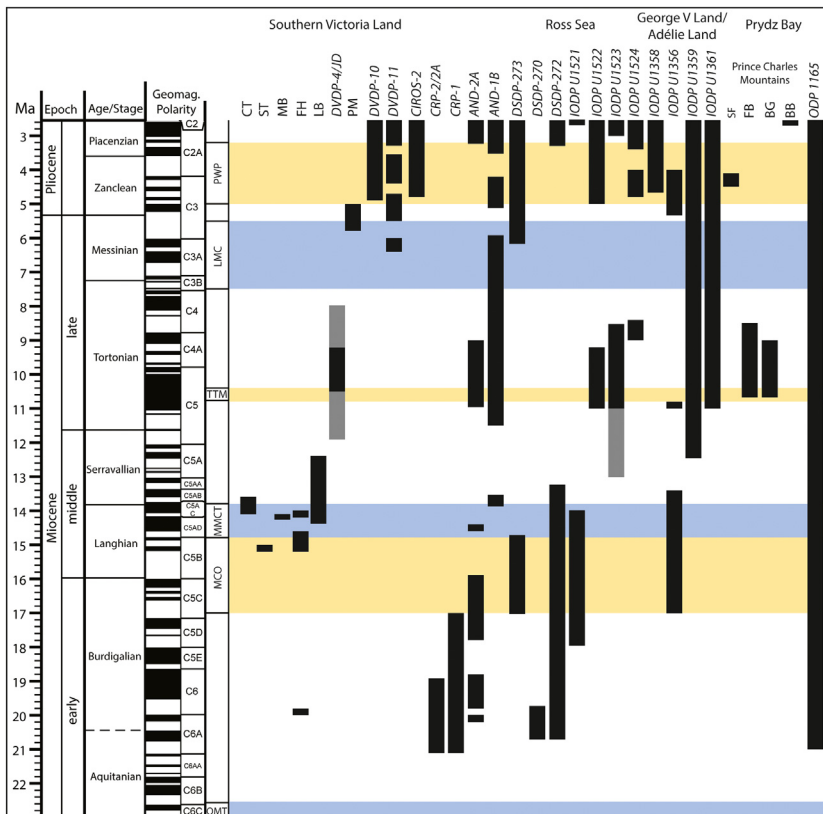


FIGURE 9.5 Stratigraphic summary of key sites and records discussed in the text. Black bars indicate approximate interval of geologic time preserved in each record. Grey bars indicate intervals for which ages are less well constrained. Italics = drill core records, regular type face = outcrop. *CT*, Cirque till; *ST*, Sessrumminir till; *MB*, Mount Boreas; *FH*, Friis Hills; *LB*, Labyrinth; *DVDP*, Dry Valleys Drilling Project; *JD*, Jason diamicton; *PM*, Prospect Mesa Gravels; *CIROS*, Cenozoic Investigations in the Ross Sea; *CRP*, Cape Roberts Project; *AND*, ANDRILL; *DSDP*, Deep Sea Drilling Project; *SF*, Sørsvåg Formation; *FB*, Fischer Bench Formation; *BG*, Battye Glacier Formation; *BB*, Bardin Bluffs Formation. Significant climate intervals and transitions include the *OMT*, Oligocene/Miocene Transition; *MCO*, Miocene Climatic Optimum; *MMCT*, Middle Miocene Climate Transition; *TTM*, Tortonian Thermal Maximum; *LMC*, Late Miocene Cooling; *PWP*, Pliocene Warm Period.

9.2.2 George V Land to Wilkes Land Margin

9.2.2.1 Geological setting

The segment of the East Antarctic continental margin between the north-western Ross Sea (164°E) and Prydz Bay (90°E) is characterised by two major subglacial basins, the Wilkes subglacial basin (WSB) and Aurora subglacial basin (ASB) (Fig. 9.1), two areas where the EAIS is largely grounded below sea level (Fretwell et al., 2013; Morlighem et al., 2020). The WSB is the biggest of the EAIS and its marine-based portion alone contains an ice volume of 3–4 m sea level equivalent (Golledge et al., 2017a; Mengel and Levermann, 2014; Pollard et al., 2015). The WSB is 1400 km long and 200 to 600 km wide and is located east of the Mertz Shear Zone and west of the Transantarctic Mountains, inland of the George V Coast (Fig. 9.2) (Drewry, 1983; Drewry and Jordan, 1983; Ferraccioli et al., 2009; Fretwell et al., 2013; Mengel and Levermann, 2014; Morlighem et al., 2020). Below a thick ice cover, the northern WSB presents plateau-like surfaces, which are laterally continuous over tens to hundreds of kilometres (Paxman et al., 2019a). The flat surfaces are separated by a complex network of sub-basins up to 80 km wide, wherein the ice sheet bed lies up to 2.1 km below sea level (Ferraccioli et al., 2009). The elevations of the flat plateau-like surfaces are broadly uniform across the basin, with a modal elevation of 560 m below sea level. Subglacial topography exerts a fundamental influence on the dynamics of the AIS (Austermann et al., 2015; Colleoni et al., 2018; Gasson et al., 2015; Golledge et al., 2017a; Paxman et al., 2020; Wilson et al., 2013). Glaciers draining through the WSB, including the Cook, Ninnis and Mertz, have inland-sloping bedrock topography (Fretwell et al., 2013; Morlighem et al., 2020), which makes them more vulnerable to rapid ice sheet retreat in response to ocean and climate warming (DeConto and Pollard, 2016; Golledge et al., 2015, 2017a, 2017b; Mengel and Levermann, 2014; Pollard et al., 2015). Therefore, it is necessary to reconstruct past bedrock topography for particular time slices in order to accurately simulate AIS dynamics during those times in the past (Paxman et al., 2019b, 2020).

In front of the WSB, the continental shelf has an average width of 125 km and an average water depth of 450–500 m. The shelf exhibits an overdeepened and landward-sloping bathymetric profile that is caused by glacial erosion and sediment loading (Ten Brink and Cooper, 1992; Vanney and Johnson, 1979a, 1979b). The inner and outer shelf topography is irregular, with troughs that contain inner shelf deep basins ($>1000\text{ m}$) that shoal towards the shelf break and are bound by shallow flat shelf banks (the Adélie and Mertz Banks). The continental shelf troughs were eroded by ice streams during times of glacial advances while the banks illustrate where grounded ice was slow moving (Beaman et al., 2010; De Santis et al., 2003; Eittreim et al., 1995; Escutia et al., 2005). The continental slope, which

extends from the shelf break to about 2000–2500 m water depth, is steep, narrow and incised by submarine canyons (Escutia et al., 2000; Porter-Smith et al., 2003). Deposition dominates the eastern flank of the channel, with the asymmetry between the levees, the result of the Coriolis effect (Donda et al., 2003; Escutia et al., 2000). Seaward of the slope, the continental rise is also relatively steep and rugged because of (1) the presence of a complex network of tributary-like channels that continue from the slope canyons, (2) the very high-relief levee systems associated to the channels, and (3) a system of sediment ridges (Escutia et al., 2000; Escutia et al., 2002).

The ASB extends up to 1000 km inland from the Antarctic coast from 106°E to 122°E, and it is composed of smaller subglacial basins, including the Vincennes and Sabrina subglacial basins (Aitken et al., 2016; Drewry, 1976; Roberts et al., 2011). The Sabrina basin, closest to the coast, is separated by a discontinuous ridge from the inland Aurora basin on the west side and Vestfold basin inland on the east. The main ice drainage is through the Totten Glacier, with Vanderford Glacier to the west and Sabrina Coast glaciers (including the Moscow University Glacier) to the east. Several overdeepened basins (Aitken et al., 2016; Young et al., 2011) and an active subglacial hydrology (Wright et al., 2021) characterise the catchment and ultimately imply it may be susceptible to coupled atmospheric and oceanic forcings with a potential ice volume contribution of ~4 m of sea level rise equivalent (SLE) (Aitken et al., 2016).

In front of the ASB, the continental shelf width increases from 130 km at the eastern end of the Moscow University ice shelf terminus to 180 km at the Totten Glacier terminus (Fernandez et al., 2018), but narrows to 40 km in the Budd Coast. The continental shelf exhibits an irregular overdeepened morphology with a cross-shelf trough offshore the Moscow University with depths ranging from over 1000 m water depth close to the coast to 450–550 m at the shelf edge (Fernandez et al., 2018; O'Brien et al., 2020). The continental slope is relatively gently dipping (~2°) and is incised by northeast-southwest trending canyons that are separated by topographic ridges (O'Brien et al., 2020). Two distinct areas are defined by their geomorphology. To the east of the Totten Glacier Canyons, sediment ridges between canyons are fed by fine sediments from turbidity currents and hemipelagic deposition being entrained by westward flowing currents. To the west, the ridges form by accretion of suspended sediment moving along the slope as a broad plume.

9.2.2.2 Oceanography of the Adélie coast

Today, the suite of sites drilled in the Georges V Land and the eastern Wilkes Land margin by the DSDP Leg 28 and IODP Expedition 318 lie south of the Antarctic PF, between the Southern Boundary of the ACC, near the Antarctic Divergence at ~63°S (i.e., IODP Site U1356) and north of the

Southern Antarctic Counter Current Front (i.e., DSDP Site 269) ([Bindoff et al., 2000; Orsi et al., 1995](#)).

The Adélie Coast continental shelf is one of the locations where the Antarctic Bottom Waters (AABW), the densest water masses of the world ocean fuelling the global ocean circulation, are produced by brine rejection during sea ice formation and the heat loss to the atmosphere ([Gordon and Tchernia, 1978; Orsi et al., 1999](#)). The Adélie Land Bottom Water (ALBW) fills the bottom of the Australian sector of the Southern Ocean ([Aoki et al., 2005](#)) and contributes ~25% of the AABW volume ([Campagne et al., 2015](#)). ALBW is produced when warm modified Circumpolar Deep Water (mCDW) flow southward across the shelf break into the Adélie Depression. Brine rejection in the Mertz Glacier Polynya system produces High-Salinity Shelf Water (HSSW), which circulates across the depression and melts the base of the Mertz Glacier Tongue to produce Ice Shelf Water (ISW). ISW ascends and supplies freshwater to the upper shelf waters. Mixing of the ISW and HSSW with other shelf waters produces Dense Shelf Water (DSW) that is exported through the Adélie sill ([Williams and Bindoff, 2003; Williams et al., 2008, 2010](#)). As these waters flow north of the continental shelf, they descend as dense cold water plumes and gravity currents into the complex channel-levee system along the Wilkes Land margin ([Caburlotto et al., 2010; Williams et al., 2010](#)). This water is funnelled through the canyons and produces ALBW, some of which is incorporated into the Antarctic Slope Current where it mixes with Ross Sea Bottom Water ([Williams et al., 2008](#)). A large polynya occurs to the west of the Mertz Glacier and is an area of high biological productivity.

9.2.2.3 Seismic stratigraphy off the George V Land to Wilkes Land Margin

The Georges V Land and Adélie Coast margins ([Fig. 9.2](#)) have been a target for unravelling the Cenozoic glacial history of Antarctica through acquisition of seismic stratigraphic and sedimentological data over many decades of national and international expeditions. A review of the main regional unconformities, seismic units, and their seismic attributes is provided by ([Cooper et al., 2008; Escutia et al., 2005](#)). Sediments recovered along this margin during IODP Expedition 318 ([Escutia et al., 2011a](#)) have provided unique chronostratigraphic control for the previously defined seismic units ([Fig. 9.6](#)), which is summarised in the chapter by [McKay et al. \(2021\)](#).

Recent studies collate available seismic reflection profiles along the Adélie Coast and Wilkes Land margin (west of 145°E) and across to the conjugate Australian margin ([Sauermilch et al., 2019](#)). These authors provide for the first time a consistent seismic stratigraphic framework across the

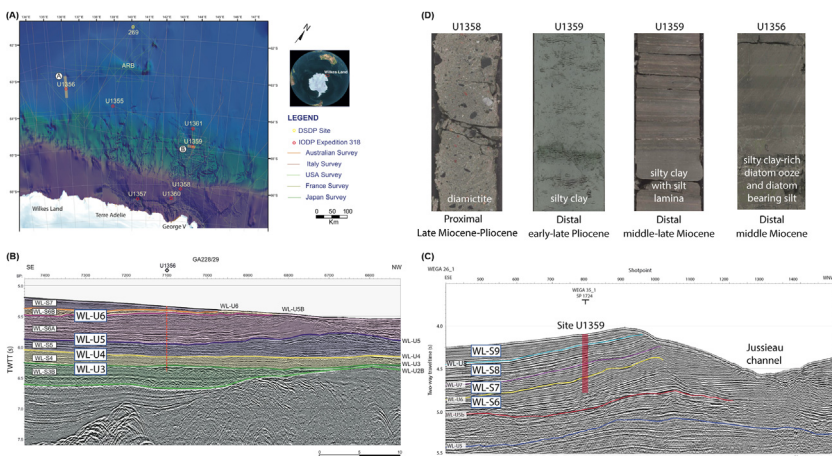


FIGURE 9.6 (A) Location of sites drilled off the George V and Adélie Land continental margin during IODP Expedition 318. Sites U1358, U1359, U1361 and U1356 recovered sediments of Miocene and Pliocene age (Escutia et al., 2011a). (B and C) Seismic reflection profiles across sites U1356 and U1359, respectively, and include seismic units (WL-S) and bounding unconformities (WL-U). WL-S9: Pliocene-Pleistocene; WL-S8: late Miocene-early Pliocene; WL-S7: middle-late Miocene; WL-S6: early-middle Miocene (Escutia et al., 2011a, 2011b). (D) Examples of Miocene and Pliocene facies that characterise the range of depositional environments recovered by drilling at each site.

Australian-Antarctic basin, revising the horizons and seismic units defined by different authors ranging from the Cretaceous to the Miocene.

9.2.2.4 Drill core records from the George V Land to Wilkes Land Margin

The first drilling offshore the Wilkes Land margin and Adélie Coast that recovered Pliocene and older sediments took place in 1973 during DSDP Leg 28 at Sites 268 and 269 on the continental rise and abyssal plain, respectively (Hayes et al., 1975a) (Figs 9.2 and 9.5).

DSDP Site 268 (63.949°S, 105.155°E) was drilled at a water depth of ~3500 m and reached a sub-bottom depth of 474.5 m with an average core recovery of 35%. Recovered clays, silty clays and nannofossil oozes with varying amount of Ice Rafted Debris (IRD) were dated Oligocene to Quaternary. Oligocene to Miocene sediments were interpreted to be dominated by contourites (Piper and Brisco, 1975), deposited when the ice sheet first advanced onto the shelf (Hayes et al., 1975c). However, water at the time was warm enough to support calcareous biogenic sedimentation, but ice rafting and contourite deposits provide evidence for nearby ice on East Antarctica and existing bottom water currents. Pliocene and Quaternary

deposition was dominated by turbidites, which was interpreted to result from progradation of the margin ([Piper and Brisco, 1975](#)).

DSDP Site 269 (61.6761°S, 140.0701°E) drilled two holes 269 and 269A at water depth of ~4300 m, near the southeastern edge of the South Indian abyssal plain ([Hayes et al., 1975a](#)). Drilling penetrated 958 m below seafloor (mbsf) and recovered an average 42% of the cored sediments. The recovered section was assigned a tentative age of late Eocene-early Oligocene based on several reworked specimens of dinoflagellates, to Quaternary ([Hayes et al., 1975a](#)). The base of the drilled section has been assigned a late Oligocene age (24.2 Ma) based on magnetostratigraphy constrained by dinocyst and calcareous nannofossil biostratigraphy ([Evangelinos et al., 2020](#)). These authors show late Oligocene-earliest Miocene sedimentation to be dominated by persistent reworking by the ACC of sediments sourced by gravity flows and hemipelagic settling, recording fluctuating current intensities driven by the migration of the frontal system in response to climatic changes.

In 2010 IODP Expedition 318 drilled seven sites offshore the Adélie Coast ([Fig. 9.6A](#)). Four of the Sites U1356, U1358, U1359, and U1361 recovered sediments from the Miocene and Pliocene ([Escutia et al., 2011a](#)) ([Fig. 9.5](#)).

IODP Site U1356 (63.3102°S, 135.999°E) was drilled at a water depth of 3997 m, ~350 km offshore the Adélie Coast, just south of the Antarctic Divergence, an upwelling area south of the Antarctic PF, where mean annual ocean temperatures are ~0°C. The site was drilled to a depth of 1006.4 mbsf with an average recovery of 35% of the cored section ([Escutia et al., 2011](#)). Miocene sediments were recovered in Hole 1356A between 97 and 431.5 mbsf (Cores 11R to 46R, lithological Units I, II and III, recovery ~29%) ([Escutia et al., 2011a; Tauxe et al., 2012](#)). Sediments from 97 to 400 mbsf span the interval from ~10.8 to 17 Ma, with a hiatus from ~11 to 13.4 Ma ([Sangiorgi et al., 2018; Tauxe et al., 2012](#)) ([Fig. 9.5](#)). Sediments at 431.5 mbsf were dated earliest Miocene ([Tauxe et al., 2012](#)). The record from Site U1356A thus includes the MCO and the MMCT. Miocene sediments mostly consist of clay-rich diatom ooze, diatom-rich and diatom-bearing silty clays, with different degrees of lamination and bioturbation ([Escutia et al., 2011a; Salabarnada et al., 2018; Sangiorgi et al., 2018](#)).

IODP Site U1359 (64.904°S, 143.9603°E) drilled four holes at a water depth 3014 m ([Escutia et al., 2011a](#)). The site is located on the eastern levee of the Jussieu submarine channel: one of the many channel systems along the margin that act as conduits for dense water masses and sediment transport from the continental shelf to the deep ocean ([Escutia et al., 2000](#)). This site was positioned in an upper fan environment where the levee relief is ~400 m ([Escutia et al., 2000, 2011a](#)). Pliocene sediments were recovered from Holes U1359A-C (lithologic Units IIa and IIb) and middle to upper Miocene sediments from ~6 to 12.5 Ma from Hole U1359D (Cores 4R to

46R, lithologic Units IIb, IIc and III) ([Escutia et al., 2011a; Tauxe et al., 2012](#)) ([Fig. 9.5](#)).

Based on shipboard visual core descriptions ([Escutia et al., 2011a](#)), middle to late Miocene sediments mostly consist of laminated clays and silty clays with a higher clast abundance in the late Miocene sediments (Unit IIc), and an upper Miocene nannofossil-bearing mudstone. Although delivery of sediment to the continental rise may have been derived from turbidity currents, the laminated clays in this interval are characterised by persistent sub-mm to mm silt laminae with sharp top and bottom contacts, consistent with redeposition by contour currents in a poorly ventilated benthic environment. However, upper Miocene to upper Pliocene sediments are bioturbated diatom-bearing to diatom-rich silty clays interbedded with massive and laminated silty clays. In this interval, the laminated silty clays are characterised by graded silt laminae fining upwards into massive silty clays, consistent with deposition by low-density overbank turbidity currents in a levee environment ([Escutia et al., 2011a](#)). The diatom content in the sediments is suggestive of increased surface water productivity or reduction in terrigenous input. As the continental shelf margin continued to prograde and the channels became more proximal to the sediment source during the late Miocene and Pliocene, low-density muddy turbidity currents resulted in the deposition of well-defined packages of silt laminations on the levee. In general, the depositional environment at Site U1359 during the Miocene was characterised by open, well ventilated waters during interglacial periods, and enhanced sediment delivery and reduced ventilation during glacials.

IODP Site U1361 (64.4095°S, 143.8867°E) drilled two holes on the lower continental rise ([Escutia et al., 2011a](#)), ~280 km north of the Adélie Coast and ~200 km south of the southern boundary of the ACC. Hole U1361A penetrated to 386 mbsf with a recovery of 87%. It was drilled in the east (right) levee bank of the Jussieu submarine channel. Site U1361 recovered more than 200 m of upper middle to upper Miocene (12.5 to 5.33 Ma) sediments (Lithologic Unit IIb. and lower Unit IIa; Cores 14H to 41X, ~134–386 mbsf) ([Escutia et al., 2011a; Tauxe et al., 2012](#)) ([Fig. 9.5](#)).

This site was cored on the same levee system as Site U1359. The facies associations are essentially the same and are characterised by alternating beds of bioturbated diatom-rich mudstones and laminated silty clays (with a shift in laminae style between the Late Miocene and Pliocene). However, for the late Miocene, post-cruise analysis of Cores 33X and 37X (~302–350 mbsf) focused on an interval with anomalous bioturbated mudstones beds deposited between 11.7 to 10.8 Ma, whereby diatom content was either replaced or diluted by calcareous nannofossils. This nannofossil ooze was initially (and tentatively) interpreted to have formed in response to an increase in surface freshwater as the EAIS melted at this time. An increase in freshwater run off

may have enhanced surface water stratification and nutrient delivery via turbid meltwater plumes ([Escutia et al., 2011a](#)).

Site U1361 also recovered a substantial Pliocene section from 34.9 to 134 mbsf (Unit IIa). Pliocene sediments are characterised by repetitive interbedded laminated olive-grey silty clays and bioturbated greenish grey diatom-rich silty clay, but with persistent ice rafted debris throughout. As with Site U1359, it is interpreted as being deposited by low-density overbank turbidity currents in a levee environment, superimposed by ice rafting processes, and with enhanced pelagic sedimentation (or reduced turbidite input) and bottom current reworking during interglacials ([Patterson et al., 2014](#)). Sediments contain high abundances of reworked sporomorphs suggesting continuous strong erosion in the hinterland ([Escutia et al., 2011a](#)).

9.2.2.5 Neogene history of the George V Land to Wilkes Land margin

Multiproxy palynological, geochemical and sedimentological analyses of IODP Expedition 318 sediments ([Bijl et al., 2018a; Hartman et al., 2018; Sangiorgi et al., 2018](#)) indicate warm-temperate ice-free ocean conditions characterised the Adelie Coast during much of the MCO. TEX₈₆-based paleothermometry indicates upper ocean temperatures ranged between 11.2 and 16.6°C ± 2.8°C ([Sangiorgi et al., 2018](#)). These warm upper ocean conditions favoured ice melt and sustained ice-free conditions at the continental margin ([Halberstadt et al., 2021; Levy et al., 2019; Sangiorgi et al., 2018](#)) where temperate vegetation grew in-situ under mild atmospheric temperatures ([Passchier et al., 2013b; Strother et al., 2017](#)). Temperature gradients between southern high and mid latitudes (South Tasmanian Sea) were significantly weaker than today ([Sangiorgi et al., 2018](#)), whereas the gradient between the Adélie Coast and Ross Sea was significantly higher than today ([Levy et al., 2016; Sangiorgi et al., 2018](#)). Mean Annual Precipitation (MAP) reconstructions based on the Chemical Index of Alteration of sediments indicate elevated values (500–800 mm/year) compared to the present-day (150–400 mm/year) ([Passchier et al., 2013b](#)). Sediments deposited during the MCO contain no sea-ice indicators ([Bijl et al., 2018a](#)) or ice rafted debris, which suggests ice sheets terminated landward of the coastal margin ([Halberstadt et al., 2021; Levy et al., 2019; Sangiorgi et al., 2018](#)).

Proxy data at Site U1356 indicate a major environmental transition occurred after the onset of the MMCT at 14.8 Ma. TEX₈₆-based paleothermometry indicate ocean temperatures off the Adélie Coast cooled by ~6°C between ~16.5 and 14.5 Ma and dinocyst assemblages suggest sea-ice became a more persistent feature by ~14.2 Ma ([Sangiorgi et al., 2018](#)). An increase in sedimentary clasts at ~14.6 Ma indicates nearby glaciers extended into ocean and that IRD-bearing icebergs transported debris across the drill site. Clast occurrence and abundance peaked between 14 and 13.8 Ma and

dropped again between 13.8 and 13.5 Ma (Sangiorgi et al., 2018). Clast provenance studies suggest the clasts were derived from an inland source area that extended along the eastern part of the Adélie Craton (the western margin of the WSB) (Pierce et al., 2017). These data suggest a dynamic coastal environment in which an ice sheet repeatedly advanced and retreated from interior regions across the WSB shelf throughout the MMCT (Pierce et al., 2017) and that the ice sheet and glaciers reached their maximum extent between 14 and 13.8 Ma.

Sediments and seismic sequences that overly a major hiatus (WL-U5b) between 13.4 and ~11 Ma at Site U1356 (Fig. 9.6), formed as channel levee systems migrated across the site when the margin of the expanded EAIS advanced and retreated over the continental shelf (Escutia et al., 2011a; Sangiorgi et al., 2018). The abundance of soil organic matter in these sediments is lower than in sediments deposited during the MCO, consistent with a reduction in soil formation and extent due to colder climatic conditions and extensive regional ice cover (Sangiorgi et al., 2018). Vegetation composition (from pollen) remained broadly unchanged between the MCO and late Miocene, although an increase in the relative abundance of southern beech (*Nothofagus* spp.) suggest temperatures were colder (Sangiorgi et al., 2018). Geochemical proxies indicate mean annual terrestrial temperatures between 6°C–8°C at 10.8 Ma compared to temperatures of 7°C–12°C indicated through the MCO (Passchier et al., 2013a; Sangiorgi et al., 2018). TEX₈₆-based temperature estimates show upper ocean temperatures were between 4°C and 10°C (±4°C). A decrease in the relative abundance of protoperidinoid dinocysts suggests a decrease in sea-ice at this time. Nannofossil-rich sediments appear in a discrete sequence at Site U1361 (Pretty, 2019) and indicate that between 11.7 and 11 Ma, temperatures were either warm enough to support coccolithophore growth (Balch et al., 2016) or the local CCD deepened enough to allow carbonate deposition. Together proxy environmental data from Sites U1356 and U1361 indicate warming of water masses that outcrop close to the continent along the George V and Adélie Coasts in the late Miocene (DeCesare and Pekar, 2016; Evangelinos et al., 2020), well after the end of the MMCT. However, the increase in diatomaceous sediments after 11 Ma suggests this late Miocene warming was relatively short-lived, at least offshore of the Adélie Coast (Pretty, 2019; Sangiorgi et al., 2018).

Younger sediments recovered from the continental rise at Sites U1359 and U1361 indicate the EAIS margin remained dynamic into and through the Pliocene. Sedimentological data including lithofacies characterisation, grain size, and major and minor trace element ratios from continental shelf sediments helped identify oscillating periods of open-marine conditions and glacial advances to the outer shelf during the Pliocene (Orejola and Passchier, 2014; Patterson et al., 2014; Reinardy et al., 2015). The geochemical provenance of fine-grained detrital sediments recovered at

continental rise Site U1361 suggests a dynamic early Pliocene (5.3 to 3.3 Ma) ice sheet margin, with repeated ice sheet advance and retreat well into the WSB (Cook et al., 2013), as indicated by the relative contribution of inland lithologies of the Ferrar and Beacon supergroup lithologies to the detrital sediment signature offshore. Analyses of a variety of geochemical and mineralogical provenance proxies in the Pliocene sediments (clay mineralogy, fine-grained Sr and Nd isotope composition, ice rafted hornblende $^{40}\text{Ar}/^{39}\text{Ar}$ ages) highlight that ice sheet reconstructions are more robust when multiple methods are deployed. For example, the provenance of ice rafted hornblende grains points to far-travelled sources, indicating ice sheet instability in West Antarctica at the same time ice retreat occurred into the WSB (Cook et al., 2017).

Geochemical proxies, including Mn/Al and biogenic barite, have been used to determine oceanic redox conditions at Site U1359 and point to possible incursions of CDW onto the continental shelf, which may have promoted glacial retreat in the Pliocene (Hansen and Passchier, 2017). Fossil diatom and silicoflagellate assemblage data furthermore suggest that the warmest interglacials coincided with a poleward shift of Southern Ocean frontal systems. Such periods were characterised by prolonged ice-free open water conditions with higher productivity and strong surface ocean stratification (Armbrecht et al., 2018; Taylor-Silva and Riesselman, 2018).

Pliocene fluctuations in ice sheet volume and extent, as well as surface ocean conditions in the vicinity of the WSB, appear to be paced by changes in incoming solar radiation through astronomical (orbital) cycles (Armbrecht et al., 2018; Hansen et al., 2015; Patterson et al., 2014; Taylor-Silva and Riesselman, 2018). Data from offshore cores show that during the warm Early Pliocene marine based margins of the EAIS responded to \sim 40-kyr changes in mean annual southern high latitude insolation paced by changes in Earth's axial tilt (obliquity). Between 3.5 and 3.3 Ma significant shift in EAIS dynamics occurred in response to Southern Ocean cooling and development of a perennial sea-ice cover which limited the role of oceanic forcing on ice sheet extent (Patterson et al., 2014). After \sim 3.3 Ma, substantial retreat of the ice sheet margin occurred only during austral summer insolation maxima that are controlled by 20-kyr precession cycles modulated by changes in short (100 kyr) eccentricity cycles.

High-resolution far-field sea level records recovered from the Whanganui Basin of New Zealand support these findings and suggest that the average amplitude of sea-level changes during the mid-Pliocene (3.3–2.7 Ma) was \sim 7 to 18 m and oscillated in response to Antarctic ice volume changes that were driven by 20-kyr changes in local insolation (Grant et al., 2019). These data contradict estimates of ice volume and temperature derived from a global stack of benthic $\delta^{18}\text{O}$ records (Lisiecki and Raymo, 2005), which suggest 40-kyr changes in mean annual insolation drove ice volume change at this time

(de Boer et al., 2015; Pollard and DeConto, 2009). Explanations for the apparent dominance of obliquity at this time have been proposed (Huybers and Tziperman, 2008; Raymo and Nisancioglu, 2003; Raymo et al., 2006) but these new sea level data suggest that further investigation is required. The Wanganui sea level record also suggests the magnitude of glacial retreat was much larger during the KM3 (3.158 Ma) oxygen isotope event than during the M1 (3.251 Ma) and KM5 (3.198 Ma) events. This observation is supported by diatom assemblage data from Site U1361 that imply a major poleward migration of the Antarctic PF during this interval of warmth, which destabilised the ice sheet margins (Taylor-Silva and Riesselman, 2018). Oxygen isotope event KM3 is an important interval to examine Antarctic ice sheet sensitivity to climate warming. The 18 m amplitude change in sea level observed during this interglacial is best explained by mass loss from Antarctica's marine-based ice sheet margins with limited contribution from the Greenland Ice Sheet (Grant et al., 2019; Shakun et al., 2018). If the contribution to sea level from Greenland was small, then the observed magnitude of sea level change requires complete melt of the WAIS and major retreat of the EAIS across East Antarctica's large subglacial basins, including the WSB and ASB (Fig. 9.2).

High resolution (suborbital) geochemical provenance data from Site U1361 (Figs 9.2 and 9.6), alongside XRF records of oceanic productivity and records of IRD mass accumulation during selected Pliocene warm intervals indicate a strong coupling of changes in provenance (e.g., ice sheet margin retreat) and marine biological productivity (e.g., sea ice melting). Increases in iceberg calving appear to precede ice sheet retreat in this sector and may have contributed to fertilising the Southern Ocean (Bertram et al., 2018). These high-resolution data indicate that the time between deglacial onset and maximum grounding line retreat within the WSB was a few thousand years (Bertram et al., 2018), a conclusion that is consistent with modelling results (Golledge et al., 2017a, 2017b; Pollard et al., 2015).

Satellite-based analyses of modern ice sheet and sea ice dynamics suggest that the Wilkes Land margin is more vulnerable to warming temperatures than the George V margin (Miles et al., 2013, 2016). However, glaciers that drain the ASB (including the Totten and Moscow University Glaciers) sit on beds with geomorphological features and slopes that promote glacial stability (Morlighem et al., 2020) and will have to retreat several km inland before they reach a destabilising retrograde bed. Whether or not the margin of the EAIS along the Wilkes Land coastal region was highly dynamic during the warm Pliocene is unclear. Evidence for glacial destabilisation and ice margin retreat within the ASB during the Pliocene comes from sedimentologic evidence for diatom oozes (Gulick et al., 2017) and geochemical studies of ice rafted debris in cores from offshore the ASB and Prydz Bay (Cook et al., 2014; Williams et al., 2010). Geochemical data suggest iceberg armadas entered the Southern Ocean from the Wilkes Land margin, and possibly the

adjacent low-lying ASB, during the early Pliocene (Cook et al., 2014; Williams et al., 2010). These icebergs may have carried sedimentary detritus with a characteristic provenance fingerprint of the rocks from the Wilkes Land region all the way to Prydz Bay, despite elevated SSTs. However, multichannel seismic data from offshore the ASB catchment suggest a muted glacial response to Pliocene warmth (Gulick et al., 2017). Modelling studies also produce contrasting results; some suggest little retreat across the ASB during peak Pliocene warmth (de Boer et al., 2015; Golledge et al., 2017b), while others indicate significant grounding zone retreat can occur across the region (de Boer et al., 2015; Pollard et al., 2015). Further insight into past glacial dynamics in this potentially sensitive region remains elusive as no continuous marine sedimentary record currently exists from the Sabrina Coast (Gulick et al., 2017). However, current efforts are underway to develop a drilling program to recover new records (Gulick et al., 2017; McKay et al., 2021; Montelli et al., 2019).

9.2.3 The Ross Sea Embayment and Southern Victoria Land

9.2.3.1 Geological setting

The Ross Sea Embayment (RSE) is bordered by the 3500 km long Transantarctic Mountain (TAM) chain to the west and Marie Byrd Land (MBL) and Siple Coast to the east (Fig. 9.2). The modern WAIS is grounded within the lower topographic relief of the West Antarctic Rift System (WARS), one of Earth's major continental extension zones extending across Antarctica from the western RSE to the Antarctic Peninsula (AP) and separating West and East Antarctica (Jordan et al., 2020). Most of the WAIS sits on continental crust that lies well below sea level, in places reaching depths well over two kilometres (Fretwell et al., 2013; Morlighem et al., 2020). Clastic and biogenic sediments have accumulated in the sedimentary basins that formed as the WARS evolved through the Cretaceous and Cenozoic (Decesari et al., 2005, 2007; Jordan et al., 2020; Luyendyk et al., 2001; Wilson et al., 2009). Clastic sediments that comprise the Miocene and Pliocene sequences reviewed herein are sourced from pre-Quaternary rocks from the TAM and beneath West Antarctica. Sediment provenance studies have become important tools for reconstructing past ice dynamics across the area so here we provide a brief overview of the regional geology. See Talarico et al. (2021) for a more comprehensive review.

Basement rocks exposed along the TAM primarily comprise early Paleozoic igneous intrusives of the Ross Orogeny (Allibone et al., 1993; Cox et al., 2012; Goode et al., 2012; Gunn, 1963; Gunn and Warren, 1962; Paulsen et al., 2013; Stump, 1995). Post Ross Orogeny exhumation and erosion of the granitic and metamorphic basement provided Kukri Peneplain upon which the clastic Beacon Supergroup was deposited (Barrett, 1971;

Barrett et al., 1972, 1986; McKelvey et al., 1977). This sequence was intruded by Ferrar Dolerite at c.180 Ma (Compston et al., 1968; Ferrar, 1907; Harrington, 1958; Licht et al., 2014). Little is known of the basement rocks inland of the TAM because these are covered by the EAIS (Palmer et al., 2012). Late Cenozoic volcanics in the western Ross Sea region comprise the McMurdo Volcanic Group, part of the Erebus Volcanic Province (Kyle, 1990a, 1990b), which range in age from ~19 Ma to present. Drillcore evidence extends the volcanic record in the western Ross Sea back to 26 Ma (Di Vincenzo et al., 2009; Gamble et al., 1986; McIntosh, 1998; 2000).

The best exposed basement rocks in West Antarctica are in Marie Byrd Land and comprise the Neoproterozoic to Cambrian Swanson Formation and Devonian to mid Cretaceous magmatic rocks (Korhonen et al., 2010; Pankhurst et al., 1998; Siddoway, 2008; Siddoway and Fanning, 2009; Tingey, 1991). Starting in the Oligocene, the region was subjected to intense alkaline volcanism and uplift of the Marie Byrd Land Dome (Hole and LeMasurier, 1994; Winberry and Anandakrishnan, 2004), although other studies suggest this uplift event began in the early Miocene ~10 million years later (Spiegel et al., 2016). Today the Marie Byrd Land Dome extends to an altitude of 2700 m and is a feature that likely shed sediment into the WARS over the Miocene and Pliocene. Eighteen major volcanoes and many smaller centres across MBL are composed of felsic alkaline lavas (Panter et al., 2000). Other volcanic centres likely exist under the WAIS and have been imaged via aerogeophysical surveys (Behrendt et al., 1996, 2002, 2004). Some of the MBL volcanoes have been active during the Pleistocene-Holocene, potentially affecting geothermal heat flow and basal WAIS dynamics (de Vries et al., 2017).

Basins on the mid to outer continental shelf in the RSE contain sedimentary rocks dating to the late Eocene (Barrett, 1989, 2009; Galeotti et al., 2012; Harwood and Levy, 2000; Levy and Harwood, 2000a, 2000b). However, reworked palynomorphs in seabed surface samples collected across the Ross Sea indicate terrestrial sedimentary rocks dating to the Cretaceous were deposited across West Antarctica (Truswell and Drewry, 1984), but in-situ sediments have yet to be recovered. Reworked marine microfossils are also common components in glacial sediments recovered from beneath the WAIS and offer insight into the likely in-situ sequences that occur beneath the WAIS. Siliceous microfossils from discrete time intervals in the early Miocene, middle Miocene and late Miocene are preserved in sediment clasts and matrix from the Ross Ice Shelf Project (RISP) J-9 core (Harwood et al., 1989) and indicate in situ Neogene sediments occur upstream of the site. Microfossil analyses also show that reworked Eocene, Miocene, Pliocene, and Pleistocene diatoms are widespread beneath the Whillans and Kamb ice streams (Coenen et al., 2020; Scherer et al., 1998). Whereas these data provide tantalising

evidence for the occurrence of Neogene strata beneath the WAIS and inner Ross Ice Shelf, thus far no in-situ pre-LGM samples have been collected. These strata are a target of future drilling efforts (McKay et al., 2021). In contrast, sedimentary basins located north of the Ross Ice Shelf have been the target of multiple drilling campaigns and offer the most complete and comprehensive stratigraphy's through the Miocene and Pliocene and are discussed in detail below.

9.2.3.2 Oceanography and climate in the Ross Sea Region

The Ross Sea Embayment covers an area of approximately 1,137,000 km² and includes an extensive ocean cavity beneath the world's largest ice shelf. Relatively warm CDW enters the cyclonic flow of the Ross Gyre at its eastern limb (Orsi and Wiederwohl, 2009; Whitworth et al., 1998). At the continental shelf break, CDW locally flows onto the continental shelf and mixes to become mCDW with temperatures of 1°C to 1.5°C (Budillon and Spezie, 2000; Dinniman et al., 2003, 2007). Sea-ice formation in the Ross Sea converts AASW and/or shoaling mCDW, into cold and dense High Salinity Shelf Water (HSSW). Cyclonic circulation of HSSW beneath the Ross Ice Shelf is inferred to occur within the major troughs that connect the continental slope with the grounding line of the Ross Ice Shelf (RIS) (Dinniman and Klinck, 2002). Ice shelf water (ISW) is created via contact between water and the Ross Ice Shelf at depth and is characterised by temperatures below the surface freezing point. Supercooled ISW emerges from beneath the Ross Ice Shelf in the west central region of the continental shelf (Dinniman et al., 2003).

HSSW is exported from the Ross Sea continental shelf where it mixes with CDW and contributes to AABW. At present, most of the abyssal layers of the world's oceans are filled with water that is influenced by AABW that primarily originates from the Weddell and Ross Seas. Thus, changes in ice shelf extent, water temperature, and/or meltwater input to the Ross Sea could significantly disrupt present-day global meridional overturning circulation (MOC) (Jacobs et al., 2002; Orsi et al., 2002; Purkey and Johnson, 2010). Over the past 40 years, Ross Sea-derived AABW have freshened as a result of increased meltwater input to the Amundsen and Bellingshausen Seas from melting ice shelves/glacial systems upstream from the Ross Sea (Jacobs and Giulivi, 2010; Jacobs et al., 2002; Silvano et al., 2018). Recent hydrographic observations in the late 2010s have revealed a reversal of the freshening trend hinting at the existence of decadal variations or oscillations in meltwater contribution from the Ross Sea region (Aoki et al., 2020; Castagno et al., 2019).

At present, the strong westward-flowing Antarctic Slope Current (ASC) and its sharp subsurface front (Antarctic Slope Front – ASF), separates AASW from CDW on the lower continental slope. The ASF serves as a dynamical barrier that limits the transfer of CDW onto the Ross Sea continental shelf (Ainley

and Jacobs, 1981; Smith et al., 2012; Thompson et al., 2018). However, a decrease in wind shear stress across the ASF may cause shoaling of isopycnals and enhanced eddy-driven transport of CDW across the continental shelf margin (Stewart and Thompson, 2014). Furthermore, modelling indicates that flow of CDW onto the Ross Sea continental shelf is directly influenced by the volume of dense waters that descend off the continental shelf to form AABW (Morrison et al., 2020). Incursion of warm CDW is sensitive to the morphology of the continental margin, vigour of the ASC (and associated eddy activity), and production of AASW and AABW (Thompson et al., 2018). Changes in atmospheric and ocean dynamics at the continental shelf margin clearly influence the incursion of warm water onto the Ross Sea Continental Shelf and will likely increase ice shelf and ice sheet melt. Positive feedbacks associated with increasing melt and freshwater flux will enhance intrusion of CDW and potentially accelerate ice sheet retreat.

Terrestrial rock outcrops span the western and eastern margins of the Ross Sea Region (Fig. 9.2). The McMurdo Dry Valleys (MDV) are the best studied and monitored and are the focus of the terrestrial environmental records discussed in this review. The MDV represent one of the largest ice-free regions in Antarctica, covering approximately 4000 km² in the central Transantarctic Mountains. Today, the Dry Valleys feature a hyperarid, cold-desert climate. Mean annual temperature at Lake Bonney, on the floor of Taylor Valley is -17.9°C (Doran et al., 2002). Climate at higher elevations in the MDV is difficult to constrain due to a lack of long-term monitoring data. However, a meteorological station at 1581 m above sea level in the Friis Hills recorded weather conditions from 2005 to 2010 (Bliss et al., 2011). During this period, mean summer temperature was -13.2°C with an average wind speed of 4.7 m/s. The winter mean was -29.7°C with an average wind speed of 4.2 m/s (Bliss et al., 2011). Based on measured regional lapse rate of $6.4^{\circ}\text{C}/\text{km}$ (Bliss et al., 2011), the range in mean annual temperature in the Friis Hills, Asgard and Olympus ranges would approach -24°C to -28°C . Additional weather station data collected from the Friis Hills between 2011 to 2018 recorded an average mean annual air temperature of $-22.7^{\circ}\text{C} \pm 1.3^{\circ}\text{C}$ (Doran and Fountain, 2019). Climate in the Friis Hills and other high elevation regions of the MDV (Fig. 9.2) is classified as a severe polar desert with sub-freezing temperatures and strong winds occurring throughout the year (Lewis and Ashworth, 2015). Precipitation measured at Lake Bonney is less than 150 mm/year, which falls as snow (Fountain et al., 1999). Precipitation at locations farther inland and higher is likely less (Doran et al., 2002).

9.2.3.3 Seismic stratigraphic records in the Ross Sea

The Ross Sea Embayment contains a dense network of seismic profiles (McKay et al., 2021). Regional interpretation of the major stratigraphic discontinuities allows for a well-defined seismic-stratigraphic framework, constrained

by deep-drilling sites from across the Ross Sea (McKay et al., 2021) (Fig. 9.7). The broad seismic stratigraphy of the Ross Sea was first resolved by the SCAR Antarctic Offshore Stratigraphy project, ANTOSTRAT (Brancolini et al., 1995a; Cooper and Davey, 1987). Above the seismic basement, the underlying sequence holds syn-rift sediments of Mesozoic to early Eocene age (Cooper and Davey, 1987). The overlying sedimentary sequence contains

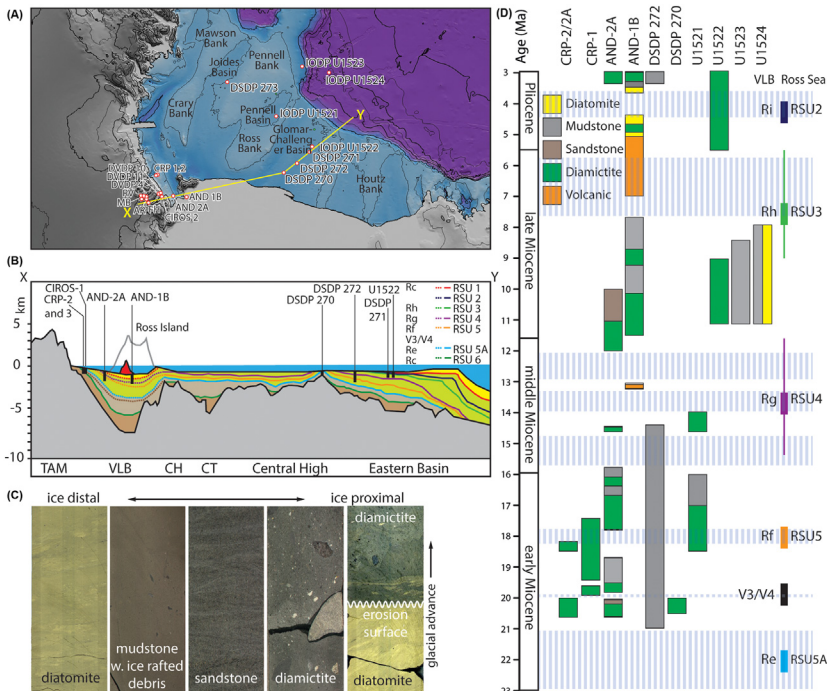


FIGURE 9.7 (A) Ross Sea region with location of key drill cores and outcrop discussed in the text: *DVD*, Dry Valley Drilling Project; *MB*, Mount Boreas; *AR*, Asgard Range; *RV*, Rude Valley; *FH*, Friis Hills; *CRP*, Cape Roberts Project; *CIROS*, Cenozoic Investigations in the Ross Sea; *AND*, ANDRILL; *DSDP*, Deep Sea Drilling Project; *IODP*, Integrated Ocean Discovery Program. Line X–Y indicates approximate location of cross section shown in (B). (B) Generalised cross section from the Transantarctic Mountains (TAM) to the continental shelf margin. Solid coloured lines indicate major Ross Sea seismic unconformities (RSUs). Correlative surfaces in the Victoria Land Basin (VLB) are dashed as direct correlations are ambiguous due to the occurrence of basement highs and faults at the VLB margin. (C) Representative examples of sediment/facies types and transitions observed in Ross Sea drillcores. (D) Chronostratigraphic framework and generalised lithofacies for drill cores discussed in this text. Dashed blue horizontal lines highlight episodes where drill core unconformities coincide with seismic unconformities, which are indicated by coloured lines at right of diagram (thin vertical lines indicate age uncertainty). Drill core chronostratigraphy is based on published age models (Florindo et al., 2005; Levy et al., 2016; McKay et al., 2019; Naish et al., 2009; Wilson et al., 2012b) and/or has been adjusted to fit up-to-date ages for key biostratigraphic datums (Crampton et al., 2016; Florindo et al., 2013).

seven major unconformities referred to as Ross Sea Unconformities (RSU's) that bound eight intervening seismic sequences named Ross Sea Sequences (RSS's) (McKay et al., 2021). The RSS are largely defined by studies in the Eastern and Central basins of the Ross Sea, whereas different nomenclatures exist in the active rift zones of the Western Ross Sea (Davey et al., 2000; Fielding, 2018; Fielding et al., 2008; Henrys et al., 1998, 2001; Levy et al., 2016). Here we describe briefly the seismic stratigraphic sequences and unconformities through the Miocene and Pliocene.

Seismic-stratigraphic sequences RSS2 to RSS6 (oldest to youngest) are Miocene (Brancolini et al., 1995a). RSS2 sits above RSU6 and grades upwards into well-stratified reflections that are laterally continuous. RSU6 has never been drilled but an age of >27 Ma is generally accepted (Busetti and Cooper, 1994). This unconformity is restricted to the deepest sedimentary basins, where it forms the top of stratified sediments infilling channels and structural valleys and onlaps structural highs (De Santis et al., 1995). RSS2 is thickest along the inner continental shelf and is thin to absent along a SE-NW band over Glomar Challenger Basin and the Ross and Iselin banks (Brancolini et al., 1995a; De Santis et al., 1995). RSU5 (~18 Ma) forms the top of RSS2 and is expressed regionally as a high amplitude reflection that is locally erosive on the eastern and inner part of the continental shelf. RSS3 overlies RSU5 and includes thick prograding wedges that occupy the main sedimentary basins of the Ross Sea continental shelf. Locally, strata within the upper part of the unit exhibit aggradational features (Pérez et al., 2021a). RSU4a (~17 to 16.4 Ma) defines the top of RSS3 and is characterised by a regionally extensive lateral reflection that locally truncates underlying sediments. RSS4 occurs above RSU4a and includes seismic facies with regionally variable amplitudes and laterally discontinuous reflectors. The sequence is thick and extends across the central basins. RSS4 is truncated by RSU4 (~14.6 to 12 Ma), an erosional surface that extends across most of the Ross Sea continental shelf. RSS5 and RSS6 are relatively discrete units that occur locally in the central and eastern Ross Sea, where they thicken towards and along the outer shelf. These sequences typically comprise prograding wedges that are bounded by RSU3 (~8 to 6 Ma), which is generally considered an erosional surface across much of the inner to mid Ross Sea continental shelf (De Santis et al., 1995). RSU2 generally deepens landwards (De Santis et al., 1999) and has an estimated age between 4.0 and 2.8 Ma in the western Ross Sea (Brancolini et al., 1995b; Granot et al., 2010).

The origin of the RSUs has been linked to a range of processes including tectonic events, glacial erosion, and sea level oscillations (Alonso et al., 1992; Anderson and Bartek, 1992; Bartek et al., 1991; Busetti et al., 1993; Brancolini et al., 1995a; Cooper et al., 1995; De Santis et al., 1995; Hinz and Block, 1984). The aggradational pattern in the upper part of RSS2 is inferred to reflect ice distal glaciomarine conditions in the Ross Sea that preceded deposition of ice proximal progradational wedges within RSS3. These

prograding strata likely represent a period of ice sheet advance into marine environments across the Ross Sea continental shelf (De Santis et al., 1995, 1999; Pérez et al., 2021a). The regionally variable but erosive signature of RSU4a suggests expansion of ice caps from local highs at locations across the Ross Sea formed this feature. The relatively uniform stratified pattern that characterises RSS4 likely reflects a period of open marine conditions and hemipelagic sedimentation with little evidence of ice advance and retreat across the Ross Sea during the MCO (De Santis et al., 1995; McKay et al., 2019; Pérez et al., 2021a). The regional erosional signature of RSU4 reflects an episode of extensive ice sheet advance across the continental shelf of the Ross Sea (Bart and De Santis, 2012; De Santis et al., 1995, 1999; McKay et al., 2019; Pérez et al., 2021a). Prograding wedges that form RSS5 and RSS6 were deposited during multiple episodes of marine ice sheet advance and retreat during late Miocene, which delivered glacial marine sediments to the outer continental shelf. The landward deepening surface of RSU2 formed as a thick and extensive marine ice sheet grounded across the continental shelf during the late Pliocene and early Pleistocene (De Santis et al., 1999; Lindeque et al., 2016).

9.2.3.4 Stratigraphic records from drill cores in the Ross Sea

The history of geological drilling in the Ross Sea is relatively long and has contributed significant discoveries that are fundamental to our understanding of Antarctic ice sheets and environmental evolution. In December 1973, Leg 28 of the Deep Sea Drilling Project (DSDP) (Hayes et al., 1975b) recovered upper Oligocene to lower Miocene glacial sediments at Site 270, instantly extending our known history of Cenozoic glaciation back some 25 million years (Barrett, 1975; Hayes et al., 1975d). Miocene and Pliocene sediments were recovered at Sites 272 and 273, providing insight into the history of glacial advance and retreat across the Ross Sea continental shelf. In 2018, IODP Expedition 374 drilled five holes and recovered Miocene to Pleistocene sediments that add to our expanding knowledge of marine ice sheet behaviour in the central Ross Sea through the Neogene (Figs 9.5 and 9.6) (McKay et al., 2019).

Site U1521 (75.6839°S , 179.6718°W) recovered a 648 m sequence of Miocene to Recent sediments that is divided into seven lithostratigraphic units (I–VII) (McKay et al., 2019). Contacts between the units range from sharp to gradational. Mudstone and diamictite account for $\sim 90\%$ of the recovered core, and minor lithofacies include chert and conglomerate. The assemblage of facies reflects open-marine to ice-proximal depositional environments at this location since at least the early Miocene (~ 18 Ma). Site U1521 drilled through a thick seismic sequence of progradational foresets above RSU5 and recovered a ~ 300 m interval (Units VII and VI) of diamictites interbedded with thin mudstone layers that suggest input of a large

volume of glacially eroded material by marine-terminating glaciers or ice sheets. Unit V is a 40 m interval of poorly recovered chert nodules and silica cemented mudstone. Unit IV is a ~70 m of dark grey massive to stratified diatom-bearing clast-poor sandy diamictite. Unit III includes an ~120 m-thick interval of diatom-rich muds and diatom oozes provisionally assigned an age spanning 16.7 to 15.8 Ma (McKay et al., 2019). These predominantly open water sediments were deposited during an interval of ice sheet retreat spanning the earliest part of the MCO. Unit II includes an ~80 m thick sequence of dark grey massive clast-poor muddy diamictite interbedded with bioturbated diatom-bearing/rich mudstone with dispersed clasts. The lower ~40 m of the unit consists of diamictite and includes a disconformity that correlates with RSU4 and preliminary age constraints date this surface at ~14.6 Ma (Pérez et al., 2021a). Facies in Lithostratigraphic Unit II indicate highly truncated cycles of subglacial, glaciomarine and open marine sedimentation (McKay et al., 2019) that reflect repetitive cycles of marine-based ice sheet advance and retreat across the Ross Sea continental shelf since the middle Miocene (Pérez et al., 2021a).

Site U1522 (76.5538°S , 174.7578°W) penetrated to 701 m below the sea floor and recovered 279.57 m of core (40%). The 696 m thick succession of upper Miocene to Recent sediments is divided into four lithostratigraphic units (McKay et al., 2019). Lithostratigraphic Unit II spans the Pliocene and includes consists of ~195 m of massive interbedded diatom-bearing/rich sandy/muddy diamictite with mudstone laminae. Units III and IV recovered upper Miocene sediments spanning the interval from ~11 to 9 Ma. Unit III includes 250 m of muddy diatomite and diatom-bearing/rich diamictite and is divided into three subunits based on the style of interbedding and presence of lithologic accessories. Unit IV consists of ~50 m of interbedded diatom-bearing sandy diamictite and muddy diatomite. RSU3 intersects the core between 400 and 500 mbsf, which constrains the age of this surface to <9 and >5.5 Ma.

Site U1523 (74.1503°S , 176.7951°W) was cored on the outermost continental shelf, at a site under the influence of the ASC. A range of coring systems were deployed at Site U1523 as the operations crew attempted to recover material from the location in challenging coring conditions. A total of sixty-four cores were collected from five holes. These cores provide an ~220 m-thick composite sequence spanning the (?)middle Miocene to Pleistocene. The sequence is divided into three lithostratigraphic units and (?)middle Miocene and Pliocene sediments occur in unit II and III and are characterised by sand/gravel-rich beds alternating with diatom-bearing/rich mud – interpreted to reflect shifting ASC current strength through time. Due to the unconsolidated nature of the facies in this interval, and the rotary coring methods, core recovery of Unit III was extremely poor and, while the sequence may extend back to 13 Ma, lithological information is restricted to strata younger than 11 Ma, although downhole logs measurement were

conducted throughout this interval of Site U1523, and will continuous records of the downhole variability/cyclicity of facies. Approximately 50 m of upper Miocene sediments within Unit III include massive to laminated diatom-bearing/rich mud interbedded at the decimetre scale with diatom-bearing diamict (McKay et al., 2019).

Site U1524 (74.21738° S, 173.6336° W) is located on the continental rise, and drilled an expanded levee of the Hillary Canyon, one of the largest conduits of AABW feeding the abyssal ocean from the Ross Sea continental rise and includes three holes, the deepest of which was cored to 441.9 m bsf. A composite sequence recovered in three holes includes upper Miocene to Pleistocene sediment that is divided into three lithostratigraphic units (I–III) (McKay et al., 2019). Contacts between units and subunits are mostly gradational and are distinguished by gradual changes in diatom content. Unit II is mid Pliocene and consists of ~ 117 m of massive to laminated muddy diatom ooze interbedded with bioturbated to laminated diatom ooze and diatom-rich sandy mud. Unit III is 120 m thick and consists of massive to laminated mud interbedded with massive diatom-rich sandy mud with dispersed clasts of muddy diamict and muddy diatom ooze. A major disconformity at ~ 320 mbsf spans the interval from 8.4 and 4.8 Ma and separates Unit III and II. The fine-grained, and graded nature of the laminae is interpreted as representing a largely continuous record of turbidity current activity associated with AABW flow down the Hillary Canyon, with an ultra-expanded mid- to Late Pliocene section (McKay et al., 2019).

A series of onshore to nearshore geological drilling projects between 1976 and 2008 that have revealed much about Antarctic Cenozoic climate history is the southwest corner of the Ross Sea (Fig. 9.7). These drilling campaigns recovered sediments from discrete intervals through the past 36 million years (McKay et al., 2021). Neogene strata were recovered from onshore drilling within the Dry Valley Drilling Project (McGinnis, 1981; McKelvey, 1975) and from offshore locations during the McMurdo Sound Sediment and Tectonic Studies drilling Project (Barrett, 1986), Cenozoic Investigations in the Ross Sea Project (Barrett, 1989), Cape Roberts Project (Barrett et al., 1998; Barrett and Ricci, 2000, 2001; Davey et al., 2001), and the ANDRILL McMurdo Ice Shelf (Naish et al., 2007; Naish et al., 2008) and Southern McMurdo Sound Projects (Harwood et al., 2008, 2009) (Fig. 9.5). These drill cores provide detailed records of environmental variability and reveal the evolution of glacial marine conditions in Southern Victoria Land through the Neogene and are described in more detail below.

The *Cape Roberts Project* drilled at three locations recovering a composite stratigraphy comprising stratigraphic snap shots from the late Eocene to Pleistocene (Figs 9.2D, 9.5, 9.7). Lower Miocene sediments were recovered between 23 and 184 mbsf in CRP-2/2A (77.006° S, 163.719° E) and 50 and

150 mbsf in CRP-1 (77.008°S , 163.755°E) (Florindo et al., 2005). The Miocene sediments consist of six recurrent lithofacies: diamictite, rhythmically interlaminated fine-grained sandstone and siltstone, well-stratified sandstone, poorly-stratified muddy sandstone, coarse-grained siltstone and fine-grained siltstone (Cape-Roberts-Science-Team, 1998). These data indicate multiple phases of advance and retreat of the McKay glacier occurred through the early Miocene.

The ANDRILL-2A drill core (77.76°S , 165.28°E), a 1,138-m-long stratigraphic archive of climate and ice sheet variability from the McMurdo Sound sector of the western Ross Sea (Figs 9.2D, 9.7), was recovered in 2008 by drilling from an ~ 8.5 -m-thick floating sea ice platform in 380 m of water, located ~ 30 km off the coast of Southern Victoria Land. The core offers an ice-proximal stratigraphic archive over the period c.20.2–14.2 Ma, with a more fragmentary record of Late Miocene and Pliocene time (Figs 9.5, 9.7). The sedimentary sequence is divided into 74 high-frequency glacimarine cycles recording repeated advances and retreats of glaciers into and out of the Victoria Land Basin (Fielding et al., 2011; Jovane et al., 2019; Levy et al., 2016; Passchier et al., 2011).

The ANDRILL-1B hole (77.89°S , 167.09°E) (Figs 9.2D, 9.7) was cored to 1284.85 m bsf and was completed on 26 December 2007 (Naish et al., 2007). Rock and sediments below ~ 150 mbsf are upper Miocene to Pliocene (Naish et al., 2007, 2009; Wilson et al., 2007) (Figs 9.5, 9.7). Sedimentary facies in the core are highly cyclic, comprising stratified and massive diamictite, breccia, conglomerate, sandstone, siltstone, mudstone and diatomite (Krissek et al., 2007b), and three distinct facies associations (termed Motifs) were identified in the cores highlighting major shifts in the glacial mass balance controls, as well as strong orbital pacing of ice sheet volume, over the past ~ 13.6 Ma (McKay et al., 2009; Naish et al., 2009; Rosenblume and Powell, 2019).

CIROS-2 (77.6833°S , 163.5333°E) was drilled in 1984 from a sea-ice platform near the middle of Ferrar Fjord, western McMurdo Sound in 211 m of water (Figs 9.2E, 9.7). The hole penetrated 166.47 m of Plio-Pleistocene sediments, terminating in basement gneiss. The core includes 13 lithologic units which alternate between massive and stratified diamictite, faintly stratified mudstone, and fine and very fine sand and sandstone (Barrett and Hambrey, 1992). The lowermost sequence (162 to 100 mbsf) covers most of the Pliocene (Levy et al., 2012) and is dominated by diamictite but is interbedded with thin (dm to m-scale) marine mudstone beds.

The *Dry Valley Drilling Project (DVDP)*, run by the United States Antarctic Program in the early to mid-1970s, recovered geological data from onshore sites at Ross Island and in the MDV (Figs 9.2E, 9.7). DVDP holes-10 (77.5833°S , 163.5166°E) and -11 (77.5833°S , 163.4167°E) were drilled during 1974/75 at the eastern end of Taylor Valley (McKelvey, 1975, 1981; Mudrey and McGinnis, 1975; Treves and McKelvey, 1975). DVDP-10

penetrated to 185.47 m and recovered a sequence dating back to the early Pliocene (~5.0 Ma) (Levy et al., 2012; Ohneiser and Wilson, 2012). DVDP 11 penetrated to 328 m and recovered a sequence dating back to ~6 Ma (Levy et al., 2012; Ohneiser and Wilson, 2012). DVDP-10 contains five lithostratigraphic units that include sandstone, pebbly sandstone, conglomerate, diamictite, breccia and laminated sandy mudstone (McKelvey, 1975, 1981). Units 4 and 5 are Pliocene. DVDP-11 was divided into eight lithostratigraphic units (McKelvey, 1975, 1981). The lowermost units (9–13) are Pliocene to upper Miocene and comprise an ~130-metre-thick sequence of sediments dominated by diamictite and minor sandy mudstone with some conglomerate (Levy et al., 2012; McKelvey, 1981).

9.2.3.5 Terrestrial records from Southern Victoria Land

Geological and glaciological research on the terrestrial records in Southern Victoria Land has a long history, beginning with observations by members of Scott and Shackleton's expeditions (David and Priestley, 1914; Ferrar, 1907; Wright and Priestley, 1922). While many of the subsequent early studies centred on mapping extensive exposures of Paleozoic and Mesozoic rocks in the mountains and valleys (Gunn and Warren, 1962), efforts were also made to decipher the glacial history preserved in the regional geomorphology and more recent sedimentary record (Bull et al., 1962; Calkin, 1974; Denton et al., 1971; Selby, 1971; Selby and Wilson, 1971). Since this early work, there have been extensive studies on the geomorphological and climatic evolution of the Dry Valleys region since the Miocene (Denton et al., 1984; Hall and Denton, 2005; Kowalewski et al., 2006; Lewis et al., 2006, 2007, 2008; Marchant et al., 1993; Prentice et al., 1993; Prentice and Krusic, 2005; Sugden and Denton, 2004; Sugden et al., 1991, 1995). Importantly, many of these deposits and landforms are mantled by, or interbedded with, volcanic ash and tephra, which provide critical age constraints (Lewis and Ashworth, 2015; Lewis et al., 2006; Marchant et al., 1993, 1996; Schiller et al., 2019).

Terrestrial sedimentary deposits of Miocene and Pliocene age in the Ross Embayment are primarily located in the MDV but are relatively few and most post-date the MCO (Table 9.1). These records are composed of tills, fluvial-lacustrine sequences and colluvium. Many tills consist of unconsolidated units that are often metres thick with characteristics including striated clasts, underlying striated bedrock and cross bedding suggesting fluvial processes likely from supraglacial melting. Some of the oldest well dated terrestrial glacial deposits observed in the Ross Embayment occur in the Friis Hills (Lewis and Ashworth, 2015), Western Olympus Range (Lewis et al., 2007) and Asgard Range (Marchant et al., 1993) (Fig. 9.2D).

TABLE 9.1 Summary of key terrestrial deposits in the McMurdo Dry Valleys listed in chronostratigraphic order.

Feature	Location	Age	Ref
Alpine II	East-Central Wright Valley	$<2.8 \pm 0.2$ Ma	Hall et al. (1997)
Onyx drift	Lower Wright Valley	$<3.3 \pm 0.3$ Ma	Hall and Denton (2005)
Wright drift	Lower Wright Valley	$<3.4 \pm 0.2$ Ma	Hall and Denton (2005)
Valkyrie drift	Lower Wright Valley		
Loop drift	Lower Wright Valley	$<3.3 \pm 0.3$ Ma	Hall and Denton (2005)
Alpine III	East-Central Wright Valley	$<3.3 \pm 0.2$ Ma	Hall et al. (1997)
Till (lateral moraines (WUIII))	Upper Wright Valley	Overlies Peleus <3.8 Ma (<3.5 Ma)*	Bockheim and McLeod (2006)
Alpine IV	Lower Wright Valley	Overlies Peleus	
Peleus Till/ WU IV	Wright Valley	$>3.8 <5.5$ (<3.5 to >3)*	Bockheim (2010); Prentice (1998); Summerfield et al. (1999)
Pecten Gravels (Prospect Mesa)	Wright Valley	Stratigraphically below Peleus (>3.5)*	
Jason Glaciomarine Diamicton	Wright Valley	9 ± 1.5 Ma	Prentice et al. (1993)
Rock Glaciers	Western Asgard Range	<12.5 Ma	Marchant et al. (1993)
Jotunheim Till	Western Asgard Range	>10.5 Ma	Marchant et al. (1993)
Dido drift 1	Western Olympus Range	>12.44 Ma	Lewis et al. (2007)
Dido till 2a	Western Olympus Range	$<13.62 >12.44$ Ma	Lewis et al. (2007)
Dido till 2b	Western Olympus Range	$<13.72 >13.62$ Ma	Lewis et al. (2007)

(Continued)

TABLE 9.1 (Continued)

Feature	Location	Age	Ref
Nibelungun Till	Western Asgard Range	<15.2**>13.6** Ma	Marchant et al. (1993)
Channels and Potholes in Asgard Range (Sessrumnir Valley)	Western Asgard Range	Inferred to post-date Asgard Till	Sugden et al. (1991)
Asgard Till	Western Asgard Range	<15.2**>13.6 Ma	Marchant et al. (1993), Sugden et al. (1991)
Dido till 2c	Western Olympus Range	>13.85 Ma	Lewis et al. (2007)
Dido drift 2	Western Olympus Range	>13.94 Ma	Lewis et al. (2007)
Electra Colluvium	Western Olympus Range	>13.94 Ma**	Lewis et al. (2007)
Circe Till	Western Olympus Range	>13.94 Ma	Lewis et al. (2007)
Mount Boreas	Western Olympus Range	14.07 ± 0.05 Ma**	Lewis et al. (2008)
Friis II drift (upper)	Eastern and Central Friis Hills	~14.2 to 13.9 Ma	Chorley (2021)
Friis II drift (lower)	Eastern and Central Friis Hills	~15.1 to 14.4 Ma	Chorley (2021)
Koenig Colluvium	Western Asgard Range	>15.2 Ma	Marchant et al. (1993)
Inland Forts Till	Western Asgard Range	>13.5 Ma	Marchant et al. (1993)
Sessrumnir Till	Western Asgard Range	>15.2 to 15 Ma	Marchant et al. (1993)
Friis I Drift	Eastern Friis Hills	19.76 ± 0.11 Ma	Lewis and Ashworth (2015)

The Friis Hills (Figs 9.2, 9.8) are located at the head of the Taylor Valley in the MDV and, at an average elevation of 1325 metres (m) above sea level, constitute an isolated inselberg with peaks up to 1500 m above sea level. Their unique position has allowed for Miocene terrestrial glacio-fluvial-

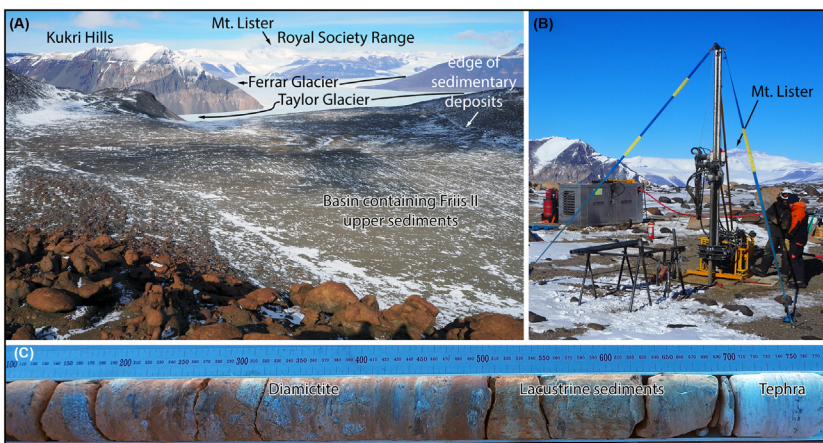


FIGURE 9.8 Images from the Friis Hills, upper Taylor Valley, Southern Victoria Land, Antarctica. (A) View from the northern peak in the Friis Hills looking across the broad south-eastern facing Friis central valley that contains glacial lacustrine sediments of the Friis II drift (Lewis and Ashworth, 2015). (B) Drill rig used to recover core shown in (C). (C) Core showing diamictite, lacustrine sediments and tephra from middle Miocene Friis II upper sediments.

lacustrine sediments to be preserved in high-elevation basins that have been protected from subsequent EAIS ice sheet expansions (Lewis and Ashworth, 2015). The Friis I drift sits on striated granitic basement within a small paleovalley in the easternmost region of the Friis Hills and includes an upper and lower diamicton interpreted as subglacial (lodgement/traction) tills up to 5.5 m-thick, separated stratigraphically by an interval of interbedded fluvio-lacustrine muds, sands, gravels and a volcanic ash with an $^{40}\text{Ar}/^{39}\text{Ar}$ age of 19.76 ± 0.11 Ma (Lewis and Ashworth, 2015). This relatively thin deposit is the only well-dated glacial sequence in the Transantarctic Mountains that pre-dates 15.2 Ma.

The stratigraphically younger Friis II drift occurs above Friis I drift within the paleovalley in the eastern Friis Hills but is most extensive across the central basin where it is deposited on top of basement rocks (Fig. 9.8A). The Friis II sequence includes at least sixteen sedimentary cycles comprising diamicts and interbeds of well-sorted, fine grained interglacial fluvial and lacustrine deposits (Chorley, 2021; Lewis and Ashworth, 2015; Verret et al., 2020). Friis II lower units were deposited during advance and retreat of wet-based temperate style glaciers flowing to the southeast. The Friis II upper sequence includes diamict that likely records a transition to more regionally expansive eastward directed glacial advance (Lewis and Ashworth, 2015). Fossiliferous beds in the Friis II drift record a *Nothofagus* shrub tundra with mean summer temperatures of $\sim 6^\circ\text{C}$ – 7°C (Lewis and Ashworth, 2015). The Friis II drift was cored in 2017 and tephra recovered in the cored

sequence and a paleomagnetic stratigraphy indicate an age between ~ 15.1 and 13.8 Ma for the Friis II upper sequence (Chorley, 2021; Verret et al., 2020). These age constraints are consistent with meteoric beryllium analyses that suggest the Friis Hills sequence is older than ~ 14 Ma (Valletta et al., 2015).

Miocene sedimentary deposits in the western Asgard Range include the Sessrumnir, Inland Forts, Asgard, Nibelungan and Jotenheim tills and the Koenig colluvium (Marchant, 1993). These sequences contain tephra that constrain the age of the glacial sediments to between ~ 15.2 and 10.5 Ma (Table 9.1). Nibelungan and Jotenheim tills are restricted in areal extent, whereas the other deposits are more extensive and are discussed in more detail here. Sessrumnir till is an poorly sorted massive and unconsolidated sandy diamict that overlies striated and moulded Ferrar Dolerite and granite bedrock and was likely deposited by alpine glaciers that extended from local alpine ice caps at the end of the MCO (Marchant, 1993). Inland Forts till is a silt-rich and unconsolidated diamict that mantles the striated sandstone bedrock floor (Fig. 9.9) and is inferred to have formed beneath a southward flowing wet-based glacier that occupied Inland Forts, similar to nearby Sessrumnir till (Ackert, 1990; Marchant, 1993). Asgard till is a silt-rich and

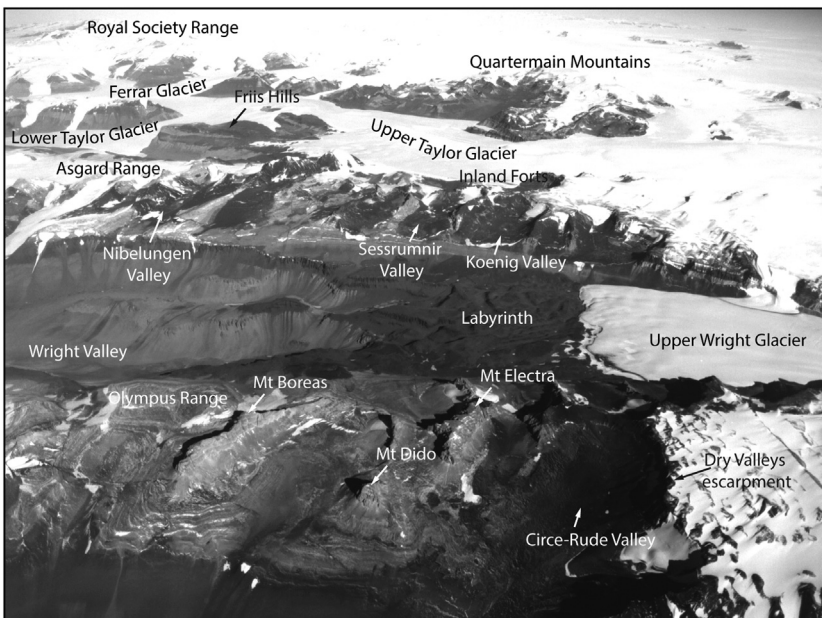


FIGURE 9.9 Oblique aerial photograph (USN TMA2299 0063) looking southwest towards the Olympus Range (foreground), Asgard Range (mid image), Quartermain Mountains and Royal Society Range (top of image). Features and locations containing Miocene terrestrial deposits discussed in text are labelled.

unconsolidated diamict containing granite erratics and striated sandstone and dolerite clasts. It is the most widespread surface deposit in the region and generally occurs in lobate map patterns at the mouths of hanging valleys in the Asgard Range and Quartermain Mountains. Radioisotopic dates on sanidine crystals in ash from deposits beneath the till indicate a maximum age of 14.8 Ma and from ash in sand wedges that cut the till indicate a minimum age of 13.6 Ma (Marchant, 1993). The Asgard till post-dates the MCO and was deposited during the MMCT (14.8 to 13.6 Ma) (Table 9.1). The sandstone and granite clasts and erratics and the morphological features of the Asgard till indicate that depositing ice flowed from the east, down major trunk valleys and spilled southwards into hanging valleys and likely reflects the influence of larger regional scale ice sheets (Marchant, 1993). However, thermal conditions at the base of the ice were likely highly variable with warm-wet conditions in the linear valleys and cold-frozen conditions across the plateaus with minimal disruption to underlying deposits.

Koenig colluvium is a bright orange (highly oxidised) and poorly sorted diamictite, composed of well-developed ventifacts within a sandy matrix that is stratigraphically between the underlying Sessrumnir till and overlying Asgard till. There are no striated, moulded or glacially polished clasts in Koenig colluvium and the deposit is inferred to reflect minor hillslope degradation and subaerial weathering in a desert climate. The age of Koenig colluvium is constrained by phonolitic ash that rests on buried ventifact pavement that covers the colluvium. Radioisotopic dates from sanidine in the ash indicate Koenig colluvium is older than 14.8 Ma and was deposited prior to the onset of the MCT (Table 9.1). This ash also provides a maximum age for the Asgard till which overlies the colluvium (Marchant, 1993).

Miocene sedimentary deposits in the Olympus Range include Circe till, Electra colluvium, Dido drift (Lewis et al., 2007) and fossil-rich moraine-dammed glacial-lacustrine deposits (Lewis et al., 2008). Circe till is a remnant of regional alpine glaciation originating from Circe-Rude Valley in the upper western boundary of Wright Valley (Fig. 9.9). Circe till varies from 1–4 m in thickness, sits directly on moulded and striated bedrock, and includes a lower mud-rich diamictite and upper stratified diamictite with sand and gravel lenses. Clasts are commonly striated and cross bedding is apparent in the sandy lenses. The lower unit is interpreted as a lodgement till deposited beneath wet-based ice and the upper unit an ablation till and likely represent a single cycle of glacial advance and retreat (Lewis et al., 2007). Circe till and Electra colluvium are possible equivalents to Sessrumnir/Inland Forts till and Koenig colluvium in the Asgard Range. Dido drift includes disparate patches of till comprising grain-supported sandy diamictite. These drift sediments were most likely deposited in the absence of water by sublimation of cold-based alpine glaciers (Lewis et al., 2007). The stratigraphically youngest unit (Dido Ib drift) is the only till unit in the valley that is not dissected. This feature suggests the till has not been modified due to

post-depositional glacial overriding. Age constraints for the Circe-Rude valley deposits come from volcanic ash that occurs as infill within relict sand-wedge troughs, laterally extensive interbeds, and small pods that infill voids in the Dido drift. Radioisotopic ($^{40}\text{Ar}/^{39}\text{Ar}$) dates on sanidine crystals from an ash in a wedge that dissects the lowermost Dido drift constrains the minimum age of Circe till, and the oldest episode of wet-based glaciation in the region, to $>13.94 \pm 0.75$ Ma (Lewis et al., 2007). Dates on ash in voids in the Dido Ib till suggest that regional glacial overriding at high elevations (>1200 m) has not occurred since 12.44 ± 0.15 Ma.

Middle Miocene glacial lacustrine sediments with exceptionally well-preserved fossil plants and freshwater aquatic organisms occur in a small moraine-dammed basin near Mount Boreas in the western Olympus Range (Fig. 9.9) (Lewis et al., 2008). This site is one of several that occur within north-facing valleys and contain moraine-dammed glacial-lacustrine deposits in the western Olympus Range. The lacustrine beds at the Mount Boreas site are near horizontal, unconsolidated and are comprised of glaciolacustrine silt and sand beds beneath a sequence of diatomaceous mud. The lake sediments are overlain by fluvial sands and debris flow deposits. The extent and elevation of the beds behind the moraine suggest the lake was as much as 8 m deep (Lewis et al., 2008). Exquisite examples of freeze-dried moss are abundant in the mud rich layers. Fossil diatom assemblages and well-preserved ostracods indicate the moraine-dammed lake was ice free for at least 2 to 3 months each year. The age of the fluvial lacustrine deposits is 14.07 ± 0.05 Ma and is based on correlation to a tephra in another lake deposit in Fritsen Valley to the east (Lewis et al., 2008).

The oldest known marine sedimentary deposit on the floor of the Wright Valley is the Jason Diamicton (Prentice et al., 1993). The diamicton is a pebbly muddy sand to sandy mud that crops out extensively along the north shore of Lake Vanda in Wright Valley and was recovered at the base of DVDP-4A (Prentice et al., 1993). DVDP-4A was drilled near the centre of Lake Vanda ($77^{\circ}32'\text{S } 161^{\circ}32'\text{E}$) at an elevation of 83.6 metres above sea level and recovered sediment between the lake floor at 68 m and granitic basement, which was intersected at 80.6 metres below the lake surface (Cartwright et al., 1974). The lowermost section between 5.74 and 11.2 m in DVDP-4A comprises siltstone with minor amounts of sandstone and conglomerate and contains a late Miocene marine diatom assemblage (Brady, 1979). The absence of diamictite in the marine sequence indicates the Wright Valley fjord remained ice free during deposition of the sequence. The diatom assemblage indicates the Wright Valley sediments in DVDP-4A are older than sediments at the base of DVDP-10 and 11. Whole and fragmented marine diatoms are abundant in the Jason diamicton and include *Denticulopsis dimorpha*, *D. lauta*, *Actinocyclus ingens* and *Thalassiosira nitzchioides* (Brady, 1979, 1982; Prentice et al., 1993). This assemblage indicates a depositional age between 13.66 and 9.23 Ma based on a revised biostratigraphic age presented herein (Fig. 9.10)

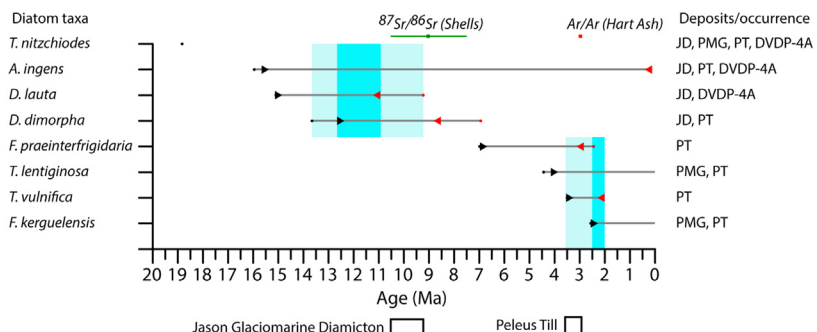


FIGURE 9.10 Diatom range chart for species reported in Dry Valley Drilling Project (DVDP) – 4A, the Jason Diamicton (JD), Peleus Till (PT) and Prospect Mesa Gravels (PMG). Ages for first appearance and last appearance datums for taxa are from the Constrained Optimisation (CONOP) hybrid range model (arrows) and total range model (dots) of Florindo et al. (2013). Deposits in which the diatoms are reported are shown at right (Prentice et al., 1993). $^{87}\text{Sr}/^{86}\text{Sr}$ date on shell from the Jason Diamicton from Prentice et al. (1993) and $^{40}\text{Ar}/^{39}\text{Ar}$ date on the Hart Ash from Schiller et al. (2019). Pale blue boxes indicate maximum likely age range of each deposit based on diatom biostratigraphy (darker blue boxes indicate minimum likely age range). Likely age of the Jason Diamicton and Peleus Till based on the combination of available chronostratigraphic data is indicated by boxes at bottom of diagram.

using total range model data for the diatom datums (Florindo et al., 2013). This age is compatible with estimates derived from $^{87}\text{Sr}/^{86}\text{Sr}$ analyses on shell fragments recovered from the diamicton, which suggests a minimum age of 9 ± 1.5 Ma (Prentice et al., 1993), indicating that the floor of the Wright Valley was a marine fjord during the late Miocene.

Pliocene sedimentary deposits in the MDV region consist of drift sheets, glacimarine sediments and volcaniclastic sequences associated with local cinder cones. Most of these deposits occur at lower elevations in the Taylor and Wright Valleys. However, at least one Pliocene glacial drift deposit occurs at relatively high elevation (1400 to 1500 m) in Vernier Valley in the Wilkniss Mountains. This drift is one of a series of four with a terminating moraine ranging from 1 to 4 metres in height, that were deposited by ice flowing from the Ferrar Glacier and into Vernier Valley. A minimum age of 3.39 ± 0.19 Ma was determined via cosmogenic ^{3}He and ^{21}Ne analysis from pyroxenes in surface boulders on the terminal moraine that extends furthest into the valley and is located at the highest elevation (Staiger et al., 2006). These data indicate that the margin of the Ferrar Glacier was at least 120 m higher than today during at least one glacial advance in the late Pliocene.

Four distinct surficial sedimentary deposits in the upper Wright Valley (WU IV through I) record major advances of the Wright Upper Glacier (Calkin and Bull, 1972), which is fed from Taylor Dome. The lowermost unit is now recognised as the Peleus Till (Prentice et al., 1993). Peleus Till is

silty, contains striated clasts and crops out discontinuously across Wright Valley from 180 m to 1150 m elevation (Hall et al., 1997; Prentice et al., 1993). The till lacks moraines and exhibits feather edges and is interpreted to be a subglacial till deposited during multiple glaciations from the west, east, or local alpine areas (Prentice et al., 1993). The age of the Peleus Till is somewhat contentious. The Peleus till has been correlated with the Asgard till (Hall et al., 1993a), which implies a depositional age of between 15 and 13 Ma and requires that the Wright Valley had been cut to its near present morphology prior to the middle Miocene. The absence of basaltic clasts in the till has been used to suggest the till predates ~ 3.8 Ma, the age of oldest clasts in overlying drifts (Hall et al., 1993a). However, the till is well exposed in a section at Prospect Mesa where a 6-m thick sequence overlies the pecten gravels (Prentice et al., 1993), which requires the till post-dates the late Miocene/early Pliocene gravels. However stratigraphic integrity at the location was questioned by Hall et al. (1997), who suggested original deposition of the till occurred before the Prospect Mesa Gravels were deposited and that the Peleus Till was remobilised down slope and emplaced on top of the Pecten Gravels. Regardless, diatoms in the Peleus Till at Prospect Mesa include *Thalassiosira vulnifica*, *T. lentiginosa*, *T. insigna* (reported as *Cosmiodiscus insignis*), and *Fragilariopsis kerguelensis* (reported as *Nitzschia kerguelensis*), which reflect a Pliocene age (Prentice et al., 1993). Currently accepted ages for the first and last appearances of these taxa (Florindo et al., 2013) (Fig. 9.10) indicate a depositional age between ~ 3.5 and 2 Ma. The Hart Ash, which has been recovered at several locations in the lower Wright Valley (Schiller et al., 2019), provides additional age constraint for the Peleus Till. Whereas no direct stratigraphic relationship between the till and ash has been observed, the ash would not survive wet-based glacial advances and therefore the ash places a minimum age on the Peleus Till. The Hart Ash was originally dated to 3.9 ± 0.3 Ma (Hall, 1992) but recent work suggests a younger age of 2.97 ± 0.02 Ma (Schiller et al., 2019). Based on available constraints presented in this review, we conclude that the Peleus Till was deposited between 3.5 and 3 Ma.

Pliocene surficial glacial sedimentary deposits in central Wright Valley include Alpine IV, III and II drifts (Hall et al., 1993a). These drifts are highly oxidised and contain weathered and fractured boulders. Alpine IV drift overlies Peleus Till and lateral moraines associated with the drift underlie moraines comprised of Alpine III and Alpine II drifts (Hall et al., 1993b). A chronology for the drifts was established through $^{40}\text{Ar}/^{39}\text{Ar}$ dating of reworked volcanic clasts contained within the drifts, which provide a maximum age for the deposits (i.e. the drifts cannot be older than the youngest dated clast). Alpine III and IV drifts contain clasts that range between 3.8 and 3.3 Ma, which indicates the drifts are younger than late Pliocene.

Relatively extensive glacial deposits in lower Wright Valley include the Valkyrie, Wright and Onyx drifts (Hall and Denton, 2005). Wright drift

overlies Alpine III and IV drifts and is dissected by Alpine II Drift. Onyx drift is a massive coarse-sand diamicton that overlies Alpine III and IV drifts but is cut by Alpine II drift. Loop drift is an unconsolidated, massive, coarse-sand diamicton with common stained and ventifacted clasts that are occasionally striated. Loop drift is inferred to be older than Valkyrie, Wright and Onyx drifts based on the degree of weathering (Hall and Denton, 2005). Basaltic clasts in the Loop, Wright and Onyx drifts constrain their maximum age to 3.4 to 3.3 Ma (Hall and Denton, 2005) (Table 9.1). Basaltic cones are not known from the eastern Wright Valley so the likely source of basalt in the drifts is McMurdo Sound, which indicates the drift sediments were deposited by ice that extended into the Wright Valley from the Ross Sea. Drift geomorphology and extent suggests they were deposited by ice that was 400 to 500 metres thicker than the present-day Wilson Piedmont Glacier (Hall and Denton, 2005).

9.2.3.6 Neogene history in the Ross Sea Region

The Ross Sea mid-continental shelf began to subside in the late Oligocene (~26 Ma) and increasingly large regions of West Antarctica became inundated by the sea (Kulhanek et al., 2019; Paxman et al., 2019b, 2020). Ice sheets and glaciers advanced and retreated across regions of the Ross Sea throughout the late Oligocene, periodically expanding from ice caps on Marie Byrd Land, topographic highs in the central and eastern Ross Sea (De Santis et al., 1995, 1999; Sorlien et al., 2007a, 2007b), and outlet glaciers through the TAM (Fielding et al., 2000). Water depths in the region around DSDP 270 reached 500 m by the early Miocene (Kulhanek et al., 2019; Leckie and Webb, 1983, 1986).

A significant transient glacial advance across the Oligocene/Miocene boundary is captured in DSDP 270 and the Cape Roberts Project cores by major disconformities that overly glacimarine glacial-interglacial sedimentary cycles leading up to 23 Ma (Florido et al., 2005; Kulhanek et al., 2019; Naish et al., 2001b, 2021). Depositional packages that immediately post-date the disconformities indicate ice retreated from these sites in the early Miocene. Whereas the composition of the pollen assemblage in DSDP Site 270 suggests terrestrial environmental conditions did not change across the O/M boundary, an increase in relative abundance of *Nothofagidites* suggests moderate climatic cooling occurred in the early Miocene (Kulhanek et al., 2019).

Environmental conditions were highly variable in the Ross Sea through much of the early and middle Miocene (Levy et al., 2016). SSTs ranged from cold sub-zero values similar to those recorded today to short intervals of warmth during which temperatures peaked at ~10°C (Levy et al., 2016; Warny et al., 2009). Whereas the AIS was generally restricted to terrestrial environments, at least four episodes of extensive marine ice sheet advances

are reflected by drill core and seismic data (Levy et al., 2016). Two of these episodes of marine ice sheet advance (MISA) occurred in the early Miocene. The first is captured by a major disconformity in AND-2A which correlates in time with RSU 5A and records advance of ice across regions of the Ross Sea continental shelf at ~ 19.8 Ma. This disconformity occurs above a sequence of strata at the base of AND-2A assigned to stratigraphic Motifs 2 and 5 (Fielding et al., 2011; Passchier et al., 2011), which are interpreted to record a broad environmental range from a sub-polar glacial regime with significant meltwater influence to minimal (distal) glacial influence (Fielding et al., 2011). Pollen in AND-2A (Griener et al., 2015; Warny et al., 2009) and sequences in the Friis Hills (Lewis and Ashworth, 2015) indicate tundra occupied regions spanning the coast to at least 60 km inland during interglacial conditions before and after the MISA at 19.8 Ma. These data reflect a highly variable climate in which the ice sheet margin advanced and retreated across the coastal margin of the Ross Sea, at times extending into marine environments.

An unusual period of cold and relatively stable climate is indicated by proxies in a prominent thick sequence of fine-grained sediments in AND-2A (Levy et al., 2016). This conspicuous stratigraphic interval is characterised by very low amounts of pollen and spores and persistently low surface water temperature (SWT = upper 200 m of water column) (-1.3°C to 2.6°C) and is thought to have accumulated in a dark environment beneath semipermanent sea ice or an ice shelf. This episode of apparent environmental stability coincides with an interval characterised by low variability in sea level (Kominz et al., 2008) and orbital eccentricity (Laskar et al., 2004, 2011; Levy et al., 2016) (Fig. 9.11). During this time, the ice sheet margin retreated from the coast and the grounding zone remained distal to the AND-2A site through many glacial–interglacial cycles (~ 700 kyrs). Variability in the $\delta^{18}\text{O}$ record decreased during this interval but glacial–interglacial amplitudes still ranged between $0.6\text{\textperthousand}$ and 1\textperthousand (Fig. 9.11). Given the apparent relative stability of the adjacent ice sheet, much of the variability in the $\delta^{18}\text{O}$ record must have been driven by changes in bottom water temperature. Today, significant volumes of bottom water are generated in the Ross Sea (Carter et al., 2021; Orsi et al., 1999). If we assume similar quantities of Earth’s bottom water was generated in the Ross Sea during the early Miocene, then the 3°C to 4°C range of SWTs recorded in AND-2A through this interval may have driven changes in BWT of similar magnitude. Changes of 3°C to 4°C in BWT can explain between 90% and 100% of the total glacial–interglacial variation in the $\delta^{18}\text{O}$ records between 19.4 and 18.6 Ma (up to 0.88% if we apply 0.22% per 1°C of bottom water temperature change). It appears possible that terrestrial portions of the AIS remained relatively stable during intervals of low variability in Earth’s eccentricity while ocean temperature at high latitudes fluctuated up to 4°C . These observations highlight the potential for distinct sensitivities of the cryosphere and ocean to

climate and raise questions regarding the fundamental mechanisms and processes that drive change in Antarctica through time.

A second episode of early Miocene marine ice sheet advance across the Ross Sea is captured in both the AND-2A and IODP Site U1521 cores and by RSU5 (Pérez et al., 2021a) (Fig. 9.7D). Disconformity U2 removed sediments equivalent to ~900 kyrs of record from AND-2A and is overlain by a 100 m-thick diamictite dominated sequence that is sheared and deformed (Fielding et al., 2011; Passchier et al., 2011). The AND-2A U2 disconformity coincides with RSU5, which marks the base of RSS-3 and correlates to the bottom of Lithostratigraphic Unit VI at 566 mbsf in Site U1521, which is a thick progradational package (McKay et al., 2019; Pérez et al., 2021a). RSU5 is not interpreted as an erosive surface at Site U1521, but the overlying interbedded massive to stratified diamictite and mudstones in Lithostratigraphic Unit VI contain shell fragments and calcium carbonate nodules and concretions that reflect advance and retreat of glaciers south of the site in the central Ross Sea. These regional disconformities and diamictite dominated sequences along the western margin and across the central Ross Sea, suggest highly erosive ice sheets and glaciers extended well beyond the Antarctic coast into marine environments between 17.8 and 17.3 Ma (Levy et al., 2016, 2019; McKay et al., 2019). This marine-based ice sheet advance approximately coincides with a prominent sea level lowstand at the New Jersey margin (Kominz et al., 2008) (Fig. 9.11E), which supports significant ice sheet growth at this time. Whereas there is no obvious excursion in recent high resolution $\delta^{18}\text{O}$ compilations (De Vleeschouwer et al., 2017; Westerhold et al., 2020), the episode does coincide with the Mi1b isotope event (Miller et al., 1991a). Furthermore, this distinct episode of marine-based ice sheet advance occurs during a prominent peak in obliquity sensitivity and diatom turnover (Fig. 9.11I and J), which is inferred to reflect AIS expansion and enhanced connection between marine-based ice sheets and the Southern Ocean (Crampton et al., 2016; Levy et al., 2019). These observations show the AIS extended well beyond the TAM and periodically occupied large regions of the Ross Sea prior to the MMCT.

Retreat of the AIS from the Ross Sea Embayment during the MCO is captured by the 124 m-thick sequence of bioturbated diatomaceous mudstone with rare clasts that constitutes Unit III in IODP Site U1521 (McKay et al., 2019). The diatomaceous unit was deposited sometime between 17 and 15 Ma (McKay et al., 2019), is bounded by sequences that include diamictites and lacks evidence for proximal glacial influence. Sequences spanning the MCO in AND-2A contain diverse lithologies, lack massive diamictites (Fielding et al., 2011; Passchier et al., 2011) and indicate temperate wet-based glaciers calved at the coastline through glacial–interglacial cycles. Several units comprise sedimentary motifs and facies associations that indicate the grounding zone of the temperate glaciers that fed the basin were distal to the drill site. However, only three short interglacial intervals contain multiproxy data that suggest peak warmth and maximum ice margin retreat.

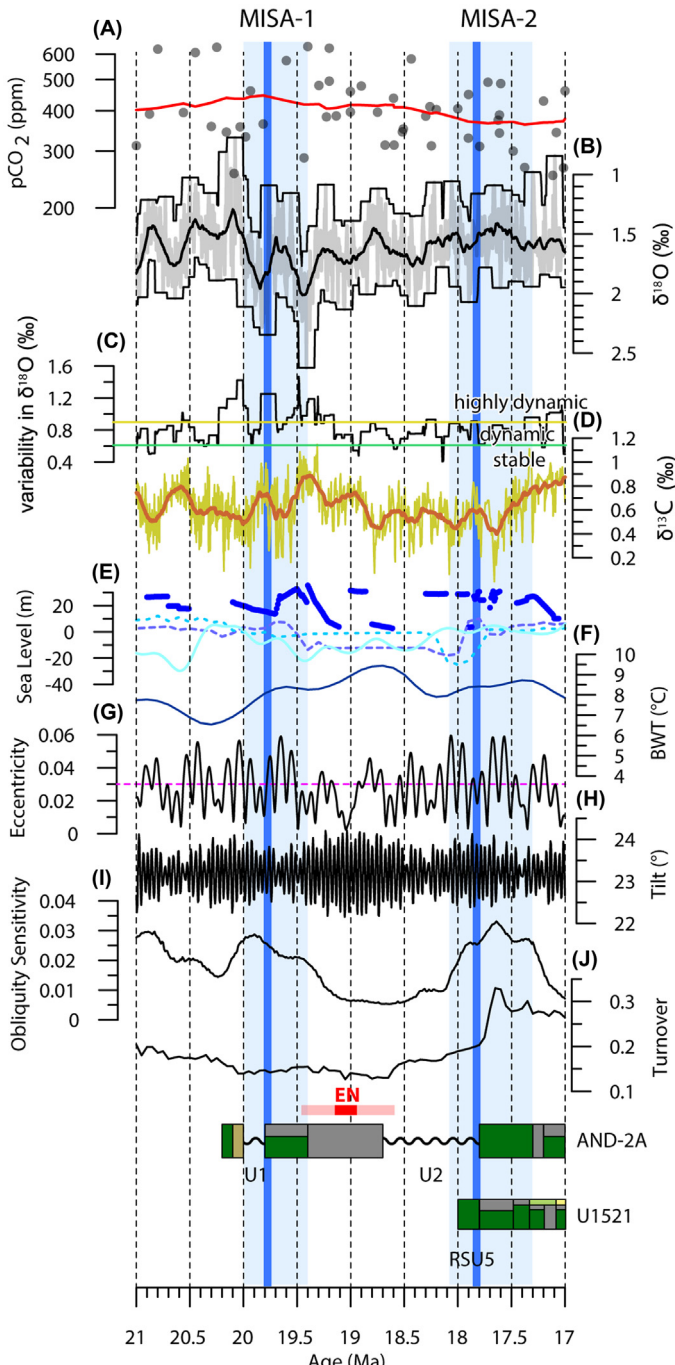


FIGURE 9.11 Environmental data from the early Miocene (21 to 17 Ma). (A) Atmospheric CO_2 compilation comprises data from a range of proxies outlined in Fig. 9.1. Solid red line displays a two million year moving average. (B) Splice of deep sea benthic foraminifera $\delta^{18}\text{O}$ data (light grey) reflect changes in ice volume and deep/bottom water temperature (De Vleeschouwer (Continued)

During the warmest of these events, SWT reached 10°C (Levy et al., 2016), diatoms and dinocyst abundance peaked, and podocarp and pollen numbers suggest tundra vegetation expanded (Griener et al., 2015; Warny et al., 2009) and perhaps reflect hydrologically active intervals during the MCO (Feakins et al., 2012). Two of these short intervals of maximum warmth captured in AND-2A (at ~16.4 and 16 Ma) coincide with oxygen and carbon isotope minima that mark intervals of unique peak warmth that align with 400 kyr eccentricity maxima (Holbourn et al., 2015).

Terrestrial environmental records through most of the MCO have not yet been recovered from the Ross Sea region. A ‘gap’ in the ash stratigraphy in the TAM occurs between the 19.76 Ma ash recovered from the Friis Hills (Lewis and Ashworth, 2015) and the oldest ash in the Asgard Range that dates to 15.15 ± 0.2 Ma (Marchant et al., 1993, 1996). Analyses of volcanic material in the AND-2A core indicate eruptions from Mount Morning continued throughout the MCO (Di Vincenzo et al., 2009; Nyland et al., 2013) so it is unclear why ash deposits from the mid Miocene are not present in the TAM. Perhaps the climate was highly variable and glaciers too dynamic and erosive through this interval to preserve sediments in the TAM? Two tephra layers have been recovered in drill cores from the central Friis Hills and indicate the sequence post-dates ~15 Ma (Chorley et al., 2021; Verret et al., 2020). Interglacial deposits contain a pollen assemblage characteristic of tundra vegetation that characterised the region since the late Oligocene. The search for Miocene terrestrial deposits should continue so that we can more

◀ et al., 2017). Solid black line displays a 150 kyr moving average. Maximum and minimum values are determined within each 150 kyr window and create the envelope (black lines) that bound the $\delta^{18}\text{O}$ data. (C) A $\delta^{18}\text{O}$ variability ‘index’, interpreted as a measure of glacial/interglacial variability, is determined by subtracting the maximum values in (B) from the minimum value, for each 150 kyr window. We indicate arbitrary ‘thresholds’ in these data (green and yellow solid lines) and suggest that values below 0.6% reflect a relatively ‘stable’ high latitude environment and values that exceed 0.9% indicate a highly dynamic environment with large changes in BWT and/or ice volume over glacial-interglacial time scales. (D) Yellow line shows high resolution deep sea benthic foraminifera $\delta^{13}\text{C}$ splice (Westerhold et al., 2020). Solid deep orange line displays a 150 kyr moving average. (E) Sea level curves are from Kominz et al. (2008) (pale blue dashed line), Kominz et al. (2016) (blue dots), Miller et al. (2005) (blue dashed line), and Miller et al. (2020) (pale blue line). (F) BWT data are derived from the compilation of Cramer et al. (2011) using Equation 7a (dark blue). (G) Astronomical eccentricity and (H) axial tilt (obliquity) from Laskar et al. (2011). (I) obliquity sensitivity after Levy et al. (2019). (J) Rate of diatom species extinction and speciation (turnover) after Crampton et al. (2016). Lithologic logs from the AND-2A and U1521 drill cores highlight disconformities (U1, U2, RSU5) and diamictite dominated intervals that are inferred to indicate marine ice sheet advances (MISA events) (Levy et al., 2016; McKay et al., 2019). Note that peak values in obliquity sensitivity and diatom turnover coincide with the MISA event between ~18 and 17.4 Ma. Red bars highlight an interval of low eccentricity that coincides with a thick mudstone unit in AND-2A and reflects a period of low variability in AIS grounding line variability and ‘stable’ glacial dynamics.

fully assess ice sheet and environmental sensitivity during peak warm intervals in the MCO.

In contrast to the MCO, terrestrial deposits that capture the transition into and through the MMCT in the Ross Sea Region are relatively common. The thickest, most continuous record occurs in the Friis Hills (Chorley, 2021; Lewis and Ashworth, 2015; Verret et al., 2020). Here, up to 80 m of strata described from outcrop (Lewis and Ashworth, 2015) and drillcore (Chorley, 2021; Verret et al., 2020) include approximately 15 glacial–interglacial cycles comprising diamictite, glacifluvial, and glaci lacustrine sediments. Most of the sediments assigned to the Friis Hills II lower sequence were deposited during the last few hundred thousand years of the MCO (~15 Ma). Diamictites in this sequence are muddy and were deposited beneath wet-based alpine glaciers. Interglacial units contain *Nothofagus* leaves, pollen and spores from a tundra vegetation, and freshwater diatoms. Friis II upper sediments are younger than 14.8 Ma (Verret et al., 2020) and contain diamictites with sedimentary features that suggest deposition under thicker ice and colder, drier climatic conditions (Lewis and Ashworth, 2015). Interglacial units still contain abundant evidence for liquid water across the region and fossil remains indicate tundra vegetation persisted through the MMCT to ~14 Ma (Valletta et al., 2015). Fossil-rich glacial-lacustrine deposits at Mount Boreas in the Olympus Range also show relatively warm and wet conditions persisted in the TAM through to at least 14.07 ± 0.05 Ma (Lewis et al., 2008). By 13.85 ± 0.03 Ma the climate had cooled by at least 8°C , muddy glacial diamictites were superseded by sandy sublimation tills indicative of drier conditions, and evidence for tundra vegetation had disappeared (Lewis et al., 2008; Lewis et al., 2007). Sedimentary deposits and geomorphological features in the Asgard Range generally support observations from sequences in the Friis Hills and Olympus Range. Wet based sediments deposited by alpine glaciers, including the Sessrumnir and Inland Forts tills, predate 15 and 13.5 Ma, respectively (Table 9.1). The laterally extensive Asgard Till is silt-rich, contains striated clasts, was deposited sometime between 13.6 and 15.2 Ma, and records expansion of a large glacier down the paleo Wright Valley (Marchant et al., 1993). Together, these terrestrial data indicate climate became colder and drier, and glaciers thicker and more extensive, during glacial episodes leading up to the final step of the MMCT between 13.9 and 13.8 Ma. But interglacial episodes remained relatively warm. These observations are reflected by an increase in glacial/higher values (colder/more ice) in the deep-sea $\delta^{18}\text{O}$ record between ~14.8 and 13.9 Ma while low interglacial/warm values (warmer/less ice) persisted until 13.9 Ma (Holbourn et al., 2014; Shevenell et al., 2004, 2008).

Marine sedimentary records support terrestrial evidence of progressive cooling and ice expansion during glacial episodes beginning at ~14.8 Ma. A major disconformity at 264 mbsf in the AND-2A core (U3) spans 14.6 to

15.8 Ma and coincides with the appearance of massive diamictites and associated facies that reflect a cold, subpolar/polar glacial regime with minor meltwater involvement (Fielding et al., 2011; Levy et al., 2016; Passchier et al., 2011). Another major disconformity at 214.13 mbsf separates sediments deposited at \sim 14.4 Ma from overlying sediments that are most likely younger than 11 Ma (Acton et al., 2008–2009). These two major unconformities are equivalent to RSU4, which suggests several shelf-wide advances of grounded marine-based ice originating from East Antarctica started between 14.8 and 14.6 Ma and continued through to \sim 11 Ma (Fig. 9.7D). This regionally extensive unconformity represents the first unequivocal seismic evidence for a glacially carved trough in the central Ross Sea (Anderson, 1999; Colleoni et al., 2018; De Santis et al., 1995; Ten Brink and Schneider, 1995). Approximately 250 m of till foreset and aggrading bottomset strata occur above RSU4 (De Santis et al., 1999) and RSU4 overlies outwash channels (tunnel valley features), suggesting the region was influenced by large volumes of erosive sediment-laden meltwater during glacial advance associated with the MMCT beginning at \sim 14.6 Ma (Anderson and Bartek, 1992; Chow and Bart, 2003; McKay et al., 2019; Pérez et al., 2021a).

Dissected drift sheets, potholes and subglacial melt channels at modern elevations $>$ 1000 m in the TAM provide evidence for glacial overriding event(s) in the middle Miocene (Sugden and Denton, 2004). The age of these features suggests ice flowing through the mountains reached its maximum thickness within 200 kyrs after the Mi3/E₃ isotope event and termination of the MMCT. For example, glacial plucking of bedrock and sedimentary deposits including the Circe and Electra tills in Western Olympus Range occurred between 13.62 and 12.44 Ma (Lewis et al., 2007). Formation of potholes and in the Asgard Range occurred after the Asgard Till was deposited between 15 and 13.6 Ma (Marchant, 1993; Sugden et al., 1995). Subglacial meltwater channels that characterise the Labyrinth formed beneath thick ice that flowed into the Wright Valley sometime between 14.4 and 12.4 Ma (Lewis et al., 2006). We note that evidence for subsequent overriding has not been recovered or reported, but that overriding events in the early and middle Miocene cannot be excluded.

The Cavendish Drift forms a series of stacked cycles of diamictite and fine-grained interbeds that blanket the southeastern margin of the Friis Hills (Lewis and Ashworth, 2015). Climbing ripples and crossbeds are common in sandy interbeds and rare dropstones are scattered throughout most beds. The sequence was deposited by wet-based ice but all beds are non-fossiliferous, which suggests tundra was no longer present in the region (Lewis and Ashworth, 2015). However, the climate was clearly warm enough during interglacial episodes to allow glacier surface melting and water to flow along the ice margin. The age of the drift is difficult to constrain; however, it truncates the Friis Hills II sequence so must be younger than 14 Ma (Lewis and

Ashworth, 2015; Valletta et al., 2015; Verret et al., 2020) and likely post-dates the episode of erosion and moulding of bedrock that occurred during glacial overriding between 13.6 and 12.4 Ma (Lewis and Ashworth, 2015; Lewis et al., 2007). A suite of $^{40}\text{Ar}/^{39}\text{Ar}$ dates indicate glacial drift was deposited on the Rhone Platform at the margin of a paleo Taylor Glacier between 10.76 and 10.39 Ma (Hartman, 1998). It is plausible that the most recent phase of downcutting of the Taylor Valley to its present depth and deposition of the Cavendish Drift occurred between \sim 11 and 10 Ma.

Geological data from neighbouring Wright Valley support a late Miocene age for the formation of modern valley topography in the MDV. Fossil marine diatoms in the Jason Diamicton deposited on the floor of the Wright Valley (Brady, 1982) indicate glacial expansion and erosion during and after the MMCT had cut the valley to its present depth sometime between 13.66 and 9.23 Ma. Furthermore, strontium isotope dates on fossil shells suggest the marine incursion that formed the deposit within the Wright Valley marine fjord occurred after 10.5 Ma (Prentice et al., 1993, 1999). This date aligns with the postulated age of deposition of the Cavendish Drift (Lewis and Ashworth, 2015). Furthermore, it coincides with the transition from diamictite-dominated sequences of Motif 1 below 1060 mbsf in AND-1B to deposition of mudstone-dominated Motif 3 (McKay et al., 2009; Wilson et al., 2012b). This distinct change in facies in AND-1B reflects an environmental shift in the western Ross Sea at \sim 10 Ma from a polar glacial regime to a subpolar meltwater dominated system that was similar to Spitsbergen today (McKay et al., 2009; Rosenblume and Powell, 2019; Wilson et al., 2012b). Sequence 67 occurs between 101.03 and 142.34 mbsf in the AND-2A core and includes an \sim 25 m-thick stratified sandstone that reflects a high-latitude temperate glacial regime with wet-based glaciers (Fielding et al., 2011; Passchier et al., 2011). Two reworked lava clasts within the sequence are dated at 11.43 ± 0.46 and 11.363 ± 0.072 Ma and provide a maximum age for the sediments (Di Vincenzo et al., 2009). The first appearance of the planktic foraminifera, *Neogloboquadrina pachyderma* at 83.80 mbsf in AND-2A indicates sediments above this depth must be younger than 11.04 Ma (Acton et al., 2008–2009; Patterson and Ishman, 2012). Together these chronostratigraphic data suggest that sequence 67 is \sim 11 Ma or younger. Evidence for ice free marine fjords in the Dry Valleys and subpolar and temperate conditions in drillcores from McMurdo Sound indicate that climate warmed and ice retreated inland between \sim 11 and 8 Ma, well after the end of the MMCT.

Sedimentary deposits from the latest Miocene (8 to 5.5 Ma) are relatively rare in the Ross Sea region (Figs 9.5 and 9.7). Preliminary age analysis of cores from IODP Expedition 374 indicate a late Miocene hiatus from \sim 9 to 5.5 Ma (McKay et al., 2019). This disconformity ties with RSU3, which defines major cross-shelf paleotroughs and is associated with enhanced progradation of the continental shelf into the Eastern Ross Sea (Bart and De

Santis, 2012; Chow and Bart, 2003; De Santis et al., 1995). RSU3 reflects expansion of marine based WAIS in the eastern Ross Sea, that likely coalesced with ice derived from the EAIS to drive continental shelf wide advances of marine-based ice sheets across the Ross Sea (De Santis et al., 1995; 1999). The latest Miocene record in the AND-1B drill core comprises an ~175 m-thick volcanic sequence (Di Roberto et al., 2010; Krissek et al., 2007a; McKay et al., 2009). The sequence is subdivided into a 70 m-thick succession of volcanic-rich mudstone and sandstone and a 105 m-thick section of interbedded tuff, lapilli tuff and volcanic diamictite that were deposited in an open water ice free environment. $^{40}\text{Ar}/^{39}\text{Ar}$ dates on a 2.81-m-thick lava flow in the middle of the sequence indicates the sequence was deposited around 6.48 Ma. Seismic and drill core data from the central Ross Sea show marine-based ice advanced across large areas of the Ross Sea in the late Miocene, but evidence from AND-1B also shows the ice sheet also episodically retreated to the terrestrial continental margin.

Importantly, the ‘missing record’ spanning ~8 to 5.5 Ma and inferred frequent expansion and retreat of a marine-based AIS associated with RSU3, approximately coincides with the episode of late Miocene cooling observed across our planet (Herbert et al., 2016; Holbourn et al., 2018). Furthermore, cosmogenic nuclides in the AND-1B core suggest major retreat at the terrestrial margins of the AIS along the TAM front has been minimal since ~8 Ma (Shakun et al., 2018). Cosmogenic nuclide studies have also been used to constrain the onset of persistent aridity in the MDV and East Antarctica. Specifically, meteoric ^{10}Be ($^{10}\text{Be}_{\text{met}}$) is a tracer of water infiltration and its migration in permafrost soils (Dickinson et al., 2012). $^{10}\text{Be}_{\text{met}}$ is formed in the upper atmosphere by cosmic rays and is transferred to Earth’s surface by precipitation or deposition of dust. $^{10}\text{Be}_{\text{met}}$ nuclides can move into soils by infiltration and clay illuviation, making it a suitable environmental tracer of water movement through soil profiles over million-year timescales. Analysis of meteoric beryllium ($^{10}\text{Be}_{\text{met}}$) in the MDV suggests water infiltrated stable upland soils until ~6.6 Ma but has not penetrated since (Dickinson et al., 2012). It appears that the dry and arid polar climate that characterises Victoria Land and the MDV today, first became a persistent feature of the Antarctic climate during the peak cold of the late Miocene.

SSTs data from several ocean basins and across a range of latitudes indicate global climate warmed again in the early Pliocene (Fig. 9.4H) (Herbert et al., 2016). Diatomites in AND-1B indicate frequent collapse of the WAIS through the Pliocene. Diatom assemblages and geochemical paleothermometry indicate ocean temperatures were as much as 4°C warmer than present during the warmest interglacial episodes (McKay et al., 2012; Naish et al., 2009). Contemporaneous paleothermometry data from the nearby DVDP-11 drill core indicates Taylor Fjord surface waters were up to 5°C warmer than today (Ohneiser et al., 2020). Despite climatic warming, the hyper arid

conditions that were established along the Victoria Land Coast at \sim 6 Ma appear to have persisted into the Pliocene. Fine grained sedimentary lithofacies in AND-1B are dominated by pelagic diatom ooze, indicating that the offshore environment was starved of terrigenous sediment supply and melt-water discharge was reduced during Pliocene interglacials. These facies are a stark contrast to the thick (10s of metres) glaciomarine mudstone-rich facies deposited during late Miocene interglacials that indicate large volumes of turbid outwash from marine and/or terrestrial-terminating glacial systems (McKay et al., 2009; Rosenblume and Powell, 2019).

A relatively thick diatomite sequence in the AND-1B core, deposited between 3.6 and 3.4 Ma, indicates warmer-than-present conditions persisted in the western Ross Sea into the early late Pliocene. However, a cooling trend is reflected in diatom assemblage data from the diatomite (McKay et al., 2012; Winter et al., 2010a, 2010b). A thick diamictite overlies the diatomite and indicates readvance of grounded ice from West Antarctica beginning at 3.4 Ma. Subsequent diatomite units contain diatom assemblages that indicate colder conditions and more persistent winter sea ice (McKay et al., 2012). The last major expansion of a wet-based glacier from the EAIS through the Wright Valley deposited the Peleus Till sometime between 3.5 and 3 Ma (Table 9.1) (Levy et al., 2012). Sand-rich alpine drift deposits were deposited between 3.8 and 3.3 Ma (Table 9.1) (Levy et al., 2012). Plant biomarkers in the DVDP-11 indicate vegetation disappeared from coastal regions of the Taylor Valley at some time between 3 and 4 Ma. This transition from silt- to sand-rich glacial deposits along valley floors in the MDV indicates a shift from wet- to cold-based glacial conditions occurred between 3.5 and 3 Ma. This observed readvance of marine ice sheets and transition from wet to dry glacial conditions in the lower MDV coincides with the major M2 glaciation recorded in $\delta^{18}\text{O}$ records (Lisiecki and Raymo, 2005). By \sim 3.0 Ma, relatively thick packages of diamictite and gravel dominated sediment accumulated in DVDP-10 and -11 at the mouths of the fjord valleys, indicating the drill sites were often covered by grounded ice, thick multiyear sea ice or an ice shelf (Levy et al., 2012).

Paleobathymetric reconstructions suggest that RSU2 formed as the continental shelf in the Ross Sea deepened inland of the continental shelf margin (De Santis et al., 1999). Overdeepening developed as marine-based ice sheets expanded and retreated across the Ross Sea continental shelf eroding middle and late Miocene sediments below RSU3. Most of the eroded sediment was transported to the continental shelf break and redeposited on the upper slope to form large trough-mouth fans (Colleoni et al., 2018; Cooper et al., 2008; De Santis et al., 1999). While the age of RSU2 is poorly constrained, we hypothesise the initial erosional event that formed this basin-wide unconformity coincided with the M2 isotope event and the transition to ‘near modern’ polar conditions in the Ross Sea between 3.4 and 3 Ma (Levy et al., 2012; McKay et al., 2012).

9.3 Numerical modelling

9.3.1 Miocene

Although there have been relatively few modelling studies of the Miocene AIS, efforts are increasingly shifting to examination of this important interval in Earth's climate history (Steinthorsdottir et al., 2020). Until recently, most ice sheet model (ISM) studies that have covered the Miocene have been long-duration simulations spanning multiple epochs or idealised studies representative of a Miocene-like Antarctic (De Boer et al., 2010; Huybrechts et al., 1993; Langebroek et al., 2009, 2010; Pollard and DeConto, 2005, 2020). Only a few recent modelling studies have specifically targeted the Miocene AIS (Colleoni et al., 2018; Gasson et al., 2016b; Halberstadt et al., 2021; Stap et al., 2019) and only recently with an Antarctic topography appropriate for the Miocene (Paxman et al., 2020). In contrast to the Pliocene (covered in the next section), there are some unique modelling challenges presented when simulating the Miocene. Intervals of the Miocene were warmer and with higher concentrations of atmospheric CO₂ (Foster et al., 2012; Greenop et al., 2014). There was greater retreat of the AIS causing greater variability in sea level (Lear et al., 2010; Miller et al., 2020). In the mid-Pliocene, ice sheet retreat was centred on the large subglacial basins of Antarctica; however, during the mid-Miocene, there was additional retreat of the terrestrial ice sheet, grounded above sea level (Gasson and Keisling, 2020). At times during the Miocene, it is likely that surface temperatures were warm enough to generate widespread surface melting of the ice sheet, although the extent of this retreat is difficult to constrain (Fielding et al., 2011; Levy et al., 2016; Passchier et al., 2011; Sangiorgi et al., 2018). Simulating this magnitude of retreat with ISMs has proven difficult (Foster and Rohling, 2013).

The first simulations of a Miocene-like AIS were transient simulations run from the onset of Antarctic glaciation across the EOT (Pollard and DeConto, 2005). These experiments showed that to reproduce the large ice volume changes inferred for the Miocene from oxygen isotope and sea level records at the time (Kominz et al., 2008; Miller et al., 2005; Zachos et al., 2001b) required a large climate forcing. This is needed to overcome the strong cooling caused by the elevation feedback during the ice sheet growth (Oerlemans, 2002). This feedback is further strengthened by albedo feedback, meaning early simulations required an Antarctic warming of ~15°C (Huybrechts et al., 1993) or an increase of atmospheric CO₂ to ~8x pre-industrial concentrations (Pollard and DeConto, 2005) to produce a negative surface mass balance and retreat of the Miocene Antarctic Ice Sheet. This is much higher than proxy records of atmospheric CO₂ for the mid-Miocene and therefore presented an enigma known as the Antarctic Ice Sheet hysteresis problem (Foster et al., 2012).

As this effect is also seen in long-term future simulations of the AIS ([Garbe et al., 2020](#)), the Miocene is an important test-bed for this effect.

Another way to simulate relatively large magnitude of AIS retreat with lower atmospheric CO₂ requires greater polar amplification than is currently simulated by coupled ocean-atmosphere climate models ([Langebroek et al., 2009](#)). [Langebroek et al. \(2009, 2010\)](#) used a reduced complexity climate box model and a 2-d ISM, which allowed them to increase or decrease Antarctic polar amplification. This study showed that when polar amplification increases, AIS hysteresis is reduced, and ice sheet retreat can be initiated at a lower concentration of atmospheric CO₂ than in the study of [Pollard and DeConto \(2005\)](#). However, the cause of this inferred increase in polar amplification in the Miocene has yet to be explored or explained. In a follow-up study, [Langebroek et al. \(2010\)](#) added oxygen isotope tracing to their model and showed that changes in the oxygen isotope composition of the ice sheet could have caused part (15%) of the shift in the oxygen isotope composition of sea water across the middle-Miocene, with the remaining 85% of the shift caused by a change in ice volume.

[Gasson et al. \(2016b\)](#) simulated a dynamic Miocene AIS (~35 m sea level equivalent changes) that was consistent with oxygen isotope records ([Lear et al., 2010](#)) and atmospheric CO₂ reconstructions ([Foster et al., 2012; Greenop et al., 2014](#)). However, they showed smaller changes in sea level than some recent reconstructions ([Miller et al., 2020](#)). In their simulations, increased retreat of the ice sheet was achieved with a high resolution asynchronously coupled ice sheet and climate model. Use of a high-resolution regional climate model allowed processes in the narrow Antarctic ablation zone to be captured. As a result, feedbacks from retreating ice on the climate were simulated, which caused a positive feedback that increased surface melting. [Gasson et al. \(2016b\)](#) also simulated changes in the oxygen isotope composition of the Antarctic Ice Sheet, following [Langebroek et al. \(2010\)](#) but with 3-d isotope tracing. Modelled changes in the oxygen isotopic composition of the ice sheet could explain ~45% of the change in the oxygen isotope composition of seawater, with the rest caused by ice mass. Importantly, this feature is something that is not accounted for in the sea level reconstruction of [Miller et al. \(2020\)](#), which may partially explain the discrepancy between those studies.

Recent transient simulations of the Miocene ice sheet suggests a highly dynamic AIS occupied Antarctica during the Miocene ([Stap et al., 2019](#)). [Stap et al. \(2019\)](#) used the COSMOS climate model, which shows a particularly strong sensitivity to a change to Miocene boundary conditions, with an increase in the global mean temperature of 2.4°C with pre-industrial CO₂ relative to a control simulation ([Stap et al., 2017, 2019; Stärz et al., 2017](#)). They highlight that transient simulations show a smaller change in volume (~66%) when compared to equilibrium simulations. This difference is largely because, in the transient simulations (and reality), the ice sheet does

not reach equilibrium with the surface climate because of a continually changing orbit. The strength of this effect will depend on how quickly the ice sheet responds to the climate forcing and highlights the possibility that equilibrium simulations may overestimate ice sheet response to climate forcing (Stap et al., 2019).

Other transient ice sheet simulations have been run across several geological epochs, including the Miocene (De Boer et al., 2010), using an inverse routine (Van de Wal et al., 2005) to force a one-dimensional ISM using the benthic $\delta^{18}\text{O}$ record (De Boer et al., 2010). This simple model produced a solution for surface temperature, ice volume and benthic $\delta^{18}\text{O}$ (De Boer et al., 2010) and atmospheric CO₂ (Stap et al., 2017). The major strength of this approach is that it calculated a self-consistent high-resolution record of Antarctic ice volume (De Boer et al., 2010), but it lacks a predictive capability as it is forced with proxy ice volume reconstructions. Therefore, the paleo data cannot be used to evaluate the model, nor can the model be used to make inferences about the future response of the AIS to climate changes. This second issue has been addressed by including atmospheric CO₂ in the inversion scheme (Stap et al., 2017). This study explored two components of the AIS hysteresis – height mass balance feedback and albedo feedback. Results showed that, for cooler climate states, albedo is the stronger feedback on the AIS, whereas in a warmer Miocene-like state the two feedbacks are balanced in strength (Stap et al., 2017).

Bed topography is one of the most important boundary conditions for an ISM and, until recently, an Antarctic topography for the Miocene has not been available. Studies have variously used the modern-day bed topography or created idealised ‘Miocene-like’ topographies by scaling between modern-day and an earlier reconstruction for the ice-free Antarctic of the late Eocene (Colleoni et al., 2018; Gasson et al., 2016b; Wilson et al., 2012a). Such studies used an idealised topography to show how the evolution for the continental shelf around Antarctica changed the ice sheet sensitivity to climate forcing, with the ice sheet effectively increasing its own sensitivity to ocean forcing. On a smaller scale, Halberstadt et al. (2021) investigated how the elevation and uplift of the TAM affected sensitivity to climate forcing in that sector. The publication of reconstructed Miocene Antarctic topography (Paxman et al., 2019b) and bathymetry (Hochmuth et al., 2020) allowed these processes to be explored in more detail and with greater confidence. Paxman et al. (2020) quantified how changing Antarctic bed has increased ice sheet sensitivity. Using an equivalent climate forcing, they found that the modern-day AIS is ~28% more sensitive to climate forcing than the mid-Miocene AIS. This result is sobering given the magnitude of sea level swings observed in the Miocene.

The climate forcing used in the studies discussed above has been ad-hoc, without a consistent set of boundary conditions (e.g., paleogeography) adopted in the various climate models used (Burls et al., 2021). A new

initiative, MIOMIP (the Miocene model intercomparison project) is seeking to change this. This will allow a clearer examination of what impact the climate forcing and the climate model used has on simulations of the Miocene AIS and how polar amplification varies across models. This is something that has been successfully achieved for the Pliocene (Dolan et al., 2018) (see below).

9.3.2 Pliocene

Over the last decade, there has been a rapid increase in efforts to understand both the broader climate of the Pliocene from a modelling perspective (for example the Pliocene Model Intercomparison Projects [PlioMIP] 1 and 2) (Haywood et al., 2013, 2020) and to also provide well-constrained geological data to assess global modelling results (Dowsett et al., 2019; McClymont et al., 2020; Tierney et al., 2019). There have also been several different and evolving approaches to understand the stability of the AIS using computer models. Building on efforts from the geological proxy data community to understand in detail specific regions or glacial drainage basins (Cook et al., 2013; Naish et al., 2009; Passchier, 2011; Patterson et al., 2014; Williams et al., 2010), and reconstructions of Pliocene sea level (Dumitru et al., 2019; Dutton et al., 2015; Grant et al., 2019; Miller et al., 2012), ice-sheet modellers have primarily focussed on reconstructing the broad-scale extent of Antarctica during this warm interval and, in that, understanding potential areas of ice sheet instability for the past and future AIS and also the impact of changes on global mean sea level (de Boer et al., 2015; DeConto and Pollard, 2016; DeConto et al., 2021; Dolan et al., 2018; Gasson et al., 2016a; Golledge et al., 2017b).

Some of the first ISM simulations that focused on the mid-Pliocene Warm Period (mPWP; 3.264–3.025 Ma) identified the WSB and ASB as areas that were most susceptible to increased temperatures (Hill et al., 2007). These studies used climatological forcing fields (temperature and precipitation) from a coupled atmosphere-ocean general circulation model (GCM; HadCM3), which had been set up with Pliocene boundary conditions, to force an offline shallow-ice approximation (SIA) ISM over East Antarctica (Hill et al., 2007). Hill et al. (2007) simulated retreat which was broadly in line with Pliocene sea-level high-stand estimates at that time (Dowsett and Cronin, 1990). Using a similar modelling framework, Dolan et al. (2011) tested the impact of Pliocene-specific extremes in orbital forcing on reconstructions of the EAIS ice sheet size, showing a possible global sea level high stand of $\sim + 21$ m under high Southern Hemisphere (SH) summer insolation scenarios. The area of EAIS retreat was again restricted to the WSB and ASB, but the overall approach was limited by the more simplistic modelling framework employed.

Simulations of the WAIS and marine-basins of the EAIS require models with the enhanced capability to simulate grounding line and ice shelf dynamics (termed shallow-shelf approximation dynamics), in addition to shallow ice approximation dynamics (SIA-SSA ISMs). Such a model, which included these dynamics and a parameterisation of the grounding line movement, was employed by [Pollard and DeConto \(2009\)](#) to simulate the evolution of the WAIS over the last 5 Ma. For the Pliocene portion of the record, the modelling results showed good agreement with the ANDRILL-1B records ([Naish et al., 2009](#)) and indicated rapid transitions with the WAIS collapsing periodically to leave only small isolated ice caps on the West Antarctic islands. However, for these simulations, only marginal ice sheet retreat in East Antarctica was demonstrated. This differs from other modelling results mentioned previously, using solely shallow ice approximation dynamics, with this difference explained by a stronger climate model forcing arising from the PRISM3 boundary conditions in the studies of [Hill et al. \(2007\)](#) and [Dolan et al. \(2011\)](#).

Inconsistencies between continental scale retrodictions of AIS extent led to efforts for a more structured assessment comparing modelled predictions of ice sheets for the Pliocene (e.g., the Pliocene Ice Sheet Modelling Intercomparison Project; PLISMIP) ([de Boer et al., 2015; Dolan et al., 2018, 2012; Yan et al., 2016](#)). [de Boer et al. \(2015\)](#) coordinated simulations from six SIA-SSA ISMs to simulate the complete Antarctic domain (including grounded and floating ice). HadCM3 climate fields from simulations comparable to those used in PlioMIP1 experiment ([Bragg et al., 2012](#)) were used to force the ISMs offline. [de Boer et al. \(2015\)](#) tested multiple scenarios within the modelling framework including the impact of different ISM initialisation methods (e.g., starting with a present-day AIS or with a reduced Pliocene AIS) and also the impact of different underlying bedrock topographies including Bedmap1 ([Lythe et al., 2001](#)) and Bedmap2 ([Fretwell et al., 2013](#)). One key result from this study was that none of the models using Bedmap1 predicted a retreat of the EAIS across the WSB and ASB as has been suggested by studies of marine sediments ([Cook et al., 2013](#)) and previous simulations. Our understanding of the vulnerability of different sectors of the ice sheet continues to evolve as improvements to bedrock topography reconstructions of Antarctica ([Morlighem et al., 2020](#)) and the identification of new subglacial basins (e.g., Recovery Basin). Reconstructions of the Antarctic topography during the geological past by accounting for the effects of glacial erosion and tectonics are also highlighting how the ice sheet sensitivity to basal conditions has changed through time ([Colleoni et al., 2018; Paxman et al., 2020](#)). Importantly, these reconstructions show minimal differences in Antarctic topography between the Pliocene and present-day, making the Pliocene a more suitable analogue for future warming than geological periods further back in time ([Paxman et al., 2019b, 2020](#)). However, [Austermann et al. \(2015\)](#) additionally show that factors such as

dynamic topography related changes in bed elevation (not accounted for in the reconstructions of [Paxman et al., 2019b](#)) during the Pliocene can also have a significant effect on the predicted stability of ice in the marine-based WSB.

Following a similar experimental design to [de Boer et al. \(2015\)](#), [Dolan et al. \(2018\)](#) used results from PlioMIP1 ([Haywood et al., 2011, 2013](#)) to test the dependency of reconstructions of the mid-Pliocene AIS on the climate model used to provide the climate forcing fields to an ISM. The outputs of seven fully coupled atmosphere-ocean climate models were used to predict the whole AIS using three ISMs (of differing levels of complexity). [Dolan et al. \(2018\)](#) showed mean sea level changes relative to the pre-industrial control simulations of $+7.8 \pm 4.1$ m for simulations starting from a reduced (PRISM3) ice sheet, and $+2.4 \pm 3.5$ m for those starting from a present-day AIS configuration within the ISMs. It was demonstrated that there is a high level of model dependency on predictions of AIS extent and volume, and that this is exacerbated by imposed initial conditions (e.g., the PRISM3 AIS) that are a necessary requirement of the coupled atmosphere-ocean GCM modelling framework (e.g., choice of AIS configuration in the underlying climate model, the impact of bedrock topography and the initial conditions within the ISM). Despite the broad range in climate forcing from the different GCMs used, none of these simulations showed retreat of the EAIS grounding line.

Despite uncertainties in geological reconstructions of Pliocene sea level, the Pliocene has also been used as a calibration target for ISMs in order to predict future sea-level rise. ISM experiments that are set-up to perform well in simulating Last Interglacial (LIG) and Pliocene sea level show that Antarctica has the potential to contribute more than a metre of sea-level rise by 2100 in the future if emissions of greenhouse gases continue unabated ([DeConto and Pollard, 2016](#)). Simulations set up for the Pliocene that use climatological inputs from a Regional Climate Model (RCM) configured with a warm austral summer orbit, atmospheric CO₂ at 400 ppmv, and 2°C of ocean warming imposed within the model, suggest that Antarctica can contribute up to 11.3 m of sea-level rise ([DeConto and Pollard, 2016](#)). Significant ice sheet retreat in these simulations occurred within marine basins of WAIS and EAIS (particularly around the present-day Ninnis, Mertz, Totten and Recovery glaciers in East Antarctica). One key difference between this work and previous modelling was the implementation of new processes, based on theoretical work ([Bassis and Walker, 2012](#)), which link atmospheric warming with hydrofracturing of buttressing ice shelves and the structural collapse of marine terminating ice cliffs (termed the Marine Ice Cliff instability or MICI) ([DeConto and Pollard, 2016; Pollard et al., 2015](#)). However, observational evidence for MICI is minimal, largely because the conditions that would trigger it have not yet been met in Antarctica. There is also considerable debate

about the theoretical basis of this process, in particular whether ice shelves can be removed rapidly enough to leave behind vulnerable ice cliffs (Robel and Banwell, 2019), whether surface meltwater can be efficiently removed from the ice shelf surface (Bell et al., 2017), and what the critical failure height of sheer ice cliffs is and how this depends of the extent of crevassing (Clerc et al., 2019). Marine-terminating glaciers of the Greenland Ice Sheet such as Jackobshavn Isbrae provide better insight into whether this process is plausible (Parizek et al., 2019). However, the relatively narrow channels of these glaciers, which have a strong seasonal cycle in calving which is arrested by ice melange during winter (Joughin et al., 2020), mean that they are not directly comparable to calving fronts of Antarctic glaciers, which can be tens of kilometres wide. There is also debate about whether these additional mechanisms are needed to explain Pliocene sea levels (Edwards et al., 2019; Gasson et al., 2016a; Gasson and Keisling, 2020). Low end estimates of Pliocene sea level (Miller et al., 2019; Raymo et al., 2018) can be explained with existing ISM physics (Edwards et al., 2019). Although there is continued debate around MICI, more recent modelling by DeConto et al. (2021) has reiterated the importance of ice-cliff calving in order to improve geological data-model comparisons and to constrain ISM physics in climate states that are warmer than seen in the satellite era. DeConto et al. (2021) show a maximum GMSL contribution of 20.85 m from their Pliocene Antarctic simulation, which is consistent with recent geological observations (Dumitru et al., 2019; Grant et al., 2019). In this study, sea level estimates from the Pliocene and LIG were used alongside observed ice loss between 1992 and 2017 (Shepherd et al., 2018) to predict future scenarios of ice sheet retreat for the Antarctic ice sheet. A median value of 34 cm by 2100 is predicted for the AIS contribution to GMSL for global mean warming limits of +3°C (DeConto et al., 2021). Improved model physics and revised atmospheric forcing in this study relative to DeConto and Pollard (2016) explain the discrepancy in future estimates of change at 2100, although the contribution to GMSL does reach 1 m by 2125. Without the Pliocene sea level constraint, these future projections have larger uncertainties (DeConto et al., 2021).

Golledge et al. (2017b) have also investigated Antarctic climate and ice sheet configuration during the early Pliocene (c.4.23 Ma). Using a regional climate model (RegCM3) coupled offline to the PISM (Parallel Ice Sheet Model) three-dimensional, thermodynamic SIA-SSA ISM, alongside a new synthesis of high-latitude paleoenvironmental proxy data to define a probable climatic envelope, they simulate an AIS contribution of 8.6 ± 2.8 m to GMSL. In the simulations presented by Golledge et al. (2017b), substantial grounding-line retreat is evident in the WSB, but the Aurora and Recovery basins are less affected by early Pliocene conditions (Dolan et al., 2011). The ISM used in this study includes a sub-grid grounding line melt

mechanism, which is used as a way of compensating for the low spatial resolution of the model. However, there is debate about this parameterisation, and experiments with higher resolution models have shown that it may overestimate ocean melting at the grounding line and generate numerical errors (Cornford et al., 2020; Seroussi and Morlighem, 2018). In their simulations the WAIS is deglaciated, with only some ice remaining on the West Antarctic islands. These results are corroborated by evidence for vegetation at the margins of a fjord in the Taylor Valley, Southern Victoria Land during the early Pliocene (Ohneiser et al., 2020). Model-based predictions for vegetation in this area are most compatible with simulations that show a complete collapse of the WAIS and significant retreat of the EAIS from the subglacial basins (including Wilkes) (Ohneiser et al., 2020).

When the modelling and the data communities work in combination to tackle a challenge there is potential for significant progress in our understanding of the nature of specific characteristics of the Pliocene AIS over the coming years. For example, cosmogenic nuclide exposure ages alongside ice sheet modelling have been used to suggest that the EAIS continental interior could have been up to 600 m higher than present around the mid-Pliocene (Yamane et al., 2015). Sediment provenance records derived from $^{40}\text{Ar}/^{39}\text{Ar}$ ages of hornblende grains from ODP Site 1165 near Prydz Bay have been combined with iceberg trajectory modelling to understand the record of IRD during the Pliocene (Cook et al., 2014). This demonstrated, that declining SSTs over the period of the mid-Pliocene allowed Wilkes Land icebergs to travel further before melting.

Oxygen isotope data (Miller et al., 2012; Winnick and Caves, 2015) combined with simulations of the oxygen isotope composition of the AIS for a range of configurations have also added to our understanding of the impact of changes to the Pliocene AIS on sea level (Gasson et al., 2016a). Gasson et al. (2016a) were able to identify ice sheet configurations that are consistent with the oxygen isotope record and conclude that a maximum contribution of ~ 13 m to Pliocene sea level highstands should be expected from Antarctica. However, there are additional uncertainties in this method that hinder accurate results (Raymo et al., 2018), determining the temperature contribution to changes in the oxygen isotope composition of benthic foraminifera is particularly difficult. There is no current consensus on the Pliocene sea level high stand using this approach.

Finally, there has been a recent focus on reconstructing the transient nature of Pliocene ice sheets (Berends et al., 2019; de Boer et al., 2017). Berends et al. (2019) used a coupled hybrid ice-sheet-climate model and a matrix method using fields from snapshot climate model simulations to reconstruct ice sheet geometry and sea level over the Late Pliocene (3.6 to 2.58 Ma). Combined simultaneous simulations of the Northern Hemisphere ice sheets and AIS, suggested a sea level drop of ~ 16 m at MIS M2, associated with a significant expansion of the AIS and surrounding ice shelves.

9.4 Synthesis/summary of key climate episodes and transitions in Antarctica through the Miocene and Pliocene

9.4.1 Early to mid-Miocene

While there is evidence that Antarctica's ice margins periodically extended into marine settings prior to the Neogene (Barrett, 1989; Carter et al., 2017; Galeotti et al., 2016; Gulick et al., 2017; Levy et al., 2000; Wilson et al., 1997), geological data suggest the first major expansion of marine ice sheets in Antarctica occurred at the Oligocene/Miocene transition (see Naish et al., 2021). Sedimentary facies analysis from drill cores (Naish et al., 2001a, 2001b), seismic data (Sorlien et al., 2007b) and geochemical proxies (Duncan et al., 2019) show that large regions of the AIS advanced into marine environments in the Ross Sea during the latest Oligocene and formed a major disconformity at ~ 23 Ma (Florindo et al., 2005; Kulhanek et al., 2019). Furthermore, an increase in mass transport deposits and ice rafted debris in the latest Oligocene a major regional unconformity (WL-U5) corresponding to a major hiatus within lower Miocene rocks at Site U1356 (Bijl et al., 2018a, 2018b; Escutia et al., 2011a; Hartman et al., 2018) suggests significant environmental change occurred across the O/M at the George V and Adélie Coasts and supports a shift to a glacial regime in which marine-ice sheet advance became more frequent. Together these data suggest that the O/M transition and Mi1 oxygen isotope event record the first extensive advance of Antarctica's ice sheets and ice caps into marine environments (Bart and De Santis, 2012; De Santis et al., 1995; Escutia and Brinkhuis, 2014; Escutia et al., 2011a; Levy et al., 2019; Sorlien et al., 2007b).

Climatic warming in the earliest Miocene ended the transient glacial advance recorded by the Mi1 isotope event (Naish et al., 2021), although we note that pollen data suggest climatic conditions in the Ross Sea embayment in the early Miocene were similar to those that characterised the late Oligocene (Kulhanek et al., 2019; Prebble et al., 2006). Proxy data suggest atmospheric CO₂ increased in the early Miocene, from values <300 ppm that characterised the Mi1 oxygen isotope event, to average concentrations around 400 ppm (Figs 9.1 and 9.13). These data support other studies that suggest 400 ppm is a threshold for marine glaciation, below which climatic conditions in the high southern latitudes are conducive to the advance of marine-based ice sheets (Gasson et al., 2016b; Halberstadt et al., 2021; Levy et al., 2019, 2016; Naish et al., 2009). Evidence for episodic advance of the AIS margin well beyond the present coastline and into glacial marine settings during the early and middle Miocene is captured by U-shaped valley features within lower to middle Miocene strata (RSS2 and RSS3) offshore of the outlet glaciers along the Southern Victoria Land coast (Brancolini et al., 1995). Thick prograding wedges characterise strata within RSS3 at many locations across the Ross Sea (De Santis et al., 1999; Pérez et al., 2021a) and

in seismic sections through the continental shelves offshore George V Land and the Adélie Coast (Eittreim et al., 1995, 2011a) and suggest glacimarine and subglacial depositional environments across the continental shelves during the early to early middle Miocene.

Whereas the age of Sirius Group rocks at locations across the TAM is mostly poorly constrained (Barrett, 2013; Scherer et al., 2016; Webb et al., 1984), the location of diamictite-rich units at Table Mountain inland of, and higher than, middle Miocene deposits in the Asgard and Olympus Ranges and Friis Hills, suggest they were potentially deposited during the early Miocene (Lewis and Ashworth, 2015). We hypothesise that these glacial sediments were deposited during episodes of ice sheet expansion that coincide with disconformities and diamictite-dominated units at Sites AND-2A (Levy et al., 2016; Passchier et al., 2011) and U1521 (McKay et al., 2019). One of these episodes of major marine ice sheet expansion occurred between 18 and 17 Ma and coincides with a significant fall in eustatic sea level and an increase in Earth system sensitivity to obliquity (Levy et al., 2019). Glacial sediments deposited at the AND-2A site during this time interval reflect a polar climatic and glacial regime (Passchier et al., 2011) and show that ‘cold-based’ glacial events and potentially arid climatic conditions occurred in Antarctica well before the MMCT (Fig. 9.13E).

Evidence from offshore Prydz Bay (Cooper and O’Brien, 2004; Haywood et al., 2008; Williams and Handwerger, 2005) and the ASB (Gulick et al., 2017) also suggest the EAIS margin was dynamic during the early Miocene. At times the ice sheet advanced across the continental shelf and others it retreated inland of the terrestrial coastal margin (Williams and Handwerger, 2005). Drill core data from the Ross Sea Embayment indicate environmental conditions were highly variable throughout the early Miocene and show that sediments were deposited under a range of glacial regimes at different times to include terrestrial, subpolar, and polar climates (Fielding, 2018; Fielding et al., 2011; Levy et al., 2016; Passchier et al., 2011) (Fig. 9.13). Large areas of West Antarctica’s land surface were either subaerial and/or significantly shallower than today in the early Miocene and this topography may have enabled ice to more easily grow and expand across the Ross Sea continental shelf (Colleoni et al., 2018; Paxman et al., 2020; Pollard and DeConto, 2020). However, climatic conditions must have occasionally been cold enough to allow thick ice margins to advance into relatively deep marine environments (Gasson et al., 2016b; Kulhanek et al., 2019; Levy et al., 2019; McKay et al., 2019). TEX₈₆-based data indicate surface water temperatures were at times similar to Holocene values and coastal environments may have supported multi-season sea ice and/or small ice shelves (Levy et al., 2016). During warmer intervals surface water temperatures reached 5°C to 6°C ± 2.8°C and tundra vegetation occupied regions from the coast (Griener

et al., 2015; Kulhanek et al., 2019; Levy et al., 2016) to at least 60 km inland within the MDV (Lewis and Ashworth, 2015).

9.4.2 Miocene Climate Optimum

Beginning at \sim 17 Ma, the onset of the MCO is reflected in the deep sea benthic foraminifera records by a major decrease in $\delta^{18}\text{O}$ values and increase in $\delta^{13}\text{C}$ values (De Vleeschouwer et al., 2017; Westerhold et al., 2020; Woodruff and Savin, 1991). While the deep-sea data and a range of paleoclimate proxies from across the globe indicate a shift to warmer conditions at this time, environmental variability through the MCO remained high. This variability is most clearly reflected by large excursions (up to 1.5‰) in the deep sea $\delta^{18}\text{O}$ data that occur on glacial–interglacial time-scales and require either large changes in ice volume (Miller et al., 2020) and/or bottom water temperature (Lear et al., 2015; Modestou et al., 2020; Shevenell et al., 2008). So, while the average climate state was warm during the MCO, environmental changes through this key interval were large and frequent.

Antarctic records of environmental conditions throughout the MCO primarily come from three key drill cores: AND-2A and IODP Site U1521 from the Ross Sea, and IODP Site U1356 from offshore the WSB. Interestingly, terrestrial records through the MCO have yet to be recovered, although snapshots from the end of the optimum occur in the Friis Hills (Chorley, 2021; Verret et al., 2020) and Asgard Range (Marchant, 1993) in the MDV. The onset of the MCO occurs at \sim 550 mbsf in AND-2A and is somewhat unremarkable as there are no obvious changes in sedimentary facies or other environmental proxies (Fielding et al., 2011; Levy et al., 2016; Passchier et al., 2011). However, sedimentary facies and sequences deposited at AND-2A during the MCO are lithologically diverse and generally mud-rich (Fielding et al., 2011; Passchier et al., 2011). Importantly, there is no evidence that glaciers extended beyond the drill site during the MCO (Fielding et al., 2011; Levy et al., 2016; Passchier et al., 2011). Environmental data through the interval between \sim 15.8 and \sim 14.6 Ma are missing in a disconformity in the AND-2A core (Levy et al., 2016). The warmth of the MCO is reflected more clearly at Site U1521 in the central Ross Sea where a distinctive change in sedimentary facies occurs at \sim 210 mbsf. This depth marks the boundary between lithostratigraphic Units IV that comprises dark grey massive diatom-bearing clast-poor sandy diamicrites and lithostratigraphic Unit III, a 124 m-thick sequence of diatom-bearing/rich mudstones (McKay et al., 2019). The paucity of coarse sediments in this interval suggests the ice sheet margin was restricted to the terrestrial coastal region across the Ross Embayment between 17 and 16 Ma at least. The environmental record between \sim 16 and \sim 14.6 Ma at Site U1521 is missing in a disconformity (McKay et al., 2019). The

stratigraphic interval spanning the MCO at Site U1356 is characterised by diatomaceous and cherty mudstones lacking outsized clasts (Escutia et al., 2011a; Sangiorgi et al., 2018). These sediments were deposited within a distal channel levee setting with subsequent minor reworking by bottom currents of variable strength and bioturbation. There is little evidence for ice rafting over the drill site during the MCO (Sangiorgi et al., 2018), which suggests the coastal marine margins across the WSB remained ice free during the MCO. However, we note that core recovery through the MCO was relatively low and inferences regarding ice sheet extent and variability at this site must consider that clast-rich intervals may not have been recovered.

Sedimentological data from three drill sites offer evidence that the AIS did not extend far beyond the terrestrial coastal margin between at least 17 and 16 Ma. However, diamictites at the base of each sedimentary cycle throughout the section spanning the MCO in AND-2A indicate ice reached the Southern Victoria Land coast during glacial episodes. Coupled ice sheet and climate modelling experiments using Miocene boundary conditions show the AIS remained land-based during cold (glacial) astronomical configurations when CO₂ forcing was set at 460 ppm or greater (Halberstadt et al., 2021). However, the simulated AIS could extend across Antarctica's continental shelves in 'cold orbit' simulations where lower CO₂ concentrations are used (Gasson et al., 2016b; Halberstadt et al., 2021; Paxman et al., 2020). These results suggest atmospheric CO₂ concentrations were unlikely to have dropped below 400 ppm during the MCO, as suggested by proxy studies (Greenop et al., 2014).

In contrast to sedimentological data that inform maximum glacial extent, direct geological constraints on minimum AIS extent and volume during the MCO are few to absent. Geochemical proxy data (BIT index) from Site U1356 suggest that soil was able to form on extensive ice-free regions along the near-coastal lowlands at the margins of the WSB during intervals of ice retreat (Sangiorgi et al., 2018). Pollen data indicate these regions were covered by woody vegetation dominated by southern beech and *Podocarpaceae* conifers growing in a temperate climate with MATs between 5.8°C and 13°C and mean summer temperatures >10°C (Sangiorgi et al., 2018). Offshore surface-water temperature reconstructions based on TEX₈₆ suggest temperatures of 11.2°C–16.7°C ± 2.8°C. Intervals that indicate peak warmth and more extensive ice margin retreat from the coast in AND-2A are rare. One such interval contains thick-shelled costate scallops and venerid clams that indicate that water temperatures were at least 5°C warmer than in the Ross Sea today (Beu and Taviani, 2013). These observations are supported by TEX₈₆ and Δ₄₇ data, which indicate surface water temperatures reached a maximum between 7.0°C ± 2.8°C and 10.4°C ± 2.5°C (Levy et al., 2016). Another interval contains abundant diatoms and dinoflagellates and minimal gravel and sand clasts, which suggests the glacier grounding line retreated

inland from the coast as ice did not calve into the marine environment. Pollen and spores are abundant in this interval and indicate a coastal vegetation of mossy tundra with shrub podocarps and southern beech and suggest a cool terrestrial climate (up to 10°C January mean air temperature) (Levy et al., 2016; Warny et al., 2009).

While these glacial marine data indicate regional temperature increases and coastal ice margin retreat during peak warm intervals of the MCO, they do not provide constraints on the extent of inland ice margin retreat. However, coupled numerical climate and ice sheet modelling experiments offer a means to examine ice sheet response to maximum warming during the MCO. Results show significant volumes of ice remained on Antarctica under warm astronomical configurations and ‘extreme’ greenhouse gas forcing (>840 ppm) (Gasson et al., 2016b; Gasson and Keisling, 2020; Halberstadt et al., 2021; Paxman et al., 2020). It appears that the terrestrial regions of the AIS are sensitive to warming under CO₂ conditions that exceed 540 ppm but they do not completely melt even under high CO₂ (>840 ppm) and warm orbits (Gasson et al., 2016b; Halberstadt et al., 2021). Ice that sits on West Antarctica and the WSB and ASB is particularly susceptible to warming. The minimum simulated ice volume produced on reconstructed Miocene topographies under high (840 ppm) atmospheric CO₂ concentration and a warm (interglacial) astronomical configuration ranges between $14.1 \times 10^6 \text{ km}^3$ (Gasson et al., 2016b) and $18.94 \times 10^6 \text{ km}^3$ (Paxman et al., 2020). These volumes are equivalent to ~53% and ~71% of the modern AIS ($26.54 \times 10^6 \text{ km}^3$ excluding ice shelves) (Fretwell et al., 2013). If we assume that maximum ice volume during glacial episodes in the MCO was no more than modern (which is generally consistent with drill core data), then the likely maximum glacial–interglacial ice volume change during the MCO ranges between 27 and 17 m sea level equivalent. These outputs are consistent with records from the Marion Plateau that indicate sea level amplitude changes of $27 \pm 1 \text{ m}$ at 16.5 and 15.4 Ma (John et al., 2011), and the New Jersey margin with maximum amplitudes of between 20 and 30 m through the MCO (Kominz et al., 2008, 2016) (Fig. 9.3E). These results contrast with a recent study that suggests complete collapse of the AIS occurred during the MCO (Miller et al., 2020).

The moderate changes in ice volume indicated by ice sheet modelling studies and sea level records require significant changes in bottom water temperature to explain the large (up to 1.5‰) excursions in deep sea δ¹⁸O records. Paleotemperature records from ODP Site 1172 in the Southern Ocean indicate bottom water temperature variations up to 3°C occurred on astronomical time scales through the MCO (Shevenell et al., 2008) (Fig. 9.3E). Relatively low resolution records derived from ODP Site 806 (western equatorial Pacific) using similar Mg/Ca-based proxy techniques indicate bottom water temperatures varied by up to 6°C over million year

time scales (Lear et al., 2015). These temperature estimates are also supported by Δ_{47} (clumped isotope) data from ODP Site 761 which indicate bottom water temperatures in the Indian Ocean were up to 9°C warmer than today during the MCO and varied by up to 4°C through the optimum (Modestou et al., 2020). These bottom waters were likely produced at high southern latitudes including in the Ross Sea Embayment and offshore George V and Adélie Land. Data from AND-2A indicate surface water temperatures ranged between -1.8°C and 10°C in the Ross Sea during the MCO. It seems reasonable to infer that the temperature of bottom water derived from these regions varied by 3°C to 6°C on interglacial time scales. This magnitude of change in BWT can explain between 0.63‰ and 1.26‰ of the change in deep sea $\delta^{18}\text{O}$ records and suggests that estimates of ice volume changes of 27 m sea level equivalent through the MCO are reasonable (e.g. Bradshaw et al., 2021).

9.4.3 Miocene Climate Transition

The onset of the middle Miocene Climate Transition is reflected in deep sea $\delta^{18}\text{O}$ records by a relatively subtle increase in glacial values and a trend towards higher average values beginning at ~ 14.8 Ma (Holbourn et al., 2014). The MMCT lasted for approximately one million years and culminated in a large ($\sim 0.4\%$) stepped increase in average $\delta^{18}\text{O}$ values at 13.8 Ma that coincides with the final major increase in deep sea $\delta^{13}\text{C}$ events (CM6) at the end of the Monterrey carbon excursion (Vincent and Berger, 1985). This last major step in the MMCT coincides with a drop in atmospheric CO_2 concentration below 300 ppm (Badger et al., 2013b) (Fig. 9.12A). It has long been inferred that the MMCT records the expansion and stabilisation of the EAIS and the cooling and aridification of Antarctica's terrestrial environments (Clapperton and Sugden, 1990; Sugden and Denton, 2004; Sugden et al., 1993). This inference is primarily based on extensive evidence from deposits at high elevation (>1000 m) in the TAM (Sugden et al., 1993) but also relies on the deep sea $\delta^{18}\text{O}$ data. Of particular importance to the 'stabilist' perspective are 15 million year old ash deposits in the Asgard Range of the MDV that suggest little to no landscape modification has occurred at these high elevation locations since the end of the MCO (Marchant, 1993). This inference is supported by surface exposure studies that utilise cosmogenic nuclides, which indicate little erosion has occurred at high elevations in the TAM over the past 15 million years (Spector and Balco, 2021; Valletta et al., 2015). Arguments for expansion of the EAIS during the MMCT are based on geomorphological evidence for glacial overriding including subglacial potholes in the Asgard Range (Sugden et al., 1991) and channels that form the Labyrinth in upper Wright Valley (Lewis et al., 2006). However, these results are debated, with another study suggesting that cosmogenic nuclide data indicate relatively high erosion rates at high

elevations in the MDV since the middle Miocene (Middleton et al., 2012). These results also require a much younger or more complex history for the formation of the channelised landforms in the Asgard Range and upper Wright Valley (Middleton et al., 2012).

Here we summarise environmental events in the Ross Sea and offshore George V Land that occurred through the MMCT and show that while climate cooled and the AIS advanced to the continental margin, the ice sheet expansion was a transient event (Figs 9.12 and 9.13). Disconformities in the AND-2A and Site U1521 cores at ~ 14.8 and 14.6 Ma, respectively, indicate ice grounded and expanded beyond the terrestrial coastal margin and across the Ross Sea continental shelf at this time. These disconformities correlate with Ross Sea Unconformity 4 (RSU4), which is the oldest spatially extensive erosional surface preserved within Neogene-aged seismic sequences across the Ross Sea (De Santis et al., 1995, 1999; Pérez et al., 2021a). The transition to a polar glacial regime at this time is reflected by a shift to facies sequences dominated by mud-poor massive diamictites above the disconformity in the AND-2A core (Passchier et al., 2011). Increases in deep sea $\delta^{18}\text{O}$ data align with the drill core and seismic evidence for more extensive advances of grounded ice into marine settings during glacial episodes. Furthermore, the Marion Plateau sea level record indicates maximum sea level fall of 33 ± 5 m at 14.7 Ma, which is slightly more than the maximum recorded amplitude of sea level fall during the MCO (-27 ± 1 m) and supports the near field Antarctic records and deep sea $\delta^{18}\text{O}$ data. However, it is critical to recognise that the deep sea $\delta^{18}\text{O}$ data also show ice volume decreased again during interglacial episodes through the MMCT. Importantly, flora and fauna from fossil-rich glacial–fluvial and glacial–lacustrine deposits in the Friis Hills indicate interglacial climate remained relatively warm and wet until at least 14 Ma (Chorley, 2021; Lewis and Ashworth, 2015; Verret et al., 2020) and suggest ice margins retreated from the coast. These observations indicate the AIS was highly variable throughout much of the million-year-long MMCT.

Major disconformities in AND-2A and Site U1531 post-date ~ 14.4 and ~ 14 Ma, respectively, and form major stratigraphic breaks between two and three million years in duration (Figs 9.7 and 9.13D). These major disconformities correlate with RSU4, which likely formed as AIS advance during glacial episodes became progressively more extensive during the later stages of the MMCT. By 14.2 Ma maximum values of $2.2\text{\textperthousand}$ in deep sea $\delta^{18}\text{O}$ data indicate the AIS was growing to its greatest extent and volume since the onset of the MMCT. However, the AIS still underwent significant retreat during interglacial events. A large decrease in deep sea $\delta^{18}\text{O}$ records at ~ 13.9 Ma may capture the ‘last gasp’ of relative warmth and significant inland retreat of terrestrial ice sheets during warm interglacial episodes in the middle Miocene (Fig. 9.12B). Fossil flora and fauna preserved in lacustrine deposits at Friis Hills and Mt Boreas indicate climate remained warm

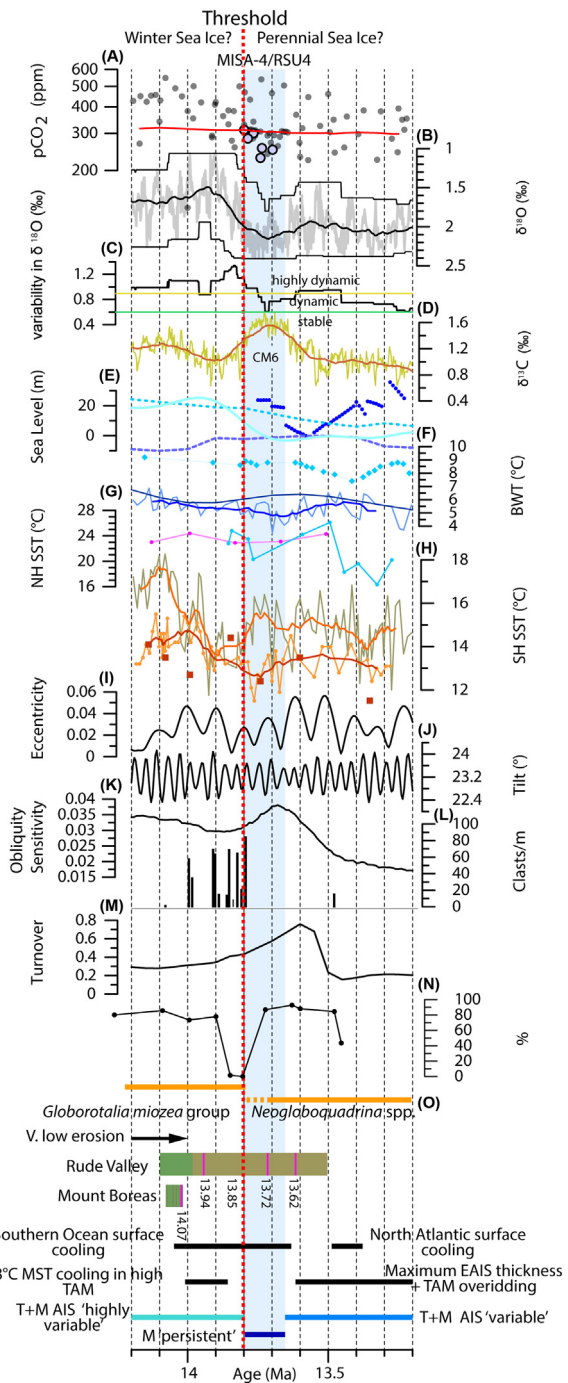


FIGURE 9.12 Environmental data from the middle Miocene (14.2 to 13.2 Ma). (A) Atmospheric CO₂ compilation comprises data from a range of proxies outlined in Fig. 9.1. Solid red line displays a two million year moving average. Purple dots highlight boron proxy data from Malta (Badger et al., 2013b). (B) Splice of deep sea benthic foraminifera $\delta^{18}\text{O}$ data (light (Continued)

enough at this time to support tundra vegetation at relatively high inland sites (Lewis and Ashworth, 2015; Lewis et al., 2008; Verret et al., 2020). Significant increases in IRD are recorded at IODP Site U1356 and ODP Site 1165 between 14.1 and 13.8 Ma (O'Brien et al. 2001; Sangiorgi et al., 2018). Geochemical provenance analysis of clasts in these cores indicates the EAIS margin

◀ grey) reflect changes in ice volume and deep/bottom water temperature (De Vleeschouwer et al., 2017). Solid black line displays a 150 kyr moving average. Maximum and minimum values are determined within each 150 kyr window and create the envelope (black lines) that bound the $\delta^{18}\text{O}$ data. (C) A $\delta^{18}\text{O}$ variability ‘index’, interpreted as a measure of glacial/interglacial variability, is determined by subtracting the maximum values in (B) from the minimum value, for each 150 kyr window. We indicate arbitrary ‘thresholds’ in these data (green and yellow solid lines) and suggest that values below 0.6‰ reflect a relatively ‘stable’ high latitude environment and values that exceed 0.9‰ indicate a highly dynamic environment with large changes in BWT and/or ice volume over glacial-interglacial time scales. (D) Yellow line shows high resolution deep sea benthic foraminifera $\delta^{13}\text{C}$ splice (Westerhold et al., 2020) and carbon maxima event CM6 (Vincent and Berger, 1985; Woodruff and Savin, 1991). Solid deep orange line displays a 150 kyr moving average. (E) Sea level curves are from Kominz et al. (2008) (pale blue dashed line), (Kominz et al., 2016) (blue dots), Miller et al. (2005) (blue dashed line) and Miller et al. (2020) (pale blue line). (F) BWT data from ODP Site 761 (Lear et al., 2010) (light blue), ODP Site 1171 (Shevenell et al., 2008) (blue), and derived from the compilation of Cramer et al. (2011) using Equation 7a (dark blue). Solid line through data from ODP Site 1171 displays a 9-pt running average. (G) SST data for the Northern Hemisphere from ODP Site 608 (Super et al., 2018) (light blue) and ODP Site 902 (Super et al., 2020) (pink). (H) SST data for the Southern Hemisphere from ODP Site 1171 using the Mg/Ca proxy (Shevenell et al., 2004) (dark brown) and the TEX₈₆ proxy (orange) (Leutert et al., 2020), using the calibration of Ho and Laepple (2016). Solid lines through the Mg/Ca and TEX₈₆ data display a 9-pt running average. Red squares display temperature estimates derived from clumped isotopes (Δ_{47}) (Leutert et al., 2020). (I) Astronomical eccentricity and (J) axial tilt (obliquity) from (Laskar et al., 2011). (K) obliquity sensitivity after Levy et al. (2019). (L) Ice rafted debris from IODP Site U1356 (Sangiorgi et al., 2018). (M) Rate of diatom species extinction and speciation (turnover) after Crampton et al. (2016). (N) Percentage protoperidinioid dinoflagellate cysts at IODP Site U1356 (Sangiorgi et al., 2018). (O) Orange bars indicate significant changes in foraminifera assemblage composition in the Southern Ocean (Verducci et al., 2009). The coincident changes in diatom (M), dinocyst (N), and foraminifera (O) assemblages suggests an increase in sea ice persistence and extent occurred after 13.8 Ma. A decrease in erosion rates in the TAM after 15 Ma is suggested by cosmogenic nuclide studies (Spector and Balco, 2021). Generalised stratigraphic data from the Olympus Range in the McMurdo Dry Valleys indicate a transition from wet-based, fossiliferous, glacial-lacustrine deposits (green), to dry-based glacial drifts (brown) occurred between 14 and 13.9 Ma based on tephra chronology (pink layers) (Lewis et al., 2008; Lewis et al., 2007). Summary of climatic events (black bars) are based on environmental proxies within this figure [interval of maximum EAIS thickness inferred from regional geomorphology in the MDV (Lewis et al., 2006; Sugden et al., 1991)]. Blue vertical band indicates interval characterised by major unconformities in Ross Sea drill cores and the occurrence of erosional seismic surface RSU4. Antarctic Ice Sheet variability and extent (T, terrestrial; M, Marine) inferred from drill core data (Levy et al., 2016; McKay et al., 2019; Sangiorgi et al., 2018), modelling studies (Gasson et al., 2016b; Halberstadt et al., 2021), obliquity sensitivity (K), and high resolution $\delta^{18}\text{O}$ records (B). Red dashed vertical line highlights likely threshold in the climate system across which atmospheric cooling enhanced sea ice and marine ice sheet expansion (see text for discussion).

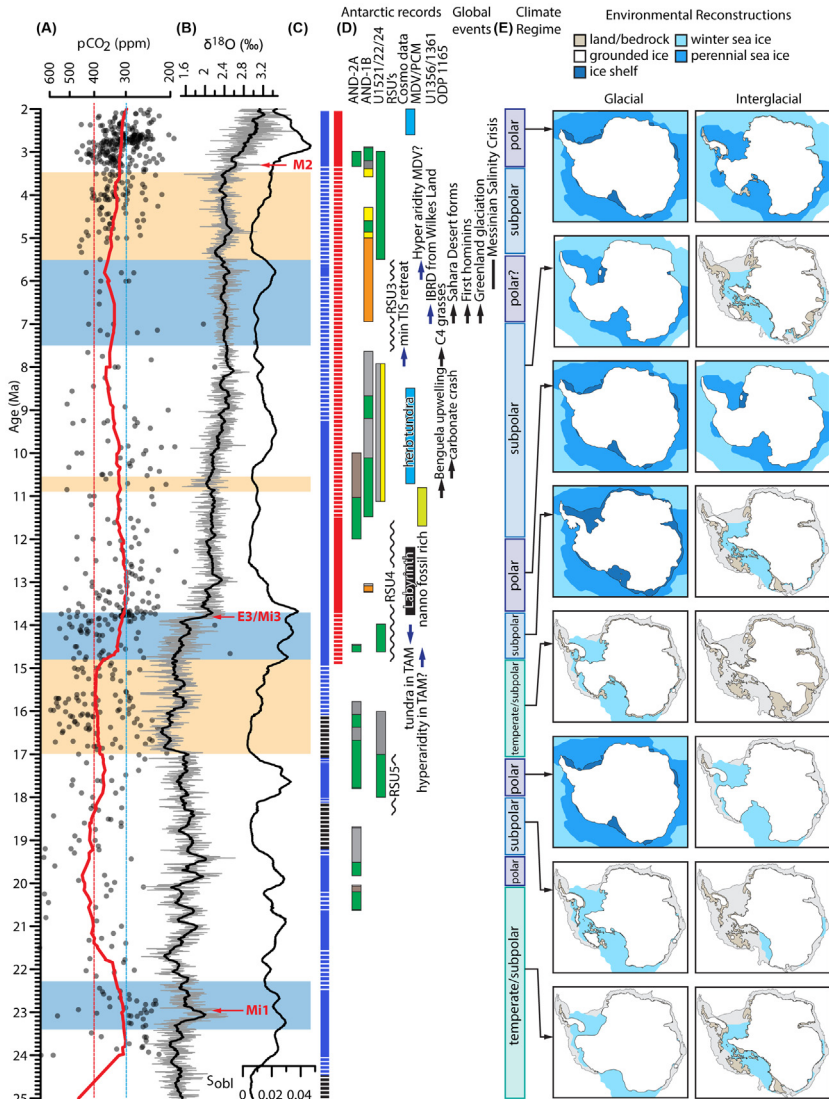


FIGURE 9.13 Summary of Antarctic ice sheet and high southern latitude climate change through the Miocene and Pliocene. (A) Atmospheric CO₂ compilation comprises data from a range of proxies outlined in Fig. 9.1. Solid red line displays a two million year moving average. (B) Splice of deep sea benthic foraminifera $\delta^{18}\text{O}$ data (light grey) reflect changes in ice volume and deep/BWT (De Vleeschouwer et al., 2017). Solid black line displays a 150 kyr moving average. (C) Obliquity sensitivity (S_{obl}) calculated from the obliquity forcing variance and the $\delta^{18}\text{O}$ record and is interpreted as a proxy for ocean-ice sheet connectivity (Levy et al., 2019). Coloured bars reflect the ice-sheet extent: T, terrestrial (black); T + M, terrestrial and marine (blue), PSI, perennial sea ice (red); dashed lines, transitional. (D) Graphical summary of key

(Continued)

repeatedly retreated inland across the WSB and Lambert Graben and advanced again into marine environments delivering IRD-rich ice to the drill sites (Pierce et al., 2017). SSTs in the Southern Ocean dropped by 2°C to 6°C between ~14.1 and 13.8 Ma (Leutert et al., 2020; Shevenell et al., 2004).

Sea level fell by 59 ± 6 m at ~13.9 Ma (John et al., 2011), which suggests the AIS expanded to the edge of the continental shelf at this time. Coupled ice sheet and climate modelling experiments show that ice volume in the mid Miocene could have increased by $\sim 18.3 \times 10^6$ km³ between warm interglacial climates under moderate CO₂ (500 ppm) and cold glacial climates under low CO₂ (280 ppm) (Gasson et al., 2016b). This change in volume would cause a 36 m fall in sea level (Gasson et al., 2016b). These results suggest that either the observed magnitude of sea level fall at the Marion Plateau is larger than eustatic (i.e. influenced by local geodynamic effects) (Austermann et al., 2015, 2017), minimum (interglacial) AIS volumes were less than modelled and/or glacial expansion was greater (climate may have been colder than simulated), or that ice sheets may have also grown in the northern hemisphere (DeConto et al., 2008).

Deep sea δ¹⁸O records and geological, paleoceanographic and paleo-ecological data from the Antarctic margin and Southern Ocean show a major environmental threshold was crossed at ~13.8 Ma (Fig. 9.12). Summer mean air temperature in the TAM cooled by 8°C between 14.07 ± 0.05 and 13.85 ± 0.03 Ma, tundra vegetation disappeared from high elevations and glacial systems became dry-based (Lewis et al., 2007, 2008). Bottom water temperature decreased by ~2°C in the Southern Ocean (Shevenell et al., 2008) between ~14 and 13.7 Ma and by $2.9^\circ\text{C} \pm 2.5^\circ\text{C}$ in the Indian Ocean by 13.5 Ma (Modestou et al., 2020). Immediately after 13.8 Ma, an episode of low variability in deep sea δ¹⁸O data (Fig. 9.12B and C) suggests the AIS ‘stabilised’ at the continental shelf margin and persisted at this position for ~150 kyrs. This period of maximum marine based ice extent coincides with the CM6 δ¹³C excursion and a peak in obliquity sensitivity (Levy et al., 2019) (Fig. 9.12D and K). A major turnover pulse in diatom species (an episode of coincident species extinction and appearance) also occurred during this interval (Fig. 9.12M) and may have happened, in part, because marine based ice sheets covered Antarctica’s continental shelves for an extended period (Crampton et al., 2016).

Climate and ice sheet modelling studies show that extensive sea ice forms around Antarctica when atmospheric CO₂ concentrations drop, orbits are particularly cold, and the AIS grows large (DeConto et al., 2007; Halberstadt

◀ Antarctic records and events and major global events discussed in text. (E) Summary of changes in climate regime (temperate, subpolar, and polar) and associated reconstructions of glacial-interglacial ice sheet, ice shelf, and sea ice extent (maps at right) is based on proxy evidence discussed in text and on climate and ice sheet modelling experiments (Gasson et al., 2016b; Golledge et al., 2017b; Halberstadt et al., 2021).

et al., 2021). These results suggest expansion and persistence of perennial sea ice across the Southern Ocean also occurred between 13.8 and 13.6 Ma, as: (1) the interval coincides with a node in obliquity and low eccentricity; (2) proxy CO₂ data show values dropped below 300 ppm (Badger et al., 2013b); and (3) geological data show the AIS expanded to the continental margin (Figs 9.12 and 9.13E). The onset of persistent and extensive perennial sea ice after 13.8 Ma is also supported by the occurrence of abundant protoperidinioid dinocyst species at Site U1356 (Sangiorgi et al., 2018) and a prominent change in formaminiferal fauna at ODP Hole 747A (Kerguelen Plateau, southern Indian Ocean). Here taxa with a warm water affinity (e.g., *Globorotalia miozea* group) were replaced by a fauna with typical polar characters and dominated by neogloboquadrinids (Verducci et al., 2009). This expansion of sea ice and transition to a ‘polar’ climate in the Southern Ocean likely contributed to the major perturbation in Southern Ocean phytoplankton at 13.6 Ma (Crampton et al., 2016). However, it is important to note that this climatic cooling in the Southern Ocean was transient and that after ~12.9 Ma warm water foraminifera species became more abundant once again (Majewski, 2010; Verducci et al., 2009).

The timeline of events and range of paleoenvironmental data outlined above is compelling and shows that climate gradually cooled and the AIS progressively expanded during glacial episodes through the MMCT but was highly dynamic until ~13.8 Ma. An environmental threshold was crossed at ~13.8 Ma, which may have been driven by a combination of favourable ‘cold’ astronomical configurations and a decrease in atmospheric CO₂ concentration below 300 ppm (Badger et al., 2013b). The AIS expanded across marine basins and continental shelves at this time and remained relatively stable for ~150 kyr. Persistent perennial sea ice occupied the circum-Antarctic ocean and ‘polar’ climatic conditions characterised the high southern latitudes (Fig. 9.13E). However, these cold polar conditions were transient and as the Antarctic climate warmed the AIS again became highly dynamic after 13.6 Ma, which highlights an ongoing puzzle regarding the timing of the onset, and subsequent persistence, of hyper arid climate in the TAM and the transition to a modern polar climate.

Cosmogenic exposure age data suggest erosion rates have been minimal since 15 to 14 Ma and are used to infer an arid climate since this time (Spector and Balco, 2021; Valletta et al., 2015). However, this inference is incongruous with data described above that indicate relatively warm interglacial climates persisted at high elevations until at least 13.9 Ma (Lewis and Ashworth, 2015; Lewis et al., 2008; Verret et al., 2020). Furthermore, mud-rich facies in AND-1B offshore the MDV indicate a subpolar glacial regime delivered plumes of terrestrial material during the warm late Miocene (McKay et al., 2009). Climate and ice sheet modelling also suggests climatic conditions that were warm and wet enough to support tundra vegetation,

which persisted at the coast even when atmospheric CO₂ concentrations were low (<460 ppm) and ice occupied most of Antarctica's terrestrial regions (Halberstadt et al., 2021). Finally, meteoric beryllium data suggest water percolated into the surface at high elevation locations into the late Neogene (Dickinson et al., 2012).

9.4.4 Late Miocene

Climate in the late Miocene was cooler than during peak warm episodes of the MCO, but proxy data show surface temperatures remained significantly warmer than today (Herbert et al., 2016; Prebble et al., 2017; Super et al., 2020). Northern high latitude temperature anomalies ranged between 10°C and 15°C higher than today between 11.5 and 8 Ma and mid-latitude temperatures in the southern hemisphere were between 5°C and 8°C warmer (Herbert et al., 2016). Whereas bottom water temperatures cooled by ~2°C across the MMCT (Modestou et al., 2020; Shevenell et al., 2008), they were still at least 6°C warmer than present in the Indian Ocean during the late Miocene (Modestou et al., 2020). Sedimentological (Passchier et al., 2011) and paleoecological (Verducci et al., 2009) data show that polar climatic conditions characterised southern high latitudes by the end of the MMCT, but a return to a subpolar glacial regime around Antarctica by the late Miocene is reflected in geological records from Wilkes Land (Pretty, 2019; Sangiorgi et al., 2018), the Ross Sea (McKay et al., 2009) and Prydz Bay (Hambrey and McKelvey, 2000; Whitehead et al., 2006a, 2006b). Geological data and observations that document this return to warm subpolar conditions at the Antarctic margin are summarised below.

The appearance of nannofossil-rich mudstones at IODP Site U1361 indicates a return to warm oceanic conditions, enhanced meltwater production and ice sheet retreat along the Wilkes Land Coast between 11.7 and 11 Ma (Pretty, 2019). TEX₈₆-based paleotemperature reconstruction from the site show surface waters was 6°C to 10°C at this time (Sangiorgi et al., 2018). These data suggest temperatures were ~8°C to 12°C above sub-zero temperatures that characterise the modern environment and are similar to the anomalies recorded at high northern latitudes and indicate a 2- to 3-times polar amplification. Sedimentary facies changes in AND-1B reflect a shift from a polar to subpolar glacial regime at ~10 Ma in the Ross Sea region (McKay et al., 2009; Rosenblume and Powell, 2019; Wilson et al., 2012b). Massive diamicts and waterlain tills deposited at ODP Site 739 indicate the Lambert ice stream was highly dynamic with multiple episodes of advance and retreat across the continental shelf in Prydz Bay during the late Miocene (Barron and Larsen, 1989). In-situ marine diatoms in the Batty Glacier and Fisher Bench Formations show the Lambert Glacier margin retreated well inland between 10 and 8.5 Ma (Hambrey and McKelvey, 2000; Whitehead et al., 2006b). Sediments deposited during

this marine incursion contain palynological assemblages that reflect a herb tundra vegetation similar in form to that of the present-day cool to cold sub-Antarctic regions (Wei et al., 2013). Pollen assemblages in AND-2A contain some elements that are similar to the Prydz Bay assemblages (Taviani et al., 2008–2009), which suggests climatic conditions that support modern sub-Antarctic flora also persisted in the Ross Sea region into the early late Miocene. The first major marine incursions up the ‘modern’ Wright Valley also occurred at this approximate time and represent relatively warm ice-free conditions at low elevations in the MDV (Brady, 1979; Prentice et al., 1993). Up to 675 m of strata have been imaged offshore the ASB (package Ms-II) that contain additional erosive surfaces that truncate reflectors and exhibit rough morphology and channels indicative of glacial erosion in a meltwater-rich environment (Gulick et al., 2017). While age constraints on this unit are few, it predates the late Miocene (~8 Ma) (Gulick et al., 2017) and may include sediments deposited during the late middle to early late Miocene. These environmental indicators show warming occurred across a range of latitudes and longitudes during the late Miocene and indicate Antarctica transitioned out of a polar regime that characterised environmental conditions for several million years through and immediately after the MMCT (Fig. 9.13).

Glacial–interglacial environmental variability reflected in deep sea $\delta^{18}\text{O}$ records was low though the late middle Miocene and suggests a relatively stable climate system persisted between ~13 and 11.5 Ma, after which these deep sea data capture a shift to a more dynamic state (De Vleeschouwer et al., 2017; Holbourn et al., 2013; Westerhold et al., 2020) (Fig. 9.4B and C). A major feature in the $\delta^{18}\text{O}$ record at ODP Site 1146 (South China Sea) is an abrupt warming event ($\delta^{18}\text{O}$ drop of ~1%) at ~10.8 Ma that is associated with a large decline in $\delta^{13}\text{C}$ of ~1‰ (Holbourn et al., 2013). Several subsequent abrupt warming events ($\delta^{18}\text{O}$ drops) occur in the Site 1146 record between 9 and 10 Ma. This interval has been identified as the Tortonian thermal maximum (Westerhold et al., 2020). The ‘hyperthermal’ at 10.8 Ma approximately coincides with an abrupt but transient (2°C to 4°C) increase in bottom water temperature recorded in a relatively low resolution Mg/Ca record from ODP Site 747 (Billups and Schrag, 2002). These warm events coincide with evidence for warm surface water temperatures (Sangiorgi et al., 2018) and glacial retreat at the Antarctic margin (Whitehead et al., 2006a, 2006b), including the carbonate rich unit from offshore Wilkes Land (Escutia et al., 2011a; Pretty, 2019), and suggest the AIS was sensitive to global climate change and remained highly dynamic following the end of the MMCT. This interval of time certainly warrants more attention.

Environmental records through the interval from ~8 to 5.5 Ma are generally missing from drill cores in the Ross Sea region (Figs 9.7 and 9.13)

(Acton et al., 2008–2009; McKay et al., 2019). This major disconformity correlates with RSU3 at Site U1522 and suggests another phase of marine based ice sheet advance and retreat across the continental shelf began at the onset of the LMC. This episode of cooling and AIS advance is also reflected in beryllium data from AND-1B, which indicate that terrestrial outlet glaciers along the Victoria Land coast have not retreated much further inland of their current position since ~8 Ma (Shakun et al., 2018). Iceberg rafted debris derived from the Wilkes and Adélie Land margin of the EAIS first appears at ODP Site 1165 at ~7 Ma (Williams et al., 2010). These observations suggest that only after 7 Ma were SSTs cold enough to allow ice bergs to transit the large distance from offshore the WSB and ASB to Site 1165 without melting (Williams et al., 2010). Glacial expansion of both the EAIS and WAIS is also inferred from mass accumulation rates of terrigenous matter and iron that intensified between ~7.2 and 6.6 Ma offshore Prydz Bay and the Antarctic Peninsula (Grützner et al., 2005). Furthermore, seismic data and short cores collected offshore of the ASB reveal a 0–110-m-thick package of sub-horizontal to landward-dipping strata that are most likely younger than 6.9 Ma (Gulick et al., 2017). These strata contain no visible channels, which suggests reduced meltwater influence, and erosional surfaces in these late Miocene strata record advance and retreat of an expanded EAIS offshore the ASB. A lack of accumulation and preservation of open marine sediments suggests limited regional ice retreat or shorter interglacials since the late Miocene (Gulick et al., 2017).

Most of the evidence discussed above suggests the AIS became larger, drier and less dynamic at ~7 Ma. Meteoric beryllium data from sites in the MDV suggest modern hyper arid conditions were established at these high southern latitudes at ~6 Ma (Dickinson et al., 2012; Schiller et al., 2009). At the same time, Southern Hemisphere ocean surface water temperatures reached modern values for a brief period (Herbert et al., 2016). This late Miocene increase in Antarctic ice volume and areal extent likely peaked between 5.96 and 5.6 Ma coincident with the Messinian salinity event that impacted the Mediterranean (Garcia-Castellanos and Villaseñor, 2011; Hsü et al., 1973; Ohneiser et al., 2015). However, this interval of peak cold conditions and maximum ice volume ended as climate warmed into the early Pliocene.

9.4.5 Pliocene

The Pliocene is an important period to examine as it offers insight into the equilibrium response of the different sectors of the AIS to climate change under current atmospheric CO₂ concentration. Pliocene research also has the potential to constrain the amplitude of ice volume and sea-level change that may arise from a future deglaciation (DeConto et al., 2021). The last 10 years has seen a significant increase in the coverage

and quality of proxy data from paleoclimate archives, which in turn has driven innovation and increased performance and skill of numerical ice sheet simulations, such that the modelled ice volume changes are broadly consistent with paleoclimate constraints for the warm interglacials of the Pliocene.

ANDRILL provided geological evidence that the WAIS had grown and collapsed numerous times between 5 and 2.6 Ma in response to astronomically-paced climate cycles when atmospheric CO₂ was last ~400 ppm (McKay et al., 2012; Naish et al., 2009; Pollard and DeConto, 2009). However, results from IODP Expedition 318 showed that East Antarctic ice within the catchment of the WSB was also highly dynamic during the Pliocene (Bertram et al., 2018; Cook et al., 2013, 2017; Patterson et al., 2014; Reinardy et al., 2015) and that advance and retreat of both the EAIS and WAIS drove global sea-level changes of up to 20 m (Dumitru et al., 2019; Grant et al., 2019; Miller et al., 2012). These discoveries challenged some of the early Pliocene ISM reconstructions which displayed strong hysteresis and could only release 7–9 m of sea-level equivalent ice volume (Pollard and DeConto, 2009). Subsequent work to improve the ISMs has improved alignment between model results and geological constraints. These improvements are primarily due to: (1) better climate–ice sheet coupling to account for ice sheet–climate feedbacks (DeConto and Pollard, 2016; DeConto et al., 2021; Golledge et al., 2015, 2017b, 2019); (2) better characterisation of uncertainty associated with different modelling frameworks (de Boer et al., 2015; Dolan et al., 2018); (3) the ability to simulate instability mechanisms that act on marine-based ice, particularly the ice that sits on reverse-sloped beds; and (4) numerical representation of processes that enhance ice sheet retreat including ice-cliff failure and ice-shelf hydrofracture (DeConto and Pollard, 2016; DeConto et al., 2021; Gasson et al., 2016a; Pollard et al., 2015), although the need to employ these processes and ice sheet physics is still debated (Gasson and Keisling, 2020).

Proxy data from IODP Expedition 318 and ANDRILL imply that the marine-based sectors of both West and East Antarctica were sensitive to obliquity forcing, especially under a warmer mean climate state when CO₂ was between 350 and 400 ppm prior to ~3.3 Ma and the M2 glaciation (Naish et al., 2009; Patterson et al., 2014). Several studies have argued that this was due to the influence of obliquity on modulating the temperature gradient of the Southern Hemisphere (Raymo and Nisancioglu, 2003), promoting wind-driven upwelling of CDW with consequences for melt rates at grounding lines and in ice shelf cavities (Hansen and Passchier, 2017; Levy et al., 2019; Naish et al., 2009). While the duration of both glacimarine cycles in AND-1B and IRD mass accumulation in Site U1316 cores was dominated by obliquity prior to regional cooling associated with the M2 glaciation in benthic foraminifera

$\delta^{18}\text{O}$ records (Patterson et al., 2014), the East Antarctic WSB displays a strong eccentricity/precession-paced ice volume variability in IRD mass accumulation between 3.3 and 2.5 Ma (Fig. 9.14).

Ice sheet, SST and sea ice reconstructions from sediment cores in the Ross Sea and eastern Wilkes Land margins provide evidence for expansion of the AIS that began at ~ 3.3 Ma (Levy et al., 2012; McKay et al., 2012), essentially terminating Pliocene warmth in the southern high-latitudes. This was associated with coastal SST cooling of $\sim 2.5^\circ\text{C}$, a stepwise expansion of sea ice and polynya formation in the Ross Sea between 3.3 and 2.5 Ma (Fig. 9.14). The intensification of Antarctic cooling resulted in strengthened westerly winds and invigorated ocean circulation. The associated northward migration of Southern Ocean fronts has been linked with reduced Atlantic Meridional Overturning Circulation by restricting surface water connectivity between the ocean basins, with implications for heat transport to the high latitudes of the North Atlantic. McKay et al. (2012) imply this may in turn have preconditioned the northern hemisphere for continental-scale glaciation when atmospheric CO₂ concentration fell below 300 ppm between ~ 2.9 and 2.7 Ma (Masson-Delmotte et al., 2013).

Peak sea-level estimates during the warmest Pliocene interglacials from far-field sea-level records are as high as +40 m above present. Based on the present global ice-sheet budget the sea-level equivalent of marine-based sectors of the AIS can account for 22.7 m, the Greenland Ice Sheet contains 7.3 m, and an additional 35.6 m is available from terrestrial sectors of the AIS. Amplitudes $> +30$ m can only be explained by melting the terrestrial sectors of the AIS, and/or by having more ice on the Northern Hemisphere continents during glacial periods than can be explained by the available geological data (Thiede et al., 2011). Larger than Holocene Antarctic glacial ice volumes cannot be excluded by proximal geological data for glacials during the mPWP (Naish et al., 2009), but retreat of the EAIS inland of its terrestrial margins since ~ 8 Ma appears to be precluded by a recent study that found extremely low concentrations of cosmogenic ¹⁰Be and ²⁶Al isotopes in the ANDRILL-1B marine sediment core (Shakun et al., 2018). Therefore, the maximum contribution to GMSL from the Antarctic ice sheets during the mPWP is the volume of the marine-based sectors of the ice sheet (modern day = ~ 23 m sea-level equivalent). A recent reassessment of the far-field estimates for the warmest mid-Pliocene interglacials shows GMSL was at least +4.1 m and no more than +20.7 m, with a median of +10.7 m (Grant and Naish, 2021). This median value is consistent with ISM simulations constrained by ice proximal geological data (DeConto and Pollard, 2016; Colledge et al., 2017b; Pollard et al., 2015).

This range also implies an equilibrium polar ice-sheet sensitivity of 2–8 m of sea-level change for every degree of temperature change, with a mean value of 4 m/AIS (Grant and Naish, 2021). However, the

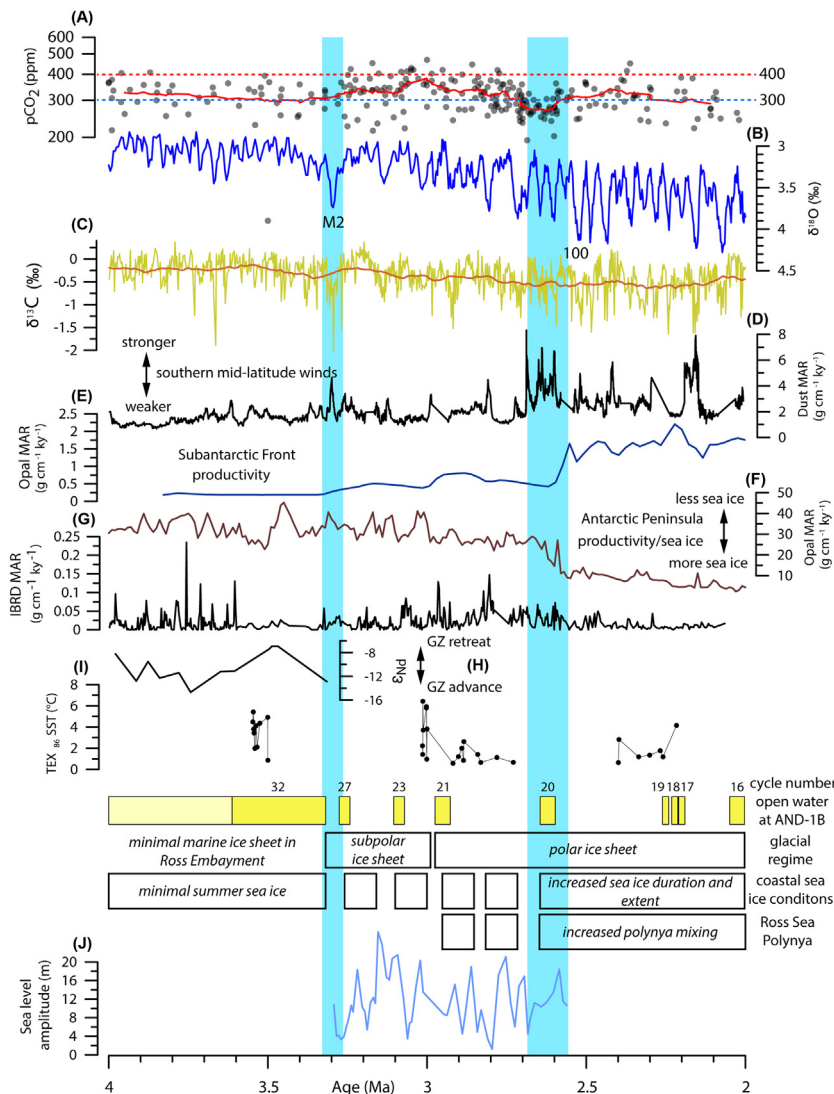


FIGURE 9.14 Environmental data from the Pliocene to early Pleistocene (4 to 2 Ma) highlight Southern Hemisphere climate system feedbacks and responses and their relationship to Antarctic climate evolution. Cooling steps in Pliocene climate at ~3.3 and ~2.6 Ma are highlighted by blue dashed lines. (A) Atmospheric CO₂ compilation comprises data from a range of proxies outlined in Fig. 9.1. Solid red line displays a 17-point running average. (B) Benthic foraminifera δ¹⁸O proxy for ice volume and temperature (Lisicki and Raymo, 2005). (C) High resolution deep sea benthic foraminifera δ¹³C splice (Westerhold et al., 2020). Solid deep orange line displays a 150 kyr moving average. (D) Atmospheric circulation (relative westerly wind strength) from dust mass accumulation rates for ODP Site 1090 (Martinez-Garcia et al., 2011). (E) Southern Ocean primary productivity based on biogenic opal mass accumulation rates at ODP Site 1091 shows a sharp increase coincident with increased windiness and nutrient supply by Fe-rich dust at ~2.6 Ma (Cortese et al., 2004; Hillenbrand and Cortese, 2006). (F) Onset of Antarctic sea ice at ~2.6 Ma marked by a decline in primary productivity recorded in biogenic opal MAR (g cm⁻¹ ky⁻¹). (G) IBRD MAR (g cm⁻¹ ky⁻¹) and TEX₈₆ SST (°C). (H) GZ retreat and GZ advance. (I) TEX₈₆ SST (°C) and cycle number. (J) Sea level amplitude (m). (Continued)

empirical estimate does not consider ice sheet dynamics, such as a potential stability threshold in the AIS, caused by the loss of ice shelves, which may be crossed at 1.5°C – 2°C of global warming, after which ongoing mass loss may be rapid and non-linear (DeConto et al., 2021; Golledge et al., 2015). Given the analogous nature of the warm Pliocene to future projections (Burke et al., 2018), the paleoclimate reconstructions presented in this chapter offer a stark warning about the potential future of the AIS if warming continues at its current rate. If a threshold is exceeded, AIS instabilities would likely be irreversible on multi-century timescales (DeConto et al., 2021; Golledge et al., 2015).

9.5 Next steps

In this chapter, we have summarised efforts over the past 50 years to obtain proxy environmental data from geological records of the Miocene and Pliocene, that are informed by modelling outputs to offer insight into AIS behaviour during key episodes and transitions through the Neogene. Despite the progress that has been made, there are many outstanding questions regarding AIS response to past climate variability that require future focus (Colleoni et al., 2021; McKay et al., 2021). There remains significant uncertainty over AIS sensitivity to past intervals of warmth when Earth's average surface temperatures were similar to those forecast for our future, particularly if we fail to achieve emissions targets to limit global warming to well below 2°C (Meinshausen et al., 2011; Rogelj et al., 2016; UNFCCC, 2015). In particular, there is a need to document and constrain the extent of ice margin retreat and amount of ice volume loss during the Miocene and Pliocene, when Earth's average surface temperatures exceeded 2°C . These data offer important benchmarks for testing ice sheet and climate models that are used for future forecasts and projections. These paleo-targets allow us to identify potential thresholds, and the resultant implications for the AIS, when key tipping points in the Earth System are crossed (DeConto et al., 2021).

Whereas sediment cores and seismic records from the margin provide information on maximum AIS extent, we still rely on sea level records and

◀ opal mass accumulation at Antarctic Peninsula ODP Site 1096 (Hillenbrand and Cortese, 2006). (G) Ice berg rafted debris mass accumulate rate from IODP Site U1361 (Patterson et al., 2014). (H) Detrital Nd isotope composition (ϵ_{Nd}) for Pliocene marine sediments from IODP Site U1361 (Cook et al., 2013, 2017). Lower values indicate grounding zone (GZ) retreat. (I) Summary of ocean, sea ice and ice sheet evolution in Ross Embayment based on the AND-1B record (McKay et al., 2012; Naish et al., 2009). Note the cooling in SST and the return of periodic grounded ice sheets to western Ross Embayment occurs at ~ 3.3 Ma, ending a ~ 1.2 Ma period of relatively warm, ice free, open ocean conditions, and the appearance of sea ice and the development Ross Sea polynya between 3.2 and 2.6 Ma. (J) Sea level record (PlioSeaNZ) from the Whanganui Basin, New Zealand, shows maximum glacial-interglacial amplitude change over 20 m (Grant et al., 2019).

deep sea benthic $\delta^{18}\text{O}$ records for estimates of minimum ice volume. Unfortunately, far field sea level records with high temporal precision and well constrained estimates of amplitude are rare (Dumitru et al., 2019; Grant and Naish, 2021; Grant et al., 2019). Furthermore, estimates of ice volume change from deep sea oxygen isotope records require independent estimates of bottom water temperature. These temperature records are difficult to obtain, and proxies are still being developed, tested and improved. Large ($\sim 1\% - 1.5\%$) changes in $\delta^{18}\text{O}$ over glacial–interglacial timescales (100 kyr) during the MCO (Holbourn et al., 2015) are particularly difficult to explain and highlight the challenge we still face in our efforts to understand Earth’s climate system. While some sea level studies propose that the AIS completely melted during peak warm episodes in the MCO (Miller et al., 2020), modelling experiments suggest large areas of inland Antarctica likely remained ice covered throughout the Miocene (Gasson et al., 2016b; Halberstadt et al., 2021; Paxman et al., 2020). Furthermore, a recent climate modelling study suggests that large spatial variability of the AIS in the Miocene was more rapid than previously thought, and in turn enabled large BWT swings (up to 4°C) (Bradshaw et al., 2021). All these studies suffer from a lack of direct evidence to constrain the maximum extent of AIS retreat during intervals of peak warmth and $\delta^{18}\text{O}$ minima.

This ‘challenge’ to better document and constrain maximum ice sheet retreat is also true for the Pliocene. Advance and retreat of the AIS across regions that were grounded below sea level likely occurred throughout the Pliocene and drove sea level amplitude variations of up to 20 m (Dumitru et al., 2019; Grant et al., 2019; Miller et al., 2012). While data from offshore of the WSB (Cook et al., 2013; Patterson et al., 2014) and in the Ross Sea (McKay et al., 2012; Naish et al., 2009) show that margins of both the WAIS and EAIS retreated during warm episodes in the Pliocene, direct observations from inland portions of these marine basins have yet to be recovered. To better investigate and explain AIS dynamics during the Neogene, we need sedimentary records from the continental interior of West and East Antarctica (McKay et al., 2016). Constraints on bed topography are also critical given the sensitivity of ISMs (and by inference the ice sheet) to this boundary condition (Paxman et al., 2020). These paleotopographic constraints are generally limited to DSDP Site 270 in the Ross Sea (Kulhanek et al., 2019; Leckie and Webb, 1983) and in-situ bedrock samples from the East Antarctic craton do not exist. Clearly, more data are needed. Efforts are underway to acquire new Miocene and Pliocene records from near the grounding zone of the WAIS at the Siple Coast and from beneath the Crary Ice Rise (Levy et al., 2020). Site survey data from beneath the EAIS are required to identify potential drilling targets but are difficult to obtain. Recent advances in overice seismic data acquisition using a vibroseis source and snow streamer recording technology show promise and offer the opportunity to more rapidly acquire high quality data sets (Eisen et al., 2015;

Hofstede et al., 2013). Drilling systems that can penetrate the thick ice to acquire rock and sediment samples from beneath the ice are also being developed (Goode and Severinghaus, 2016; Hodgson et al., 2016; Timoney et al., 2020) but have yet to be fully tested in remote locations.

While the Antarctic community endeavours to obtain new ice proximal records of ice sheet and environmental variability, new high-fidelity surface and bottom water temperature records at high temporal resolution across latitudinal transects also need to be established (Koppers and Coggon, 2020). In addition, new multi-proxy CO₂ records at high temporal resolution across key transitions need to be developed. These paleotemperature and paleo-CO₂ data will most likely be generated from deep sea sedimentary records. Legacy cores housed in repositories can be targeted for new studies at the same time new targets could be identified for future drilling through the next phase of the IODP and the International Continental Drilling Program. Finally, the PlioSEANZ record from the Wanganui Basin in New Zealand (Grant et al., 2019) highlights the value of highly resolved records of sea level amplitude change as a constraint on past ice sheet behaviour that is independent of the deep sea δ¹⁸O records. Similar records through key episodes in the Neogene are highly desirable. The MCO and MMCT are obvious targets for new proxy records but the Tortonian Thermal Maximum and late Miocene cooling are also intervals of major change for which we have few records and relatively sparse data.

Finally, next generation atmosphere-ocean models that can be fully coupled with state-of-the-art ice sheet and GIA models are highly desirable. Development of computing capacity may provide the means to run these increasingly complex models over longer (geological) timescales and will help address outstanding questions regarding the connectivity of the AIS to the broader Earth system. Outputs from these modelling experiments will be integrated with existing and new observations to improve our understanding of key processes that influence AIS dynamics and provide targets to advance our ability to reduce uncertainty and forecast change as the world warms over the coming decades and centuries. These major objectives are the focus of the new Scientific Community on Antarctic Research INStabilities and Thresholds in ANTarctica (INSTANT) Scientific Research Program.

Acknowledgements

We wish to acknowledge the support of National Antarctic Programmes and the International Scientific Drilling Programmes and Projects that have allowed our community to acquire the critical records of environmental change that have been discussed in this review. We thank Jenny Black, GNS Science, for her assistance with Fig. 9.2. R.L., T.N., R.M., C.O. and N.G. acknowledge funding support from the New Zealand Ministry of Business and Innovation and Employment through the Antarctic Science Platform

contract (ANTA1801) Antarctic Ice Dynamics Project (ASP-021-01). C.E. acknowledges funding by the Spanish Ministry of Economy, Industry and Competitiveness (grant CTM2017-89711-C2-1/2-P), co-funded by the European Union through FEDER funds. L.F.P. was funded through the European Union's Horizon 2020 research and innovation program under the Marie Skłodowska-Curie grant agreement number 792773 for the West Antarctic Margin Signatures of Ice Sheet Evolution (WAMSISE) Project.

References

- Ackert Jr., R.P., 1990. Surficial geology and geomorphology of the western Asgard Range, Antarctica: implications for late Tertiary glacial history. University of Maine, pp. 147.
- Acton, G., Crampton, J., Di Vincenzo, G., Fielding, C.R., Florindo, F., Hannah, M., et al., and ANDRILL SMS Science Team 2008–2009. Preliminary integrated chronostratigraphy of the AND-2A Core, ANDRILL Southern McMurdo Sound Project Antarctica. In: Harwood, D., Florindo, F., Talarico, F., Levy, R.H. (Eds.), Studies from the ANDRILL Southern McMurdo Sound Project, Antarctica – Initial Science Report on AND-2A. Terra Antartica, pp. 211–220.
- Adkins, J.F., McIntyre, K., Schrag, D.P., 2002. The salinity, temperature, and $\delta^{18}\text{O}$ of the glacial deep ocean. *Science* 298 (5599), 1769–1773.
- Ainley, D.G., Jacobs, S.S., 1981. Sea-bird affinities for ocean and ice boundaries in the Antarctic. *Deep Sea Research Part A. Oceanographic Research Papers* 28 (10), 1173–1185.
- Aitken, A., Roberts, J., Van Ommen, T., Young, D., Golledge, N., Greenbaum, J., et al., 2016. Repeated large-scale retreat and advance of Totten Glacier indicated by inland bed erosion. *Nature* 533 (7603), 385–389.
- Allibone, A.H., Cox, S.C., Smillie, R.W., 1993. Granitoids of the Dry Valleys area, southern Victoria Land: geochemistry and evolution along the early Paleozoic Antarctic Craton margin. *New Zealand Journal of Geology and Geophysics* 36, 299–316.
- Alonso, B., Anderson, J.B., Diaz, J.I., Bartek, L.R., Elliot, D.H., 1992. Pliocene-Pleistocene seismic stratigraphy of the Ross Sea; evidence for multiple ice sheet grounding episodes *Contributions to Antarctic research III. Antarctic Research Series* 57, 93–103.
- Amidon, W.H., Fisher, G.B., Burbank, D.W., Ciccioli, P.L., Alonso, R.N., Gorin, A.L., et al., 2017. Mio-Pliocene aridity in the south-central Andes associated with Southern Hemisphere cold periods. *Proceedings of the National Academy of Sciences* 114 (25), 6474–6479.
- Anderson, J.B., Bartek, L.R., 1992. Cenozoic glacial history of the Ross Sea revealed by intermediate resolution seismic reflection data combined with drill site information. In: Kennett, J.P., Warnke, D.A. (Eds.), *The Antarctic Paleoenvironment: A perspective on global change. American GeophysicalUnion, Washington, D.C.*, pp. 231–263. *Antarctic Research Series*.
- Anderson, J.B., 1999. *Antarctic Marine Geology*. Cambridge University Press, pp. 289.
- Aoki, S., Rintoul, S.R., Ushio, S., Watanabe, S., Bindoff, N.L., 2005. Freshening of the Adélie Land Bottom water near 140 E. *Geophysical Research Letters* 32 (23).
- Aoki, S., Yamazaki, K., Hirano, D., Katsumata, K., Shimada, K., Kitade, Y., et al., 2020. Reversal of freshening trend of Antarctic Bottom Water in the Australian-Antarctic Basin during 2010s. *Scientific Reports* 10 (1), 1–7.
- Armbrecht, L.H., Lowe, V., Escutia, C., Iwai, M., McKay, R., Armand, L.K., 2018. Variability in diatom and silicoflagellate assemblages during mid-Pliocene glacial-interglacial cycles determined in Hole U1361A of IODP Expedition 318, Antarctic Wilkes Land Margin. *Marine Micropaleontology* 139, 28–41.

- Austermann, J., Mitrovica, J.X., Huybers, P., Rovere, A., 2017. Detection of a dynamic topography signal in last interglacial sea-level records. *Science Advances* 3 (7).
- Austermann, J., Pollard, D., Mitrovica, J.X., Mouha, R., Forte, A.M., DeConto, R.M., et al., 2015. The impact of dynamic topography change on Antarctic ice sheet stability during the mid-Pliocene warm period. *Geology* 43 (10), 927–930.
- Badger, M.P., Chalk, T.B., Foster, G.L., Bown, P.R., Gibbs, S.J., Sexton, P.F., et al., 2019. Insensitivity of alkenone carbon isotopes to atmospheric CO₂ at low to moderate CO₂ levels. *Climate of the Past* 15 (2), 539–554.
- Badger, M.P., Schmidt, D.N., Mackensen, A., Pancost, R.D., 2013a. High-resolution alkenone palaeobarometry indicates relatively stable p CO₂ during the Pliocene (3.3–2.8 Ma). *Philosophical Transactions of the Royal Society A: Mathematical, Physical and Engineering Sciences* 371 (2001), 20130094.
- Badger, M.P.S., Lear, C.H., Pancost, R.D., Foster, G.L., Bailey, T.R., Leng, M.J., et al., 2013b. CO₂ drawdown following the middle Miocene expansion of the Antarctic Ice Sheet. *Paleoceanography* 28 (1), 42–53.
- Badgley, C., Barry, J.C., Morgan, M.E., Nelson, S.V., Behrensmeyer, A.K., Cerling, T.E. et al., 2008. Ecological changes in Miocene mammalian record show impact of prolonged climatic forcing. *Proceedings of the National Academy of Sciences* 105 (34), 12145–12149.
- Balch, W.M., Bates, N.R., Lam, P.J., Twining, B.S., Rosengard, S.Z., Bowler, B.C., et al., 2016. Factors regulating the Great Calcite Belt in the Southern Ocean and its biogeochemical significance. *Global Biogeochemical Cycles* 30 (8), 1124–1144.
- Ballantyne, A., Greenwood, D., Sinnenhe Damsté, J., Csank, A., Eberle, J., Rybczynski, N., 2010. Significantly warmer Arctic surface temperatures during the Pliocene indicated by multiple independent proxies. *Geology* 38 (7), 603–606.
- Ballantyne, A.P., Axford, Y., Miller, G.H., Otto-Bliesner, B.L., Rosenbloom, N., White, J. W., 2013. The amplification of Arctic terrestrial surface temperatures by reduced sea-ice extent during the Pliocene. *Palaeogeography, Palaeoclimatology, Palaeoecology* 386, 59–67.
- Barber, P.M., 1981. Messinian subaerial erosion of the proto-Nile Delta. *Marine Geology* 44 (3–4), 253–272.
- Barker, P., Thomas, E., 2004. Origin, signature and palaeoclimatic influence of the Antarctic Circumpolar Current. *Earth-Science Reviews* 66 (1–2), 143–162.
- Barker, P.F., Camerlenghi, A., Baker, P.F.e., Camerlenghi, A.e., Acton, G.D.e., Brachfeld, S.A., et al., 2002. Glacial history of the Antarctic Peninsula from Pacific margin sediments. In: Proceedings of the Ocean Drilling Program, Scientific Results, Antarctic Glacial History and Sea-Level Change; covering Leg 178 of the cruises of the drilling vessel JOIDES Resolution; Punta Arenas, Chile, to Cape Town, South Africa; sites 1095–1103; 5 February–9 April 1998. Proceedings of the Ocean Drilling Program, Scientific Results (CD-ROM), 178: 40.
- Barker, P.F., Filippelli, G.M., Florido, F., Martin, E.E., Scher, H.D., 2007. Onset and role of the Antarctic Circumpolar Current. *Deep Sea Research Part II: Topical Studies in Oceanography* 54 (21), 2388–2398.
- Barrett, P., Francis, J., Gohl, K., Haywood, A., Siddoway, C., Wilson, D., 2009. ANTscape: antarctic Paleotopographic maps for the last 100 million years, AGU Fall Meeting Abstracts, p. PP43A-1561.
- Barrett, P.J. (Ed.), 1989. Antarctic Cenozoic history from the CIROS-1 drillhole, McMurdo Sound, Antarctica. NZ DSIR Bulletin, p. 254.
- Barrett, P.J., Ricci, C.A., 2000. Studies from the Cape Roberts Project, Ross Sea, Antarctica; scientific report of CPR-2/2A. *Terra Antartica* 7 (3–4), 211–654.

- Barrett, P.J., Ricci, C.A., 2001. Studies from the Cape Roberts Project, Ross Sea, Antarctica; scientific report of CRP-3. *Terra Antarctica* 8 (3–4), 121–620.
- Barrett, P.J., 1971. Stratigraphy and paleogeography of the Beacon Supergroup in the Transantarctic Mountains. Antarctica. 2nd Gondwana Symp., Proc. Pap. 249–256.
- Barrett, P.J., 1975. Textural characteristics of Cenozoic preglacial and glacial sediments at Site 270, Ross Sea, Antarctica. Initial Reports of the Deep Sea Drilling Project 28, 757–766.
- Barrett, P.J., 1986. Antarctic Cenozoic history from the MSSTS-1 drillhole, McMurdo Sound. NZ DSIR Bulletin 237, 172.
- Barrett, P.J., 2007. Cenozoic climate and sea level history from glacimarine strata off the Victoria Land coast, Cape Roberts Project, Antarctica. In: Hambrey, M.J., Christoffersen, P., Glasser, N.F., Hubbard, B. (Eds.), *Glacial Sedimentary Processes and Products*. Blackwell: International Association of Sedimentologists, pp. 259–287.
- Barrett, P.J., 2009. Cenozoic climate and sea level history from Glacimarine Strata off the Victoria Land Coast, Cape Roberts Project, Antarctica. *Glacial Sedimentary Processes and Products*. Blackwell Publishing Ltd., pp. 259–287.
- Barrett, P.J., 2013. Resolving views on Antarctic Neogene glacial history—the Sirius debate. *Earth and Environmental Science Transactions of the Royal Society of Edinburgh* 104 (1), 31–53.
- Barrett, P.J., Hambrey, M.J., 1992. Plio-Pleistocene sedimentation in Ferrar Fjord, Antarctica. *Sedimentology* 39, 109–123.
- Barrett, P.J., Elliot, D.H., Lindsay, J.F., 1986. The Beacon Supergroup (Devonian-Triassic) and Ferrar Group (Jurassic) in the Beardmore Glacier area, Antarctica. *Antarctic Research Series* 36 (14), 339–428.
- Barrett, P.J., Fielding, C.R.A., Wise, S. (Eds.), 1998. Initial Report on CRP-1, Cape Roberts Project, Antarctica, 187. *Terra Antartica*, Siena.
- Barrett, P.J., Grindley, G.W., Webb, P.N., 1972. The Beacon Supergroup of East Antarctica. *Antarctic geology and geophysics*. International Union of Geological Sciences. Series B 1, 319–332.
- Barron, J.A., Keller, G., 1982. Widespread Miocene deep-sea hiatuses: coincidence with periods of global cooling. *Geology* 10 (11), 577–581.
- Barron, J., Larsen, B., et al., 1989. *Proc. ODP, Init. Repts.*, 119. College Station, TX (Ocean Drilling Program). Available from: <https://doi.org/10.2973/odp.proc.ir.119.1989>.
- Barron, J., Larsen, B., et al., 1991. *Proc. ODP, Sci. Results*, 119. College Station, TX (Ocean Drilling Program). Available from: <https://doi.org/10.2973/odp.proc.sr.119.1991>.
- Bart, P.J., De Santis, L., 2012. Glacial intensification during the Neogene: a review of seismic stratigraphic evidence from the Ross Sea. Antarctica, continental shelf. *Oceanography* 25 (3), 166–183.
- Bart, P.J., Owolana, B., 2012. On the duration of West Antarctic Ice Sheet grounding events in Ross Sea during the Quaternary. *Quaternary Science Reviews* 47, 101–115.
- Bartek, L.R., Vail, P.R., Anderson, J.B., Emmett, P.A., Wu, S., 1991. The effect of Cenozoic ice sheet fluctuations in Antarctica on the stratigraphic signature of the Neogene. *Journal of Geophysical Research* 96B, 6753–6778.
- Bartoli, G., Höönsch, B., Zeebe, R.E., 2011. Atmospheric CO₂ decline during the Pliocene intensification of Northern Hemisphere glaciations. *Paleoceanography* 26 (4).
- Bassis, J.N., Walker, C., 2012. Upper and lower limits on the stability of calving glaciers from the yield strength envelope of ice. *Proceedings of the Royal Society A: Mathematical, Physical and Engineering Sciences* 468 (2140), 913–931.

- Beaman, R.J., O'Brien, P.E., Post, A.L., De Santis, L., 2010. A new high-resolution bathymetry model for the Terre Adélie and George V continental margin, East Antarctica. *Antarctic Science* 23 (1), 95.
- Beerling, D.J., Fox, A., Anderson, C.W., 2009. Quantitative uncertainty analyses of ancient atmospheric CO₂ estimates from fossil leaves. *American Journal of Science* 309 (9), 775–787.
- Behrendt, J.C., Blankenship, D.D., Morse, D.L., Bell, R.E., James, T.Se, Jacka, T.He, et al., 2004. Shallow-source aeromagnetic anomalies observed over the West Antarctic ice sheet compared with coincident bed topography from radar ice sounding; new evidence for glacial “removal” of subglacially erupted late Cenozoic rift-related volcanic edifices. *Ice sheets and neotectonics. Global and Planetary Change* 42 (1–4), 177–193.
- Behrendt, J.C., Blankenship, D.D., Morse, D.L., Finn, C.A., Bell, R.E., Smellie, J.Le, et al., 2002. Subglacial volcanic features beneath the West Antarctic ice sheet interpreted from aeromagnetic and radar ice sounding. *Volcano-ice interaction on Earth and Mars. Geological Society Special Publications* 202, 337–355.
- Behrendt, J.C., Saltus, R., Damaske, D., McCafferty, A.E., Finn, C.A., Blankenship, D., et al., 1996. Patterns of late Cenozoic volcanic and tectonic activity in the West Antarctic rift system revealed by aeromagnetic surveys. *Tectonics* 15 (3), 660–676.
- Bell, R.E., Chu, W., Kingslake, J., Das, I., Tedesco, M., Tinto, K.J., et al., 2017. Antarctic ice shelf potentially stabilized by export of meltwater in surface river. *Nature* 544 (7650), 344–348.
- Berends, C.J., de Boer, B., Dolan, A.M., Hill, D.J., van de Wal, R.S.W., 2019. Modelling ice sheet evolution and atmospheric CO₂ during the Late Pliocene. *Climate of the Past* 15 (4), 1603–1619.
- Bertram, R.A., Wilson, D.J., van de Flierdt, T., McKay, R.M., Patterson, M.O., Jimenez-Espejo, F.J., et al., 2018. Pliocene deglacial event timelines and the biogeochemical response offshore Wilkes Subglacial Basin, East Antarctica. *Earth and Planetary Science Letters* 494, 109–116.
- Beu, A., Taviani, M., 2013. Early Miocene Mollusca from McMurdo Sound, Antarctica (ANDRILL 2A drill core), with a review of Antarctic Oligocene and Neogene Pectinidae (Bivalvia). *Palaeontology* 57 (2), 299–342.
- Beu, A., 1990. Molluscan generic diversity of New Zealand Neogene stages: extinction and biostratigraphic events. *Palaeogeography, Palaeoclimatology, Palaeoecology* 77 (3–4), 279–288.
- Beu, A.G., 1974. Molluscan evidence of warm sea temperatures in New Zealand during Kapitean (late Miocene) and Waipipian (middle Pliocene) time. *New Zealand Journal of Geology and Geophysics* 17 (2), 465–479.
- Bierman, P.R., Shakun, J.D., Corbett, L.B., Zimmerman, S.R., Rood, D.H., 2016. A persistent and dynamic East Greenland Ice Sheet over the past 7.5 million years. *Nature* 540 (7632), 256–260.
- Bijl, P.K., Houben, A.J., Bruls, A., Pross, J., Sangiorgi, F., 2018a. Stratigraphic calibration of Oligocene–Miocene organic-walled dinoflagellate cysts from offshore Wilkes Land, East Antarctica, and a zonation proposal. *Journal of Micropalaeontology* 37 (1), 105–138.
- Bijl, P.K., Houben, A.J., Hartman, J.D., Pross, J., Salabarnada, A., Escutia, C., et al., 2018b. Paleoceanography and ice sheet variability offshore Wilkes Land, Antarctica—part 2: insights from Oligocene–Miocene dinoflagellate cyst assemblages. *Climate of the Past* 14 (7), 1015–1033.
- Billups, K., Ravelo, A.C., Zachos, J.C., 1997. Early Pliocene deep-water circulation: stable isotope evidence for enhanced Northern Component Deep Water. *Proc. Ocean Drill. Program, Scientific Results* 154, 319–330.

- Billups, K., Schrag, D.P., 2002. Paleotemperatures and ice volume of the past 27 Myr revisited with paired Mg/Ca and $^{18}\text{O}/^{16}\text{O}$ measurements on benthic foraminifera. *Paleoceanography* 17 (1), 1003.
- Billups, K., Schrag, D.P., 2003. Application of benthic foraminiferal Mg/Ca ratios to questions of Cenozoic climate change. *Earth and Planetary Science Letters* 209, 181–195.
- Bindoff, N.L., Rosenberg, M.A., Warner, M.J., 2000. On the circulation and water masses over the Antarctic continental slope and rise between 80 and 150 E. *Deep Sea Research Part II: Topical Studies in Oceanography* 47 (12–13), 2299–2326.
- Bliss, A.K., Cuffey, K.M., Kavanaugh, J.L., 2011. Sublimation and surface energy budget of Taylor Glacier, Antarctica. *Journal of Glaciology* 57 (204), 684–696.
- Bockheim, J.G., 2010. Soil preservation and ventifact recycling from dry-based glaciers in Antarctica. *Antarctic Science* 22, 409–417.
- Bockheim, J.G., McLeod, M., 2006. Soil formation in Wright Valley, Antarctica since the late Neogene. *Geoderma* 137, 109–116.
- Böhme, M., 2003. The Miocene climatic optimum: evidence from ectothermic vertebrates of Central Europe. *Palaeogeography, Palaeoclimatology, Palaeoecology* 195 (3–4), 389–401.
- Bolton, C.T., Hernández-Sánchez, M.T., Fuertes, M.-Á., González-Lemos, S., Abrevaya, L., Méndez-Vicente, A., et al., 2016. Decrease in coccolithophore calcification and CO₂ since the middle Miocene. *Nature Communications* 7 (1), 10284.
- Bradshaw, C.D., Langebroek, P.M., Lear, C.H., Lunt, D.J., Coxall, H.K., Sosdian, S.M., et al., 2021. Hydrological impact of Middle Miocene Antarctic ice-free areas coupled to deep ocean temperatures. *Nature Geoscience* 14 (6), 429–436.
- Brady, H.T., 1979. A diatom report on DVDP cores 3, 4a, 12, 14, 15 and other related surface sections. In: Nagata, T. (Ed.), *Proceedings of the Seminar III on Dry Valley Drilling Project, 1978. Memoirs of National Institute of Polar Research, Special Issue*. pp. 150–163.
- Brady, H.T., 1982. Late Cenozoic history of Taylor and Wright valleys and McMurdo Sound inferred from diatoms in Dry Valley Drilling Project cores. In: Craddock, C. (Ed.), *Antarctic Geoscience*. University of Wisconsin Press, Madison, pp. 1123–1131.
- Bragg, F., Lunt, D.J., Haywood, A., 2012. Mid-Pliocene climate modelled using the UK hadley centre model: PlioMIP experiments 1 and 2. *Geoscientific Model Development* 5 (5), 1109–1125.
- Brancolini, G., Busetti, M., Marchetti, A., De Santis, L., Zanolla, C., Cooper, A.K., et al., 1995a. Descriptive text for the seismic stratigraphic atlas of the Ross Sea, Antarctica. *Geology and seismic stratigraphy of the Antarctic margin. Antarctic Research Series* 68, A271–A286.
- Brancolini, G., Cooper, A.K., Coren, F., Cooper, A.Ke, Barker, P.Fe, Brancolini, Ge, 1995b. Seismic facies and glacial history in the western Ross Sea (Antarctica). *Geology and seismic stratigraphy of the Antarctic margin. Antarctic Research Series* 68, 209–233.
- Brancolini, G., Cooper, A.K., Coren, F., 1995. Seismic facies and glacial history in the western Ross Sea (Antarctica). *Geology and Seismic Stratigraphy of the Antarctic Margin*, 68, pp. 209–233.
- Brierley, C., Burls, N., Ravelo, C., Fedorov, A., 2015. Pliocene warmth and gradients. *Nature Geoscience* 8 (6), 419–420.
- Brigham-Grette, J., Melles, M., Minyuk, P., Andreev, A., Tarasov, P., DeConto, R., et al., 2013. Pliocene warmth, polar amplification, and stepped Pleistocene cooling recorded in NE Arctic Russia. *Science* 340 (6139), 1421–1427.

- Brunet, M., 2010. Two new Mio-Pliocene Chadian hominids enlighten Charles Darwin's 1871 prediction. *Philosophical Transactions of the Royal Society B: Biological Sciences* 365 (1556), 3315–3321.
- Brunet, M., Guy, F., Pilbeam, D., Mackaye, H.T., Likius, A., Ahounta, D., et al., 2002. A new hominid from the Upper Miocene of Chad, Central Africa. *Nature* 418 (6894), 145–151.
- Budillon, G., Spezie, G., 2000. Thermohaline structure and variability in the Terra Nova Bay polynya, Ross Sea. *Antarctic Science* 12 (4), 493–508.
- Bull, C., McKelvey, B.C., Webb, P.N., 1962. Quaternary glaciations in southern Victoria Land, Antarctica. *Journal of Glaciology* 4 (31), 63–78.
- Burke, K., Williams, J., Chandler, M., Haywood, A., Lunt, D., Otto-Bliesner, B., 2018. Pliocene and Eocene provide best analogs for near-future climates. *Proceedings of the National Academy of Sciences* 115(52), 13288–13293.
- Burls, N.J., Bradshaw, C., De Boer, A.M., Herold, N., Huber, M., Pound, M., et al., 2021. Simulating Miocene warmth: insights from an opportunistic multi-model ensemble (MioMIP1). *Paleoceanography and Paleoclimatology* 36, e2020PA004054.
- Busetti, M., Camerlenghi, A., Carta, A., Lodo, E., Sauli, C., 1993. The Ross Sea (Antarctica): a review of the geological and geophysical exploration. *Bollettino di Geofisica Teorica ed Applicata* 35, 245–263.
- Busetti, M., Cooper, A.K., 1994. Possible ages and origins of unconformity U6 in the Ross Sea, Antarctica. *Terra Antartica* 1 (Special Issue), 341–343.
- Caburlotto, A., Lucchi, R., De Santis, L., Macrì, P., Tolotti, R., 2010. Sedimentary processes on the Wilkes Land continental rise reflect changes in glacial dynamic and bottom water flow. *International Journal of Earth Sciences* 99 (4), 909–926.
- Calkin, P.E., 1974. Subglacial geomorphology surrounding the ice-free valleys of Southern Victoria Land, Antarctica. *Journal of Glaciology* 13, 415–429.
- Calkin, P.E., Bull, C., 1972. Interaction of the East Antarctic Ice Sheet, alpine glaciations and sea-level in the Wright Valley area, southern Victoria Land. In: Adie, R.J. (Ed.), *Antarctic Geology and Geophysics*. Universitetsforlaget, Oslo, pp. 435–440.
- Campagne, P., Crosta, X., Houssais, M.-N., Swingedouw, D., Schmidt, S., Martin, A., et al., 2015. Glacial ice and atmospheric forcing on the Mertz Glacier Polynya over the past 250 years. *Nature Communications* 6 (1), 1–9.
- Cape Roberts Science Team, 1998. Miocene strata in CRP-1, Cape Roberts Project, Antarctica. *Terra Antartica* 5 (1), 63–124.
- Carlson, A.E., Dutton, A., Long, A.J., Milne, G.A., 2019. PALeo constraints on SEA level rise (PALSEA): ice-sheet and sea-level responses to past climate warming. *Quaternary Science Reviews* 212, 28–32.
- Carter, A., Curtis, M., Schwanethal, J., 2014. Cenozoic tectonic history of the South Georgia microcontinent and potential as a barrier to Pacific-Atlantic through flow. *Geology* 42 (4), 299–302.
- Carter, L., Bostock-Lyman, H., Bowen, M., 2021. Water masses, circulation and change in the modern Southern Ocean. In: Florindo, F., et al. (Eds.), *Antarctic Climate Evolution*, second ed. Elsevier (this volume).
- Carter, A., Riley, T.R., Hillenbrand, C.-D., Rittner, M., 2017. Widespread Antarctic glaciation during the Late Eocene. *Earth and Planetary Science Letters* 458, 49–57.
- Cartwright, K., Treves, S.B., Torii, T., 1974. Geology of DVDP 4, Lake Vanda, Wright Valley, Antarctica. *Dry Valley Drilling Project Bulletin* 3.

- Castagno, P., Capozzi, V., DiTullio, G.R., Falco, P., Fusco, G., Rintoul, S.R., et al., 2019. Rebound of shelf water salinity in the Ross Sea. *Nature Communications* 10 (1), 1–6.
- Cerling, T.E., 1992. Use of carbon isotopes in paleosols as an indicator of the P (CO₂) of the paleoatmosphere. *Global Biogeochemical Cycles* 6 (3), 307–314.
- Chorley, H., 2021. Antarctic ice sheet and climate evolution during the mid-Miocene. Open Access Victoria University of Wellington | Te Herenga Waka. Thesis. Available from: <https://doi.org/10.26686/wgtn.14150105.v1>.
- Chow, J.M., Bart, P.J., 2003. West Antarctic ice sheet grounding events on the Ross Sea outer continental shelf during the middle Miocene. *Palaeogeography, Palaeoclimatology, Palaeoecology* 198, 169–186.
- Clapperton, C.M., Sugden, D.E., 1990. Late Cenozoic glacial history of the Ross embayment, Antarctica. *Quaternary Science Reviews* 9 (2–3), 253–272.
- Clerc, F., Minchew, B.M., Behn, M.D., 2019. Marine ice cliff instability mitigated by slow removal of ice shelves. *Geophysical Research Letters* 46 (21), 12108–12116.
- Coenen, J., Scherer, R., Baudoin, P., Warny, S., Castañeda, I., Askin, R., 2020. Paleogene marine and terrestrial development of the West Antarctic Rift System. *Geophysical Research Letters* 47 (3), e2019GL085281.
- Colleoni, F., Santis, L. De, Naish, T., DeConto, R.M., Escutia, C., Stocchi, P., et al., 2021. Past Antarctic ice sheet dynamics and implications for future sea-level change. In: Florindo, F., et al. (Eds.), *Antarctic Climate Evolution*, second ed. Elsevier (this volume).
- Colleoni, F., Santis, De, Siddoway, L., Bergamasco, C.S., Golledge, A., Lohmann, N.R., et al., 2018. Spatio-temporal variability of processes across Antarctic ice-bed-ocean interfaces. *Nature Communications* 9 (1), 2289.
- Compston, W., McDougall, I., Heier, K., 1968. Geochemical comparison of the mesozoic basaltic rocks of Antarctica, South Africa, South America and Tasmania. *Geochimica et Cosmochimica Acta* 32 (2), 129–149.
- Cook, C.P., Hemming, S.R., van de Flierdt, T., Davis, E.L.P., Williams, T., Galindo, A.L., et al., 2017. Glacial erosion of East Antarctica in the Pliocene: a comparative study of multiple marine sediment provenance tracers. *Chemical Geology* 466, 199–218.
- Cook, C.P., Hill, D.J., van de Flierdt, T., Williams, T., Hemming, S.R., Dolan, A.M., et al., 2014. Sea surface temperature control on the distribution of far-traveled Southern Ocean ice rafted detritus during the Pliocene. *Paleoceanography* 29 (6), 533–548.
- Cook, C.P., van de Flierdt, T., Williams, T., Hemming, S.R., Iwai, M., Kobayashi, M., et al., 2013. Dynamic behaviour of the East Antarctic ice sheet during Pliocene warmth. *Nature Geoscience* 6, 765–769.
- Cooper, A.K., Barker, P.F., Brancolini, G., 1995. *Geology and Seismic Stratigraphy of the Antarctic Margin, Atlas, CD-ROMs, Antarctic Research Series*. American Geophysical Union, Washington, DC, p. 301.
- Cooper, A.K., Brancolini, G., Escutia, C., Kristoffersen, Y., Larter, R., Leitchenkov, G., et al., 2008. Cenozoic climate history from seismic reflection and drilling studies on the Antarctic continental margin. *Developments in Earth and Environmental Sciences* 8, 115–234.
- Cooper, A.K., O'Brien, P.E., 2004. Leg 188 synthesis: transitions in the glacial history of the Prydz Bay region, East Antarctica, from ODP drilling. In: *Proceedings of the Ocean Drilling Program: Scientific Results*, pp. 1–42.
- Cooper, A.K., O'Brien, P.E., Richter, C., 2004. Scientific results. *Proceedings of the Ocean Drilling Programme*, p. 188.

- Cooper, A.K., Davey, F.J., 1987. The Antarctic Continental Margin; Geology and Geophysics of the Western Ross Sea. Circum-Pacific Council for Energy and Mineral Resources, Earth Science Series, 5B, 253 pp.
- Cornford, S.L., Seroussi, H., Asay-Davis, X.S., Gudmundsson, G.H., Arthern, R., Borstad, C., et al., 2020. Results of the third Marine Ice Sheet Model Intercomparison Project (MISMIP+). *The Cryosphere* 14 (7), 2283–2301.
- Cortese, G., Gersonne, R., Hillenbrand, C.-D., Kuhn, G., 2004. Opal sedimentation shifts in the World Ocean over the last 15 Myr. *Earth and Planetary Science Letters* 224 (3–4), 509–527.
- Cox, S.C., Turnbull, I., Isaac, M., Townsend, D.B., Lytle, B.S., 2012. Geology of Southern Victoria Land, Antarctica.
- Cramer, B., Toggweiler, J., Wright, J., Katz, M., Miller, K., 2009. Ocean overturning since the Late Cretaceous: Inferences from a new benthic foraminiferal isotope compilation. *Paleoceanography* 24 (4).
- Cramer, B.S., Miller, K.G., Barrett, P.J., Wright, J.D., 2011. Late Cretaceous–Neogene trends in deep ocean temperature and continental ice volume: reconciling records of benthic foraminiferal geochemistry ($\delta^{18}\text{O}$ and Mg/Ca) with sea level history. *Journal of Geophysical Research: Oceans* 116 (C12), C12023.
- Crampton, J.S., Cody, R.D., Levy, R., Harwood, D., McKay, R., Naish, T.R., 2016. Southern Ocean phytoplankton turnover in response to stepwise Antarctic cooling over the past 15 million years. *Proceedings of the National Academy of Sciences* 113 (25), 6868–6873.
- Cui, Y., Schubert, B.A., Jahren, A.H., 2020. A 23 my record of low atmospheric CO₂. *Geology*.
- Dalziel, I.W.D., Lawver, L.A., Pearce, J.A., Barker, P.F., Hastie, A.R., Barfod, D.N., et al., 2013. A potential barrier to deep Antarctic circumpolar flow until the late Miocene? *Geology* 41 (9), 947–950.
- Davey, F., Cita, M.B., Vander Meer, J.J.M., Tessonson, F., Thomson, M.R., Barrett, P.J., et al., 2001. Drilling for Antarctic Cenozoic Climate and Tectonic History at Cape Roberts, Southwestern Ross Sea. *EOS Transactions of the American Geophysical Union* 82 (48), 585–590.
- Davey, F.J., Brancolini, G., Hamilton, R.J., Henrys, S.A., Sorlien, C.C., Bartek, L.R., 2000. A revised correlation of seismic stratigraphy at the Cape Roberts drillsites with the seismic stratigraphy of the Victoria Land basin. In: Davey, F.J., Jarrard, R.D. (Eds.), *Studies from the Cape Roberts Project, Ross Sea, Antarctica; Scientific Results of CRP-2/2A; Part I, Geophysics and Physical Properties Studies for CRP-2/2A*. Terra Antarctica, pp. 215–220.
- David, T.W.E., Priestley, R.E., 1914. Glaciology, physiography and tectonic geology of south Victoria Land: British Antarctic Expedition, 1907–09, reports of scientific investigations. *Geology* 1, 1–319.
- de Boer, B., Dolan, A.M., Bernales, J., Gasson, E., Goelzer, H., Golledge, N.R., et al., 2015. Simulating the Antarctic ice sheet in the late-Pliocene warm period: PLISMIP-ANT, an ice-sheet model intercomparison project. *The Cryosphere* 9 (3), 881–903.
- de Boer, B., Dolan, A.M., Bernales, J., Gasson, E., Goelzer, H., Golledge, N.R., et al., 2014. Simulating the Antarctic ice sheet in the Late-Pliocene warm period: PLISMIP-ANT, an ice-sheet model intercomparison project. *The Cryosphere Discuss* 8 (6), 5539–5588.
- de Boer, B., Stocchi, P., Whitehouse, P.L., van de Wal, R.S.W., 2017. Current state and future perspectives on coupled ice-sheet–sea-level modelling. *Quaternary Science Reviews* 169, 13–28.

- De Boer, B., Van de Wal, R., Bintanja, R., Lourens, L., Tuerter, E., 2010. Cenozoic global ice-volume and temperature simulations with 1-D ice-sheet models forced by benthic $\delta^{18}\text{O}$ records. *Annals of Glaciology* 51 (55), 23–33.
- De Santis, L., Anderson, J.B., Brancolini, G., Zayatz, I., 1995. Seismic record of Late Oligocene through Miocene glaciation on the central and eastern Continental shelf of the Ross Sea, *Geology and Seismic Stratigraphy of the Antarctic Margin*. Antarctic Research Series. AGU, Washington, D.C., pp. 235–260.
- De Santis, L., Brancolini, G., Donda, F., Harris, P.T., Brancolini, G., Bindoff, N.L.E., et al., 2003. Seismo-stratigraphic analysis of the Wilkes Land continental margin (East Antarctica); influence of glacially driven processes on the Cenozoic deposition. Recent investigations of the Mertz Polynya and George Vth Land continental margin, East Antarctica. *Deep-Sea Research. Part II: Topical Studies in Oceanography* 50 (8–9), 1563–1594.
- De Santis, L., Prato, S., Brancolini, G., Lovo, M., Torelli, L., 1999. The Eastern Ross Sea continental shelf during the Cenozoic: implications for the West Antarctic ice sheet development. *Global and Planetary Change* 23 (1–4), 173–196.
- De Vleeschouwer, D., Vahlenkamp, M., Crucifix, M., Pälike, H., 2017. Alternating Southern and Northern Hemisphere climate response to astronomical forcing during the past 35 m.y. *Geology* 45 (4), 375–378.
- de Vries, M.v.W., Bingham, R.G., Hein, A., 2017. A new volcanic province: an inventory of subglacial volcanoes in West Antarctica. In: Siegert, M.J., Jamieson, S.S.R., White, D.A. (Eds.), *Exploration of Subsurface Antarctica: Uncovering Past Changes and Modern Processes*. Geological Society, London, Special Publications 461.
- DeCesare, M., Pekar, S., 2016. Data report: foraminiferal stable isotope and percent calcium carbonate analysis from IODP Expedition 318 Hole U1361A. In: Proceedings of IODP, 2 pp.
- Decesari, R.C., Wilson, D.S., Faulkner, M., Luyendyk, B.P., Sorlien, C.C., 2005. A Model for Cretaceous and Tertiary Extension of the Ross Sea, Antarctica. *EOS (American Geophysical Union Transactions)*, 86(52): Fall Meet. Suppl., Abstract T53E-08.
- Decesari, R.C., Wilson, D.S., Luyendyk, B.P., Faulkner, M., 2007. Cretaceous and Tertiary extension throughout the Ross Sea, Antarctica. In: Cooper, A.K., Raymond, C.R., et al. (Eds.), *Antarctica: A Keystone in a Changing World—Online Proceedings of the 10th ISAES X*. Available from: <https://doi.org/10.3133/of2007-1047.srp3098>.
- DeConto, R.M., Pollard, D., 2003. Rapid Cenozoic glaciation of Antarctica induced by declining atmospheric CO₂. *Nature (London)* 421 (6920), 245–249.
- DeConto, R.M., Pollard, D., 2016. Contribution of Antarctica to past and future sea-level rise. *Nature* 531 (7596), 591–597.
- DeConto, R.M., Pollard, D., Harwood, D., 2007. Sea ice feedback and Cenozoic evolution of Antarctic climate and ice sheets. *Paleoceanography* 22, PA3214. Available from: <https://doi.org/10.1029/2006PA001350>.
- DeConto, R.M., Pollard, D., Kowalewski, D., 2012. Modeling Antarctic ice sheet and climate variations during Marine Isotope Stage 31. *Global and Planetary Change* 88–89, 45–52.
- DeConto, R.M., Pollard, D., Alley, R.B., Velicogna, I., Gasson, E., Gomez, N., et al., 2021. The Paris Climate Agreement and future sea-level rise from Antarctica. *Nature* 593 (7857), 83–89.
- DeConto, R.M., Pollard, D., Wilson, P.A., Pälike, H., Lear, C., Pagani, M., 2008. Thresholds for Cenozoic Bipolar Glaciation. *Nature* 455, 652–657.
- Denton, G.H., Armstrong, R.L., Stuiver, M., 1971. *The Late Cenozoic Glacial History of Antarctica: the Late Cenozoic glacial ages*. Yale University Press, New Haven, CT, pp. 267–306.
- Denton, G.H., Prentice, M.L., Kellogg, D.E., Kellogg, T.B., 1984. Late Tertiary history of the Antarctic ice sheet; evidence from the dry valleys. *Geology (Boulder)* 12 (5), 263–267.

- Di Roberto, A., Pompilio, M., Wilch, T.I., 2010. Late Miocene submarine volcanism in ANDRILL AND-1B drill core, Ross Embayment, Antarctica. *Geosphere* 6 (5), 524–536.
- Di Vincenzo, G., Bracciali, L., Del Carlo, P., Panter, K., Rocchi, S., 2009. ^{40}Ar - ^{39}Ar dating of volcanicogenic products from the AND-2A core (ANDRILL Southern McMurdo Sound Project, Antarctica): correlations with the Erebus Volcanic Province and implications for the age model of the core. *Bulletin of Volcanology* 72, 487–505.
- Dickinson, W.W., Schiller, M., Ditchburn, B.G., Graham, I.J., Zondervan, A., 2012. Meteoric Be-10 from Sirius Group suggests high elevation McMurdo Dry Valleys permanently frozen since 6 Ma. *Earth and Planetary Science Letters* 355–356, 13–19.
- Diester-Haass, L., Meyers, P.A., Bickert, T., 2004. Carbonate crash and biogenic bloom in the late Miocene: Evidence from ODP Sites 1085, 1086, and 1087 in the Cape Basin, southeast Atlantic Ocean. *Paleoceanography* 19 (1).
- Diester-Haass, L., Meyers, P.A., Vidal, L., Christensen, B.A.E., Giraudieu, J.E., 2002. The late Miocene onset of high productivity in the Benguela Current upwelling system as part of a global pattern. *Marine Geology* 180 (1–4), 87–103.
- Dinniman, M.S., Klinck, J.M., 2002. The influence of open vs periodic alongshore boundaries on circulation near submarine canyons. *Journal of Atmospheric and Oceanic Technology* 19 (10), 1722–1737.
- Dinniman, M.S., Klinck, J.M., Smith Jr, W.O., 2003. Cross-shelf exchange in a model of the Ross Sea circulation and biogeochemistry. *Deep Sea Research Part II: Topical Studies in Oceanography* 50 (22–26), 3103–3120.
- Dinniman, M.S., Klinck, J.M., Smith Jr, W.O., 2007. Influence of sea ice cover and icebergs on circulation and water mass formation in a numerical circulation model of the Ross Sea, Antarctica. *Journal of Geophysical Research: Oceans* 112 (C11).
- Dolan, A.M., Haywood, A.M., Hill, D.J., Dowsett, H.J., Hunter, S.J., Lunt, D.J., Pickering, S.J., 2011. Sensitivity of Pliocene ice sheets to orbital forcing. *Palaeogeography, Palaeoclimatology, Palaeoecology* 309, 98–110.
- Dolan, A.M., De Boer, B., Bernales, J., Hill, D.J., Haywood, A.M., 2018. High climate model dependency of Pliocene Antarctic ice-sheet predictions. *Nature Communications* 9 (1), 1–12.
- Dolan, A.M., Koenig, S.J., Hill, D.J., Haywood, A.M., DeConto, R.M., 2012. Pliocene Ice Sheet Modelling Intercomparison Project (PLISMIP)—experimental design. *Geoscientific Model Development* 5 (4), 963–974.
- Donda, F., Brancolini, G., De Santis, L., Trincardi, F., Harris, P.T.E., Brancolini, G.E., et al., 2003. Seismic facies and sedimentary processes on the continental rise off Wilkes Land (East Antarctica): evidence of bottom current activity. Recent investigations of the Mertz Polynya and George Vth Land continental margin, East Antarctica. *Deep-Sea Research. Part II: Topical Studies in Oceanography* 50 (8–9), 1509–1527.
- Doran, P., Fountain, A., 2019. McMurdo Dry Valleys LTER - High frequency measurements from Friis Hills Meteorological Station (FRSM) - Taylor Valley, Antarctica - 1993 to present ver 11. Environmental Data Initiative. Available from: <https://doi.org/10.6073/pasta/9ff39ef4762d45d4ff35576b79d63a2b>.
- Doran, P.T., McKay, C.P., Clow, G.D., Dana, G.L., Fountain, A.G., Nylen, T., et al., 2002. Valley floor climate observations from the McMurdo dry valleys, Antarctica, 1986–2000. *Journal of Geophysical Research: Atmospheres* 107 (D24), ACL 13-11–ACL 13-12.
- Dowsett, H.J., Cronin, T.M., 1990. High eustatic sea level during the middle Pliocene; evidence from the Southeastern United States Atlantic Coastal Plain; with Suppl. Data 90–13. *Geology (Boulder)* 18 (5), 435–438.

- Dowsett, H.J., Barron, J.A., Poore, R.Z., Poore, R.Ze., Sloan, L.C.E., 1996. Middle Pliocene sea surface temperatures: a global reconstruction. *Climates and climate variability of the Pliocene*. *Marine Micropaleontology* 27 (1–4), 13–25.
- Dowsett, H.J., Robinson, M.M., Foley, K.M., Herbert, T.D., Otto-Bliesner, B.L., Spivey, W., 2019. Mid-piacenzian of the North Atlantic Ocean. *Stratigraphy* 16 (3), 119–144.
- Dowsett, H.J., Robinson, M.M., Haywood, A.M., Hill, D.J., Dolan, A.M., Stoll, D.K., et al., 2012. Assessing confidence in Pliocene sea surface temperatures to evaluate predictive models. *Nature Climate Change* 2 (5), 365–371.
- Drewry, D.J., 1976. Sedimentary basins of the East Antarctic craton from geophysical evidence. *Tectonophysics* 36, 301–314.
- Drewry, D.J. (Ed.), 1983. *Antarctica: Glaciological and Geophysical Folio*. Scott Polar Research Institute, Cambridge, 8 maps pp.
- Drewry, D.J., Jordan, S.R., 1983. *The Bedrock Surface of Antarctica*. Scott Polar Research Institute, Cambridge.
- Dumitru, O.A., Austermann, J., Polyak, V.J., Fornós, J.J., Asmerom, Y., Ginés, J., et al., 2019. Constraints on global mean sea level during Pliocene warmth. *Nature* 574 (7777), 233–236.
- Duncan, B., McKay, R., Bendle, J., Naish, T., Inglis, G.N., Moosse, H., et al., 2019. Lipid biomarker distributions in Oligocene and Miocene sediments from the Ross Sea region, Antarctica: implications for use of biomarker proxies in glacially-influenced settings. *Palaeogeography, Palaeoclimatology, Palaeoecology* 516, 71–89.
- Dutton, A., Carlson, A.E., Long, A.J., Milne, G.A., Clark, P.U., DeConto, R., et al., 2015. Sea-level rise due to polar ice-sheet mass loss during past warm periods. *Science* 349 (6244).
- Eagles, G., Jokat, W., 2014. Tectonic reconstructions for paleobathymetry in Drake Passage. *Tectonophysics* 611, 28–50.
- Edwards, T.L., Brandon, M.A., Durand, G., Edwards, N.R., Golledge, N.R., Holden, P.B., et al., 2019. Revisiting Antarctic ice loss due to marine ice-cliff instability. *Nature* 566 (7742), 58–64.
- Egger, L.M., Bahr, A., Friedrich, O., Wilson, P.A., Norris, R.D., van Peer, T.E., et al., 2018. Sea-level and surface-water change in the western North Atlantic across the Oligocene–Miocene Transition: a palynological perspective from IODP Site U1406 (Newfoundland margin). *Marine Micropaleontology* 139, 57–71.
- Eisen, O., Hofstede, C., Diez, A., Kristoffersen, Y., Lambrecht, A., Mayer, C., et al., 2015. On-ice vibroseis and snowstreamer systems for geoscientific research. *Polar Science* 9 (1), 51–65.
- Eittreim, S.L., Cooper, A.K., Wannesson, J., Davies, T.Ae., Coffin, M.Fe., Wise, S.We., 1995. Seismic stratigraphic evidence of ice-sheet advances on the Wilkes Land margin of Antarctica. Selected topics relating to the Indian Ocean basins and margins. *Sedimentary Geology* 96 (1–2), 131–156.
- Ekart, D.D., Cerling, T.E., Montanez, I.P., Tabor, N.J., 1999. A 400 million year carbon isotope record of pedogenic carbonate; implications for paleoatmospheric carbon dioxide. *American Journal of Science* 299 (10), 805–827.
- Emiliani, C., 1955. Pleistocene temperatures. *Journal of Geology* 63 (6), 538–578.
- Emiliani, C., 1966. Isotopic paleotemperatures. *Science* 154, 851–857.
- Escutia, C., Brinkhuis, H., 2014. Chapter 3.3—From greenhouse to icehouse at the Wilkes Land Antarctic Margin: IODP expedition 318 synthesis of results. In: Stein, R., Blackman, D.K., Inagaki, F., Larsen, H.-C. (Eds.), *Developments in Marine Geology*. Elsevier, pp. 295–328.

- Escutia, C., Bárcena, M.A., Lucchi, R.G., Romero, O., Ballegeer, A.M., Gonzalez, J.J., et al., 2009. Circum-Antarctic warming events between 4 and 3.5Ma recorded in marine sediments from the Prydz Bay (ODP Leg 188) and the Antarctic Peninsula (ODP Leg 178) margins. *Global and Planetary Change* 69 (3), 170–184.
- Escutia, C., Brinkhuis, H., Klaus, A. and Expedition 318 Scientists (Eds.), 2011a. Proceedings of the Integrated Ocean Drilling Program. Integrated Ocean Drilling Program Management International, Inc., Tokyo.
- Escutia, C., Brinkhuis, H., Klaus, A. and the I.E.S., 2011b. IODP Expedition 318: From Greenhouse to Icehouse at the Wilkes Land Antarctic Margin. *Scientific Drilling* 12, 15–23.
- Escutia, C., De Santis, L., Donda, F., Dunbar, R., Cooper, A., Brancolini, G., et al., 2005. Cenozoic ice sheet history from East Antarctic Wilkes Land continental margin sediments. *Global and Planetary Change* 45 (1–3), 51–81.
- Escutia, C., DeConto, R.M., Dunbar, R., Santis, L.D., Shevenell, A., Naish, T., 2019. Keeping an eye on Antarctic Ice Sheet stability. *Oceanography* 32 (1), 32–46.
- Escutia, C., Eittreim, S.L., Cooper, A.K., Nelson, C.H., 2000. Morphology and acoustic character of the antarctic Wilkes Land turbidite systems; ice-sheet-sourced vs river-sourced fans. *Journal of Sedimentary Research, Section A: Sedimentary Petrology and Processes* 70 (1), 84–93.
- Escutia, C., Nelson, C.H., Acton, G.D., Eittreim, S.L., Cooper, A.K., Warnke, D.A., et al., 2002. Current controlled deposition on the Wilkes Land continental rise, Antarctica. Deep-water contourite systems; modern drifts and ancient series, seismic and sedimentary characteristics. *Memoir – Geological Society of London* 22, 373–384.
- Evangelinos, D., Escutia, C., Etourneau, J., Hoem, F., Bijl, P., Boterblom, W., et al., 2020. Late Oligocene-Miocene proto-Antarctic Circumpolar Current dynamics off the Wilkes Land margin, East Antarctica. *Global and Planetary Change* 191, 103221.
- Exon, N.F., Kennett, J.P., Malone, M.J., 2004. Leg 189 Synthesis: Cretaceous-Holocene History of the Tasmanian Gateway. In: Exon, N.F., Kennett J.P., Malone M.J. (Eds.), *Proceedings of the Ocean Drilling Program*.
- Exon, N.F., Kennett, J.P., Malone, M.J., Brinkhuis, H., Chaproniere, G.C.H., Ennyu, A., et al., 2001. *Proceedings of the Ocean Drilling Program, initial reports, the Tasmanian Gateway, Cenozoic climatic and oceanographic development; covering Leg 189 of the cruises of the drilling vessel JOIDES Resolution; Hobart, Tasmania, to Sydney, Australia; sites 1168–1172, 11 March–6 May 2000. Proceedings of the Ocean Drilling Program, Part A: Initial Reports, 189: (variously paginated)*.
- Fairbanks, R.G., Matthews, R.K., 1978. The marine oxygen isotope record in Pleistocene coral, Barbados, West Indies. *Quaternary Research (New York)* 10 (2), 181–196.
- Farrell, J.W., Raffi, I., Janecek, T.R., Murray, D.W., Levitan, M., Dadey, K.A., et al., 1995. Late Neogene sedimentation patterns in the eastern Equatorial Pacific Ocean. *Proceedings of the Ocean Drilling Program; scientific results; eastern Equatorial Pacific, covering Leg 138 of the cruises of the drilling vessel JOIDES Resolution, Balboa, Panama, to San Diego, California, Sites 844–854, 1 May–4 July 1991. Proceedings of the Ocean Drilling Program, Scientific Results, 138: 717–756.*
- Feakins, S.J., Warny, S., Lee, J.-E., 2012. Hydrologic cycling over Antarctica during the middle Miocene warming. *Nature Geoscience* 5 (8), 557–560.
- Fedorov, A.V., Brierley, C.M., Lawrence, K.T., Liu, Z., Dekens, P.S., Ravelo, A.C., 2013. Patterns and mechanisms of early Pliocene warmth. *Nature* 496 (7443), 43–49.

- Fernandez, R., Gulick, S., Domack, E., Montelli, A., Leventer, A., Shevenell, A., et al., 2018. Past ice stream and ice sheet changes on the continental shelf off the Sabrina Coast, East Antarctica. *Geomorphology* 317, 10–22.
- Ferraccioli, F., Armadillo, E., Jordan, T., Bozzo, E., Corr, H., 2009. Aeromagnetic exploration over the East Antarctic Ice Sheet: A new view of the Wilkes Subglacial Basin. *Tectonophysics* 478 (1–2), 62–77.
- Ferrar, H.T., 1907. Report on the field geology of the region explored during the “Discovery” Antarctic Expedition 1901–4. *National Antarctic Expedition 1*, 1–100 (Geology).
- Fielding, C., Whittaker, J., Henrys, S., Wilson, T., Naish, T., 2007. Seismic facies and stratigraphy of the Cenozoic succession in McMurdo Sound, Antarctica: Implications for tectonic, climatic, and glacial history, Short Research Paper 090. In: Cooper A.K., Raymond C. (Eds.), *Antarctica: A Keystone in a Changing World—Online Proceedings of the 10th ISAES*. USGS Open-File Report 2007-1047, Santa Barbara, United States, 4 p.
- Fielding, C.R., 2018. Stratigraphic architecture of the Cenozoic succession in the McMurdo Sound region, Antarctica: an archive of polar palaeoenvironmental change in a failed rift setting. *Sedimentology* 65 (1), 1–61.
- Fielding, C.R., Browne, G.H., Field, B., Florindo, F., Harwood, D.M., Krissek, L.A., et al., 2011. Sequence stratigraphy of the ANDRILL AND-2A drillcore, Antarctica: a long-term, ice-proximal record of Early to Mid-Miocene climate, sea-level and glacial dynamism. *Palaeogeography, Palaeoclimatology, Palaeoecology* 305 (1–4), 337–351.
- Fielding, C.R., Henrys, S.A., Wilson, T.J., 2005. Rift history of the Western Victoria Land Basin: a new perspective based on integration of cores with seismic reflection data. In: Fütterer, D.K., Damaske, D., Kleinschmidt, G., Miller, H., Tessensohn, F. (Eds.), *Antarctica: Contributions to Global Earth Sciences*. Springer-Verlag, Berlin, Heidelberg, New York, pp. 307–316.
- Fielding, C.R., Naish, T., Woolfe, K.J., Lavelle, M.J., 2000. Facies analysis and sequence stratigraphy of CRP-2/2A, Victoria Land Basin, Antarctica. *Terra Antarctica* 7, 323–338.
- Fielding, C.R., Whittaker, J., Henrys, S.A., Wilson, T.J., Naish, T.R., 2008. Seismic facies and stratigraphy of the Cenozoic succession in McMurdo Sound, Antarctica: implications for tectonic, climatic and glacial history. *Palaeogeography, Palaeoclimatology, Palaeoecology* 260, 8–29.
- Florindo, F., Farmer, R.K., Harwood, D.M., Cody, R.D., Levy, R., Bohaty, S.M., et al., 2013. Paleomagnetism and biostratigraphy of sediments from Southern Ocean ODP Site 744 (southern Kerguelan Plateau): implications for early-to-middle Miocene climate in Antarctica. *Global and Planetary Change* 110 (Part C), 434–454.
- Florindo, F., Roberts, A.P., 2005. Eocene-Oligocene magnetobiochronology of ODP Sites 689 and 690, Maud Rise, Weddell Sea, Antarctica. *Geological Society of America Bulletin* 117 (1–2), 46–66.
- Florindo, F., Wilson, G.S., Roberts, A.P., Sagnotti, L., Verosub, K.L., 2005. Magnetostratigraphic chronology of a late Eocene to early Miocene glacimarine succession from the Victoria Land Basin, Ross Sea, Antarctica. *Global and Planetary Change* 45 (1–3), 207–236.
- Flower, B.P., 1999. Warming without high CO₂? *Nature (London)* 399 (6734), 313–314.
- Flower, B.P., Kennett, J.P., 1993a. Middle Miocene ocean-climate transition: high-resolution oxygen and carbon isotopic records from Deep Sea Drilling Project Site 588A, southwest Pacific. *Paleoceanography* 8 (6), 811–843.

- Flower, B.P., Kennett, J.P., 1993b. Relations between Monterey Formation deposition and middle Miocene global cooling; Naples Beach section, California. *Geology* (Boulder) 21 (10), 877–880.
- Flower, B.P., Kennett, J.P., 1994. The middle Miocene climatic transition: East Antarctic ice sheet development, deep ocean circulation and global carbon cycling. *Palaeogeography, Palaeoclimatology, Palaeoecology* 108 (3–4), 537–555.
- Foster, G.L., Rohling, E.J., 2013. Relationship between sea level and climate forcing by CO₂ on geological timescales. *Proceedings of the National Academy of Sciences* 110 (4), 1209–1214.
- Foster, G.L., Lear, C.H., Rae, J.W.B., 2012. The evolution of pCO₂, ice volume and climate during the middle Miocene. *Earth and Planetary Science Letters* 341–344, 243–254.
- Fountain, A.G., Lyons, W.B., Burkins, M.B., Dana, G.L., Doran, P.T., Lewis, K.J., et al., 1999. Physical controls on the Taylor Valley ecosystem, Antarctica. *Bioscience* 49 (12), 961–971.
- Frank, M., Whiteley, N., Kasten, S., Hein, J.R., O’Nions, K., 2002. North Atlantic Deep Water export to the Southern Ocean over the past 14 Myr: evidence from Nd and Pb isotopes in ferromanganese crusts. *Paleoceanography* 17 (2), 12-11–12-19.
- Fretwell, P., Pritchard, H.D., Vaughan, D.G., Bamber, J.L., Barrand, N.E., Bell, R., et al., 2013. Bedmap2: improved ice bed, surface and thickness datasets for Antarctica. *The Cryosphere* 7 (1), 375–393.
- Galeotti, S., DeConto, R., Naish, T., Stocchi, P., Florindo, F., Pagani, M., et al., 2016. Antarctic Ice Sheet variability across the Eocene-Oligocene boundary climate transition. *Science* 352 (6281), 76–80.
- Galeotti, S., Lanci, L., Florindo, F., Naish, T.R., Sagnotti, L., Sandroni, S., et al., 2012. Cyclochronology of the Eocene–Oligocene transition from the Cape Roberts Project-3 core, Victoria Land basin, Antarctica. *Palaeogeography, Palaeoclimatology, Palaeoecology* 335–336, 84–94.
- Gamble, J.A., Barrett, P.J., Adams, C.J., 1986. Basaltic clasts from Unit 8. In: Barrett, P.J. (Ed.), *Antarctic Cenozoic History from the MSSTS-1 Drillhole, McMurdo Sound*, DSIR Bulletin. Science Information Publishing Centre, Wellington, pp. 145–152.
- Garbe, J., Albrecht, T., Levermann, A., Donges, J.F., Winkelmann, R., 2020. The hysteresis of the Antarctic Ice Sheet. *Nature* 585 (7826), 538–544.
- Garcia-Castellanos, D., Villaseñor, A., 2011. Messinian salinity crisis regulated by competing tectonics and erosion at the Gibraltar arc. *Nature* 480 (7377), 359–363.
- Gasson, E., DeConto, R., Pollard, D., 2015. Antarctic bedrock topography uncertainty and ice sheet stability. *Geophysical Research Letters* 42 (13), 5372–5377.
- Gasson, E., DeConto, R.M., Pollard, D., 2016a. Modeling the oxygen isotope composition of the Antarctic ice sheet and its significance to Pliocene sea level. *Geology* 44 (10), 827–830.
- Gasson, E., DeConto, R.M., Pollard, D., Levy, R.H., 2016b. Dynamic Antarctic ice sheet during the early to mid-Miocene. *Proceedings of the National Academy of Sciences* 113 (13), 3459–3464.
- Gasson, E.G., Keisling, B.A., 2020. The Antarctic Ice Sheet. *Oceanography* 33 (2), 90–100.
- Gohl, K., Wellner, J.S., Klaus, A., and the Expedition 379 Scientists, 2019. Expedition 379 Preliminary Report: Amundsen Sea West Antarctic Ice Sheet History. International Ocean Discovery Program. Available from: <https://doi.org/10.14379/iodp.pr.379.2019>.
- Goldner, A., Herold, N., Huber, M., 2014. The challenge of simulating the warmth of the mid-Miocene climatic optimum in CESM1. *Climate of the Past* 10 (2), 523–536.

- Golledge, N.R., Keller, E.D., Gomez, N., Naughten, K.A., Bernales, J., Trusel, L.D., et al., 2019. Global environmental consequences of twenty-first-century ice-sheet melt. *Nature* 566 (7742), 65–72.
- Golledge, N.R., Kowalewski, D.E., Naish, T.R., Levy, R.H., Fogwill, C.J., Gasson, E.G.W., 2015. The multi-millennial Antarctic commitment to future sea-level rise. *Nature* 526 (7573), 421–425.
- Golledge, N.R., Levy, R.H., McKay, R.M., Naish, T.R., 2017a. East Antarctic ice sheet most vulnerable to Weddell Sea warming. *Geophysical Research Letters* 44 (5), 2343–2351.
- Golledge, N.R., Thomas, Z.A., Levy, R.H., Gasson, E.G.W., Naish, T.R., McKay, R.M., et al., 2017b. Antarctic climate and ice-sheet configuration during the early Pliocene interglacial at 4.23 Ma. *Climate of the Past* 13 (7).
- Goodge, J.W., Severinghaus, J.P., 2016. Rapid Access Ice Drill: a new tool for exploration of the deep Antarctic ice sheets and subglacial geology. *Journal of Glaciology* 62 (236), 1049–1064.
- Goodge, J.W., Fanning, C.M., Norman, M.D., Bennett, V.C., 2012. Temporal, isotopic and spatial relations of early Paleozoic Gondwana-margin arc magmatism, central Transantarctic Mountains, Antarctica. *Journal of Petrology* 53 (10), 2027–2065.
- Gordon, A.L., Tchernia, P.L., 1978. Waters of the continental margin off Adélie Coast, Antarctica. *Antarctica Oceanology II: The Australian–New Zealand Sector* 19, 59–69.
- Gradstein, F.M., Ogg, J.G., 2020. Chapter 2—The chronostratigraphic scale. In: Gradstein, F.M., Ogg, J.G., Schmitz, M.D., Ogg, G.M. (Eds.), *Geologic Time Scale 2020*. Elsevier, pp. 21–32.
- Granot, R., Cande, S.C., Stock, J.M., Davey, F.J., Clayton, R.W., 2010. Postspreading rifting in the Adare Basin, Antarctica: regional tectonic consequences. *Geochemistry, Geophysics, Geosystems* 11 (Q08005), 29.
- Grant, G., Naish, T., 2021. Pliocene sea-level revisited: is there more than meets the eye? *PAGES Magazine* 29.
- Grant, G.R., Naish, T.R., Dunbar, G.B., Stocchi, P., Kominz, M.A., Kamp, P.J.J., et al., 2019. The amplitude and origin of sea-level variability during the Pliocene epoch. *Nature* 574 (7777), 237–241.
- Greenop, R., Foster, G.L., Wilson, P.A., Lear, C.H., 2014. Middle Miocene climate instability associated with high-amplitude CO₂ variability. *Paleoceanography* 29 (9), 2014PA002653.
- Greenop, R., Sosdian, S.M., Henehan, M.J., Wilson, P.A., Lear, C.H., Foster, G.L., 2019. Orbital forcing, ice vVolume, and CO₂ across the Oligocene-Miocene Transition. *Paleoceanography and Paleoclimatology* 34 (3), 316–328.
- Griener, K.W., Warny, S., Askin, R., Acton, G., 2015. Early to middle Miocene vegetation history of Antarctica supports eccentricity-paced warming intervals during the Antarctic ice-house phase. *Global and Planetary Change* 127, 67–78.
- Grützner, J., Hillenbrand, C.-D., Rebesco, M., 2005. Terrigenous flux and biogenic silica deposition at the Antarctic continental rise during the late Miocene to early Pliocene: implications for ice sheet stability and sea ice coverage. *Global and Planetary Change* 45 (1–3), 131–149.
- Gulick, S.P.S., Shevenell, A.E., Montelli, A., Fernandez, R., Smith, C., Warny, S., et al., 2017. Initiation and long-term instability of the East Antarctic Ice Sheet. *Nature* 552, 225.
- Gunn, B.M., 1963. Geological structure and stratigraphic correlation in Antarctica. *New Zealand Journal of Geology and Geophysics* 6 (3), 423–443.
- Gunn, B.M., Warren, G., 1962. Geology of Victoria Land between the Mawson and Mulock Glaciers, Antarctica. *New Zealand Geological Survey Bulletin* 100 (71), 157.
- Guo, Z.T., Sun, B., Zhang, Z.S., Peng, S.Z., Xiao, G.Q., Ge, J.Y., et al., 2008. A major reorganization of Asian climate by the early Miocene. *Climate of the Past* 4 (3), 153–174.

- Haile-Selassie, Y., Suwa, G., White, T.D., 2004. Late Miocene teeth from Middle Awash, Ethiopia, and early hominid dental evolution. *Science* 303 (5663), 1503–1505.
- Halberstadt, A.R.W., Chorley, H., Levy, R.H., Naish, T., DeConto, R.M., Gasson, E., et al., 2021. CO₂ and tectonic controls on Antarctic climate and ice-sheet evolution in the mid-Miocene. *Earth and Planetary Science Letters* 564, 116908.
- Hall, B.L., Denton, G.H., 2005. Surficial geology and geomorphology of eastern and central Wright Valley, Antarctica. *Geomorphology* 64 (1–2), 25–65.
- Hall, B.L., 1992. Surficial geology and geomorphology of eastern Wright Valley, Antarctica: Implications for Plio-Pleistocene ice-sheet dynamics. Master of Science thesis, University of Maine.
- Hall, B.L., Denton, G.H., Lux, D.R., Bockheim, J.G., 1993a. Late Tertiary Antarctic Paleoclimate and Ice-Sheet Dynamics inferred from surficial deposits in Wright Valley. *Geografiska Annaler. Series A, Physical Geography* 75 (4), 239–267.
- Hall, B.L., Denton, G.H., Lux, D.R., Schluechter, C., 1997. Pliocene paleoenvironment and Antarctic ice sheet behavior; evidence from Wright Valley. *Journal of Geology* 105 (3), 285–294.
- Hall, B.L., Denton, G.H., Lux, D.R., Bockheim, J.G., Sugden, D.E.e., Marchant, D.R.e. et al., 1993b. Late Tertiary Antarctic paleoclimate and ice-sheet dynamics inferred from surficial deposits in Wright Valley. The case for a stable East Antarctica ice sheet. *Proceedings. Geografiska Annaler. Series A: Physical Geography* 75 (4), 239–267.
- Hambrey, M.J., McKelvey, B.C., 2000. Neogene fjordal sedimentation on the western margin of the Lambert Graben, East Antarctica. *Sedimentology* 47 (3), 577–607.
- Hamon, N., Sepulchre, P., Lefebvre, V., Ramstein, G., 2013. The role of eastern Tethys seaway closure in the Middle Miocene Climatic Transition (ca. 14 Ma). *Climate of the Past* 9 (6), 2687–2702.
- Hansen, M.A., Passchier, S., 2017. Oceanic circulation changes during early Pliocene marine ice-sheet instability in Wilkes Land, East Antarctica. *Geo-Marine Letters* 37 (3), 207–213.
- Hansen, M.A., Passchier, S., Khim, B.-K., Song, B., Williams, T., 2015. Threshold behavior of a marine-based sector of the East Antarctic Ice Sheet in response to early Pliocene ocean warming. *Paleoceanography* 30 (6), 789–801.
- Haq, B.U., Hardenbol, J., Vail, P.R., 1987. Chronology of fluctuating sea levels since the Triassic. *Science* 235 (4793), 1156–1167.
- Harrington, H.J., 1958. Nomenclature of Rock Units in the Ross Sea Region, Antarctica. *Nature* 182 (4631), 290.
- Hartman, B.N., 1998. Miocene Paleoclimate and Ice-Sheet Dynamics as Recorded in Central Taylor Valley, Antarctica. Boston University. Boston, Massachusetts 179.
- Hartman, J.D., Sangiorgi, F., Salabarnada, A., Peterse, F., Houben, A.J.P., Schouten, S., et al., 2018. Paleoceanography and ice sheet variability offshore Wilkes Land, Antarctica—part 3: insights from Oligocene–Miocene TEX86-based sea surface temperature reconstructions. *Climate of the Past* 14 (9), 1275–1297.
- Harwood, D., Florindo, F., Talarico, F., Levy, R.H. (Eds.), 2008–2009. Studies from the ANDRILL Southern McMurdo Sound Project, Antarctica – Initial Science Report on AND-2A, 235 pp.
- Harwood, D., Florindo, F., Talarico, F., Levy, R., Kuhn, G., Naish, T., et al., 2009. Antarctic Drilling recovers stratigraphic records from the continental margin. *EOS, Transactions of the American Geophysical Union* 90 (11), 90–91.

- Harwood, D.M., Levy, R.H., 2000. The McMurdo erratics: introduction and overview. In: Stilwell, J.D., Feldmann, R.M. (Eds.), *Paleobiology and Paleoenvironments of Eocene Rocks, McMurdo Sound, East Antarctica: Antarctic Research Series*. American Geophysical Union, Washington, D.C., pp. 1–18.
- Harwood, D.M., Scherer, R.P., Webb, P.-N., 1989. Multiple Miocene marine productivity events in West Antarctica as recorded in upper Miocene sediments beneath the Ross Ice Shelf (Site J-9). *Marine Micropaleontology* 15 (1), 91–115.
- Hayes, D.E., Frakes, L.A. and Shipboard Scientific Party, 1975d. Sites 270, 271, 272. In: Hayes, D.E., Frakes, L.A. (Eds.), *Initial Reports of the Deep Sea Drilling Project, Leg 28*, pp. 211–334.
- Hayes, D.E., Frakes, L.A., Barrett, P.J., Burns, D.A., Chen, P.-H., Ford, A.B., et al., 1975a. Freemantle, Australia, to Christchurch, New Zealand; December 1972–February 1973. *Initial Reports of the Deep Sea Drilling Project* 28, 1017.
- Hayes, D.E., Frakes, L.A., Barrett, P.J., Burns, D.A., Chen, P.-H., Ford, A.B., et al., 1975b. Introduction. *Initial Reports of the Deep Sea Drilling Project* 28, 5–18.
- Hayes, D.E., Frakes, L.A., Barrett, P.J., Burns, D.A., Chen, P.-H., Ford, A.B., et al., 1975c. Site 268. *Initial Reports of the Deep Sea Drilling Project* 28, 153–178.
- Haywood, A.M., Dowsett, H.J., Dolan, A.M., Rowley, D., Abe-Ouchi, A., Otto-Bliesner, B., et al., 2016. The Pliocene Model Intercomparison Project (PlioMIP) phase 2: scientific objectives and experimental design. *Climate of the Past* 12 (3), 663–675.
- Haywood, A.M., Hill, D.J., Dolan, A.M., Otto-Bliesner, B.L., Bragg, F., Chan, W.L., et al., 2013. Large-scale features of Pliocene climate: results from the Pliocene Model Intercomparison Project. *Climate of the Past* 9 (1), 191–209.
- Haywood, A.M., Smellie, J.L., Ashworth, A.C., Cantrill, D.J., Florindo, F., Hambrey, M.J., et al., 2008. Middle Miocene to Pliocene history of Antarctica and the southern ocean. *Developments in Earth and Environmental Sciences* 8, 401–463.
- Haywood, A.M., Tindall, J.C., Dowsett, H.J., Dolan, A.M., Foley, K.M., Hunter, S.J., et al., 2020. The Pliocene Model Intercomparison Project Phase 2: large-scale climate features and climate sensitivity. *Climate of the Past* 16 (6), 2095–2123.
- Holland, P., Holmes, M.A., 1997. Surface textural analysis of quartz sand grains from ODP Site 918 off the southeast coast of Greenland suggests glaciation of southern Greenland at 11 Ma. *Palaeogeography, Palaeoclimatology, Palaeoecology* 135 (1–4), 109–121.
- Henrys, S.A., Bartek, L.R., Brancolini, G., Luyendyk, B.P., Hamilton, R.J., Sorlien, C.C., et al., 1998. Seismic stratigraphy of the pre-Quaternary strata off Cape Roberts and their correlation with strata cored in the CIROS-1 drillhole, McMurdo Sound Studies from the Cape Roberts Project; Ross Sea, Antarctica; scientific report of CRP-1. *Terra Antarctica* 5 (3), 273–279.
- Henrys, S.A., Buecker, C.J., Niessen, F., Bartek, L.R., Buecker, C., Davey, F.J., 2001. Correlation of seismic reflectors with the CRP-3 drillhole, Victoria Land Basin, Antarctica Studies from the Cape Roberts Project; Ross Sea, Antarctica; scientific report of CRP-3; Part 1, Geophysics and tectonic studies for CRP-3. *Terra Antarctica* 8 (3), 127–136.
- Henrys, S.A., Wilson, T.J., Whittaker, J.M., Fielding, C.R., Hall, J., Naish, T.R., 2007. Tectonic history of mid-Miocene to present southern Victoria Land Basin, inferred from seismic stratigraphy in McMurdo Sound, Antarctica. USGS and National Academies, USGS OF-2007-1047, Short Research Paper 049.
- Herbert, T.D., Lawrence, K.T., Tzanova, A., Peterson, L.C., Caballero-Gill, R., Kelly, C.S., 2016. Late Miocene global cooling and the rise of modern ecosystems. *Nature Geoscience* 9 (11), 843–847.

- Hill, D.J., Haywood, A.M., Hindmarsh, R.C.A., Valdes, P.J., 2007. Characterizing ice sheets during the Pliocene: evidence from data and models. In: Williams, M., Haywood, A.M., Gregory, F.J., Schmidt, D.N., (Eds.) Deep-time perspectives on climate change: marrying the signal from computer models and biological proxies, 517–538. London, Geological Society of London. (*Micropalaeontological Society special publications*).
- Hill, D.J., Bolton, K.P., Haywood, A.M., 2017. Modelled ocean changes at the Plio-Pleistocene transition driven by Antarctic ice advance. *Nature Communications* 8, 14376.
- Hill, D.J., Haywood, A.M., Valdes, P.J., Francis, J.E., Lunt, D.J., Wade, B.S., et al., 2013. Paleogeographic controls on the onset of the Antarctic circumpolar current. *Geophysical Research Letters* 40 (19), 2013GL057439.
- Hillenbrand, C.-D., Cortese, G., 2006. Polar stratification: A critical view from the Southern Ocean. *Palaeogeography, Palaeoclimatology, Palaeoecology* 242 (3–4), 240–252.
- Hinz, K., Block, M., 1984. Results of geophysical investigations in the Weddell Sea and in the Ross Sea, Antarctica, Proceedings 11th World Petroleum Congress, London. Wiley, New York, pp. 279–291.
- Ho, S.L., Laepple, T., 2016. Flat meridional temperature gradient in the early Eocene in the subsurface rather than surface ocean. *Nature Geoscience* 9 (8), 606–610.
- Hochmuth, K., Gohl, K., Leitchenkov, G., Sauermilch, I., Whittaker, J.M., Uenzelmann-Neben, G., et al., 2020. The evolving paleobathymetry of the circum-Antarctic Southern Ocean since 34 Ma: a key to understanding past cryosphere-ocean developments. *Geochemistry, Geophysics, Geosystems* 21 (8), e2020GC009122.
- Hodel, F., Grespan, R., de Rafélis, M., Dera, G., Lezin, C., Nardin, E., et al., 2021. Drake Passage gateway opening and Antarctic Circumpolar Current onset 31 Ma ago: the message of foraminifera and reconsideration of the Neodymium isotope record. *Chemical Geology* 570, 120171.
- Hodell, D.A., Venz-Curtis, K.A., 2006. Late Neogene history of deepwater ventilation in the Southern Ocean. *Geochemistry, Geophysics, Geosystems* 7 (9).
- Hodell, D.A., Elmstrom, K.M., Kennett, J.P., 1986. Latest Miocene benthic ^{18}O changes, global ice volume, sea level and the "Messinian salinity crisis". *Nature (London)* 320 (6061), 411–414.
- Hodgson, D.A., Bentley, M.J., Smith, J.A., Klepacić, J., Makinson, K., Smith, A.M., et al., 2016. Technologies for retrieving sediment cores in Antarctic subglacial settings. *Philosophical Transactions of the Royal Society A: Mathematical, Physical and Engineering Sciences* 374 (2059), 20150056.
- Hofstede, C., Eisen, O., Diez, A., Jansen, D., Kristoffersen, Y., Lambrecht, A., et al., 2013. Investigating englacial reflections with vibro- and explosive-seismic surveys at Halvfarryggen ice dome, Antarctica. *Annals of Glaciology* 54 (64), 189–200.
- Holbourn, A., Kuhnt, W., Clemens, S., Prell, W., Andersen, N., 2013. Middle to late Miocene stepwise climate cooling: evidence from a high-resolution deep water isotope curve spanning 8 million years. *Paleoceanography* 28 (4), 688–699.
- Holbourn, A., Kuhnt, W., Kochhann, K.G.D., Andersen, N., Sebastian Meier, K.J., 2015. Global perturbation of the carbon cycle at the onset of the Miocene Climatic Optimum. *Geology* 43 (2), 123–126.
- Holbourn, A., Kuhnt, W., Lyle, M., Schneider, L., Romero, O., Andersen, N., 2014. Middle Miocene climate cooling linked to intensification of eastern equatorial Pacific upwelling. *Geology* 42 (1), 19–22.
- Holbourn, A., Kuhnt, W., Schulz, M., Erlenkeuser, H., 2005. Impacts of orbital forcing and atmospheric carbon dioxide on Miocene Ice Sheet expansion. *Nature* 438, 483–487.

- Holbourn, A., Kuhnt, W., Schulz, M., Flores, J.-A., Andersen, N., 2007. Orbitally-paced climate evolution during the middle Miocene “Monterey” carbon-isotope excursion. *Earth and Planetary Science Letters* 261 (3–4), 534–550.
- Holbourn, A.E., Kuhnt, W., Clemens, S.C., Kochhann, K.G.D., Jöhnck, J., Lübers, J., et al., 2018. Late Miocene climate cooling and intensification of southeast Asian winter monsoon. *Nature Communications* 9 (1), 1584.
- Hole, M., LeMasurier, W., 1994. Tectonic controls on the geochemical composition of Cenozoic, mafic alkaline volcanic rocks from West Antarctica. *Contributions to Mineralogy and Petrology* 117 (2), 187–202.
- Hornbrook, Nd.B., 1992. New Zealand Cenozoic Marine Paleoclimates: A Review Based on the Distribution of Some Shallow Water and Terrestrial Biota. *Pacific Neogene: Environment, Evolution, and Events*. University of Tokyo Press, Tokyo, pp. 83–106.
- Hsü, K.J., Bernoulli, D., 1978. Genesis of the Tethys and the Mediterranean. Available from: <https://doi.org/10.2973/dsdp.proc.42-1.149.1978>.
- Hsü, K.J., Ryan, W.B., Cita, M.B., 1973. Late Miocene desiccation of the Mediterranean. *Nature* 242 (5395), 240–244.
- Huber, M., Nof, D., 2006. The ocean circulation in the southern hemisphere and its climatic impacts in the Eocene. *Palaeogeography, Palaeoclimatology, Palaeoecology* 231 (1–2), 9–28.
- Huybers, P., Tziperman, E., 2008. Integrated summer insolation forcing and 40,000-year glacial cycles: the perspective from an ice-sheet/energy-balance model. *Paleoceanography* 23 (1).
- Huybrechts, P., Sugden, D.E.e., Marchant, D.R.e., Denton, G.H.E., 1993. Glaciological modelling of the late Cenozoic East Antarctic ice sheet; stability or dynamism? The case for a stable East Antarctica ice sheet; proceedings. *Geografiska Annaler. Series A: Physical Geography* 75 (4), 221–238.
- IPCC, 2013. Climate change 2013: the physical science basis. In: Stocker, T.F., Qin, D., Plattner, G.-K., Tignor, M., Allen, S.K., Boschung, J., Nauels, A., Xia, Y., Bex, V., Midgley, P.M. (Eds.), Contribution of Working Group I to the Fifth Assessment Report of the Intergovernmental Panel on Climate Change. Cambridge University Press, Cambridge, UK and New York, NY, p. 1535.
- Jacobs, S.S., Giulivi, C.F., 2010. Large multidecadal salinity trends near the Pacific–Antarctic continental margin. *Journal of Climate* 23 (17), 4508–4524.
- Jacobs, S.S., Giulivi, C.F., Mele, P.A., 2002. Freshening of the Ross Sea during the late 20th century. *Science* 297 (5580), 386–389.
- Ji, S., Nie, J., Lechler, A., Huntington, K.W., Heitmann, E.O., Breecker, D.O., 2018. A symmetrical CO₂ peak and asymmetrical climate change during the middle Miocene. *Earth and Planetary Science Letters* 499, 134–144.
- John, C.M., Karner, G.D., Browning, E., Leckie, R.M., Mateo, Z., Carson, B., et al., 2011. Timing and magnitude of Miocene eustasy derived from the mixed siliciclastic-carbonate stratigraphic record of the northeastern Australian margin. *Earth and Planetary Science Letters* 304 (3–4), 455–467.
- Jordan, T.A., Riley, T.R., Siddoway, C.S., 2020. The geological history and evolution of West Antarctica. *Nature Reviews Earth & Environment* 1 (2), 117–133.
- Joughin, I., Shean, D.E., Smith, B.E., Floricioiu, D., 2020. A decade of variability on Jakobshavn Isbrae: ocean temperatures pace speed through influence on mélange rigidity. *The cryosphere* 14 (1), 211–227.
- Jovane, L., Florindo, F., Acton, G., Ohneiser, C., Sagnotti, L., Strada, E., et al. (2019). Miocene glacial dynamics recorded by variations in magnetic properties in the ANDRILL-2A

- drillcore. *Journal of Geophysical Research: Solid Earth* 124, 2297–2312. Available from: <https://doi.org/10.1029/2018JB016865>.
- Kasbohm, J., Schoene, B., 2018. Rapid eruption of the Columbia River flood basalt and correlation with the mid-Miocene climate optimum. *Science Advances* 4 (9), eaat8223.
- Kender, S., Kaminski, M.A., 2013. Arctic Ocean benthic foraminiferal faunae change associated with the onset of perennial sea ice in the Middle Miocene. *Journal of Foraminiferal Research* 43 (1), 99–109.
- Kennett, J.P., 1977. Cenozoic evolution of Antarctic Glaciation, the Circum-Antarctic Ocean, and their impact on global paleoceanography. *Journal of Geophysical Research* 82 (27), 3843–3859.
- Kennett, J.P., Barker, P.F., 1990. Latest Cretaceous to Cenozoic climate and oceanographic developments in the Weddell Sea, Antarctica: an ocean-drilling perspective. In: *Proceedings of the Ocean Drilling Program. Scientific Results*, 113, pp. 937–960.
- Kennett, J.P., Houtz, R.E., Andrews, P.B., Edwards, A.R., Gostin, V.A., Hajos, M., et al., 1975. Cenozoic paleoceanography in the Southwest Pacific Ocean, Antarctic glaciation, and the development of the Circum-Antarctic Current. *Initial Reports of the Deep Sea Drilling Project* 29, 1155–1169.
- Kennett, J.P., von der Borch, C.C., Baker, P.A., Barton, C.E., Boersma, A., Caulet, J.P., et al., 1986. Miocene to early Pliocene oxygen and carbon isotope stratigraphy in the Southwest Pacific, Deep Sea Drilling Project Leg 90. *Initial reports of the Deep Sea Drilling Project covering Leg 90 of the cruises of the drilling vessel Glomar Challenger, Noumea, New Caledonia, to Wellington, New Zealand, December 1982–January 1983. Initial Reports of the Deep Sea Drilling Project 90 (Part 2)*, 1383–1411.
- Kerr, A., Huybrechts, P., van der Wateren, F.Me, Cloetingh, S.A.P.L.E., 1999. The response of the East Antarctic ice-sheet to the evolving tectonic configuration of the Transantarctic Mountains. *Lithosphere dynamics and environmental change of the Cenozoic West Antarctic Rift system. Global and Planetary Change* 23 (1–4), 213–229.
- Kerr, A., Sugden, D.E., Summerfield, M.A., 2000. Linking tectonics and landscape development in a passive margin setting: the Transantarctic Mountains. In: Summerfield, M.A. (Ed.), *Geomorphology and Global Tectonics*. John Wiley & Sons, pp. 303–319.
- Knorr, G., Lohmann, G., 2014. Climate warming during Antarctic ice sheet expansion at the Middle Miocene transition. *Nature Geoscience* 7 (5), 376–381.
- Kominz, M.A., Browning, J.V., Miller, K.G., Sugarman, P.J., Mizintseva, S., Scotese, C.R., 2008. Late Cretaceous to Miocene sea-level estimates from the New Jersey and Delaware coastal plateau coreholes: an error analysis. *Basin Research* 20, 211–226.
- Kominz, M.A., Miller, K.G., Browning, J.V., Katz, M.E., Mountain, G.S., 2016. Miocene relative sea level on the New Jersey shallow continental shelf and coastal plain derived from one-dimensional backstripping: A case for both eustasy and epeirogeny. *Geosphere* 12 (5), 1437–1456. Available from: <https://doi.org/10.1130/GES01241.1>.
- Koppers, A.A.P., Coggon, R. (Eds.), 2020. *Exploring Earth by Scientific Ocean Drilling: 2050 Science Framework*. 124 pp. Available from: <https://doi.org/10.6075/J0W66J9H>.
- Korhonen, F., Saito, S., Brown, M., Siddoway, C., Day, J., 2010. Multiple generations of granite in the Fosdick Mountains, Marie Byrd Land, West Antarctica: implications for polyphase intracrustal differentiation in a continental margin setting. *Journal of Petrology* 51 (3), 627–670.
- Kowalewski, D.E., Marchant, D.R., Levy, J., Head, J., 2006. Quantifying low rates of summer-time sublimation for buried glacier ice in Beacon Valley, Antarctica. *Antarctic Science* 18 (3), 421–428.

- Krissek, L., Browne, G., Carter, L., Cowan, E., Dunbar, G., McKay, R., et al., and ANDRILL MIS Science Team 2007a. Sedimentology and Stratigraphy of the AND-1B core, ANDRILL McMurdo Ice Shelf Project, Antarctica. In: Naish, T., Powell, R., Levy, R. (Eds.), *Studies from the ANDRILL, McMurdo Ice Shelf Project, Antarctica—Initial Science Report on AND-1B*. Terra Antarctica, pp. 185–222.
- Krissek, L., Browne, G., Carter, L., Cowan, E.A., Dunbar, G., McKay, R., et al., 2007b. Sedimentology and stratigraphy of the AND-1B core, ANDRILL McMurdo Ice Shelf Project, Antarctica. *Terra Antarctica* 14 (3), 185–222.
- Kulhanek, D.K., Levy, R.H., Clowes, C.D., Prebble, J.G., Rodelli, D., Jovane, L., et al., 2019. Revised chronostratigraphy of DSDP Site 270 and late Oligocene to early Miocene paleoecology of the Ross Sea sector of Antarctica. *Global and Planetary Change* 178, 46–64.
- Kürschner, W.M., Kvaček, Z., Dilcher, D.L., 2008. The impact of Miocene atmospheric carbon dioxide fluctuations on climate and the evolution of terrestrial ecosystems. *Proceedings of the National Academy of Sciences* 105 (2), 449–453.
- Kurschner, W.M., Van der Burgh, J., Visscher, H., Dilcher, D.L., 1996. Oak leaves as biosensors of late Neogene and early Pleistocene paleoatmospheric CO₂ concentrations. *Marine Micropaleontology* 27 (1–4), 299–312.
- Kwiek, P.B., Ravelo, A.C., 1999. Pacific Ocean intermediate and deep water circulation during the Pliocene. *Palaeogeography, Palaeoclimatology, Palaeoecology* 154, 191–217.
- Kyle, P.R., 1990a. Erebus Volcanic Province. In: LeMasurier, W.E., Thomson, J.W. (Eds.), *Volcanoes of the Antarctic Plate and Southern Ocean, Antarctic Research Series*. American Geophysical Union, Washington, D. C, pp. 81–145.
- Kyle, P.R., 1990b. McMurdo Volcanic Group, western Ross embayment. In: LeMasurier, W.E., Thomson, J.W. (Eds.), *Volcanoes of the Antarctic Plate and Southern Oceans, Antarctic Research Series*. American Geophysical Union, Washington, D. C, pp. 19–25.
- Lamy, F., Winckler, G., Alvarez Zarikian, C.A., and the Expedition 383 Scientists, 2019. Expedition 383 Preliminary Report: Dynamics of the Pacific Antarctic Circumpolar Current. International Ocean Discovery Program. Available from: <https://doi.org/10.14379/iodp.pr.383.2019>.
- Langebroek, P.M., Paul, A., Schulz, M., 2009. Antarctic ice-sheet response to atmospheric CO₂ and insolation in the Middle Miocene. *Climate of the Past* 5 (4), 633–646.
- Langebroek, P.M., Paul, A., Schulz, M., 2010. Simulating the sea level imprint on marine oxygen isotope records during the middle Miocene using an ice sheet–climate model. *Paleoceanography* 25 (4).
- Larsen, H.C., Saunders, A.D., Clift, P.D., Beget, J., Wei, W., Spezzaferri, S., 1994. Seven Million Years of Glaciation in Greenland. *Science* 264 (5161), 952–955.
- Laskar, J., Fienga, A., Gastineau, M., Manche, H., 2011. La2010: a new orbital solution for the long-term motion of the Earth. *Astronomy & Astrophysics* 532, 15.
- Laskar, J., Robutel, P., Gastineau, M., Correia, A.C.M., Levrard, B., 2004. A long term numerical solution for the insolation quantities of the Earth. *Astronomy and Astrophysics* 428, 261–285.
- Lawrence, K.T., Herbert, T.D., Brown, C.M., Raymo, M.E., Haywood, A.M., 2009. High-amplitude variations in North Atlantic sea surface temperature during the early Pliocene warm period. *Paleoceanography* 24 (2).
- Lawver, L.A., Gahagan, L.M., 2003. Evolution of Cenozoic seaways in the circum-Antarctic region. *Palaeogeogr. Palaeoclimatol. Palaeoecol.* Available from: [https://doi.org/10.1016/S0031-0182\(03\)00392-4](https://doi.org/10.1016/S0031-0182(03)00392-4).

- Lear, C.H., Coxall, H.K., Foster, G.L., Lunt, D.J., Mawbey, E.M., Rosenthal, Y., et al., 2015. Neogene ice volume and ocean temperatures: Insights from infaunal foraminiferal Mg/Ca paleothermometry. *Paleoceanography* 30 (11), 1437–1454.
- Lear, C.H., Mawbey, E.M., Rosenthal, Y., 2010. Cenozoic benthic foraminiferal Mg/Ca and Li/Ca records: toward unlocking temperatures and saturation states. *Paleoceanography* 25 (4), PA4215.
- Lear, C.H., Rosenthal, Y., Wright, J.D., 2003. The closing of a seaway: ocean water masses and global climate change. *Earth and Planetary Science Letters* 210 (3–4), 425–436.
- Lear, C.H., Rosenthal, Y., Wright, J.D., 2020. Compiled bottom water temperatures of ODP site 154–926. In: Lear, C.H., et al., (Eds.), Atlantic and Pacific Benthic Mg/Ca Temperatures 0–12 Ma. PANGAEA. Available from: <https://doi.org/10.1594/PANGAEA.913906>.
- Leckie, R.M., Webb, P.-N., 1983. Late Oligocene-early Miocene glacial record of the Ross Sea, Antarctica; evidence from DSDP Site 270. *Geology* (Boulder) 11 (10), 578–582.
- Leckie, R.M., Webb, P.-N., 1986. Late Paleogene and early Neogene foraminifers of Deep Sea Drilling Project Site 270, Ross Sea, Antarctica. In: Kennett, J.P., van der Borch, C.C. (Eds.), Initial Reports DSDP, Leg 90, Noumea, New Caledonia to Wellington, New Zealand, Part 2. United States Government Printing Office, Washington, D.C., pp. 1,093–091,142.
- Leutert, T.J., Auderset, A., Martínez-García, A., Modestou, S., Meckler, A.N., 2020. Coupled Southern Ocean cooling and Antarctic ice sheet expansion during the middle Miocene. *Nature Geoscience* 13 (9), 634–639.
- Levy, R., Harwood, D., Florindo, F., Sangiorgi, F., Tripathi, R., von Eynatten, H., et al., 2016. Antarctic ice sheet sensitivity to atmospheric CO₂ variations in the early to mid-Miocene. *Proceedings of the National Academy of Sciences* 113 (13), 3453–3458.
- Levy, R., Patterson, M., van de Flierdt, T., Jiménez Espejo, F.J., Stocchi, P., Klages, J., et al., 2020. The SWAIS 2C Project-sensitivity of the West Antarctic ice sheet in a warmer world.
- Levy, R.H., Harwood, D.M., 2000a. Sedimentary lithofacies of the McMurdo Sound Erratics. In: Stilwell, J.D., Feldmann, R.M. (Eds.), Paleobiology and Paleoenvironments of Eocene Rocks, McMurdo Sound, East Antarctica: Antarctic Research Series. American Geophysical Union, Washington, D.C, pp. 39–60.
- Levy, R.H., Harwood, D.M., 2000b. Tertiary marine palynomorphs from the McMurdo Sound Erratics. In: Stilwell, J.D., Feldmann, R.M. (Eds.), Paleobiology and Paleoenvironments of Eocene Rocks, McMurdo Sound, East Antarctica: Antarctic Research Series. American Geophysical Union, Washington, D.C, pp. 183–242.
- Levy, R.H., Cody, R.D., Crampton, J., Fielding, C., Golledge, N., Harwood, D.M., et al., 2012. Late Neogene climate and glacial history of the Southern Victoria Land coast from integrated drill core, seismic and outcrop data. *Global and Planetary Change* 80–81 (Special Issue), 61–84.
- Levy, R.H., Harwood, D.M., Stilwell, J.D., Feldmann, R.M., 2000. Sedimentary lithofacies of the McMurdo Sound erratics. Paleobiology and paleoenvironments of Eocene rocks, McMurdo Sound, East Antarctica. *Antarctic Research Series* 76, 39–61.
- Levy, R.H., Meyers, S.R., Naish, T.R., Golledge, N.R., McKay, R.M., Crampton, J.S., et al., 2019. Antarctic ice-sheet sensitivity to obliquity forcing enhanced through ocean connections. *Nature Geoscience* 12 (2), 132–137.
- Lewis, A.R., Ashworth, A.C., 2015. An early to middle Miocene record of ice-sheet and landscape evolution from the Friis Hills, Antarctica. *Geological Society of America Bulletin*.
- Lewis, A.R., Marchant, D.R., Ashworth, A.C., Hedenäs, L., Hemming, S.R., Johnson, J.V., et al., 2008. Mid-Miocene cooling and the extinction of tundra in continental Antarctica. *Proceedings of the National Academy of Sciences* 105 (31), 10676–10680.

- Lewis, A.R., Marchant, D.R., Ashworth, A.C., Hemming, S.R., Machlus, M.L., 2007. Major middle Miocene global climate change: evidence from East Antarctica and the Transantarctic Mountains. *Geological Society of America Bulletin* 119 (11–12), 1449–1461.
- Lewis, A.R., Marchant, D.R., Kowalewski, D.E., Baldwin, S.L., Webb, L.E., 2006. The age and origin of the Labyrinth, western Dry Valleys, Antarctica: evidence for extensive middle Miocene subglacial floods and freshwater discharge to the Southern Ocean. *Geology* 34 (7), 513–516.
- Licht, K.J., Hennessy, A.J., Welke, B.M., 2014. The U-Pb detrital zircon signature of West Antarctic ice stream tills in the Ross embayment, with implications for Last Glacial Maximum ice flow reconstructions. *Antarctic Science* 26 (6), 687–697.
- Liebrand, D., de Bakker, A.T.M., Beddow, H.M., Wilson, P.A., Bohaty, S.M., Ruessink, G., et al., 2017. Evolution of the early Antarctic ice ages. *Proceedings of the National Academy of Sciences* 114 (15), 3867–3872.
- Liebrand, D., Lourens, L.J., Hodell, D.A., de Boer, B., van de Wal, R.S.W., Pälike, H., 2011. Antarctic ice sheet and oceanographic response to eccentricity forcing during the early Miocene. *Climate of the Past* 7 (3), 869–880.
- Lindeque, A., Gohl, K., Wobbe, F., Uenzelmann-Neben, G., Henrys, S., Davy, B., 2016. Pre-glacial to full glacial sedimentation along the Pacific margin of West Antarctica: Record of shifting pattern of supply and transport, SCAR Open Science Conference, Kuala Lumpur, Malaysia, 10 August - 20 August 2016.
- Lisiecki, L.E., Raymo, M.E., 2005. A Pliocene-Pleistocene stack of 57 globally distributed benthic ^{18}O records. *Paleoceanography* 20 (PA 1003), 1–17.
- Livermore, R., Hillenbrand, C.D., Meredith, M., Eagles, G., 2007. Drake Passage and Cenozoic climate: an open and shut case? *Geochemistry, Geophysics, Geosystems* 8 (1).
- Londoño, L., Royer, D.L., Jaramillo, C., Escobar, J., Foster, D.A., Cárdenas-Rozo, A.L., et al., 2018. Early Miocene CO₂ estimates from a Neotropical fossil leaf assemblage exceed 400 ppm. *American Journal of Botany* 105 (11), 1929–1937.
- Loutit, T.S., Kennett, J., 1979. Application of Carbon Isotope Stratigraphy to Late Miocene Shallow Marine Sediments, New Zealand. *Science* 204 (4398), 1196–1199.
- Lübbers, J., Kuhnt, W., Holbourn, A.E., Bolton, C.T., Gray, E., Usui, Y., et al., 2019. The middle to late Miocene “Carbonate Crash” in the equatorial Indian Ocean. *Paleoceanography and Paleoclimatology* 34 (5), 813–832.
- Lunt, D.J., Haywood, A.M., Schmidt, G.A., Salzmann, U., Valdes, P.J., Dowsett, H.J., et al., 2012. On the causes of mid-Pliocene warmth and polar amplification. *Earth and Planetary Science Letters* 321–322, 128–138.
- Luyendyk, B.P., Sorlien, C.C., Wilson, D.S., Bartek, L.R., Siddoway, C.S., 2001. Structural and tectonic evolution of the Ross Sea Rift in the Cape Colbeck region, eastern Ross Sea, Antarctica. *Tectonics* 20 (6), 933–958.
- Lyle, M., Dadey, K.A., Farrell, J.W., 1995. The Late Miocene (11–8 Ma) Eastern Pacific Carbonate Crash: evidence for reorganization of deep-water Circulation by the closure of the Panama Gateway. In: 1995 Proceedings of the Ocean Drilling Program, Scientific Results, 138.
- Lyle, M., Gibbs, S., Moore, T., Rea, D., 2007. Late Oligocene initiation of the Antarctic Circumpolar Current: evidence from the South Pacific. *Geology* 35 (8), 691–694.
- Lythe, M.B., Vaughan, D.G., Lambrecht, A., Miller, H., Nixdorf, U., Oerter, H., et al., 2001. BEDMAP; a new ice thickness and subglacial topographic model of Antarctica. *Journal of Geophysical Research, B, Solid Earth and Planets* 106 (6), 11335–11,351.
- Majewski, W., 2010. Planktonic foraminiferal response to Middle Miocene cooling in the Southern Ocean (ODP Site 747, Kerguelan Plateau). *Acta Palaeontologica Polonica* 55 (3), 541–560. 520.

- Maldonado, A., Barnolas, A., Bohoyo, F., Galindo-Zaldivar, J., Hernandez-Molina, J., Lobo, F., et al., 2003. Contourite deposits in the central Scotia Sea; the importance of the Antarctic Circumpolar Current and the Weddell Gyre flows Antarctic Cenozoic palaeoenvironments; geologic record and models. ANTOSTRAT Symposium; The Geologic Record of the Antarctic Ice Sheet from Drilling, Coring and Seismic Studies 198 (1–2), 187–221.
- Maldonado, A., Bohoyo, F., Galindo-Zaldívar, J., Hernández-Molina, F.J., Lobo, F.J., Lodolo, E., et al., 2014. A model of oceanic development by ridge jumping: opening of the Scotia Sea. *Global and Planetary Change* 123, 152–173.
- Marchant, D.R., 1993. Miocene glacial stratigraphy and landscape evolution of the western Asgard Range, Antarctica. *Geografiska Annaler. Series A: Physical Geography* 303–330.
- Marchant, D.R., Denton, G.H., Sugden, D.E., Swisher III, C.C., 1993. Miocene glacial stratigraphy and landscape evolution of the western Asgard Range, Antarctica. *Geografiska Annaler: Series A, Physical Geography* 75 (4), 303–330.
- Marchant, D.R., Denton, G.H., Swisher III, C.C., Potter Jr., N., 1996. Late Cenozoic Antarctic paleoclimate reconstructed from volcanic ashes in the dry valleys region of southern Victoria Land. *Geological Society of America Bulletin* 108 (2), 181–194.
- Markwick, P.J., 2007. The palaeogeographic and palaeoclimatic significance of climate proxies for data-model comparisons. In: Williams, M., Haywood, A.M., Gregory, F.J., Schmidt, D. N. (Eds.), *Deep-Time Perspectives on Climate Change: Marrying the Signal from Computer Models and Biological Proxies*. The Micropalaeontological Society, Special Publications. The Geological Society, London, 251–312.
- Marshall, J., Speer, K., 2012. Closure of the meridional overturning circulation through Southern Ocean upwelling. *Nature Geoscience* 5 (3), 171–180.
- Martinez-Botí, M.A., Foster, G.L., Chalk, T.B., Rohling, E.J., Sexton, P.F., Lunt, D.J., et al., 2015. Plio-Pleistocene climate sensitivity evaluated using high-resolution CO₂ records. *Nature* 518 (7537), 49–54.
- Martinez-Garcia, A., Rosell-Mele, A., Jaccard, S.L., Geibert, W., Sigman, D.M., Haug, G.H., 2011. Southern Ocean dust-climate coupling over the past four million years. *Nature* 476 (7360), 312–315.
- Martos, Y.M., Maldonado, A., Lobo, F.J., Hernández-Molina, F.J., Pérez, L.F., 2013. Tectonics and palaeoceanographic evolution recorded by contourite features in southern Drake Passage (Antarctica). *Marine Geology* 343, 76–91.
- Masson-Delmotte, V., M. Schulz, A. Abe-Ouchi, J. Beer, A. Ganopolski, J.F. González Rouco, E. Jansen, K. Lambeck, J. Luterbacher, T. Naish, T. Osborn, B. Otto-Bliesner, T. Quinn, R. Ramesh, M. Rojas, X. Shao and A. Timmermann, 2013: Information from Paleoclimate Archives. In: *Climate Change 2013: The Physical Science Basis. Contribution of Working Group I to the Fifth Assessment Report of the Intergovernmental Panel on Climate Change* [Stocker, T.F., D. Qin, G.-K. Plattner, M. Tignor, S.K. Allen, J. Boschung, A. Nauels, Y. Xia, V. Bex and P.M. Midgley (eds.)]. Cambridge University Press, Cambridge, United Kingdom and New York, NY, USA.
- McClymont, E.L., Ford, H.L., Ho, S.L., Tindall, J.C., Haywood, A.M., Alonso-Garcia, M., et al., 2020. Lessons from a high-CO₂ world: an ocean view from ~3 million years ago. *Climate of the Past* 16 (4), 1599–1615.
- McGinnis, L.D., 1981. Dry Valley Drilling Project. American Geophysical Union, Washington, D.C. p. 465.
- McIntosh, W.C., 1998. 40Ar/39Ar geochronology of volcanic clasts and pumice in CRP-1 Core, Cape Roberts, Antarctica. *Studies from the Cape Roberts Project; Ross Sea, Antarctica; scientific report of CRP-1. Terra Antartica* 5 (3), 683–690.

- McIntosh, W.C., 2000. $^{40}\text{Ar}/^{39}\text{Ar}$ geochronology of tephra and volcanic clasts in CRP-2A, Victoria Land Basin, Antarctica. Studies from the Cape Roberts Project, Ross Sea, Antarctica; scientific report of CRP-2/2A; part II, chronology and chronostratigraphy for CRP-2/2A. *Terra Antarctica* 7 (4–5), 621–630.
- McKay, R., Browne, G., Carter, L., Cowan, E., Dunbar, G., Krissek, L., et al., 2009. The stratigraphic signature of the late Cenozoic Antarctic Ice Sheets in the Ross Embayment. *Geological Society of America Bulletin* 121 (11–12), 1537–1561.
- McKay, R., Escutia, C., Santis, L. De., Donda, F., Duncan, B., Gohl, K., 2021. A history of Antarctic Cenozoic Glaciation. In: Florindo, F. et al. (Eds.), *Antarctic Climate Evolution*, second ed. Elsevier (this volume).
- McKay, R., Naish, T., Carter, L., Riesselman, C., Dunbar, R., Sjunneskog, C., et al., 2012. Antarctic and Southern Ocean influences on Late Pliocene global cooling. *Proceedings of the National Academy of Sciences* 109 (17), 6423–6428.
- McKay, R., De Santis, L., Kulhanek, D., Expedition 374 Scientists, 2019. Ross Sea West Antarctic Ice Sheet History, *Proceedings of the International Ocean Discovery Program*. International Ocean Discovery Program, College Station.
- McKay, R.M., Barrett, P.J., Levy, R.S., Naish, T.R., Golledge, N.R., Pyne, A., 2016. Antarctic Cenozoic climate history from sedimentary records: ANDRILL and beyond. *Philosophical Transactions of the Royal Society A: Mathematical, Physical and Engineering Sciences* 374 (2059).
- Mckelvey, B., Webb, P., Kohn, B., 1977. Stratigraphy of the Taylor and lower Victoria Groups (Beacon Supergroup) between the Mackay Glacier and Boomerang Range, Antarctica. *New Zealand Journal of Geology and Geophysics* 20 (5), 813–863.
- Mckelvey, B.C., 1975. Preliminary site reports, DVDP sites 10 and 11, Taylor Valley. In: Mudrey Jr., M.G., McGinnis, L.D. (Eds.), *Dry Valley Drilling Project (DVDP) Bulletin*. pp. 16–60.
- Mckelvey, B.C., 1981. The lithologic logs of DVDP cores 10 and 11, Eastern taylor Valley. In: McGinnis, L.D. (Ed.), *Dry Valley Drilling Project. Antarctic Research Series*. American Geophysical Union, pp. 63–94.
- Meinshausen, M., Smith, S.J., Calvin, K., Daniel, J.S., Kainuma, M.L.T., Lamarque, J.F., et al., 2011. The RCP greenhouse gas concentrations and their extensions from 1765 to 2300. *Climatic Change* 109 (1–2), 213–241.
- Mejía, L.M., Méndez-Vicente, A., Abrevaya, L., Lawrence, K.T., Ladlow, C., Bolton, C., et al., 2017. A diatom record of CO₂ decline since the late Miocene. *Earth and Planetary Science Letters* 479, 18–33.
- Mengel, M., Levermann, A., 2014. Ice plug prevents irreversible discharge from East Antarctica. *Nature Climate Change* 4 (6), 451–455.
- Methner, K., Campani, M., Fiebig, J., Löffler, N., Kempf, O., Mulch, A., 2020. Middle Miocene long-term continental temperature change in and out of pace with marine climate records. *Scientific Reports* 10 (1).
- Middleton, J.L., Ackert Jr, R.P., Mukhopadhyay, S., 2012. Pothole and channel system formation in the McMurdo Dry Valleys of Antarctica: new insights from cosmogenic nuclides. *Earth and Planetary Science Letters* 355, 341–350.
- Miles, B.W.J., Stokes, C.R., Jamieson, S.S.R., 2016. Pan–ice-sheet glacier terminus change in East Antarctica reveals sensitivity of Wilkes Land to sea-ice changes. *Science Advances* 2 (5).
- Miles, B.W.J., Stokes, C.R., Vieli, A., Cox, N.J., 2013. Rapid, climate-driven changes in outlet glaciers on the Pacific coast of East Antarctica. *Nature* 500 (7464), 563–566.
- Miller, K.G., Browning, J.V., Schmelz, W.J., Kopp, R.E., Mountain, G.S., Wright, J.D., 2020. Cenozoic sea-level and cryospheric evolution from deep-sea geochemical and continental

- margin records. *Science Advances* 6 (20), eaaz1346. Available from: <https://doi.org/10.1126/sciadv.aaz1346>.
- Miller, K.G., Kominz, M.A., Browning, J.V., Wright, J.D., Mountain, G.S., Katz, M.E., et al., 2005. The Phanerozoic record of global sea-level Change. *Science* 310 (5752), 1293–1298.
- Miller, K.G., Raymo, M., Browning, J., Rosenthal, Y., Wright, J., 2019. Peak sea level during the warm Pliocene: errors, limitations, and constraints. *PAGES Magazine* 27 (1), 1–2.
- Miller, K.G., Wright, J.D., Farbanks, R.G., 1991b. Unlocking the ice house: Oligocene-Miocene oxygen isotopes, eustasy, and margin erosion. *Journal of Geophysical Research* 96 (B4), 6829–6848.
- Miller, K.G., Wright, J.D., Browning, J.V., Kulpecky, A., Kominz, M., Naish, T.R., et al., 2012. High tide of the warm Pliocene: implications of global sea level for Antarctic deglaciation. *Geology* 40 (5), 407–410.
- Miller, K.G., Wright, J.D., Fairbanks, R.G., Cloetingh, S.E., 1991a. Unlocking the ice house; Oligocene-Miocene oxygen isotopes, eustasy, and margin erosion. Special section on long-term sea level changes. AGU Chapman Conference on Causes and consequences of Long-Term Sea Level Changes 96 (4), 6829–6848.
- Modestou, S.E., Leutert, T.J., Fernandez, A., Lear, C.H., Meckler, A.N., 2020. Warm middle Miocene Indian Ocean bottom water temperatures: comparison of clumped isotope and Mg/Ca-based estimates. *Paleoceanography and Paleoclimatology* 35 (11), e2020PA003927.
- Molnar, P., Boos, W.R., Battisti, D.S., 2010. Orographic controls on climate and paleoclimate of Asia: thermal and mechanical roles for the Tibetan Plateau. *Annual Review of Earth and Planetary Sciences* 38 (1), 77–102.
- Montelli, A., Gulick, S.P.S., Fernandez, R., Frederick, B.C., Shevenell, A.E., Leventer, A., et al., 2019. Seismic stratigraphy of the Sabrina Coast shelf, East Antarctica: early history of dynamic meltwater-rich glaciations. *GSA Bulletin* 132 (3–4), 545–561.
- Morlighem, M., Rignot, E., Binder, T., Blankenship, D., Drews, R., Eagles, G., et al., 2020. Deep glacial troughs and stabilizing ridges unveiled beneath the margins of the Antarctic ice sheet. *Nature Geoscience* 13, 132–137.
- Morrison, A., Hogg, A.M., England, M.H., Spence, P., 2020. Warm Circumpolar Deep Water transport toward Antarctica driven by local dense water export in canyons. *Science Advances* 6 (18), eaav2516. Available from: <https://doi.org/10.1126/sciadv.aav2516>.
- Mosbrugger, V., Utescher, T., Dilcher, D.L., 2005. Cenozoic continental climatic evolution of Central Europe. *Proceedings of the National Academy of Sciences of the United States of America* 102 (42), 14964–14969.
- Mudrey, M.G., Jr., McGinnis, L.D., 1975. Dry Valley Drilling Project (DVDP) Bulletin, 280 pp.
- Naish, T., Duncan, B., Levy, R., McKay, R., Escutia, C., Santis, L. De., et al., 2021. Antarctic Ice Sheet dynamics during the Late Oligocene and Early Miocene: climatic conundrums revisited. In: Florindo, F., et al. (Eds.), Antarctic Climate Evolution, second ed. Elsevier (this volume).
- Naish, T., Powell, R., Levy, R. (Eds.), 2007. Studies from the ANDRILL, McMurdo Ice Shelf Project, Antarctica—Initial Science Report on AND-1B, pp. 121–327.
- Naish, T., Powell, R., Levy, R., Wilson, G., Scherer, R., Talarico, F., et al., 2009. Obliquity-paced Pliocene West Antarctic ice sheet oscillations. *Nature* 458 (7236), 322–328.
- Naish, T.R., Wilson, G.S., 2009. Constraints on the amplitude of Mid-Pliocene (3.6–2.4 Ma) eustatic sea-level fluctuations from the New Zealand shallow-marine sediment record. *Philosophical Transactions of the Royal Society A: Mathematical, Physical and Engineering Sciences* 367 (1886), 169–187.

- Naish, T.R., Barrett, P.J., Dunbar, G.B., Wolfe, K.J., Dunn, A.G., Henrys, S.A., et al., 2001a. Sedimentary cyclicity in CRP drillcore, Victoria Land Basin, Antarctica. Studies from the Cape Roberts Project, Ross Sea, Antarctica; scientific report of CRP-3; part I, sedimentary environments for CRP-3. *Terra Antartica* 8 (3), 225–244.
- Naish, T.R., Powell, R.D., Barrett, P.J., Levy, R.H., Henrys, S., Wilson, G.S., et al. and ANDRILL MIS Science Team, 2008. Late Cenozoic Climate History of the Ross Embayment from the AND-1B Drill Hole: Culmination of three decades of Antarctic Margin Drilling. In: Cooper, A.K., Barrett, P.J., Stagg, H., Storey, B., Stump, E., Wise, W., and the 10th ISAES Editorial Team (Eds.), *Antarctica: A Keystone in a Changing World*. Proceedings of the 10th International Symposium on Antarctic Earth Sciences. The National Academies Press, Washington, D.C., pp. 71–82. Available from: <https://doi.org/10.3133/of2007-1047.kp3107>.
- Naish, T.R., Wolfe, K.J., Barrett, P.J., Wilson, G.S.E.A., 2001b. Orbitally induced oscillations in the East Antarctic ice sheet at the Oligocene/Miocene boundary. *Nature* 413, 719–723.
- Newkirk, D.R., Martin, E.E., 2009. Circulation through the Central American Seaway during the Miocene carbonate crash. *Geology* 37 (1), 87–90.
- Nyland, R.E., Panter, K.S., Rocchi, S., Di Vincenzo, G., Del Carlo, P., Tiepolo, M., et al., 2013. Volcanic activity and its link to glaciation cycles: Single-grain age and geochemistry of Early to Middle Miocene volcanic glass from ANDRILL AND-2A core, Antarctica. *Journal of Volcanology and Geothermal Research* 250, 106–128.
- O'Brien, P., Post, A., Edwards, S., Martin, T., Caburlotto, A., Donda, F., et al., 2020. Continental slope and rise geomorphology seaward of the Totten Glacier, East Antarctica (112 E-122 E). *Marine Geology* 427, 106221.
- O'Brien, P.E., Cooper, A.K., Richter, C., et al., 2001. Proc. ODP, Init. Repts., 188: College Station, TX (Ocean Drilling Program). Available from: <https://doi.org/10.2973/odp.proc.ir.188.2001>.
- Oerlemans, J., 2002. On glacial inception and orography. *Quaternary International* 95–96, 5–10.
- Ohneiser, C., Florindo, F., Stocchi, P., Roberts, A.P., DeConto, R.M., Pollard, D., 2015. Antarctic glacio-eustatic contributions to late Miocene Mediterranean desiccation and reflooding. *Nature Communications* 6 (1), 1–10.
- Ohneiser, C., Wilson, G.S., 2012. Revised magnetostratigraphic chronologies for New Harbour Drill cores, southern Victoria Land, Antarctica. *Global and Planetary Change* 82–83 (Special Issue), 12–24.
- Ohneiser, C., Wilson, G.S., Beltran, C., Dolan, A.M., Hill, D.J., Prebble, J.G., 2020. Warm fjords and vegetated landscapes in early Pliocene East Antarctica. *Earth and Planetary Science Letters* 534, 116045.
- Olbers, D., Borowski, D., Völker, C., Wolff, J.-O., 2004. The dynamical balance, transport and circulation of the Antarctic Circumpolar Current. *Antarctic Science* 16 (4), 439–470.
- Orejola, N., Passchier, S., 2014. Sedimentology of lower Pliocene to upper Pleistocene diamictites from IODP site U1358, Wilkes Land margin, and implications for East Antarctic Ice Sheet dynamics. *Antarctic Science* 26 (2), 183.
- Orsi, A.H., Johnson, G.C., Bullister, J.L., 1999. Circulation, mixing, and production of Antarctic Bottom Water. *Progress in Oceanography* 43 (1), 55–109.
- Orsi, A.H., Smethie Jr, W.M., Bullister, J.L., 2002. On the total input of Antarctic waters to the deep ocean: A preliminary estimate from chlorofluorocarbon measurements. *Journal of Geophysical Research: Oceans* 107 (C8), 31-1–31-14.

- Orsi, A.H., Whitworth, T., Nowlin, W.D., 1995. On the meridional extent and fronts of the Antarctic Circumpolar Current. Deep Sea Research Part I: Oceanographic Research Papers 42 (5), 641–673.
- Orsi, A.H., Wiederwohl, C.L., 2009. A recount of Ross Sea waters. Deep Sea Research Part II: Topical Studies in Oceanography 56 (13–14), 778–795.
- Osborne, C.P., Beerling, D.J., 2006. Nature's green revolution: the remarkable evolutionary rise of C₄ plants. Philosophical Transactions of the Royal Society B: Biological Sciences 361 (1465), 173–194.
- Pagani, M., Arthur, M.A., Freeman, K.H., 1999a. Miocene evolution of atmospheric carbon dioxide. Paleoceanography 14 (3), 273–292.
- Pagani, M., Freeman, K.H., Arthur, M.A., 1999b. Late Miocene atmospheric CO₂ concentrations and the expansion of C₄ grasses. Science 285 (5429), 876–879.
- Pagani, M., Huber, M., Liu, Z., Bohaty, S.M., Henderiks, J., Sijp, W., et al., 2011. The role of carbon dioxide during the onset of Antarctic Glaciation. Science 334 (6060), 1261–1264.
- Pagani, M., Liu, Z., LaRiviere, J., Ravelo, A.C., 2010. High Earth-system climate sensitivity determined from Pliocene carbon dioxide concentrations. Nature Geoscience 3 (1), 27–30.
- Pälike, H., Lyle, M.W., Nishi, H., Raffi, I., Ridgwell, A., Gamage, K., et al., 2012. A Cenozoic record of the equatorial Pacific carbonate compensation depth. Nature 488 (7413), 609–614.
- Palmer, E.F., Licht, K.J., Swope, R.J., Hemming, S.R., 2012. Nunatak moraines as a repository of what lies beneath the East Antarctic ice sheet. Geological Society of America Special Paper 487, 97–104.
- Pankhurst, R.J., Weaver, S.D., Bradshaw, J.D., Storey, B.C., Ireland, T.R., 1998. Geochronology and geochemistry of pre-Jurassic superterrane in Marie Byrd Land, Antarctica. Journal of Geophysical Research 1033 (B2), 2529–2547.
- Panter, K.S., Hart, S.R., Kyle, P.R., Blusztajn, J., Wilch, T.I., 2000. Geochemistry of late Cenozoic basalts from the Crary Mountains: characterization of mantle sources in eastern Marie Byrd Land, Antarctica. Chemical Geology 165, 215–241.
- Paolo, F.S., Fricker, H.A., Padman, L., 2015. Volume loss from Antarctic ice shelves is accelerating. Science 348 (6232), 327–331.
- Parizek, B.R., Christianson, K., Alley, R.B., Voytenko, D., Vařková, I., Dixon, T.H., et al., 2019. Ice-cliff failure via retrogressive slumping. Geology 47 (5), 449–452.
- Passchier, S., 2011. Linkages between East Antarctic Ice Sheet extent and Southern Ocean temperatures based on a Pliocene high-resolution record of ice rafted debris off Prydz Bay, East Antarctica. Paleoceanography 26 (4).
- Passchier, S., Bohaty, S.M., Jiménez-Espejo, F., Pross, J., Röhl, U., van de Flierdt, T., et al., 2013a. Early Eocene to middle Miocene cooling and aridification of East Antarctica. Geochemistry, Geophysics, Geosystems 14 (5), 1399–1410.
- Passchier, S., Browne, G., Field, B., Fielding, C.R., Krissek, L.A., Panter, K., et al. and Science Team, A.-S., 2011. Early and middle Miocene Antarctic glacial history from the sedimentary facies distribution in the AND-2A drill hole, Ross Sea, Antarctica. Geological Society of America Bulletin, B30334.30331.
- Passchier, S., Falk, C.J., Florindo, F., 2013b. Orbitally paced shifts in the particle size of Antarctic continental shelf sediments in response to ice dynamics during the Miocene climatic optimum. Geosphere 9 (1), 54–62.
- Patterson, M.O., Ishman, S.E., 2012. Neogene benthic foraminiferal assemblages and paleoenvironmental record for McMurdo Sound, Antarctica. Geosphere 8 (6), 1331–1341.

- Patterson, M.O., McKay, R., Naish, T., Escutia, C., Jimenez-Espejo, F.J., Raymo, M.E., et al., 2014. Orbital forcing of the East Antarctic ice sheet during the Pliocene and Early Pleistocene. *Nature Geoscience* 7 (11), 841–847.
- Paulsen, T., Encarnación, J., Grunow, A., Valencia, V., Pecha, M., Layer, P., et al., 2013. Age and significance of ‘outboard’ high-grade metamorphics and intrusives of the Ross orogen, Antarctica. *Gondwana Research* 24 (1), 349–358.
- Paxman, G.J., Jamieson, S.S., Ferraccioli, F., Bentley, M.J., Ross, N., Watts, A.B., et al., 2019a. The role of lithospheric flexure in the landscape evolution of the Wilkes Subglacial Basin and Transantarctic Mountains, East Antarctica. *Journal of Geophysical Research: Earth Surface* 124 (3), 812–829.
- Paxman, G.J.G., Gasson, E.G.W., Jamieson, S.S.R., Bentley, M.J., Ferraccioli, F., 2020. Long-term increase in Antarctic Ice Sheet vulnerability driven by bed topography evolution. *Geophysical Research Letters* 47 (20), e2020GL090003.
- Paxman, G.J.G., Jamieson, S.S.R., Hochmuth, K., Gohl, K., Bentley, M.J., Leitchenkov, G., et al., 2019b. Reconstructions of Antarctic topography since the Eocene–Oligocene boundary. *Palaeogeography, Palaeoclimatology, Palaeoecology* 535, 109346.
- Pekar, S., DeConto, R.M., 2006. High-resolution ice-volume estimates for the early Miocene: Evidence for a dynamic ice sheet in Antarctica. *Palaeogeography, Palaeoclimatology, Palaeoecology* 231 (1–2), 101–109.
- Pekar, S.F., DeConto, R.M., Harwood, D.M., 2006. Resolving a late Oligocene conundrum: deep sea warming and Antarctic glaciation. *Palaeogeography, Palaeoclimatology, Palaeoecology* 231 (1–2), 29–40.
- Pérez, L.F., De Santis, L., McKay, R.M., Larter, R.D., Ash, J., Bart, P.J., et al. and IODP Expedition 374 Scientists, 2021a. Early and middle Miocene ice sheet dynamics in the Ross Sea: results from integrated core-log-seismic interpretation. *GSA Bulletin*. Available from: <https://doi.org/10.1130/B35814.1>.
- Pérez, L.F., Hernández-Molina, F.J., Lodolo, E., Bohoyo, F., Galindo-Zaldívar, J., Maldonado, A., 2019. Oceanographic and climatic consequences of the tectonic evolution of the southern scotia sea basins, Antarctica. *Earth-Science Reviews* 198, 102922.
- Pérez, L.F., Martos, Y.M., García, M., Weber, M.E., Raymo, M.E., Williams, T., et al., 2021b. Miocene to present oceanographic variability in the Scotia Sea and Antarctic ice sheets dynamics: Insight from revised seismic-stratigraphy following IODP Expedition 382. *Earth and Planetary Science Letters* 553, 116657.
- Pérez, L.F., Nielsen, T., Knutz, P.C., Kuijpers, A., Damm, V., 2018. Large-scale evolution of the central-east Greenland margin: New insights to the North Atlantic glaciation history. *Global and Planetary Change* 163, 141–157.
- Peterson, L., Murray, D., Ehrmann, W., Hempel, P., 1992. Cenozoic carbonate accumulation and compensation depth changes in the Indian Ocean. *Synthesis of Results from Scientific Drilling in the Indian Ocean* 70, 311–333.
- Pfuhl, H.A., McCave, I.N., 2005. Evidence for late Oligocene establishment of the Antarctic Circumpolar Current. *Earth and Planetary Science Letters* 235 (3), 715–728.
- Pierce, E.L., van de Flierdt, T., Williams, T., Hemming, S.R., Cook, C.P., Passchier, S., 2017. Evidence for a dynamic East Antarctic ice sheet during the mid-Miocene climate transition. *Earth and Planetary Science Letters* 478 (Supplement C), 1–13.
- Piper, D., Brisco, C., 1975. Deep-water continental-margin sedimentation, DSDP Leg 28, Antarctica. *Initial Reports of the Deep Sea Drilling Project* 28, 727–755.
- Pollard, D., DeConto, R.M., 2005. Hysteresis in Cenozoic Antarctic ice-sheet variations. *Global and Planetary Change* 45, 9–21.

- Pollard, D., DeConto, R.M., 2007. A coupled ice-sheet/ice-shelf/sediment model applied to a marine-margin flowline: Forced and unforced variations. In: Hambrey, M., Christoffersen, P., Glasser, N.F., Hubbard, B. (Eds.), *Glacial Sedimentary Processes and Products*. Blackwell, pp. 37–52.
- Pollard, D., DeConto, R.M., 2009. Modelling West Antarctic ice sheet growth and collapse through the past five million years. *Nature* 458, 329–332.
- Pollard, D., DeConto, R.M., 2020. Continuous simulations over the last 40 million years with a coupled Antarctic ice sheet-sediment model. *Palaeogeography, Palaeoclimatology, Palaeoecology* 537, 109374.
- Pollard, D., DeConto, R.M., Alley, R.B., 2015. Potential Antarctic Ice Sheet retreat driven by hydrofracturing and ice cliff failure. *Earth and Planetary Science Letters* 412, 112–121.
- Poore, R.Ze., Sloan, L.Ce., 1996. Climates and climate variability of the Pliocene. *Marine Micropaleontology* 27 (1–4), 326.
- Porter-Smith, R., Harris, P.T.E., Brancolini, G.E., Bindoff, N.L.E., De Santis, L.E., 2003. Bathymetry of the George Vth land shelf and slope. Recent investigations of the Mertz Polynya and George Vth Land continental margin, East Antarctica. *Deep-Sea Research. Part II: Topical Studies in Oceanography* 50 (8–9), 1337–1341.
- Prebble, J.G., Raine, J.I., Barrett, P.J., Hannah, M.J., 2006. Vegetation and climate from two Oligocene glacioeustatic sedimentary cycles (31 and 24 Ma) cored by the Cape Roberts Project, Victoria Land Basin, Antarctica. *Palaeogeography, Palaeoclimatology, Palaeoecology* 231 (1), 41–57.
- Prebble, J.G., Reichgelt, T., Mildenhall, D.C., Greenwood, D.R., Raine, J.I., Kennedy, E.M., et al., 2017. Terrestrial climate evolution in the Southwest Pacific over the past 30 million years. *Earth and Planetary Science Letters* 459, 136–144.
- Preiss-Daimler, I., Zarkogiannis, S.D., Kontakiotis, G., Henrich, R., Antonarakou, A., 2021. Paleoceanographic perturbations and the marine carbonate System during the Middle to Late Miocene Carbonate Crash—a critical review. *Geosciences* 11 (2), 94.
- Prentice, M.L., Bockheim, J.G., Wilson, S.C., Burckle, L.H., Hodell, D.A., Schluchter, C., et al., 1993. Late Neogene Antarctic glacial history: evidence from central Wright Valley. In: Kennett, J.P., Warnke, D.A. (Eds.), *The Antarctic Paleoenvironment: A Perspective on Global Change, Part Two: Antarctic Research Series*. American Geophysical Union, Washington, D.C, pp. 207–250.
- Prentice, M.L., Kleman, J.L., Stroeven, A.P., 1998. The composite glacial erosional landscape of the northern McMurdo Dry Valleys: Implications for Antarctic Tertiary glacial history. *Ecosystem Dynamics in a Polar Desert: the McMurdo Dry Valleys*. Antarctica 72, 1–38.
- Prentice, M.L., Ishman, S.E., Clemens, S.C., McIntosh, W.C., Clarke, K., 1999. Late Neogene stable isotope records from fjords within the McMurdo Dry Valleys, Antarctica. In: Skinner, D.N.B. (Ed.), *8th International Symposium on Antarctic Earth Sciences*. Victoria University of Wellington, New Zealand, p. 249.
- Prentice, M.L., Krusic, A.G., 2005. Early Pliocene alpine glaciation in Antarctica: terrestrial vs tidewater glaciers in Wright Valley. *Geografiska Annaler, Series A* 87, 87–109.
- Pretty, R., 2019. Ice dynamics and ocean productivity during the Late Miocene, offshore Wilkes Land, East Antarctica. Victoria University of Wellington, Wellington, p. 148.
- Pritchard, H.D., Ligtenberg, S.R.M., Fricker, H.A., Vaughan, D.G., van den Broeke, M.R., Padman, L., 2012. Antarctic ice-sheet loss driven by basal melting of ice shelves. *Nature* 484 (7395), 502–505.

- Purkey, S.G., Johnson, G.C., 2010. Warming of global abyssal and deep Southern Ocean waters between the 1990s and 2000s: contributions to global heat and sea level rise budgets. *Journal of Climate* 23 (23), 6336–6351.
- Raffi, I., Wade, B.S., Pälike, H., Beu, A.G., Cooper, R., Crundwell, M.P., et al., 2020. Chapter 29 – The Neogene period. In: Gradstein, F.M., Ogg, J.G., Schmitz, M.D., Ogg, G. M. (Eds.), *Geologic Time Scale 2020*. Elsevier, pp. 1141–1215.
- Raitzsch, M., Bijma, J., Bickert, T., Schulz, M., Holbourn, A., Kučera, M., 2021. Atmospheric carbon dioxide variations across the middle Miocene climate transition. *Climate of the Past* 17 (2), 703–719.
- Ravelo, A.C., Andreasen, D.H., 2000. Enhanced circulation during a warm period. *Geophysical Research Letters* 27 (7), 1001–1004.
- Raymo, M.E., Nisancioglu, K.H., 2003. The 41 kyr world; Milankovitch's other unsolved mystery. *Paleoceanography* 18 (1), 11.11–11.16.
- Raymo, M.E., Ruddiman, W.F., 1992. Tectonic forcing of late Cenozoic climate. *Nature (London)* 359 (6391), 117–122.
- Raymo, M.E., 1994. The initiation of Northern Hemisphere glaciation. *Annual Review of Earth and Planetary Sciences* 22, 353–383.
- Raymo, M.E., Kozdon, R., Evans, D., Lisiecki, L., Ford, H.L., 2018. The accuracy of mid-Pliocene $\delta^{18}\text{O}$ -based ice volume and sea level reconstructions. *Earth-Science Reviews* 177, 291–302.
- Raymo, M.E., Lisiecki, L., Nisancioglu, K.H., 2006. Plio-Pleistocene ice volume, Antarctic climate, and the global $\delta^{18}\text{O}$ record. *Science* 313 (5786), 492–495.
- Raymo, M.E., Mitrovica, J.X., O'Leary, M.J., DeConto, R.M., Hearty, P.J., 2011. Departures from eustasy in Pliocene sea-level records. *Nature Geoscience* 4 (5), 328–332.
- Reichgelt, T., D'Andrea, W.J., Fox, B.R.S., 2016. Abrupt plant physiological changes in southern New Zealand at the termination of the Mi-1 event reflect shifts in hydroclimate and pCO_2 . *Earth and Planetary Science Letters* 455, 115–124.
- Reichgelt, T., D'Andrea, W.J., Valdivia-McCarthy, A.C., Fox, B.R.S., Bannister, J.M., Conran, J.G., et al., 2020. Elevated CO_2 , increased leaf-level productivity, and water-use efficiency during the early Miocene. *Clim. Past* 16, 1509–1521. Available from: <https://doi.org/10.5194/cp-16-1509-2020>.
- Reinardy, B., Escutia, C., Iwai, M., Jimenez-Espejo, F., Cook, C., van de Flierdt, T., et al., 2015. Repeated advance and retreat of the East Antarctic Ice Sheet on the continental shelf during the early Pliocene warm period. *Palaeogeography, Palaeoclimatology, Palaeoecology* 422, 65–84.
- Retallack, G.J., 2009a. Greenhouse crises of the past 300 million years. *Geological Society of America Bulletin* 121 (9–10), 1441–1455.
- Retallack, G.J., 2009b. Refining a pedogenic-carbonate CO_2 paleobarometer to quantify a middle Miocene greenhouse spike. *Palaeogeography, Palaeoclimatology, Palaeoecology* 281 (1), 57–65.
- Rintoul, S., Silvano, A., Pena-Molino, B., van Wijk, E., Rosenberg, M., Greenbaum, J. et al., 2016. Ocean heat drives rapid basal melt of the Totten Ice Shelf. *Science Advances*.
- Rintoul, S.R., da Silva, C.E., 2019. Antarctic Circumpolar Current \star . In: Cochran, J.K., Bokuniewicz, H.J., Yager, P.L. (Eds.), *Encyclopedia of Ocean Sciences*, third ed. Academic Press, Oxford, pp. 248–261.
- Rintoul, S.R., 1991. South Atlantic interbasin exchange. *Journal of Geophysical Research* 96, 5493–5550.

- Rintoul, S.R., 2018. The global influence of localized dynamics in the Southern Ocean. *Nature* 558 (7709), 209–218.
- Rintoul, S.R., Hughes, C.W., Olbers, D., 2001. The Antarctic Circumpolar Current System, *International Geophysics*. Elsevier, pp. 271–XXXVI.
- Robel, A.A., Banwell, A.F., 2019. A speed limit on ice shelf collapse through hydrofracture. *Geophysical Research Letters* 46 (21), 12092–12100.
- Roberts, J.L., Warner, R.C., Young, D., Wright, A., van Ommen, T.D., Blankenship, D.D., et al., 2011. Refined broad-scale sub-glacial morphology of Aurora Subglacial Basin, East Antarctica derived by an ice-dynamics-based interpolation scheme. *Cryosphere* 5 (3), 551–560.
- Rogelj, J., den Elzen, M., Höhne, N., Fransen, T., Fekete, H., Winkler, H., et al., 2016. Paris Agreement climate proposals need a boost to keep warming well below 2°C. *Nature* 534 (7609), 631–639.
- Rohling, E., Foster, G.L., Grant, K., Marino, G., Roberts, A., Tamisiea, M.E., et al., 2014. Sea-level and deep-sea-temperature variability over the past 5.3 million years. *Nature* 508 (7497), 477–482.
- Rommerskirchen, F., Condon, T., Mollenhauer, G., Dupont, L., Schefuss, E., 2011. Miocene to Pliocene development of surface and subsurface temperatures in the Benguela Current system. *Paleoceanography* 26 (3).
- Rosenblume, J.A., Powell, R.D., 2019. Glacial sequence stratigraphy of ANDRILL-1B core reveals a dynamic subpolar Antarctic Ice Sheet in Ross Sea during the late Miocene. *Sedimentology* 66 (6), 2072–2097.
- Rovere, A., Pappalardo, M., Richiano, S., Aguirre, M., Sandstrom, M.R., Hearty, P.J., et al., 2020. Higher than present global mean sea level recorded by an Early Pliocene intertidal unit in Patagonia (Argentina). *Communications Earth & Environment* 1 (1), 1–10.
- Rovere, A., Raymo, M.E., Mitrovica, J., Hearty, P.J., O’Leary, M., Inglis, J., 2014. The Mid-Pliocene sea-level conundrum: glacial isostasy, eustasy and dynamic topography. *Earth and Planetary Science Letters* 387, 27–33.
- Salabarnada, A., Escutia, C., Röhl, U., Nelson, C.H., McKay, R., Jiménez-Espejo, F.J., et al., 2018. Paleoceanography and ice sheet variability offshore Wilkes Land, Antarctica—Part 1: insights from late Oligocene astronomically paced contourite sedimentation. *Climate of the Past* 14 (7), 991–1014.
- Salzmann, U., Haywood, A., Lunt, D., Valdes, P., Hill, D., 2008. A new global biome reconstruction and data-model comparison for the middle Pliocene. *Global Ecology and Biogeography* 17 (3), 432–447.
- Salzmann, U., Riding, J.B., Nelson, A.E., Smellie, J.L., 2011. How likely was a green Antarctic Peninsula during warm Pliocene interglacials? A critical reassessment based on new palynofloras from James Ross Island. *Palaeogeography, Palaeoclimatology, Palaeoecology* 309 (1–2), 73–82.
- Sangiorgi, F., Bijl, P.K., Passchier, S., Salzmann, U., Schouten, S., McKay, R., et al., 2018. Southern Ocean warming and Wilkes Land ice sheet retreat during the mid-Miocene. *Nature Communications* 9 (1), 317.
- Sauermilch, I., Whittaker, J.M., Bijl, P.K., Totterdell, J., Jokat, W., 2019. Tectonic, oceanographic, and climatic controls on the Cretaceous-Cenozoic sedimentary record of the Australian-Antarctic Basin. *Journal of Geophysical Research: Solid Earth* 124 (8), 7699–7724.
- Scher, H.D., Martin, E.E., 2006. Timing and climatic consequences of the opening of Drake passage. *Science* 312 (5772), 428–430.
- Scher, H.D., Whittaker, J.M., Williams, S.E., Latimer, J.C., Kordes, W.E.C., Delaney, M.L., 2015. Onset of Antarctic Circumpolar Current 30 million years ago as Tasmanian Gateway aligned with westerlies. *Nature* 523 (7562), 580–583.

- Scherer, R.P., Aldahan, A.A., Tulaczyk, S., Possnert, G., Engelhardt, H., Kamb, B., 1998. Pleistocene collapse of the West Antarctic ice sheet. *Science* 281 (5373), 82–85.
- Scherer, R.P., DeConto, R.M., Pollard, D., Alley, R.B., 2016. Windblown Pliocene diatoms and East antarctic ice sheet retreat. *Nature Communications* 7 (1), 1–9.
- Schiller, M., Dickinson, W., Ditchburn, R.G., Graham, I.J., Zondervan, A., 2009. Atmospheric ^{10}Be in an Antarctic soil: Implications for climate change. *Journal of Geophysical Research* 114 (F1), F01033.
- Schiller, M., Dickinson, W.W., Iverson, N.A., Baker, J.A., 2019. A re-evaluation of the Hart Ash, an important stratigraphic marker: Wright Valley, Antarctica. *Antarctic Science* 31 (3), 139–149.
- Schuster, M., Duringer, P., Ghienne, J.-F., Vignaud, P., Mackaye, H.T., Likius, A., et al., 2006. The age of the Sahara Desert. *Science* 311 (5762), 821.
- Seki, O., Foster, G.L., Schmidt, D.N., Mackensen, A., Kawamura, K., Pancost, R.D., 2010. Alkenone and boron-based Pliocene pCO_2 records. *Earth and Planetary Science Letters* 292 (1–2), 201–211.
- Selby, M.J., 1971. Slopes and their development in an ice-free, arid area of Antarctica. *Geografiska Annaler: Series A, Physical Geography* 53 (3–4), 235–245.
- Selby, M.J., Wilson, A.T., 1971. The Origin of the Labyrinth, Wright Valley, Antarctica. *GSA Bulletin* 82 (2), 471–476.
- Seroussi, H., Morlighem, M., 2018. Representation of basal melting at the grounding line in ice flow models. *The Cryosphere* 12 (10), 3085–3096.
- Shackleton, N., 1967. Oxygen isotope analyses and pleistocene temperatures re-assessed. *Nature (London)* 215 (5096), 15–17.
- Shackleton, N.J., Kennett, J.P., 1975a. Late Cenozoic oxygen and carbon isotope changes at DSDP Site 284: Implications for glacial history of the northern hemisphere and Antarctica. Initial Report Deep Sea Drilling Project 29, 801–807.
- Shackleton, N.J., Kennett, J.P., 1975b. Paleotemperature history of the Cenozoic and the initiation of Antarctic glaciation; oxygen and carbon isotope analyses in DSDP sites 277, 279, and 281. Initial Reports of the Deep Sea Drilling Project 29, 743–755.
- Shakun, J.D., Corbett, L.B., Bierman, P.R., Underwood, K., Rizzo, D.M., Zimmerman, S.R., et al., 2018. Minimal East Antarctic Ice Sheet retreat onto land during the past eight million years. *Nature* 558 (7709), 284–287.
- Shepherd, A., Ivins, E., Rignot, E., Smith, B., van den Broeke, M., Velicogna, I., et al., 2018. Mass balance of the Antarctic Ice Sheet from 1992 to 2017. *Nature* 558 (7709), 219–222.
- Shevenell, A.E., Kennett, J.P., Lea, D.W., 2004. Middle Miocene Southern Ocean Cooling and Antarctic Cryosphere Expansion. *Science* 305 (5691), 1766–1770.
- Shevenell, A.E., Kennett, J.P., Lea, D.W., 2008. Middle Miocene ice sheet dynamics, deep-sea temperatures, and carbon cycling: a Southern Ocean perspective. *Geochemistry Geophysics Geosystems* 9 (2), Q02006.
- Siddoway, C.S., Fanning, C.M., 2009. Paleozoic tectonism on the East Gondwana margin: Evidence from SHRIMP U–Pb zircon geochronology of a migmatite–granite complex in West Antarctica. *Tectonophysics* 477 (3–4), 262–277.
- Siddoway, C.S., 2008. Tectonics of the West Antarctic Rift System: new light on the history and dynamics of distributed intracontinental extension. In: Cooper, A.K., Barrett, P.J., Stagg, H., Storey, B., Stump, E., Wise, W., The 10th ISAES Editorial Team (Eds.), *Antarctica: A Keystone in a Changing World. Proceedings of the 10th International Symposium on Antarctic Earth Sciences*. The National Academies Press, Washington, D.C., pp. 91–114. Available from: <http://doi.org/10.3133/of2007-1047.kp3109>.

- Siesser, W.G., 1980. Late Miocene origin of the Benguela upswelling system off northern Namibia. *Science* 208 (4441), 283–285.
- Sijp, W.P., England, M.H., 2004. Effect of the Drake passage throughflow on global climate. *Journal of Physical Oceanography* 34 (5), 1254–1266.
- Silvano, A., Rintoul, S.R., Peña-Molino, B., Hobbs, W.R., van Wijk, E., Aoki, S., et al., 2018. Freshening by glacial meltwater enhances melting of ice shelves and reduces formation of Antarctic Bottom Water. *Science Advances* 4 (4), eaap9467.
- Śliwińska, K.K., Dybkjær, K., Schoon, P.L., Beyer, C., King, C., Schouten, S., et al., 2014. Paleoclimatic and paleoenvironmental records of the Oligocene–Miocene transition, central Jylland, Denmark. *Marine Geology* 350, 1–15.
- Smith Jr, W.O., Sedwick, P.N., Arrigo, K.R., Ainley, D.G., Orsi, A.H., 2012. The Ross Sea in a sea of change. *Oceanography* 25 (3), 90–103.
- Sokolov, S., Rintoul, S.R., 2007. On the relationship between fronts of the Antarctic Circumpolar Current and surface chlorophyll concentrations in the Southern Ocean. *Journal of Geophysical Research: Oceans* 112 (C7).
- Sorlien, C.C., Luyendyk, B.P., Wilson, D.S., Decesari, R.C., Bartek, L.R., Diebold, J.B., 2007a. Buried Oligocene glacial topography beneath a smooth middle Miocene unconformity in the southeast Ross Sea: From temperate to glacial West Antarctica? In: Cooper, A. K., Raymond C.R., et al. (Eds.), *Antarctica: A Keystone in a Changing World—Online Proceedings of the 10th ISAES X*. United States Geological Survey and The National Academies, pp. Extended Abstract 099; 091-094. <<http://pubs.usgs.gov/of/2007/1047/ea/of2007-1047ea2099.pdf>>.
- Sorlien, C.C., Luyendyk, B.P., Wilson, D.S., Decesari, R.C., Bartek, L.R., Diebold, J.B., 2007b. Oligocene development of the West Antarctic Ice Sheet recorded in eastern Ross Sea strata. *Geology* 35 (5), 467–470.
- Sorlien, C.C., Wilson, D.S., Luyendyk, B.P., Wardell, N., Santis, L.D., Bart, P.J.C.S., et al., 2012. Subsidence and tilting of pre-25Ma wave-cut platform in Ross Sea, Antarctica. In: SCAR Open Science Conference, Portland, Oregon.
- Sosdian, S.M., Babilia, T.L., Greenop, R., Foster, G.L., Lear, C.H., 2020. Ocean Carbon Storage across the middle Miocene: a new interpretation for the Monterey Event. *Nature Communications* 11 (1), 134.
- Sosdian, S.M., Greenop, R., Hain, M.P., Foster, G.L., Pearson, P.N., Lear, C.H., 2018. Constraining the evolution of Neogene ocean carbonate chemistry using the boron isotope pH proxy. *Earth and Planetary Science Letters* 498, 362–376.
- Spector, P., Balco, G., 2021. Exposure-age data from across Antarctica reveal mid-Miocene establishment of polar desert climate. *Geology* 49 (1), 91–95.
- Spiegel, C., Lindow, J., Kamp, P.J.J., Meisel, O., Mukasa, S., Lisker, F., et al., 2016. Tectonomorphic evolution of Marie Byrd Land—implications for Cenozoic rifting activity and onset of West Antarctic glaciation. *Global and Planetary Change* 145, 98–115.
- St John, K.E., Krissek, L.A., 2002. The late Miocene to Pleistocene ice-rafting history of south-east Greenland. *Boreas* 31 (1), 28–35.
- St. John, K., 2008. Cenozoic ice-rafting history of the central Arctic Ocean: terrigenous sands on the Lomonosov Ridge. *Paleoceanography* 23 (1).
- Staiger, J.W., Marchant, D.R., Schaefer, J.M., Oberholzer, P., Johnson, J.V., Lewis, A.R., et al., 2006. Plio-Pleistocene history of Ferrar Glacier, Antarctica: implications for climate and ice sheet stability. *Earth and Planetary Science Letters* 243, 489–503.

- Stap, L.B., Sutter, J., Knorr, G., Stärz, M., Lohmann, G., 2019. Transient variability of the Miocene Antarctic Ice Sheet smaller than equilibrium differences. *Geophysical Research Letters* 46 (8), 4288–4298.
- Stap, L.B., Van De Wal, R.S., Boer, Bd, Bintanja, R., Lourens, L.J., 2017. The influence of ice sheets on temperature during the past 38 million years inferred from a one-dimensional ice sheet–climate model. *Climate of the Past* 13 (9), 1243–1257.
- Stärz, M., Jokat, W., Knorr, G., Lohmann, G., 2017. Threshold in North Atlantic-Arctic Ocean circulation controlled by the subsidence of the Greenland-Scotland Ridge. *Nature Communications* 8 (1), 1–13.
- Steinþorsdóttir, M., Coxall, H.K., de Boer, A.M., Huber, M., Barbolini, N., Bradshaw, C.D., et al., 2020. The Miocene: the future of the past. *Paleoceanography and Paleoclimatology* 35, e2020PA004037.
- Steinþorsdóttir, M., Jardine, P.E., Rember, W.C., 2021. Near-Future pCO₂ During the Hot Miocene Climatic Optimum. *Paleoceanography and Paleoclimatology* 36 (1), e2020PA003900.
- Stewart, A.L., Thompson, A.F., 2014. Eddy-mediated transport of warm circumpolar deep water across the Antarctic Shelf Break. *Geophysical Research Letters* 2014, GL062281.
- Stickley, C.E., Brinkhuis, H., McGonigal, K., Chaproniere, G.C.H., Fuller, M., Kelly, D.C., et al., 2004. Late Cretaceous-Quaternary biomagnetostratigraphy of ODP Sites 1168, 1170, 1171, and 1172, Tasmanian Gateway. In: Exon, N.F., Kennett, J.P., and Malone, M.J. (Eds.), *Proceedings of the Ocean Drilling Program, Scientific Results Volume 189*, pp.1–57.
- Strother, S.L., Salzmann, U., Sangiorgi, F., Bijl, P.K., Pross, J., Escutia, C., et al., 2017. A new quantitative approach to identify reworking in Eocene to Miocene pollen records from offshore Antarctica using red fluorescence and digital imaging. *Biogeosciences* 14 (8), 2089–2100.
- Stump, E., 1995. The Ross Orogen of the Transantarctic Mountains. Cambridge University Press.
- Sugden, D., Denton, G., 2004. Cenozoic landscape evolution of the Convoy Range to Mackay Glacier area, Transantarctic Mountains; onshore to offshore synthesis. *Geological Society of America Bulletin* 116 (7–8), 840–857.
- Sugden, D.E., Denton, G.H., Marchant, D.R., 1991. Subglacial meltwater channel systems and ice sheet overriding, Asgard Range, Antarctica. *Geografiska Annaler. Series A: Physical Geography* 73 (2), 109–121.
- Sugden, D.E., Denton, G.H., Marchant, D.R., 1995. Landscape evolution of the dry valleys, transantarctic mountains: tectonic implications. *Journal of Geophysical Research: Solid Earth* 100 (B6), 9949–9967.
- Sugden, D.E., Marchant, D.R., Denton, G.H., 1993. The case for a stable East Antarctic Ice Sheet. *Geografiska Annaler* 75A, 151–351.
- Summerfield, M.A., Sugden, D.E., Denton, G.H., Marchant, D.R., Cockburn, H.A.P., Stuart, F. M., 1999. Cosmogenic isotope data support previous evidence of extremely low rates of denudation in the Dry Valleys region, 162. Geological Society, London, Special Publications, Southern Victoria Land, Antarctica, pp. 255–267.
- Super, J.R., Thomas, E., Pagani, M., Huber, M., O'Brien, C., Hull, P.M., 2018. North Atlantic temperature and pCO₂ coupling in the early-middle Miocene. *Geology* 46 (6), 519–522.
- Super, J.R., Thomas, E., Pagani, M., Huber, M., O'Brien, C.L., Hull, P.M., 2020. Miocene evolution of North Atlantic sea surface temperature. *Paleoceanography and Paleoclimatology* 35 (5), e2019PA003748.
- Talarico, F., Ghezzo, C., Kleinschmidt, G., 2021. The Antarctic Continent in Gondwana: a perspective from the Ross Embayment and Potential Research Targets for Future

- Investigations. In: Florindo, F., et al. (Eds.), Antarctic Climate Evolution, second ed. Elsevier (this volume).
- Tauxe, L., Stickley, C.E., Sugisaki, S., Bijl, P.K., Bohaty, S.M., Brinkhuis, H., et al., 2012. Chronostratigraphic framework for the IODP Expedition 318 cores from the Wilkes Land Margin: Constraints for paleoceanographic reconstruction. *Paleoceanography* 27 (2) . Available from: <https://doi.org/10.1029/2012PA002308>.
- Taviani, M., Hannah, M., Harwood, D.M., Ishman, S.E., Johnson, K., Olney, M., et al., and ANDRILL SMS Science Team 2008–2009. Palaeontological characterization and analysis of the AND-2A Core, ANDRILL Southern McMurdo Sound Project Antarctica. In: Harwood, D., Florindo, F., Talarico, F., Levy, R.H. (Eds.), Studies from the ANDRILL Southern McMurdo Sound Project, Antarctica—Initial Science Report on AND-2A. Terra Antarctica, pp. 113–146.
- Taylor-Silva, B., Riesselman, C., 2018. Polar frontal migration in the warm late Pliocene: diatom evidence from the Wilkes Land margin, East Antarctica. *Paleoceanography and Paleoclimatology* 33 (1), 76–92.
- Ten Brink, U., Cooper, A., 1992. Modeling the bathymetry of Antarctic continental margins. *Recent Progress in Antarctic Earth Science*. Terra Scientific Publishing Co, Tokyo, pp. 763–772.
- Ten Brink, U.S., Schneider, C., 1995. Glacial morphology and depositional sequences of the Antarctic continental shelf. *Geology (Boulder)* 23 (7), 580–584.
- Thiede, Jr., Jessen, C., Knutz, P., Kuijpers, A., Mikkelsen, N., Spielhagen, R.F., 2011. Millions of years of Greenland Ice Sheet history recorded in ocean sediments. *Polarforschung* 80 (3), 141–159.
- Thoma, M., Jenkins, A., Holland, D., Jacobs, S., 2008. Modelling circumpolar deep water intrusions on the Amundsen Sea continental shelf, Antarctica. *Geophysical Research Letters* 35 (18), L18602.
- Thompson, A.F., Stewart, A.L., Spence, P., Heywood, K.J., 2018. The Antarctic slope current in a changing climate. *Reviews of Geophysics* 56 (4), 741–770. Available from: <https://doi.org/10.1029/2018RG000624>.
- Tian, J., Yang, M., Lyle, M.W., Wilkens, R., Shackford, J.K., 2013. Obliquity and long eccentricity pacing of the Middle Miocene climate transition. *Geochemistry, Geophysics, Geosystems* 14 (6), 1740–1755.
- Tierney, J.E., Haywood, A.M., Feng, R., Bhattacharya, T., Otto-Bliesner, B.L., 2019. Pliocene warmth consistent with greenhouse gas forcing. *Geophysical Research Letters* 46 (15), 9136–9144.
- Timoney, R., Worrall, K., Firstbrook, D., Harkness, P., Rix, J., Ashurst, D., et al., 2020. A low resource subglacial bedrock sampler: the percussive rapid access isotope drill (P-RAID). *Cold Regions Science and Technology* 177, 103113.
- Tingey, R.J., 1991. The regional geology of Archaean and Proterozoic rocks in Antarctica. In: Tingey, R.J. (Ed.), *The Geology of Antarctica*, Oxford Monographs on Geology and Geophysics. Clarendon Press, Oxford, pp. 1–73.
- Tipple, B.J., Pagani, M., 2007. The early origins of terrestrial C4 photosynthesis. *Annual Review of Earth and Planetary Sciences* 35, 435–461.
- Treves, S.B., McKelvey, B.C., 1975. Drilling in Antarctica, September–December, 1974/1975. In: Mudrey Jr., M.G., McGinnis, L.D. (Eds.), *Dry Valley Drilling Project (DVDP) Bulletin*. pp. 5–10.
- Truswell, E.M., Drewry, D.J., 1984. Distribution and provenance of recycled palynomorphs in surficial sediments of the Ross Sea, Antarctica. *Marine Geology* 59 (1–4), 187–214.

- UNFCCC, 2015. Adoption of the Paris agreement. FCCC/CP/2015/L.9/Rev.1. United Nations Framework Convention on Climate Change. Available from: http://unfccc.int/paris_agreement/items/9485.php.
- Utescher, T., Bruch, A.A., Micheels, A., Mosbrugger, V., Popova, S., 2011. Cenozoic climate gradients in Eurasia—a palaeo-perspective on future climate change? *Palaeogeography, Palaeoclimatology, Palaeoecology* 304 (3–4), 351–358.
- Valletta, R.D., Willenbring, J.K., Lewis, A.R., Ashworth, A.C., Caffee, M., 2015. Extreme decay of meteoric beryllium-10 as a proxy for persistent aridity. *Scientific Reports* 5, 17813.
- van de Lagemaat, S.H.A., Swart, M.L.A., Vaes, B., Kosters, M.E., Boschman, L.M., Burton-Johnson, A., et al., 2021. Subduction initiation in the Scotia Sea region and opening of the Drake Passage: when and why? *Earth-Science Reviews* 215, 103551.
- Van de Wal, R., Greuell, W., van den Broeke, M.R., Reijmer, C., Oerlemans, J., 2005. Surface mass-balance observations and automatic weather station data along a transect near Kangerlussuaq, West Greenland. *Annals of Glaciology* 42, 311–316.
- Van der Burgh, J., Visscher, H., Dilcher, D.L., Kuerschner, W.M., 1993. Paleoatmospheric signatures in Neogene fossil leaves. *Science* 260 (5115), 1788–1790.
- Vanney, J.-R., Johnson, G., 1979a. Wilkes land continental margin physiography, East Antarctica. *Polarforschung* 49 (1), 20–29.
- Vanney, J.-R., Johnson, G.L., 1979b. The sea floor morphology seaward of Terre Adélie (Antarctica). *Deutsche Hydrografische Zeitschrift* 32 (2), 77–87.
- Verducci, M., Foresi, L.M., Scott, G.H., Sprovieri, M., Lirer, F., Pelosi, N., 2009. The Middle Miocene climatic transition in the Southern Ocean: evidence of paleoclimatic and hydrographic changes at Kerguelen plateau from planktonic foraminifers and stable isotopes. *Palaeogeography, Palaeoclimatology, Palaeoecology* 280 (3), 371–386.
- Verret, M., Dickinson, W., Lacelle, D., Fisher, D., Norton, K., Chorley, H., et al., 2020. Cryostratigraphy of mid-Miocene permafrost at Friis Hills, McMurdo Dry Valleys of Antarctica. *Antarctic Science* 1–15.
- Vignaud, P., Duringer, P., Mackaye, H.T., Likius, A., Blondel, C., Boissarie, J.-R., et al., 2002. Geology and palaeontology of the Upper Miocene Toros-Menalla hominid locality, Chad. *Nature* 418 (6894), 152–155.
- Vincent, E., Berger, W.H., 1985. Carbon dioxide and polar cooling in the Miocene; the Monterey Hypothesis. In: Sundquist, E.T., Broecker, W.S. (Eds.), *The Carbon Cycle and Atmospheric CO₂: Natural Variations Archean to Present*. pp. 455–468. *Geophysical Monograph* 32.
- Waddell, L.M., Hendy, I.L., Moore, T.C., Lyle, M.W., 2009. Ventilation of the abyssal Southern Ocean during the late Neogene: a new perspective from the subantarctic Pacific. *Paleoceanography* 24 (3).
- Wan, S., Tian, J., Steinke, S., Li, A., Li, T., 2010. Evolution and variability of the East Asian summer monsoon during the Pliocene: evidence from clay mineral records of the South China Sea. *Palaeogeography, Palaeoclimatology, Palaeoecology* 293 (1–2), 237–247.
- Warny, S., Askin, R.A., Hannah, M.J., Mohr, B.A.R., Raine, J.I., Harwood, D.M., et al., and the SMS Science Team 2009. Palynomorphs from a sediment core reveal a sudden remarkably warm Antarctica during the middle Miocene. *Geology* 37 (10), 955–958.
- Webb, P.-N., Harwood, D.M., 1991. Late Cenozoic glacial history of the Ross Embayment, Antarctica. *Quaternary Science Reviews* 10 (2–3), 215–223.
- Webb, P.-N., Harwood, D.M., McKelvey, B.C., Mercer, J.H., Stott, L.D., 1984. Cenozoic marine sedimentation and ice-volume variation on the East Antarctic craton. *Geology* 12 (5), 287–291.

- Weber, M.E., Raymo, M.E., Peck, V.L., Williams, T., and the Expedition 382 Scientists, 2019. Expedition 382 Preliminary Report: Iceberg Alley and Subantarctic Ice and Ocean Dynamics. International Ocean Discovery Program. Available from: <https://doi.org/10.14379/iodp.pr.382.2019>.
- Wei, L.J., Raine, J.I., Liu, X.H., 2013. Terrestrial palynomorphs of the Cenozoic Pagodroma Group, northern Prince Charles Mountains, East Antarctica. Antarctic Science 26, 69–79.
- Westerhold, T., Marwan, N., Drury, A.J., Liebrand, D., Agnini, C., Anagnostou, E., et al., 2020. An astronomically dated record of Earth's climate and its predictability over the last 66 million years. Science 369 (6509), 1383–1387.
- Whitehead, J.M., Bohaty, S.M., 2003. Pliocene summer sea surface temperature reconstruction using silicoflagellates from Southern Ocean ODP Site 1165. Paleoceanography 18 (3), 1075.
- Whitehead, J.M., Ehrmann, W., Harwood, D.M., Hillenbrand, C.-D., Quilty, P.G., Hart, C., et al., 2006a. Late Miocene paleoenvironment of the Lambert Graben embayment, East Antarctica, evident from: mollusc paleontology, sedimentology and geochemistry. Global and Planetary Change 50 (3–4), 127–147.
- Whitehead, J.M., Quilty, P.G., McKelvey, B.C., O'Brien, P.E., 2006b. A review of the Cenozoic stratigraphy and glacial history of the Lambert Graben—Prydz Bay region, East Antarctica. Antarctic Science 18 (1), 83–99.
- Whitehead, J.M., Wotherspoon, S., Bohaty, S.M., 2005. Minimal Antarctic sea ice during the Pliocene. Geology 33 (2), 137–140.
- Whitworth III, T., Orsi, A., Kim, S., Nowlin, W., Locarnini, R., 1998. Ocean, ice, and atmosphere: interactions at the Antarctic Continental Margin. In: Jacobs, S.S., Weiss, R.F. (Eds.), Antarctic Research Series, vol. 75. pp. 1–28.
- Williams, G., Bindoff, N., 2003. Wintertime oceanography of the Adélie Depression. Deep Sea Research Part II: Topical Studies in Oceanography 50 (8–9), 1373–1392.
- Williams, G., Aoki, S., Jacobs, S., Rintoul, S., Tamura, T., Bindoff, N., 2010. Antarctic bottom water from the Adélie and George V Land coast, East Antarctica (140–149 E). Journal of Geophysical Research: Oceans 115 (C4).
- Williams, G., Bindoff, N., Marsland, S., Rintoul, S., 2008. Formation and export of dense shelf water from the Adélie Depression, East Antarctica. Journal of Geophysical Research: Oceans 113 (C4).
- Williams, T., Handwerger, D., 2005. A high-resolution record of early Miocene Antarctic glacial history from ODP Site 1165, Prydz Bay. Paleoceanography 20 (2).
- Williams, T., Flierdt, Tvd, Hemming, S.R., Chunga, E., Roya, M., Goldstein, S.L., 2010. Evidence for iceberg armadas from East Antarctica in the Southern Ocean during the late Miocene and early Pliocene. Earth and Planetary Science Letters 290, 351–361.
- Wilson, D.J., Bertram, R.A., Needham, E.F., van de Flierdt, T., Welsh, K.J., McKay, R.M., et al., 2018. Ice loss from the East Antarctic Ice Sheet during late Pleistocene interglacials. Nature 561 (7723), 383–386.
- Wilson, D.S., Jamieson, S.S.R., Barrett, P.J., Leitchenkov, G., Gohl, K., Larter, R.D., 2012a. Antarctic topography at the Eocene-Oligocene Boundary. Palaeogeography, Palaeoclimatology, Palaeoecology 335–336, 24–34.
- Wilson, D.S., Luyendyk, B., Pollard, D., DeConto, R., 2009. Antarctic paleotopography estimates at the Eocene-Oligocene climate transition and their implications for Ice Sheet Growth (invited). In: Escutia Dotti, C. (Ed.), Program: First Antarctic Climate Evolution Symposium. SCAR, Granada, p. 30.
- Wilson, D.S., Pollard, D., DeConto, R.M., Jamieson, S.S.R., Luyendyk, B.P., 2013. Initiation of the West Antarctic Ice Sheet and estimates of total Antarctic ice volume in the earliest Oligocene. Geophysical Research Letters 40, 1–5.

- Wilson, G.S., 1995. The Neogene East Antarctic ice sheet: a dynamic or stable feature? *Quaternary Science Reviews* 14 (2), 101–123.
- Wilson, G.S., Levy, R.H., Naish, T.R., Powell, R.D., Florindo, F., Ohneiser, C., et al., 2012b. Neogene tectonic and climatic evolution of the Western Ross Sea, Antarctica—Chronology of events from the AND-1B drill hole. *Global and Planetary Change* 96–97, 189–203.
- Wilson, G.S., Roberts, A.P., Veresub, K.L., Florindo, F., Sagnotti, L., 1997. Magnetobiostratigraphic chronology of the Eocene-Oligocene transition in the CIROS-1 core, Victoria Land margin, Antarctica: implications for Antarctic glacial history. *Geological Society of America Bulletin* 109 (12), 2–14.
- Wilson, G.S., Levy, R., Browne, G., Cody, R., Dunbar, N., Florindo, F., et al., 2007. Preliminary Integrated Chronostratigraphy of the AND-1B Core, ANDRILL McMurdo Ice Shelf Project, Antarctica. In: Naish, T., Powell, R., Levy, R. (Eds.), *Studies from the ANDRILL, McMurdo Ice Shelf Project, Antarctica - Initial Science Report on AND-1B. Terra Antartica*. pp. 297–316.
- Winberry, J.P., Anandakrishnan, S., 2004. Crustal structure of the West Antarctic rift system and Marie Byrd Land hotspot. *Geology* 32 (11), 977–980.
- Winnick, M.J., Caves, J.K., 2015. Oxygen isotope mass-balance constraints on Pliocene sea level and East Antarctic Ice Sheet stability. *Geology* 43 (10), 879–882.
- Winter, D.M., Sjunneskog, C., Harwood, D., 2010a. Early to mid-Pliocene environmentally constrained diatom assemblages from the AND-1B drillcore, McMurdo Sound, Antarctica. *Stratigraphy* 7 (2–3), 207–227.
- Winter, D.M., Sjunneskog, C., Scherer, R.P., Maffioli, P., Riesselman, C., Harwood, D.M., 2010b. Pliocene-Pleistocene diatom biostratigraphy of nearshore Antarctica from the AND-1B drillcore, McMurdo Sound. *Global and Planetary Change*. (2), 96–97. Available from: <https://doi.org/10.1016/j.gloplacha.2010.04.004>.
- Witkowski, C.R., Weijers, J.W.H., Blais, B., Schouten, S., Sinninghe Damsté, J.S., 2018. Molecular fossils from phytoplankton reveal secular Pco_2 trend over the Phanerozoic. *Science Advances* 4 (11), eaat 4556.
- Wood, B., Harrison, T., 2011. The evolutionary context of the first hominins. *Nature* 470 (7334), 347–352.
- Woodard, S.C., Rosenthal, Y., Miller, K.G., Wright, J.D., Chiu, B.K., Lawrence, K.T., 2014. Antarctic role in Northern Hemisphere glaciation. *Science* 346 (6211), 847–851.
- Woodruff, F., Savin, S., 1991. Mid-Miocene Isotope stratigraphy in the Deep Sea: high-resolution correlations, paleoclimatic cycles, and sediment preservation. *Paleoceanography* 6 (6), 755–806.
- Woodruff, F., Savin, S.M., 1989. Miocene deepwater oceanography. *Paleoceanography* 4 (1), 87–140.
- Wright, A.P., Young, D.A., Roberts, J.L., Dowdeswell, J.A., Bamber, J.L., Young, N., LeBrocq, A.M., Warner, R.C., Payne, A.J., Blankenship, D.D., van Ommen, T. and Siegert, M.J., 2021. Evidence for a hydrological connection between the ice divide and ice sheet margin in the Aurora Subglacial Basin sector of East Antarctica. *Journal of Geophysical Research, Earth Surface* 117, F01033, 15pp. Available from: <https://doi.org/10.1029/2011JF002066>.
- Wright, C., Priestley, R., 1922. *Glaciology, British Antarctic (Terra Nova) Expedition 1910–13. Harrison & Sons, Ltd., London*, p. 581.
- Wright, J.D., Miller, K.G., Fairbanks, R., 1992. Early and middle Miocene stable isotopes: implications for deepwater circulation and climate. *Paleoceanography* 7, 357–389.
- Yamane, M., Yokoyama, Y., Abe-Ouchi, A., Obrochta, S., Saito, F., Moriwaki, K., et al., 2015. Exposure age and ice-sheet model constraints on Pliocene East Antarctic ice sheet dynamics. *Nature Communications* 6 (1), 1–8.

- Yan, Q., Wei, T., Korty, R.L., Kossin, J.P., Zhang, Z., Wang, H., 2016. Enhanced intensity of global tropical cyclones during the mid-Pliocene warm period. *Proceedings of the National Academy of Sciences* 113 (46), 12963–12967.
- You, Y., 2010. Climate-model evaluation of the contribution of sea-surface temperature and carbon dioxide to the Middle Miocene Climate Optimum as a possible analogue of future climate change. *Australian Journal of Earth Sciences: An International Geoscience Journal of the Geological Society of Australia* 57 (2), 207–219.
- You, Y., Huber, M., Müller, R.D., Poulsen, C.J., Ribbe, J., 2009. Simulation of the Middle Miocene Climate Optimum. *Geophysical Research Letters* 36, 1–5.
- Young, D.A., Wright, A.P., Roberts, J.L., Warner, R.C., Young, N.W., Greenbaum, J.S., et al., 2011. A dynamic early East Antarctic Ice Sheet suggested by ice-covered fjord landscapes. *Nature* 474, 72–75.
- Zachos, J., Pagani, M., Sloan, L., Thomas, E., Billups, K., 2001a. Trends, rhythms, and aberrations in global climate 65Ma to present. *Science* 292 (5517), 686–693.
- Zachos, J.C., Dickens, G.R., Zeebe, R.E., 2008. An early Cenozoic perspective on greenhouse warming and carbon-cycle dynamics. *Nature* 451, 279–283.
- Zachos, J.C., Pagani, M., Sloan, L., Thomas, E., Billups, K., 2001b. Trends, rhythms, and aberrations in global climate 65 Ma to present. *Science* 292, 686–693.
- Zachos, J.C., Shackleton, N.J., Revenaugh, J.S., Palike, H., Flower, B.P., 2001c. Climate response to orbital forcing across the Oligocene-Miocene boundary. *Science* 292 (5515), 274–278.
- Zelilidis, A., Piper, D.J.W., Kontopoulos, N., 2002. Sedimentation and basin evolution of the Oligocene-Miocene Mesohellenic Basin, Greece. *AAPG Bulletin* 86 (1), 161–182.
- Zhang, J., Scott, D.B., 1996. Messinian deep-water turbidites and glacioeustatic sea-level changes in the North Atlantic: linkage to the Mediterranean salinity crisis. *Paleoceanography* 11 (3), 277–297.
- Zhang, R., Zhang, Z., Jiang, D., 2018. Global cooling contributed to the establishment of a modern-like East Asian Monsoon Climate by the Early Miocene. *Geophysical Research Letters* 45 (21), 11,941–911,948.
- Zhang, Y.G., Pagani, M., Liu, Z., 2014. A 12-million-year temperature history of the Tropical Pacific Ocean. *Science* 344 (6179), 84–87.
- Zhang, Y.G., Pagani, M., Liu, Z., Bohaty, S.M., DeConto, R., 2013. A 40-million-year history of atmospheric CO₂. *Philosophical Transactions of the Royal Society A: Mathematical, Physical and Engineering Sciences* 371 (2001).
- Zhisheng, A., Kutzbach, J.E., Prell, W.L., Porter, S.C., 2001. Evolution of Asian monsoons and phased uplift of the Himalaya-Tibetan Plateau since late Miocene times. *Nature (London)* 411 (6833), 62–66.